THE UNIVERSITY *of* EDINBURGH

Advanced Load Modelling for Power System Studies

Adam John Collin

Doctor of Philosophy

THE UNIVERSITY OF EDINBURGH

2013

Abstract

Although power system load modelling is a mature research area, there is a renewed interest in updating available load models and formulating improved load modelling methodologies. The main drivers of this interest are the introduction of new types of non-conventional (e.g. power electronic interfaced) loads, the requirement to operate power supply systems with increasing levels of renewable distributed generation and the implementation of various load control functionalities (e.g. demand side management). As the majority of existing load models do not allow for a full and precise analysis of these new operating conditions, it is essential to develop new load models and update load modelling techniques.

This thesis presents a detailed study of modern loads, focussing on the requirements for their correct representation in power system analysis. The developed models of the individual loads are then combined using a new load aggregation methodology for developing aggregate load models, suitable for the analysis of both existing and future power supply systems (so called 'smart grids'). The methodology uses a circuit-based load modelling approach, as this allows reproduction of the instantaneous current waveforms of the modelled load for any given supply voltage. This approach retains all electrical characteristics of the loads and provides a more realistic representation of some important phenomena (e.g. harmonic cancellation and attenuation due to load and supply system interactions) which are often neglected in traditional load modelling procedures.

Case studies of the UK residential and commercial load sectors are presented as illustrations of the load aggregation methodology. The results show significant short-term and long-term temporal variations in the load characteristics, which are not available or reported in the existing literature. This information allows for a more comprehensive assessment of demand-side management functionalities and correlation with locally connected distributed generation. Both of these effects are investigated in the thesis by quantifying the possible extent and range of changes in power system performance for some expected near future changes in load configurations and network operating conditions.

Acknowledgements

Firstly, I would like to thank my supervisor, Dr Sasa Djokic, for his honesty, patience and continued support during the PhD study. Thanks are also extended to the thesis examiners, Dr Ewen Macpherson, Prof. Chengke Zhou and Prof. Kai Strunz, for their time and effort in reviewing the thesis. The valued contribution of Dr Jan Meyer and Ms Ana Maria Blanco in providing measured data during the course of this research is duly acknowledged.

Thanks to my colleagues and friends at the Institute for Energy Systems, particularly all those who have passed through Rm 4.120, for providing such a good working environment. Special mention goes to Dr Charles Cresswell for laying the foundations of this research and his support during the formative stages of the PhD, and to Dr Jorge Acosta, Mr Ignacio Hernando-Gil and Dr Barry Hayes for their efforts in collaboration.

Arriving at this point would not have been possible without the support of friends and family over the years. I am grateful to Mum, Dad and Robert for their encouragement; without their belief in me, it would have been much harder to succeed. Last, but by no means least, I would like to extend my heartfelt thanks to Kirsty for living this with me and always being there. I promise not to use the words 'working' and 'weekend' together quite so often in the future.

Declaration

I declare that this thesis was composed by myself, that the work contained herein is my own except where explicitly stated otherwise in the text, and that this work has not been submitted for any other degree or professional qualification except as specified.

Adam John Collin

Contents

List of Figures

List of Tables

Acronyms and abbreviations

ac	Alternating current
AC	Air conditioner
ADNC	Active distribution network cells
a-PFC	Active power factor correction
ASD	Adjustable speed drive
CC	Constant current
CE	Consumer electronics
CFL	Compact fluorescent lamp
CFT	Compact fluorescent tube
CHP	Combined heat and power
CIGRE	International Council on Large Electrical Systems
CP	Constant power
CPE	Constant phase element
CRI	Colour rendering index
CRT	Cathode ray tube
CSIR	Capacitor start - inductor run
CSR	Capacitor start - capacitor run
CT	Constant torque
CV	Constant voltage
DBR	Diode bridge rectifier
dc	Direct current
DF_h	Harmonic diversity factor
DG	Distributed generation
DHW	Domestic hot water
DSM	Demand-side management
EDL	Electrochemical double layer
EECM	Electrical equivalent circuit model
EIS	Electrochemical impedance spectroscopy
EL	Electronic load
EMI	Electromagnetic interference
EPRI	Electric Power Research Institute
EV	Electric vehicle
GHG	Greenhouse gas emissions

GIL	General incandescent lamp
GSP	Grid supply point
HID	High-intensity discharge
HIL	Halogen incandescent lamp
HP	High-power
HV	High-voltage
IC	Integrated circuit
ICT	Information and communication technology
IEEE	Institute for Electronics and Electrical Engineers
IES	Institute for Energy Systems
IGBT	Insulated gate bipolar transistor
IM	Induction motor
LCD	Liquid-crystal display
LED	Light-emitting diode
LED LS	LED light source
LFL	Linear fluorescent lamp
Li-ion	Lithium ion
LP	Low-power
LV	Low-voltage
MFD	Multifunction device
MG	Microgeneration
MV	Medium-voltage
NTC	Negative temperature coefficient
OLTC	On-load tap changing transformer
OPF	Optimal power flow
PC	Personal computer
PE a-PFC	Power electronics loads with active power factor correction
PE no-PFC	Power electronics loads with no power factor correction
PE p-PFC	Power electronics loads with passive power factor correction
PFC	Power factor correction
PHEV	Plug-in hybrid electric vehicle
p-PFC	Passive power factor correction
pu	Per-unit
PV	Photovoltaic
QT	Quadratic torque
rms	Root-mean-square
RP	Rear projector
RSIR	Resistor start - inductor run

SH	Space heating
SMPS	Switch-mode power supply
SOC	State of charge
SPIM	Single-phase induction motor
THD	Total harmonic distortion
TV	Television
VT	Variable torque
V2G	Vehicle-to-grid
WECC	Western Electricity Coordinating Council
WH	Water heating
WT	Wind turbine
ZIP	Polynomial load model
3PIM	Three-phase induction motor

Nomenclature

B	Diffusion coefficient (Li-ion battery)
C_{dc}	DC link capacitor
C_{EMI}	EMI filter capacitance
C_{res}	Resonant circuit capacitance
f	Supply system frequency
f_0	Nominal/rated system frequency
I_A	Current in amperes
I_{base}	Base current
i_{dc}	Instantaneous value of dc link current
$i_{dc,batt}$	Instantaneous value of Li-ion battery current
I_f	Diode forward current
I_h	RMS current magnitude of h^{th} harmonic current component
i_{in}	Instantaneous input current
I_p	Constant current component of active power polynomial/ZIP model
I_{pu}	Current expressed in per-unit
I_q	Constant current component of reactive power polynomial/ZIP model
I_0	Diode reverse saturation current
k	Boltzmann constant
k_f	Load model frequency coefficient
L_{PFC}	Power factor correction inductance
L_{res}	Resonant circuit inductance
L_{total}	Total input inductance
n	Diode ideality factor
n_p	Coefficient of active power exponential load model
n_q	Coefficient of reactive power exponential load model
$n_{1,2}$	Empircal exponent of constant phase element (Li-ion battery)
O	Capacitance of diffusion impedance (Li-ion battery)
P	Active power demand
P_p	Constant power component of active power polynomial/ZIP model
P_q	Constant power component of reactive power polynomial/ZIP model
P_{rated}	Load rated power
$P_{WT_{aggregate}}$	Power output (wind turbine model)
P_0	Nominal/rated active power demand

PF	True power factor
PF_d	Distortion power factor
PF_1	Displacement power factor
q	Constant of electron charge
Q_0	Nominal/rated reactive power demand
Q_1	Fundamental reactive power demand
R_{base}	Base resistance
R_{CFL}	CFL input resistance
R_{ct}	Charge transfer resistance (Li-ion battery)
r_{eq}	Equivalent dc link resistance
$r_{eq,batt}$	Equivalent resistance of Li-ion battery
$R_{eq,charging}$	Charging equivalent resistance (of CFL model)
$R_{eq,discharging}$	Discharging equivalent resistance (of CFL model)
R_0	Ohmic resistance (Li-ion battery)
R_P	Passivation film resistance (Li-ion battery)
R_{pu}	Resistance expressed in per-unit
R_s	Diode internal resistance
R_{total}	Total input resistance
R_Ω	Resistance in ohms
t	Time
T	Temperature
THD_I	Current THD
THD_V	Voltage THD
v	Input wind speed (wind turbine model)
V	RMS supply voltage
V_A	Diode applied voltage
v_{dc}	Instantaneous value of dc link voltage
$v_{dc,batt}$	Instantaneous value of Li-ion battery voltage
V_F	Diode forward voltage
V_{pu}	Voltage expressed in per-unit
v_{rect}	Instantaneous value of rectified supply voltage
V_{rms}	RMS value of supply voltage
v_{start}	DC link voltage at start of discharge period
v_{supply}	Instantaneous value of supply voltage
V_T	Diode thermal voltage
V_0	Nominal/rated rms supply voltage
X	Reactance
Y_0	Capacitance of constant phase element (Li-ion battery)

Z_{eq}	Network equivalent impedance
Z_p	Constant impedance component of active power polynomial/ZIP model
Z_q	Constant impedance component of reactive power polynomial/ZIP model
Z_{sys}	System impedance
Z_W	Warburg impedance (Li-ion battery)
Δt	Simulation time step
ω	Angular frequency of supply voltage
Ψ	Load adjustment factor
θ_h	Phase angle of h^{th} harmonic current component
θ_1	Phase angle between voltage and current fundamental components

Chapter 1

Introduction

Electrical power systems planning and operation decisions are based on the results of power flow and stability simulation studies, which should carefully assess the network performance for a range of possible operating conditions. Accurate modelling of all network components is crucial to obtain realistic results, and the need to include correct modelling of loads, and their electrical characteristics, is widely recognised and accepted [1]. There are several examples from history which confirm the importance of accurate load representation, with notable power system collapses, e.g. the Swedish blackout in 1983 [2] and the Tokyo network collapse of 1987 [3], being attributed to the incorrect representation of load characteristics. Accordingly, significant effort has been expended in developing accurate load models for a range of power system studies throughout the years, e.g. [3, 4, 5].

Since the last major review of load models in the 1990s, however, there have been many changes in the operation of the electrical power system and the electrical characteristics of loads themselves. Therefore, there is a need to update existing load modelling practice and develop models of new loads which are able to satisfy the requirements for analysis of modern power systems. This is reflected by a renewed interest in the load modelling research area in both industry and academia [6].

This interest is partly driven by the increasing levels of variable generation units connected to the distribution network, which requires a more detailed representation of the distribution network and the connected load. Traditionally, these power system components would have been represented by aggregate load models, including both the supply network and a large number of individual loads, for the analysis of higher voltage level networks. At this level of aggregation, the influence of individual load components is reduced, and the aggregate load behaviour is relatively insensitive to variations in the individual loads. This allows for the use of relatively simple load models. However, at the distribution level, load representation will consist of smaller sized aggregates, i.e. smaller customer groups, and the aggregate load models and network performance are more sensitive to variations within the individual load components. This is demonstrated in several studies, e.g. [7, 8], which have shown that the selected load models used in the analysis of distribution networks will influence the optimal placement and size of distributed generation (DG) units.

The operation of the inverter-interfaced DG units will also impact on the power quality of the distribution network and will interact with the local load. This will introduce interactions at harmonic frequencies, as well as possible voltage rise and unbalance conditions. As the number of non-linear loads also continues to increase within the power system, e.g. the proliferation of consumer electronics devices and the replacement of incandescent light bulbs with energy saving alternatives, accurate models capable of reproducing these complex interactions are necessary to analyse modern power systems.

The other contributing factor to the growing interest in load modelling is that the role which loads play within the power system may change in the future. Economic considerations are placing greater stress on the operation of power systems [9], and controlling the demand, i.e. applying demand-side management (DSM), is being considered as one of many viable approaches to defer investment in upgrading power system infrastructure. Although DSM measures have been implemented for several decades, they have generally been applied to larger individual customers. There is potential to utilise advances in communication technologies to coordinate reduction in smaller, distributed customers, i.e. in residential and commercial load sectors, to provide additional network support. A better understanding of low-voltage (LV) loads and their interactions with nearby power system components and users is essential to model and exploit any possible operational advantages in near future electricity networks. Load modelling is required to implement these scenarios in power system analysis to assess their impact throughout the power system.

1.1 The need for improved load models

Although it is difficult to predict the evolution of the power system, there are several operational challenges which will have to be addressed to maintain system reliability and quality of supply. The growing volume of installed DG and the possible implementation of DSM schemes are only two areas which are of interest to the research community. The potential widespread adoption of electric vehicles (EV) may significantly increase the demand within LV residential networks, and will require increased levels of control in the power system. These examples suggest that electrical power system components must become more sophisticated and more flexible; and this should be reflected in power system simulation tools.

From a load modelling viewpoint, this can be interpreted as a requirement to preserve more of the load electrical characteristics, allowing the developed load model to be easily converted between different load model forms. Traditional power system load models were, generally, presented in only one form (which are discussed in more detail in Chapter 2) and could be applied to one specific area of power system analysis. With advances in computational power, it is possible to derive and simulate more detailed load models which are suitable for a range of power system analysis, and the development of new load models should aim to include this functionality.

Clearly, new load models must be developed when new loads are introduced to the power system in large numbers. In recent years, several new devices have been produced which are expected to be widely used, e.g. light-emitting diode (LED) light sources (LED LSs) and EV battery chargers, and, although the use of these technologies is not yet widespread, detailed load models of these emerging technologies should be available for power system analysis. Regardless of the introduction of new loads, there is always a need to regularly review and update existing load models to ensure that they are representative of the loads which are currently used within the power system. Changes in technological trends, or the introduction of performance legislation, are both likely to alter the electrical characteristics of loads. Since the last major load modelling review, there have been a handful of papers which have presented updated load models of the most prevalent individual loads, e.g. [10, 11, 12]. The load models published in these papers show several differences with the previously developed model of the similar load type, highlighting the need to continually update load models.

Furthermore, technological changes of individual loads or the introduction of new loads will alter the aggregate load composition, and, consequently, the electrical characteristics of aggregate load. For example, the increasing penetration of energy saving light sources will reduce the overall contribution of the lighting load and increase the contribution of all other loads. Therefore, there is an increasing need to understand and identify the contribution of individual loads within the aggregate demand to analyse changes in the load mix. This is particularly pertinent for DSM actions, and is reflected in the recent approaches to aggregate model development. As the majority of this research has taken place in the US, there is very little publicly available information on the corresponding models for UK based loads.

However, perhaps the most important area for possible improvement in power systems load modelling practice is in the representation of temporal load variations. Previously developed load models present, at most, only one set of load model parameters for each characteristic loading condition (i.e. minimum and maximum demands), as these are the system operating conditions that will have the greatest influence on planning decisions. As the number of stochastic generation units embedded within the system continues to increase, appreciation of the shorter time variations in the electrical characteristics of the connected load may help to improve strategic decisions. In the UK, there have been significant efforts to model load-use and demand patterns, e.g. [13, 14, 15, 16, 17], but this has never been converted into actual load models, which include the information required for use in power system studies.

1.2 Load modelling research at the Institute for Energy Systems

The research presented in this thesis is a continuation of previous load modelling research at the Institute for Energy Systems (IES) [18]. The previous research developed individual load models of the most important loads, in terms of quantity and power consumption, of the UK residential load sector. As will be shown in this thesis, many of these models are also suitable for use in modelling of the UK commercial load sector. The main functional requirement of these models was the ability to reproduce the instantaneous input current waveform of the modelled load for any given supply voltage, therefore, preserving all electrical characteristics.

The methodology defined in the previous work at IES can be divided into the following stages:

1. Development of detailed 'full circuit' model.
2. Reduction of detailed 'full circuit' model to 'equivalent' circuit model.
3. Estimation of generic values of 'equivalent circuit' model parameters.

The detailed full circuit models were developed in specialist circuit software, i.e. PSpice [19], to allow for the correct representation of the individual electronic components. However, the high switching frequency of modern loads requires very small simulation time steps (between 1 - 10 μs) and, when coupled with the full representation of the complex circuits and switching components, results in long simulation run times. Furthermore, specialist circuit software is not easily integrated with typical power system analysis tools, and the level of detail provided by the full circuit model is generally not required.

Therefore, an equivalent circuit model was developed by reducing the full circuit model to only a few key components. Due to the simple form, the equivalent circuit model can be directly implemented in some power system analysis software. If this integration is not possible, the electrical characteristics required for the specific power system analysis can be extracted from the equivalent circuit model in the suitable form, e.g. by performing a Fourier transform to obtain harmonic current injections for harmonic power flow.

The final stage in the equivalent circuit model development was defining a generic value of the equivalent circuit model parameters. This was achieved by using the developed models to investigate the influence of variations in the values of the equivalent circuit components on the key electrical requirements of the device, e.g. to satisfy harmonic legislation, and by comparing against available manufacturers' data and measurements. It is at this stage in the load model development process that the research presented in this thesis begins, and a more detailed description of the load model development process is available in Section 2.5.

The ultimate purpose of the load modelling research efforts is to build a comprehensive load model library which includes the most important loads currently found in the UK residential and commercial load sectors. The main (expected) future loads should also be included to allow for the assessment of their impact before widespread use. Once the correct generic load models of the main load categories have been developed, they can be combined as required and applied to perform a wide range of power system analysis.

Although load-use statistics are typically presented by 'end-use', e.g. as 'wet' loads, consumer electronics, etc., in this thesis, the loads in the load model library are classified into five main load categories based, predominately, on the electrical characteristics of the load. Some consideration is also given to the end-use to make the classification as intuitive as possible. For example, the consumer electronics load type includes: TVs, audio and video equipment, set-top boxes etc. The number of individual load types far exceeds the reasonable level which can be considered for power system simulation. However, all of these load types have similar electrical supply and control circuits and, therefore, comparable electrical characteristics. So they can all be classed as the same load category.

The main load categories used in this research are shown in Figure 1.1. These are discussed in more detail in the main body of the thesis, with a brief overview given in the following text.

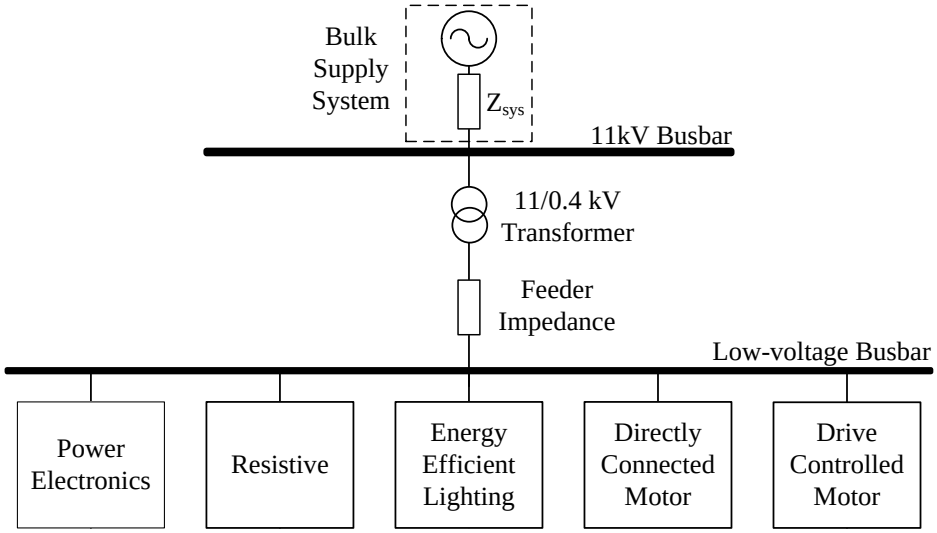

Figure 1.1: Main load categories.

Power electronics load category

Modern electronic loads are sensitive to voltage variations and require a regulated dc voltage supply, commonly referred to as a switch-mode power supply (SMPS). These devices are widely used and examples include: PCs, monitors, laptops, TVs etc. Apart from the time of use and contribution to the total load sector demand, there are no major differences between power electronics devices in the residential and commercial load sectors.

Resistive load category

Electrical devices classed as resistive load category are assumed to behave as an ideal resistor when supplied from mains voltage. Therefore, they can be modelled as a constant resistance and do not require further consideration from a load modelling point of view. These devices include space and water heaters and electrical cookers. As with the power electronics load category, the same load model is suitable for both the residential and commercial load sector.

Energy efficient lighting load category

The widely advocated phase-out of incandescent lamps has increased the contribution of the energy efficient lighting load category. At present, compact fluorescent lamps (CFLs) are the most developed technology in this category. However, in the near future, the contribution from LED LSs is expected to increase as the technology matures. Different lighting technologies will be found in the residential and commercial load sector, which are discussed in Chapter 4.

Directly connected motor load category

Directly connected induction motors (IMs) are used for a range of applications, including: fridge/freezers, washing machines and dishwashers. In the residential load sector, these will be predominantly single-phase IMs (SPIMs), which will also be largely utilised in the commercial load sector. In the commercial load sector, three-phase IMs (3PIM) may be used in larger facilities, where this type of connection is available. As the electrical models of this load category are well represented in existing literature, they are not considered in detail in this thesis.

Drive controlled motor load category

Drive controlled IMs include a power electronics drive which allows for greater control of speed/torque characteristics, improving performance and efficiency. They are most commonly used in higher power applications, i.e. in the commercial and industrial load sectors, but are expected to increase in numbers in residential applications. Accordingly, these devices are not considered in the analysis presented in this thesis, but are discussed in the further work section.

1.3 Research objectives and scope

The main purpose of this research is to develop aggregate load models for power system analysis. This requires various stages of aggregation, and begins by consideration of the characteristics of individual devices of each load category. As explained above, the resistive and motor load categories are not considered in this thesis, as their representation for power system analysis is well defined in literature. This thesis will focus on the power electronics and energy efficient lighting load categories, which are of particular interest for load modelling research for two reasons. First of all, the contribution of both load categories is increasing within the aggregate load mix. Furthermore, both load categories include a significant percentage of non-linear loads, which are responsible for harmonic emissions within the power system.

Aggregate models of these load categories are developed with consideration of the complex interactions between load harmonics. These load category models are then combined based on available UK load-use statistics to develop aggregate load models for the UK residential and commercial load sector, which may be directly applied in power system studies. This includes appreciation of the temporal variations in load characteristics, which offers a substantial improvement on existing models.

During the various stages of the aggregation process, information on the individual loads is lost. However, as the approach taken in this research begins from the detailed consideration of each individual load category, this information is available. Therefore, from the models presented in this thesis, it is possible to extract information on individual loads, an aggregation of loads from the same load category or an aggregate load representing a specific load sector.

The specific research objectives were defined as:

- To gain an understanding of how individual load characteristics impact on aggregate load behaviour and how these can be included in power system analysis.
- To develop load models of future electrical loads.
- To develop a methodology for representing the developed LV load models at the medium-voltage (MV) level for use in wider power system analysis.
- To analyse temporal variations in the electrical characteristics of the aggregate load models.
- To reproduce the instantaneous input current waveform of all modelled loads for a given supply voltage.

The scope and boundaries of the research were defined as:

- The research contained in this thesis is primarily focussed on the UK residential load sector, but reference is made to the UK commercial sector to illustrate how the techniques may be transferred.
- The load models developed in the research are able to reproduce the electrical characteristics of the modelled load for the voltage range $V_{pu} \in [0.8, 1.2]$.
- The frequency range considered is up to and including the 39^{th} harmonic order, i.e. 1.95 kHz, which is the limit of harmonic legislation applied to UK residential and commercial sector loads [20, 21].
- The research will focus on the representation of non-linear loads in the power electronics and energy efficient lighting load categories. When required, all other load models are taken from the previous research [18] or literature.

It should be noted that the presentation of results in the thesis will change between the different stages of aggregation, and this reflects the various forms which are commonly applied in different types of power system analysis. For the representation of the individual loads for a specific load category, and the aggregate representation of these, the models are presented as a range of equivalent circuit model parameters. More common load model forms and the corresponding harmonic current injections are also presented.

As the analysis moves to the MV level, the results are presented using standard steady-state load model forms (which are introduced in Chapter 2). The rationale for this is to present the work in a way which is of most use to wider power system community, and also for collaboration with colleagues within IES. More detailed discussions are presented where necessary in the main body text.

1.4 Main contributions of the thesis

The results from this research have been presented in one journal paper [22] and 15 international conference papers [23, 24, 25, 26, 27, 28, 29, 30, 31, 32, 33, 34, 35, 36, 37]. The work was awarded the Basil Papadias prize for best student paper at the IEEE PowerTech Conference 2011 and contributed to the CIGRE C4.605 Working Group on Modelling and Aggregation of Loads in Flexible Power Networks [38].

The main contributions, and associated publications, can be summarised as:

- Proposal of generic compact fluorescent tube model for use in CFL modelling.
- Investigation into harmonic injections of aggregate loads of:
  SMPS [23] and CFL.
- Development of load models for expected future loads:
  LED LSs [24, 25] and EV battery chargers [26].
- Development of improved load aggregation methodology [27, 28, 29].
- Investigation into the network influence of load models:
  with locally connected microgeneration (MG) [29, 30, 31],
  harmonic power flow [31, 32],
  distribution network [31, 33].

In further collaborations with colleagues in the IES, the developed load models have also been applied for transmission level studies and power system reliability analysis. Although not included in the thesis, further details are available in [34, 35, 36, 37].

1.5 Thesis structure

This thesis is divided into eight chapters, with additional material provided in the Appendices.

Chapter 2 reviews the main principles of load modelling for power system analysis and begins by introducing several important load modelling definitions as used throughout this thesis. This is followed by an overview of the load modelling approaches commonly used today. This includes both static and dynamic load models, as well as harmonic and circuit-based load models, which are of particular interest to the work presented in this thesis. The chapter concludes with an overview of the load modelling approach applied in this research.

Chapter 3 presents the techniques used to develop aggregate load representation of the power electronics load category. This approach starts with detailed consideration of the key electrical components within typical power electronics device and how this load category must be further subdivided as a result of harmonic legislation and technological variations. The Monte Carlo simulation technique is then used to simulate a large number of these devices using the expected range of model parameters, to determine the generic aggregate load characteristics. The developed aggregate load models fully consider the effect of harmonic cancellation and harmonic attenuation within the aggregate, which is a result of the interactions with the supply system,

for three different levels of system impedance. This chapter also includes the derivation of the analytical load modelling tool which is used throughout the rest of the research. *Publications from this chapter: [22, 23].*

The aggregate modelling of the other main non-linear load category, energy-efficient lighting, is described in **Chapter 4**. This load category is divided into the two energy saving varieties: CFLs and LED LSs. The majority of this chapter is focussed on the modelling of CFLs, as they are poised to become the main residential light source in the near future, and the techniques developed in Chapter 3 are applied to the modelling of this load category. Although they are not currently widely used in the UK residential load sector, the electrical characteristics of available LED LSs are also investigated and modelled. *Publications from this chapter: [24, 25].*

Chapter 5 contains information on the modelling of EV battery chargers, which are expected to become an important load in future power systems. Limited measurements were available and access to the electronic charging circuits was restricted, but it is shown that the modelling approach defined in Chapters 3 and 4 allows for the development of a new set of load models for this load category. A range of EV applications is considered to highlight the difference in electrical characteristics as the size and connection of the EV charger changes. *Publications from this chapter: [26].*

Chapter 6 gives an overview of the aggregation methodology for representing LV load models at the MV level. This is a crucial stage in the load model development, as standard power system analysis will generally not consider the LV level, i.e. less than 11 kV level in the UK. The methodology consists of six stages which are described in detail and illustrated using the residential load category as an example. It is shown that there are considerable short-term, i.e. half hourly, and medium-term, i.e. seasonal, variations in the aggregate load characteristics. *Publications from this chapter: [27, 28, 29].*

A range of case studies are presented in **Chapter 7** to illustrate the flexibility of the previously developed load models. The case studies include an example of how simple changes in the load composition, as a result of technological changes and DSM interventions, will change the electrical characteristics of the aggregate load and influence the results of standard load flow and harmonic power flow simulations. The aggregation methodology is also revisited in this chapter to develop load models of the UK commercial load sector and to consider how to include locally connected MG within the aggregate load model formulation. *Publications from this chapter: [28, 29, 30, 31, 32, 33].*

The final **Chapter 8** reviews the main findings of the research and the contributions to the load modelling research area. Recommendations for further development and improvement of the methodologies from this research are given, and other relevant areas of work are also discussed.

Chapter 2

Load modelling review

2.1 Introduction

Load modelling is a general term which can be used to describe both the development and implementation of different load models for power system analysis. This chapter introduces the reader to the basic concepts of the load modelling area and begins by defining the load modelling terminology, as used in this thesis. This is followed by an overview of the most widely used load modelling practices, with consideration to the requirements of load models for specific types of network analysis. The final section of this chapter describes the load modelling approach applied in this thesis.

2.2 Load modelling terminology

The previous work in the load modelling research area has produced a large number of different terms and definitions to describe power system loads and their representation for use in power system analysis. As the terms and definitions may vary in different texts, the terminology used in this thesis is defined as follows:

Load model In this thesis, a **load model** is defined as an analytical, mathematical, equivalent circuit based, physical component based, or any other suitable representation of electrical equipment (or group of these), which describes changes in the electrical characteristics of the modelled equipment as a function of variations in the relevant supply conditions (e.g. supply system voltage).

Electrical characteristics A set of parameters which characterise the electrical behaviour and response of the modelled load for various changes in system operating and loading conditions. Generally, the two most important load characteristics are the variations of active and reactive power demands given as a function of supply system voltage.

Static load models describe the electrical characteristics of the modelled load as function of the known or specified system parameters. Static load models use only the present state supply conditions to determine the required load characteristics, i.e. it is assumed that the load response to changes in the operating conditions is instantaneous.

Dynamic load models describe changes in the load characteristics as a function of the previous and current state of the supply conditions, e.g. in response to time-dependent transient changes in the supply conditions.

Aggregate load model A load model can represent either individual loads or aggregate loads and the term is often used interchangeably. However, as both individual load models and aggregate load models are covered in the main body of this thesis, it is important to make a clear distinction between the two. In this thesis, the term **load model** refers to the model of an individual load, while the term **aggregate load model** refers to a load model which represents the electrical characteristics of a group of individual loads.

Load type A group of individual loads with the same intended end-use, e.g. TVs, which may have similar or different electrical characteristics. This is generally how load-use statistics are presented, e.g. in government level reports, where loads are typically grouped into the following broad load types: consumer electronics, information and communication technology (ICT) equipment, lighting, wet, cold, cooking and space and water heating.

Load category A group of electrical devices which, for the purpose of load modelling, have the same, or similar, electrical characteristics. This may consist of devices from more than one load type. A load category may be further divided into several subcategories due to variations in electrical circuits.

Load sectors are defined as 'places where similar activities are performed'. Therefore, there are inherent similarities in the load composition, i.e. load types and load categories present in the aggregate load, and also in the load-use patterns. The most common classification of load sectors is residential, commercial and industrial [39], but more extensive definitions may include subsectors, e.g bank office, hospital, hotel, factory and retail, as subsectors of the commercial sector in [40]. This may also be referred to as the **load class**.

Load composition is the percentage contribution of different load categories to the total active power demand of a group of loads connected at one point of delivery for end-use consumption of electricity. This may also be referred to as the **load mix**.

2.3 Load model implementation

Although there are many forms of load models, some are more widely used than others. When selecting a suitable load model, the user must consider the type of analysis to be performed and the electrical characteristics of the load. In this section, the results of a recent survey of network operators from around the world are used to highlight and introduce current load modelling practice for steady-state and dynamic power system analysis. Full details of survey responses are available in [6]. Furthermore, harmonic load models and circuit-based load models are introduced as they are of particular interest to the research presented in this thesis.

2.3.1 Static load models

For steady-state power flow analysis of electrical power systems, the connected load can be represented by simple static load models. In traditional power system analysis, static loads are defined as one of three general load models:

- Constant impedance load - for which the active and reactive power demands of the load vary proportionally to the square of the supply voltage magnitude.
- Constant current load - for which the active and reactive power demands of the load vary in direct proportion (i.e. linearly) to the supply voltage magnitude.
- Constant power load - for which the load will draw constant active and reactive power, irrespective of the changes in supply voltage magnitude. When both active and reactive power are modelled in this way, it is generally referred to as a constant PQ load model.

These characteristics are illustrated in Figure 2.1.

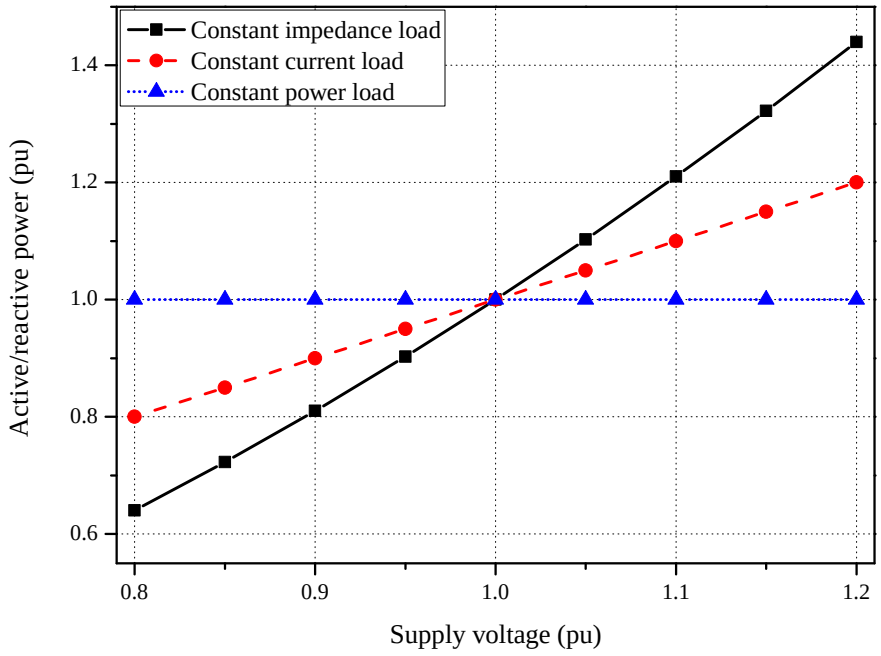

Figure 2.1: The three general static load model characteristics.

Based on the results of the recent load model survey [6], static load models are still widely used for both steady-state (Figure 2.2) and dynamic (Figure 2.3, discussed in Section 2.3.2) power system analysis. However, the constant PQ load model is by far the most widely used load model for steady-state analysis. The main explanation for this is that, at higher voltage levels, the distribution system transformer tap changers will operate to regulate the customer voltage to the nominal, or rated, value. If the voltage is constant, the load characteristics do not change

and appear as constant PQ. While this assumption is valid at the MV levels, where such voltage control technologies are present, it is not applicable in the lower voltage networks, where no voltage control is (currently) installed. The other main conclusion which can be drawn from the survey in [6] is that, for steady-state analysis, the same load model form is applied to represent both active and reactive power.

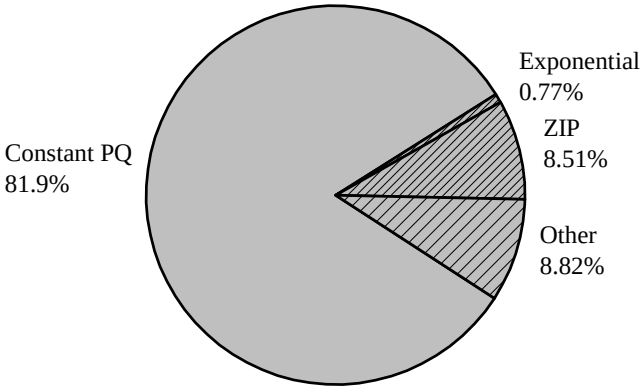

Figure 2.2: Currently used load models for steady-state analysis [6].

Although the constant PQ load model is the most common load model form, there is still significant use of other load models, as illustrated in Figure 2.2 and Figure 2.3. One reason for this is that the traditional constant impedance, constant current and constant power load models cannot accurately represent the electrical characteristics of non-linear loads. These are better expressed using more sophisticated load models.

The exponential load model

The exponential load model is a static load model that uses two exponents, n_p and n_q, to define the relationship between active and reactive power demand P and Q and supply system voltage V, (2.1) - (2.2). When $n_p = n_q = 2$, the load is a constant impedance load; when $n_p = n_q = 1$ the load is a constant current load; when $n_p = n_q = 0$, the load is a constant power load. The exponents may also be set to an arbitrary value in order to more accurately represent the power demand characteristics of the modelled load.

$$P = P_0 \left(\frac{V}{V_0} \right)^{n_p} \tag{2.1}$$

$$Q = Q_0 \left(\frac{V}{V_0} \right)^{n_q} \tag{2.2}$$

where: P and Q are the actual active and reactive power demands of the load, V is the actual supply voltage at the considered load bus (where the load is connected), V_0 is the nominal/rated system voltage, P_0 and Q_0 are nominal/rated active and reactive powers of the load, and n_p and n_q are the exponential model coefficients.

Most static load models exclude frequency variations in the supply system as the steady-state frequency variations are generally much smaller than voltage magnitude variations. However, frequency dependency can be included in the load model by multiplying the exponential load model with a frequency dependency term of the form:

$$1 + k_f (f - f_0) \tag{2.3}$$

where: f is the actual bus frequency, f_0 is the nominal/rated system frequency and k_f is the frequency dependent load model coefficient.

The second order polynomial load model

The second order polynomial load model is a static load model that represents the load power demand characteristic as the sum of the constant impedance Z, constant current I, and constant power P load characteristics, (2.4)-(2.5), and is often referred to as the "ZIP model".

$$P = P_0 \left[Z_p \left(\frac{V}{V_0} \right)^2 + I_p \left(\frac{V}{V_0} \right) + P_p \right] \tag{2.4}$$

$$Q = Q_0 \left[Z_q \left(\frac{V}{V_0} \right)^2 + I_q \left(\frac{V}{V_0} \right) + P_q \right] \tag{2.5}$$

where: P and Q are the actual active and reactive power demands of the load, V is the actual supply voltage at the considered load bus (where the load is connected), V_0 is the nominal/rated system voltage, P_0 and Q_0 are nominal/rated active and reactive powers of the load, and Z_p, I_p, P_p, Z_q, I_q, P_q are the polynomial model coefficients for active and reactive power, respectively.

As a result of the more complex analytical form, the polynomial load model can provide better matching of non-linear load characteristics than the exponential load model. As the active power polynomial coefficients must sum to plus one, the active power ZIP model coefficients may be interpreted to have some physical significance when modelling aggregate loads, i.e. they can indicate the percentage contribution of different load categories within the aggregate. However, as the coefficients are the result of mathematical curve fitting routines, the physical interpretation of the individual coefficients should be treated with caution. Generally, the individual coefficients should lie between zero and one, however, the values may take a negative value to represent a negative trend.

The reactive power ZIP model coefficients can sum to plus/minus one (with a positive value for an inductive load and a negative value for a capacitive load). However, the coefficients can also be presented as a sum to the actual reactive power demand, typically given as $Q_{0,pu}$. This, coupled with the fact that the reactive power load characteristics will tend to have more non-linear behaviour than the active power characteristics, and will often have individual coefficients greater than plus/minus one, makes the physical interpretation of the reactive power coefficients more complex.

Similar to the exponential form, it is possible to introduce a frequency dependent term (2.3) in the polynomial load model. It is also possible to convert the polynomial load model coefficients into one single value for use in a corresponding exponential load model using (2.6) and (2.7) [6]. This conversion is particularly useful when describing load characteristics. Although the ZIP model will provide a more accurate representation of load characteristics and should be implemented in simulation software, it is more straightforward to describe load characteristics, particularly if they change in time, using the single coefficient of the exponential form.

$$n_p = \frac{Z_p * 2 + I_p * 1 + P_p * 0}{Z_p + I_p + P_p} \tag{2.6}$$

$$n_q = \frac{Z_q * 2 + I_q * 1 + P_q * 0}{Z_q + I_q + P_q} \tag{2.7}$$

where: all parameters are as previously defined.

2.3.2 Dynamic load models

The assumption when using static load models is that the response of most loads to variations in the supply conditions is fast, resulting in reaching a new steady-state operating condition within a single simulation time step. While this assumption is adequate for steady-state power flow analysis, it is not suitable for dynamic power system analysis, which will focus on the transient response of the system and loads to various disturbances. The use of more detailed load models for dynamic power system analysis is confirmed by the survey results [6].

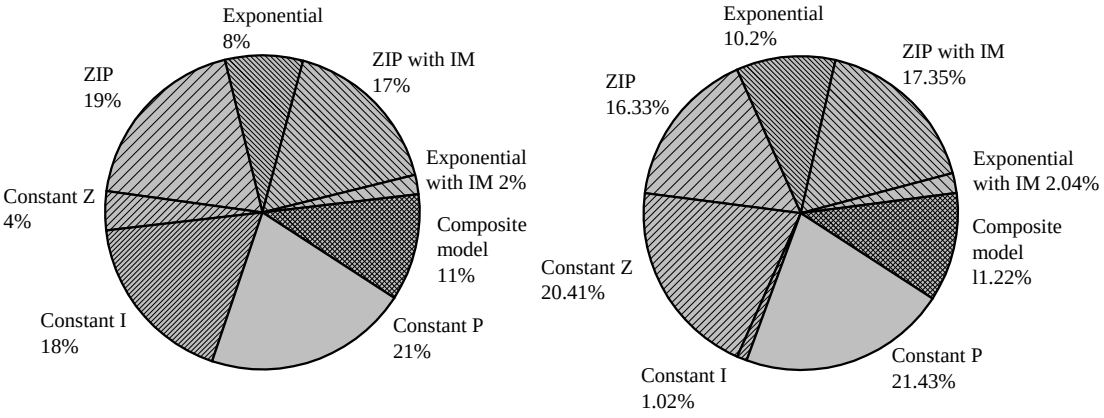

(a) active power (b) reactive power

Figure 2.3: Currently used load models for dynamic stability studies [6].

These results show that the dominance of the constant PQ load model is severely diluted and there is a more even spread of applied load models, with the use of voltage dependent load models much more prevalent than in steady-state analysis. The results also show that the load model selected to represent the active and reactive power characteristics may not be the same, as was the case with static load models. However, the main difference in the survey results is the inclusion of the IM load model as a separate dynamic load component.

Although dynamic load models are not considered in the analysis in this thesis, the natural evolution of the research is to progress to modelling the dynamic characteristics of the load. Therefore, the most common forms of dynamic load models are now briefly introduced.

Induction motor load models

Due to their large numbers, IMs have traditionally been represented by a separate load model. Another reason for the separation is that IMs have the main influence on the dynamic characteristics of the aggregate load [1, 3, 39]. This is confirmed by the results in Figure 2.3 which indicate that around 20% of network operators include detailed representation of this load for dynamic studies.

The complex dynamic behaviour of IM motor loads is normally represented in power system analysis using the 'dq' reference frame transformation, which converts the three phase ac quantities to a system of equations formed with respect to only two axes. The standard dq representation of a symmetrical three-phase induction motor is given by the set of equations (2.8) - (2.15), and the derivation of these equations is discussed in detail in [41].

Stator flux linkages Ψ:

$$\Psi_{qs} = L_s i_{qs} + L_m i'_{qr} \tag{2.8}$$

$$\Psi_{ds} = L_s i_{ds} + L_m i'_{dr} \tag{2.9}$$

Rotor flux linkages Ψ:

$$\Psi'_{qr} = L'_r i'_{qr} + L_m i_{qs} \tag{2.10}$$

$$\Psi'_{dr} = L'_r i'_{dr} + L_m i_{ds} \tag{2.11}$$

Stator voltages v:

$$v_{qs} = R_s i_{qs} + \frac{d\Psi_{qs}}{dt} + \omega_s \Psi_{ds} \tag{2.12}$$

$$v_{ds} = R_s i_{ds} + \frac{d\Psi_{ds}}{dt} - \omega_s \Psi_{qs} \tag{2.13}$$

Rotor voltages v:

$$v'_{qr} = R'_r i'_{qr} + \frac{d\Psi'_{qr}}{dt} + (\omega_s - \omega)\Psi'_{dr} \tag{2.14}$$

$$v'_{dr} = R'_r i'_{dr} + \frac{d\Psi'_{dr}}{dt} - (\omega_s - \omega)\Psi'_{qr} \tag{2.15}$$

where: R, i, L and ω are the resistance, current, inductance and angular frequency variables and subscripts d, q, s, r denote the d-axis and q-axis components of the stator and rotor windings, respectively.

Note: $L_s = L_{ls} + L_m$ and $L'_r = L'_{lr} + L_m$, where: subscripts m and l represent the magnetising and leakage inductance.

The rotor acceleration is determined by the mismatch in the electromagnetic torque T_e and the mechanical torque load T_m, i.e.:

$$T_e - T_m = J\frac{d\omega}{dt} \tag{2.16}$$

where: J is the moment of inertia of the rotor and the connected load.

As the full dynamic IM model is defined by five differential equations, the model is commonly referred to as the fifth-order model. This may be reduced to a third-order model if stator transients are neglected, i.e. $\frac{d\Psi_{qs}}{dt} = \frac{d\Psi_{ds}}{dt} = 0$, which can be applied if stator resistance is high, resulting in reduced stator transients [42, 43].

Exponential dynamic recovery model

At the higher voltage levels, the dynamic response of the demand will include both the load and the network components. More specifically, this refers to the operation of on-load tap changing (OLTC) transformers within the distribution network, which will act to restore nominal supply voltage following a voltage disturbance. The exponential dynamic recovery model is based on field measurements of the typical active and reactive power response of loads subjected to a step change in voltage at the high-voltage (HV) busbars [2]. Therefore, it is suitable for use in long-term stability studies, but will not provide accurate representation of the dynamics of IMs.

The response, shown in Figure 2.4, is characterised by the following stages: i) a step change in power ΔP immediately follows the step change in voltage ii) following this, the lower voltage OLTC transformers, and other control devices, will act to restore the voltage. As the voltage increases, the power demand will also increase until iii) a new steady-state condition P_s is reached. These times are indicated in Figure 2.4, however, it should be repeated that the voltage recovery is not shown, as this model represents the response at the higher voltage levels, while the initial voltage recovery will take place within the aggregate load.

This response is modelled as a first order differential equation which contains both the steady-state P_s and P_t transient load response components (2.17) and (2.18). Note: similar expressions exist for reactive power demand response.

$$T_P\frac{dP_r}{dt} + P_r = P_s(V) - P_t(V) = P_0\left(\frac{V}{V_0}\right)^{\alpha_s} - P_0\left(\frac{V}{V_0}\right)^{\alpha_t} \tag{2.17}$$

$$P_d = P_r + P_0\left(\frac{V}{V_0}\right)^{\alpha_t} \tag{2.18}$$

where: P_d is the active power consumption, P_r is the active power recovery, P_0 is the pre-fault value of active power, V is the supply voltage, V_0 is the pre-fault supply voltage, T_P is the active power recovery time constant, α_s is the steady-state active power voltage exponent, α_t is the transient active power voltage exponent and P_s and P_t represent the static and transient components/responses of the aggregate load.

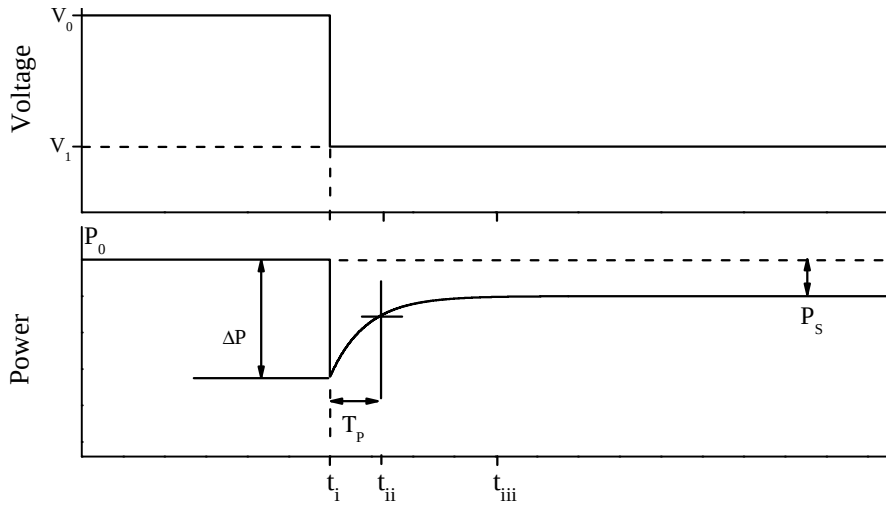

Figure 2.4: Typical response of the exponential dynamic recovery model [2].

Composite load models

As suggested by the name, a composite load model consists of more than one load model. This typically includes at least one static load model and at least one dynamic load model, normally an induction motor model, connected in parallel. The general form is shown in Figure 2.5. This load model is typically implemented by the analytical expressions corresponding to the different load models of the aggregate load. References [1, 44, 45, 46] give good examples of the implementation of this load model form.

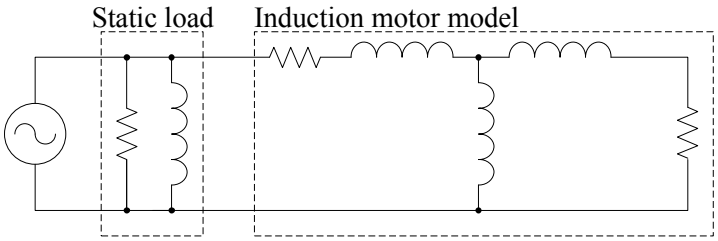

Figure 2.5: General form of the composite load model [44].

2.3.3 Harmonic load model

The previously shown load model forms are able to retain information on the active and reactive power demands of the modelled load. However, the information on harmonic injections is completely lost. As the proportion of non-linear loads continues to increase, analysis of the impact of increasing harmonic injections may become an important area of power system analysis. Harmonic load models are notoriously difficult to obtain with any degree of confidence, as they are highly variable and sensitive to changes within the power system, and statistical approaches are normally used to characterise the harmonic emissions of loads.

Harmonic loads in a power system are usually modelled by current source harmonic injections, consisting of a large number of harmonic current sources defined by their magnitude, phase angle and frequency, which are set to replicate the characteristics of the modelled load up to the desired harmonic order (2.19) [40, 47].

$$I = \sum_{h=1}^{H} |I|_h \angle \theta_h \tag{2.19}$$

where: $|I|_h$ and θ_h are the magnitude and phase angle of the h^{th} harmonic current component and H is the predetermined maximum harmonic order.

As harmonics are vector quantities, characterised by their magnitude and a phase angle, harmonic cancellation due to phase angle dispersion will occur between same-order harmonics within aggregate loads. The level of harmonic cancellation is difficult to predict and model, as this effect will occur between all time-variable harmonic sources connected to the same supply system, and will also depend on the specific operating conditions and impedances of the network. However, the harmonic diversity factor (DF_h) is a widely used indicator to quantify the harmonic cancellation effects between power system loads [48]. The DF_h is the ratio of the vector sum of magnitudes of individual current harmonics in the aggregate load to their algebraic sum (2.20).

$$DF_h = \left| \frac{\sum_n^N I_h^n}{\sum_n^N |I_h^n|} \right| \tag{2.20}$$

where: $I_h^n = |I_h^n| \angle \theta_h^n$ is the harmonic vector current of order h injected by the n^{th} load and N is the number of loads in the aggregate.

The value of DF_h will lie between one and zero: where DF_h of one indicates that no harmonic cancellation has occurred, while any value less than one indicates harmonic cancellation within the aggregate load. This is important to consider when representing aggregate loads, as it shows that assuming a fixed value of harmonic injection from one source will not yield accurate simulation results. In the absence of more detailed information, the diversity factor DF_h may be used to scale the expected harmonic injections of a particular load to obtain a more realistic value of the harmonic injections of the aggregate load [47].

2.3.4 Circuit-based load modelling

The previously introduced forms of load modelling are, generally, able to represent load characteristics for only one type of power system analysis. Circuit-based load models are able to reproduce the instantaneous input current waveform, to some degree of accuracy, and, therefore, retain more information on the load electrical characteristics. By processing the input current waveform, it is theoretically possible to extract any required load characteristic.

The circuit-based approach begins by considering the electrical components within the circuits of electrical loads and developing models based on the circuit topology. As the electronic circuits utilised in many modern loads are normally very complex, and often contain large numbers of active and passive electronic components, they require long simulation times and high levels of modelling detail. Accordingly, detailed full circuit models are not suitable for use in power system analysis and they are often reduced to equivalent circuit models.

Circuit-based models have been used to assess the transient behaviour of single-phase rectifier loads, e.g. [49, 50, 51], and the harmonic injections from modern electronic loads, e.g. [48, 52, 53, 54]. This clearly demonstrates their versatility.

2.4 Identification of load model parameters

Once the form of the load model is selected, the parameter values of the load model must be identified. It should be noted that, in some cases, the form of the load model can only be decided upon once the electrical characteristics of the load have been ascertained. There are two widely used methods to determine the parameter values: the measurement-based approach and the component-based approach. The description of these approaches in the following text refers to the development of aggregate load models, but it is possible to apply the general principles for the formulation of individual load models.

2.4.1 Measurement-based load modelling

The measurement-based load modelling approach obtains the input data for load model parameters from measurement devices installed in the actual power system. These devices will measure voltage and/or frequency variations and the resulting changes in load characteristics to either staged or naturally occurring disturbances, which are then fitted to the selected load model form. Good examples of this modelling approach are available in references [55, 56]. The main advantage of this modelling approach is that it is based on physical data and will provide accurate load models for the measured location and time. The main drawback of this approach is that naturally occurring seasonal variations in the load are hard to account for, without additional load composition data and extensive measurement campaigns. Furthermore, it is not possible to determine the load characteristics over a wide range of supply conditions and the model can only be applied at other network locations where the load composition and network configuration is similar to the site of the model development.

As the traditional measurement-based load modelling approach represents the actual load as a black box, there is no identification of the load composition. This is a particularly important requirement to analyse the impact of expected near-future load changes on the operation and performance of the power system. However, it is possible to combine the measurement and component-based load modelling approaches through the use of 'load signatures', i.e. by using a set of known load characteristics to determine the load composition from the measured data. This technique is demonstrated in [42].

2.4.2 Component-based load modelling

If the measurement-based load modelling approach can be considered a 'top-down' technique, the component-based load modelling approach can be described as 'bottom-up' approach, as the aggregate load model is constructed from the models of the individual load components within the aggregate load. The main advantage of this modelling approach is that no measurements of the power system are required to develop the aggregate load model. However, this must be compensated for by gathering large amounts of data to determine the load composition of the modelled aggregate load.

In general, only two datasets are required to implement the component-based load modelling approach:

1. Load models: representation of the required electrical characteristics of the individual loads which are present in the aggregate load. These individual load models are combined with the load composition data to form the aggregate load model.

2. Load composition data: the load mix giving the percentage contribution of each individual load to the total aggregate demand.

This classification is applicable only if the aggregate load consists of one load sector. However, if the aggregate load includes a large area of the network, it is highly likely to include different load sectors, e.g. a mix of residential and commercial buildings. Therefore, it is more intuitive to divide the second dataset into two separate parts to also include the load sector mix. This acknowledges the contribution of different load sectors to the total aggregate demand:

1. Individual load models: as previously defined.

2. Load sector composition data: the load mix giving the percentage contribution of each individual load to the total load sector demand.

3. Load sector mix: the percentage contribution of each load sector to the total load demand.

This is illustrated in Figure 2.6. The main purveyors of this load modelling approach are the Western Electricity Coordinating Council (WECC), while the Electric Power Research Institute (EPRI) have focussed more on combining the measurement-based and component-based approaches. As WECC and EPRI are two of the most active groups in load model research, they provide a good source of comparison for the models and approaches proposed in this thesis. Both show that motor loads are normally represented by specific IM models, with power electronics loads also included as a separate category [39, 57]. However, WECC group all other loads as 'static' [57], while EPRI include different lighting technologies and thermostatic loads as individual load components [39].

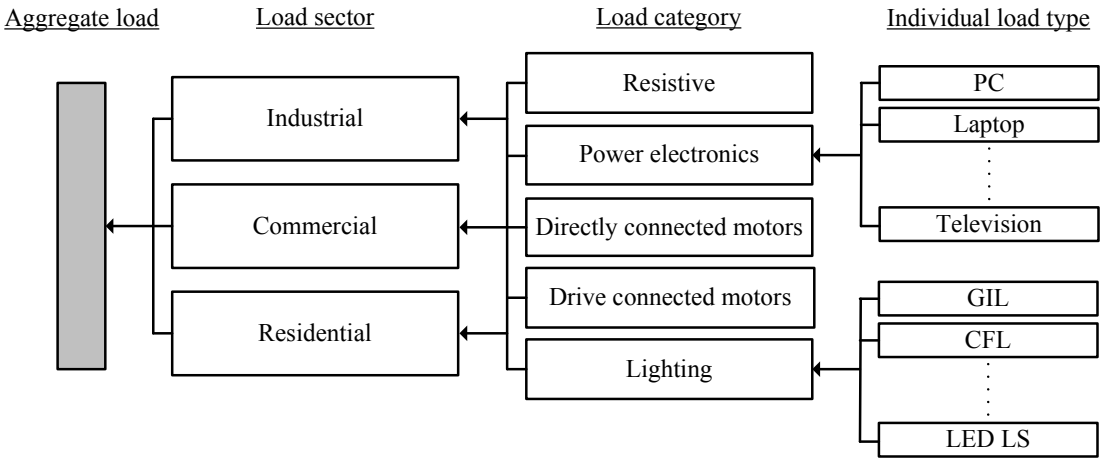

Figure 2.6: Component-based load modelling approach.

2.5 Load modelling approach implemented in this thesis

The purpose of the research presented in this thesis is to provide a flexible load modelling approach which is suitable for the analysis of modern and future power systems. Accordingly, the most flexible load modelling practices should be selected, and the developed load models should be available in forms for use in a wide range of power system analysis. These aims are best served by combining the use of circuit-based load models within a component-based load modelling framework. As previously discussed, circuit-based load models will reproduce the instantaneous input current waveform and allow the electrical characteristics of the modelled load to be converted into any required load model form.

This is achieved by the load model development process illustrated by the flow chart in Figure 2.7, which includes details on the required transformations and data flows between different stages of the modelling approach. It should be noted that this flow chart describes the steps required to model the individual load categories identified in Figure 1.1. The developed models of the load categories can then be combined to produce aggregate models of specific load sectors, and the aggregation methodology for this is discussed in Chapter 6.

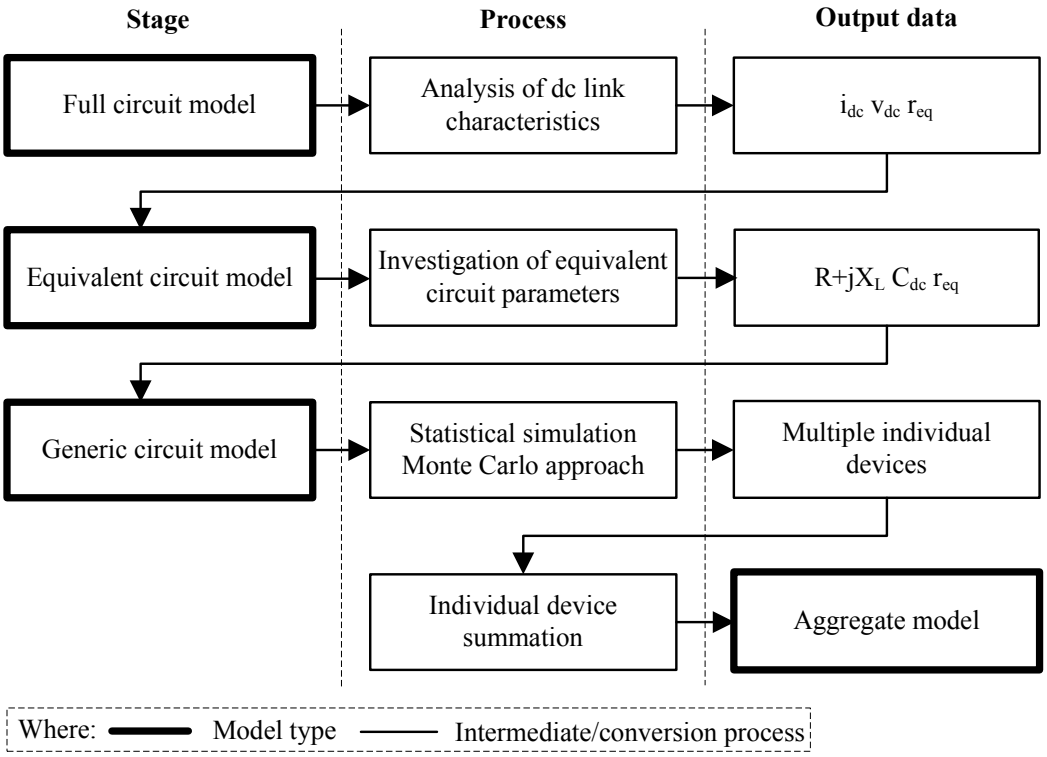

Figure 2.7: Load category model development flow chart.

The modelling of the individual load categories begins by consideration of the most important electronic components within a detailed full circuit model, which are obtained from previous research in [18]. For the modern non-linear loads considered in this thesis, which all include an ac-dc rectification stage, the full circuit model is reduced to an equivalent circuit form by analysing the current i_{dc} and voltage v_{dc} characteristics at the dc link to form an equivalent resistance r_{eq}. The resulting equivalent circuit model consists of only four parameters: the impedance in the input current conduction path $R + jX_L$, a diode bridge rectifier, smoothing dc link capacitor C_{dc} and r_{eq}. To define the generic circuit model, typical values, and expected ranges, of each equivalent circuit model parameter are identified.

The full circuit, equivalent circuit and generic circuit models all provide instantaneous input current waveforms, from which the required load model parameters may be extracted. By applying statistical simulation techniques, the range of generic model values can be utilised to simulate a large number of individual devices. At this stage in the model development process, these individual devices may be used to define individual models of each individual load or an aggregate load category model can be obtained by summing the required characteristics of the individual loads. In this research, the aggregate models of the individual load categories are calculated by summing the input current waveforms of the individual devices, as this will also include the effect of harmonic cancellation.

For the analysis presented in the thesis, it is not necessary to present coefficients of the developed load models for all of the previously identified load model forms. To demonstrate the flexibility of the developed circuit-based load models, the input current waveforms are processed to present results in standard load model forms suitable for two important areas of power system analysis: steady-state power flow analysis and harmonic analysis. The required functionality of the load model is significantly different for these two studies, and serves to highlight the flexibility of the developed circuit-based load models.

The exponential and polynomial load model forms are selected to illustrate the load characteristics for steady-state power flow, as the results of the recent survey indicates the widespread use of these model forms [6]. Therefore, the outcomes are produced in the form which is of most practical use. These models are obtained by varying the supply voltage in the range $V_{pu} \in [0.8, 1.2]$ and the active and reactive power demand for each voltage are calculated from the input current and voltage waveforms. A curve fitting routine is then applied to determine the value of the exponential and polynomial load model coefficients for the simulated power demands. As only one coefficient is required to describe the exponential model, this form is more widely used in the thesis to illustrate the temporal variations in the load characteristics. The corresponding polynomial models are included in the Appendices.

The exponential and polynomial load model forms are suitable for steady-state power flow analysis and also, as shown by the survey responses, are used for certain dynamic studies. As the purpose of these models is only to represent information on the active and reactive power magnitude, they do not contain any information on the harmonic emissions of modern power system loads. The increasing number of non-linear loads indicates that correct representation of the harmonic currents drawn by power system loads will be a useful resource for the community. Therefore, the harmonic injections obtained by Fourier analysis of the input current waveforms are also included in the presented results. It should be noted, however, that statistical models are typically used to represent harmonic loads. Although not extensively covered in this thesis, it is demonstrated that the modelling approach can produce this information if required.

The path taken in this thesis differs from WECC and EPRI, both of whom are producing load models for dynamic system studies, and tend to focus on the correct identification and representation of motor load dynamics. As the ultimate goals of the load modelling approaches are not the same, it is believed that the approaches are complementary, rather than contradictory.

2.6 Chapter summary

This chapter has presented a general overview of the load modelling research area. A review of current load modelling practice has been used to introduce the most commonly implemented load modelling forms. Existing load modelling practice has been assessed in its suitability for the analysis of modern, and future, power systems. From these conclusions, the load modelling methodology which is applied in this thesis has been introduced as a combination of the circuit- and component-based load modelling approaches.

Chapter 3

Power electronics load category

3.1 Introduction

In this thesis, the power electronics load category is defined as a combination of two major load types: consumer electronics loads and ICT loads. The individual loads included in this category cover a wide range of end-use applications, from televisions and set-top boxes, to desktop computers and laptops. Although the end-use of these loads is different, they all require dc voltage to operate, which is obtained using standard ac-dc rectifier circuits. Therefore, there are similarities in the electrical characteristics of these loads.

Due to the large number of power electronics devices currently in use, this load category is responsible for a significant percentage of the UK electricity consumption. The contribution of the power electronics load category to the total UK residential electricity demand has increased year on year, as a result of the initial boom in consumer electronics in the 1980's, plus the increasing demand for computing power (which is visible in all load sectors). This trend is shown in Figure 3.1. Although the overall consumption of the residential load sector has reduced recently, the consumption of power electronics loads is still increasing.

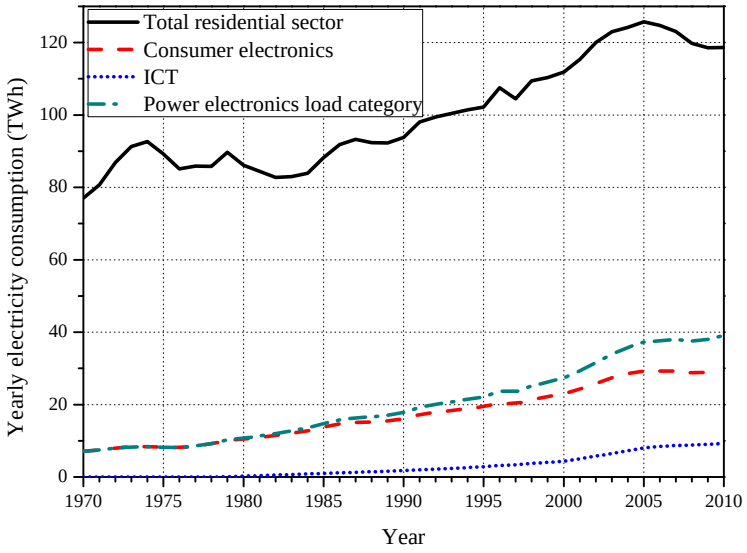

Figure 3.1: Consumption statistics of the power electronics load category [58].

In addition to the growing penetration of these devices, there is another important reason for the efforts to develop more accurate load models of the power electronics load category. The conversion of the ac supply voltage to regulated dc voltage requires the use of a SMPS. The SMPS operation will result in a discontinuous current waveform being drawn from the ac supply system, which will draw current at harmonic frequencies from the ac supply system. As the number of harmonic sources connected to the network increases, careful modelling is required to assess the impact of this load category on network performance.

These issues are considered in this chapter, which develops generic models and aggregate models of the power electronics load category. The analysis begins with a consideration of the electrical components within the load and their influence on the input electrical characteristics. The reduced equivalent circuit model form is then introduced, along with its analytical representation and generic/typical value for each component. A sensitivity analysis on the influence of each equivalent circuit model parameter to the load electrical characteristics is performed before the Monte Carlo simulation technique is applied to determine the harmonic cancellation between different power electronics loads, which allows for the development of more accurate aggregate models of this load category.

3.1.1 Available power electronics load models in literature

Existing load models offer some insight into the general characteristics of the power electronics load category, Table I. Most literature agrees that modern power electronic loads have constant, or approximately constant, active power characteristics with a very high displacement power factor (approximately unity) [4, 60, 63]. However, the available load models for this load category are the standard exponential or polynomial forms which do not include information on harmonic injections. Furthermore, the classification of these loads is often too specific, or vague, to allow for widespread implementation in aggregate load modelling methodologies.

Table 3.1: Power electronics load models identified in literature.

Ref.	Year.	Load	PF_1	Exp. Model		Polynomial/ZIP Model					
				n_p	n_q	Z_p	I_p	P_p	Z_q	I_q	P_q
[59]	1982	TV	0.8	2	5.1	ns	ns	ns	ns	ns	ns
[4]	1992	EL	ns	0	0	ns	ns	ns	ns	ns	ns
[60]	1998	OE 1	1	0.24	0	0.34	-0.35	0.98	0	0	0
[60]	1998	OE 2	1	0.2	0	0.08	0.07	0.84	0	0	0
[61]	2004	TV/Comp	ns	2	5.2	ns	ns	ns	ns	ns	ns
[62]	2004	EL	1	ns	ns	0	0	1	0	0	0
[63]	2008	TV CRT	1	ns	ns	0	0	1	0	0	0.15
[63]	2008	TV LCD	1	ns	ns	0	0	1	0	0	0.15

where: ns - not stated, EL - electronic load, OE - office equipment, Comp - computer load, CRT - cathode ray tube (TV), LCD - liquid-crystal display (TV) and PF_1 is the displacement power factor (as defined in (3.1) in Section 3.2.4).

3.2 General power electronics load topology

Power electronic loads require a tightly regulated dc supply voltage to operate, which is obtained by rectifying the ac supply voltage to dc and then by controlling the dc voltage to the supplied electronic circuitry. The standard method for ac-dc voltage conversion is an uncontrolled diode bridge rectifier (DBR). However, the DBR alone does not satisfy the performance criteria for power electronics load, as any fluctuations in the supply voltage will be transferred directly to the dc load. Therefore, extra control circuitry and components are included to provide a regulated dc voltage. The combination of DBR with controlled dc-dc converter is widely referred to as a SMPS, as it will utilise a high frequency switching signal to regulate the dc voltage. The general topology of a SMPS load is shown in Figure 3.2.

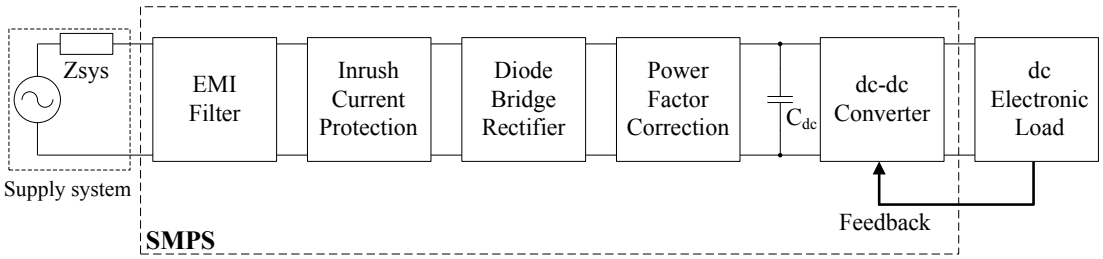

Figure 3.2: General block diagram of the power electronics load category.

A clear understanding of the purpose of each block will help to determine the influence of each circuit component on the electrical characteristics of the power electronics load. Accordingly, a brief overview of each component block is included in the following text. However, it is not the purpose of this thesis to accurately model the full SMPS circuit, as a detailed full circuit model is not a directly usable tool for load aggregation, due to the complex circuits and long simulation times. Full circuit models of SMPS have been developed in the previous research [18] and are widely available for download from circuit design companies, e.g. [64].

3.2.1 EMI filter

Due to the switching nature of operation, power electronic loads are a source of electromagnetic interference (EMI). EMI contains energy at high frequencies in the radio frequency range, several orders above the fundamental frequency, which is a problem not just for the operation of electrical equipment but also for radar and communication equipment. Therefore, these emissions are limited in accordance with various international standards, e.g. [65] and [66].

EMI is transmitted in two forms: radiated and conducted [67]. Radiated EMI can be reduced by metal enclosures which house the power electronics. As no additional electrical components are included, there is no effect from a load modelling viewpoint. Conducted EMI is generated into the power lines and is minimised by the use of EMI filters, the general form of which is shown in Figure 3.3.

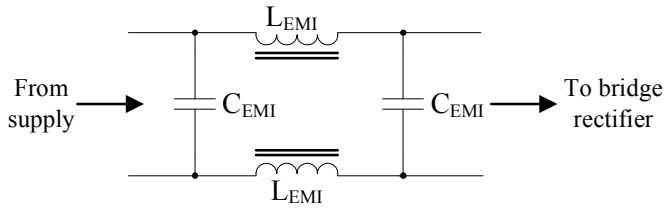

Figure 3.3: Typical switch-mode power supply EMI suppression filter circuit.

An EMI filter works by presenting a significantly higher impedance to higher frequency currents, i.e. the EMI filter is designed to act as a low-pass filter. In many devices, the values of these components are very small, and they have a negligible effect on the electrical characteristics of the load. However, larger values of EMI filter capacitors can influence the load behaviour if the dc load demand is low (as a percentage of the device rated power). This is discussed further in Section 3.5.

3.2.2 Inrush current protection

Inrush current is the term often used to describe the increased current drawn by a device at switch-on. This effect is well known in induction motors, but it will also exist in power electronic devices due to the presence of the dc link capacitor C_{dc}, shown in Figure 3.2, which is included to reduce the dc voltage ripple (refer to Section 3.2.3 for further details). When it is not energised, the C_{dc} will present a low-impedance conduction path, resulting in a large current being drawn at start-up. If not controlled, this large current may trip internal or external protection, or damage the electronic components within the device.

There are two common approaches to limit the magnitude of inrush current: by using active components, such as triacs, relays and thyristors, or by using a negative temperature coefficient (NTC) resistor. This component is often referred to as a thermistor. It is estimated that around 90 % of devices requiring inrush current protection will use the NTC method, as the cost is around 45 % of the active inrush current control system [68]. Therefore, this method is considered in the models developed in this thesis.

When current flows through the thermistor, the component will heat up. As the temperature increases, the resistance of the thermistor will decrease to an asymptotic value. This effect is illustrated in Figure 3.4 which shows that, for the typical rms current values found in the considered power electronics applications, there is not a major variation in the steady-state characteristics. An average line is also plotted, which shows the averaged NTC characteristics and can be used to define a generic response for use in the power electronics load models.

During steady-state operation, this component can be modelled as a fixed resistance. However, the dynamic characteristics in Figure 3.4 show that this component should be carefully considered for dynamic modelling of power electronics loads as the thermistor resistance will change in time. The application of the load models developed in this research to dynamic power system studies is discussed in the further work section in Chapter 8.

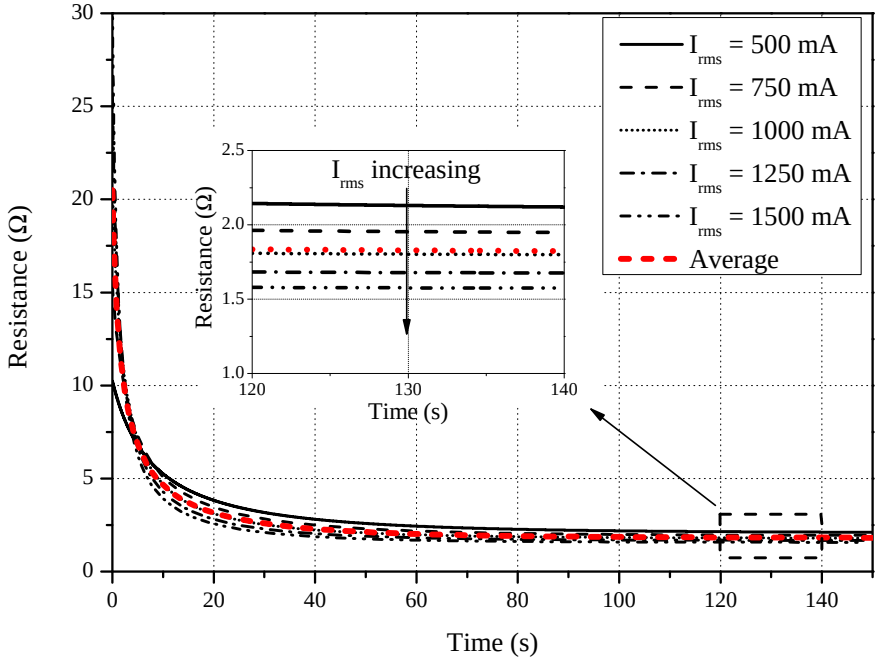

Figure 3.4: General characteristics of an NTC thermistor, based on data in [18].

3.2.3 Diode bridge rectifier

The standard method to convert ac mains supply voltage to dc voltage is by using an uncontrolled DBR. The single-phase DBR consists of four diodes, connected as shown in Figure 3.5. This configuration can be thought of as two groups of diodes. In the top group, the cathodes of D1 and D3 are at the same potential; in the bottom group the anodes of D2 and D4 are at the same potential. In the top group, the diode with the highest potential at the anode will conduct; while, in the bottom group, the diode with its cathode at the lowest potential will conduct. Therefore, when the supply voltage is positive, D1 and D2 will conduct, with D3 and D4 reverse biased. Conversely, when the supply voltage is negative, D3 and D4 will conduct, with D1 and D2 reverse biased. The resulting current flow through the dc load is in one direction. However, this simple DBR configuration produces a positive cycle voltage waveform with a large ripple component at the twice the supply system frequency, as shown in Figure 3.5(b). Therefore, a smoothing dc link capacitor, C_{dc}, is included to reduce the ripple component.

The addition of C_{dc} significantly changes the operation of the DBR circuit. When the magnitude of the rectified system voltage v_{rect} is greater than the magnitude of capacitor voltage v_{dc}, capacitor C_{dc} charges, and current is drawn from the supply. The dc link voltage v_{dc} will increase as C_{dc} charges, until it is greater than v_{rect}. When v_{dc} is greater than v_{rect}, C_{dc} will discharge through the connected electronic load, and v_{dc} will decrease, as the energy supplied to the load is taken from the capacitor C_{dc}. During the discharging stage, no current is drawn from the supply. This operation is presented in Figure 3.5(d).

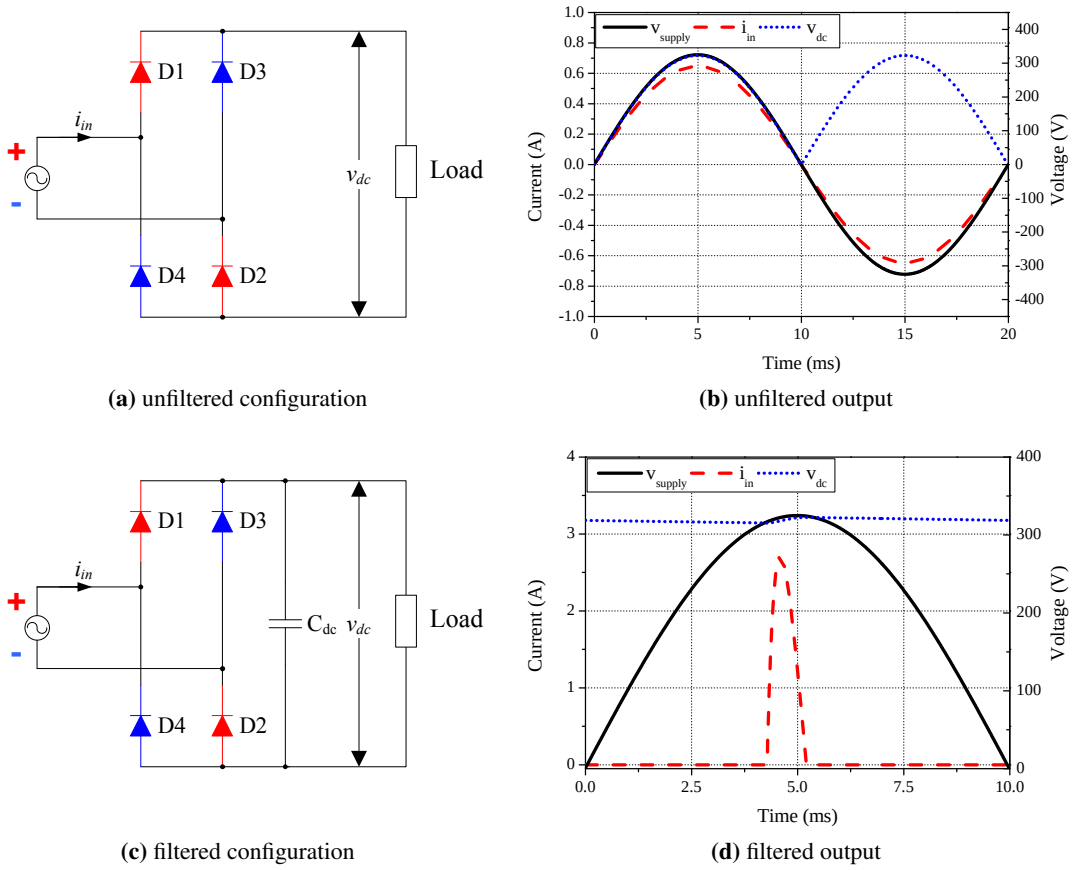

(a) unfiltered configuration

(b) unfiltered output

(c) filtered configuration

(d) filtered output

Figure 3.5: Single-phase diode bridge rectifier configuration and operation.

3.2.4 Power factor correction

As shown in Figure 3.5(d), the operation of the typical front-end DBR will result in a discontinuous current pulse waveform being drawn from the ac supply system. This current pulse waveform is rich in harmonics. The presence of harmonics has many negative effects on the operation of electricity networks, including higher thermal stresses and overloading of system components, e.g. shortening the lifetimes of transformers and cables, and increased neutral conductor currents. Harmonics may also interact with the supply system impedance, leading to distortions of the supply voltage, e.g. 'flat-top' voltage waveforms, which results in a less efficient transfer of power.

To allow for a better control of harmonic emissions, all loads connected to LV electricity networks must satisfy harmonic legislation. In the EU, harmonic emissions are governed by legislation in [20] for loads with rated current less than or equal to 16 A per phase, and by limits in legislation [21] for devices with rated current greater than 16 A but less than 75 A per phase. The majority of residential and commercial loads will be below 16 A and, therefore, have to satisfy the harmonic limits specified in [20].

In [20], power electronics devices are classed as Class D loads and must satisfy the harmonic limits shown in Table 3.2. Power electronic equipment with a rated power less than or equal to 75 W are currently exempt from the requirements in the harmonic standards. This threshold may be reduced to 50 W in the future, but it is worth noting that this reduction has not been introduced in the most recent update, from 2006 to 2009 editions.

Table 3.2: Harmonic limits for power electronics load category, (Class D) given in [20].

Harmonic number (N)	Maximum permissible harmonic current per watt (mA/W)	Maximum permissible harmonic current (A)
3	3.40	2.30
5	1.90	1.14
7	1.00	0.77
9	0.50	0.40
11	0.35	0.33
13	0.29	0.21
$15 \leq N \leq 39$	$\frac{3.85}{N}$	$\frac{2.25}{N}$

Without proper consideration of the power factor, the link between harmonics and power factor may not be instantly apparent. However, there are two simple connections between these properties. Although the displacement (or fundamental) power factor PF_1 is widely used, the true power factor PF is the ratio of total active power P to the total apparent power S. For non-linear loads, this will include a significant proportion of power transferred at the harmonic frequencies. The term distortion power factor PF_d may be applied to this component of the true power factor, which is a function of total harmonic distortion (THD). Therefore, PF_1 is a measure of the angular displacement between the fundamental components of the current and voltage, while PF_d is measure of the power demand at harmonic frequencies. These definitions are given in (3.1) - (3.4). All electrical definitions used in this thesis are grouped together and included in Appendix A.

$$PF_1 = \frac{P_1}{S_1} = cos(\theta_1) \tag{3.1}$$

$$PF_d = \frac{[1+(P_H/P_1)]}{\sqrt{1+THD_I^2+THD_V^2+(THD_I THD_V)^2}} \approx \frac{1}{\sqrt{1+THD_I^2}} \tag{3.2}$$

$$PF = \frac{P}{S} = PF_1 \times PF_d \tag{3.3}$$

$$THD_{\%} = \sqrt{\sum_{h\neq 1}\left(\frac{|I_h|}{|I_1|}\right)^2} \times 100 \tag{3.4}$$

where: P,P_1,S,S_1 are the total and fundamental active and apparent power, θ_1 is the phase angle between the voltage and current fundamental components and I_1,I_h are the current magnitude at the fundamental and h^{th} harmonic frequency.Note: THD definition is also applicable to voltage.

The second definition of distortion power factor in (3.2) is suitable for use when $THD_V < 5\%$ and $THD_I > 40\%$, which is true for the majority of the non-linear loads presented in this thesis. However, all PF_d values presented are derived from the full defintion.

From the definitions, it is theoretically possible to improve the true power factor by reducing the phase angle between the voltage and current fundamental components or by lowering the harmonic currents. In practice, power factor correction (PFC) techniques will influence both. There are two general forms of PFC, active (a-PFC) and passive (p-PFC).

Active PFC

As the name suggests, a-PFC utilises active electronic components to control the harmonic emissions. More specifically, an additional dc-dc converter is used to shape the input current to a good approximation of the sinusoidal waveform in phase with the input voltage. This is typically based on the boost converter topology [67] and is shown in Figure 3.6.

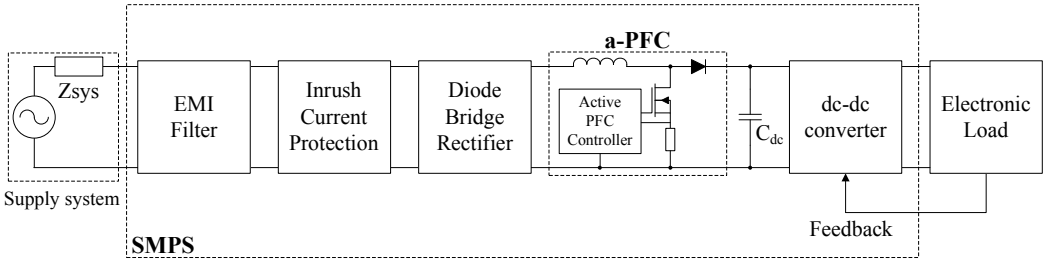

Figure 3.6: General configuration of power electronics load with a-PFC circuit.

Due to the active control, the resulting input current waveform is very close to the ideal sinusoid, with a displacement power factor very close to unity and a very low THD_I. An example of the performance of an a-PFC device (for measured laptop battery charger) is given in Figure 3.7, where the high frequency switching components are clearly visible in the input current waveform, which is a good approximation of the sinusoidal waveform.

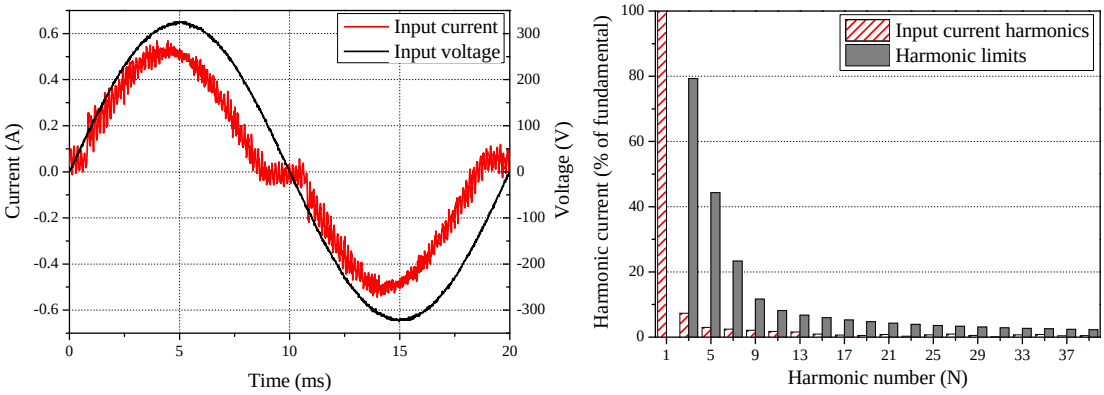

(a) input current waveform (b) associated harmonic content

Figure 3.7: Input characteristics of a-PFC power electronics loads.

Passive PFC

The harmonic emissions of power electronic loads can also be reduced by careful selection of the electronic components within the rectifier circuit. This approach is utilised in lighting ballast design (discussed further in Chapter 4). However, for stricter harmonic legislation, it may be necessary to include additional passive components in the circuit to satisfy harmonic limits. This is classified as p-PFC.

The most common p-PFC approach in the power electronics load category is to include an additional inductance in the conduction path to reduce the harmonic emissions. There are other possible technical solutions for p-PFC which are employed in other load categories, such as the valley-fill PFC circuit discussed in Section 4.3.1 in the following chapter.

As inductors oppose the change of current, this will effectively reduce the rate of change of the current pulse and 'smooth' the input current waveform, i.e. widening the current pulses and reducing their harmonic content. This is illustrated in Figure 3.8 which shows that the value of inductive reactance will have a significant effect on the input current waveform. The inductor is placed on the dc side, as shown in Figure 3.2, as this configuration was observed from inspection of actual devices. For the steady-state analysis presented in this thesis, placing the inductor on the ac side will have no impact on the circuit analysis.

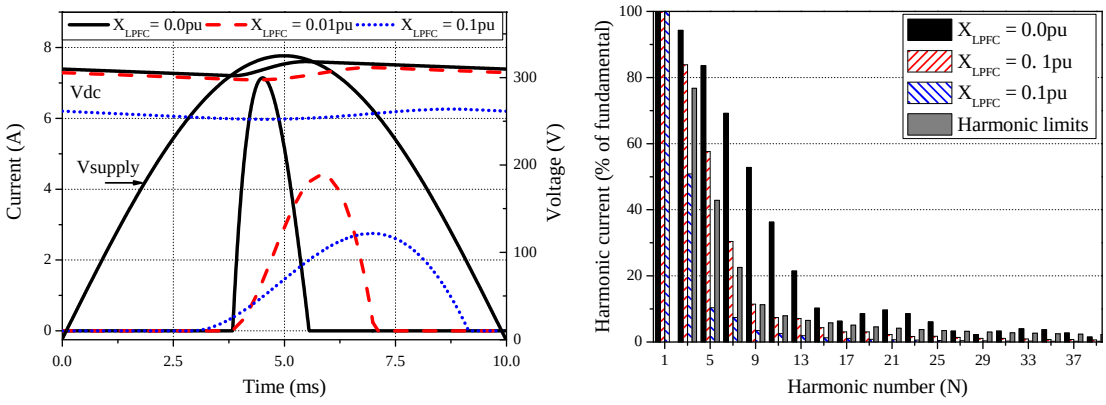

(a) input current waveform

(b) associated harmonic content

Figure 3.8: Influence of inductor size on the input characteristics of power electronics loads.

To illustrate this effect, nominal reactance values are taken: from 0 to 0.1 per-unit (pu). As the value of inductive reactance increases, the current waveform will become wider and shift to the right. The wider current pulses will have a lower harmonic content. Furthermore, as the current pulses shift to the right, the voltage fundamental will eventually lead the current fundamental and the load will become inductive. This effect can be clearly seen in Figure 3.9. Therefore, the introduction of the p-PFC inductor will reduce the displacement power factor, as the fundamental components of the current and voltage are more out of phase. However, the improvement of the distortion power factor far outweighs this effect and results in an overall improvement of the true power factor. This effect is quantified in Table 3.3.

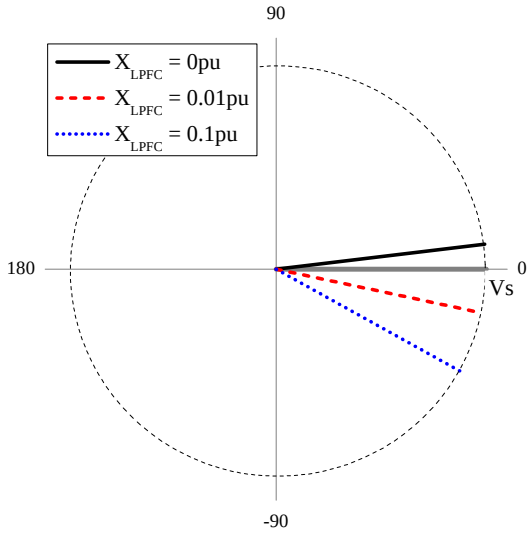

Figure 3.9: Influence of p-PFC inductor size on the phase angle of the fundamental component of the input current of power electronics loads.

Table 3.3: Effect of p-PFC inductor value on the true, displacement and distortion power factor of power electronics load.

$X_{L_{PFC}}$ (pu)	Characteristic		
	PF	PF_1	PF_d
0	0.53	0.99	0.53
0.01	0.67	0.98	0.68
0.1	0.77	0.87	0.89

Current industry practice is to use p-PFC, rather than a-PFC, due to the extra cost incurred by including an additional dc-dc converter [69]. It is expected that the increasing cost of copper based components, coupled with the falling cost of semiconductors, will make a-PFC more prominent in all power electronic equipment in the near future [70]. This is proposed as an area of future research (see Chapter 8 for discussion).

3.2.5 DC-DC converter

After the rectification stage, the dc voltage is regulated at the requried value by the dc-dc converter. Although there are a large number of configurations for dc-dc converters, the two most widely used are the flyback converter and the forward converter. Due to their low cost, flyback converters are normally used in low-power applications, while forward converters are typically used in power supplies with rated powers in the range 100 - 300 W [71].

Although the exact configuration of the components will determine the specific operation, a typical dc-dc converter for power electronic equipment will include a MOSFET-based circuit, acting as a switch, diode(s) to regulate direction of current flow and a magnetic component

to store energy. Depending on the specific configuration, switching the MOSFET on and off will cause energy to be stored in the magnetic component, or to be released to the dc load. Therefore, by controlling the frequency and duty cycle of the MOSFET switch, it is possible to regulate the voltage at the output terminals of the converter.

The dc-dc converter uses feedback from its output to monitor the dc voltage and control the switching duty cycle accordingly. This feedback control produces a regulated dc voltage and also protects the dc load from variations in the ac mains supply voltage. Modern SMPS loads contain sophisticated integrated circuit (IC) control chips, offering a range of features, including: reduced standby power, higher efficiency at reduced load and internal thermal protection. The control chip is supplied from the dc link voltage and requires a certain minimum dc voltage to function properly. If the dc link voltage is reduced, e.g. due to voltage sag or short voltage interruption, the controller will disconnect the load and maintain some energy in the capacitor after the dc voltage approaches some prescribed minimum value. This does not affect steady-state performance, but should be considered for dynamic modelling of power electronics loads.

Although many different dc-dc converter topologies are available, the purpose, from a load modelling viewpoint, is identical and is not considered in detail in this thesis. Reference [67] provides details on all dc-dc converter topologies.

3.3 Subcategories of power electronics loads

The previously discussed harmonic legislation and application of specific PFC methods effectively introduces three subcategories in the power electronics load category. In this thesis, these are defined as:

- PE no-PFC: power electronic loads with rated power 75 W or less
- PE p-PFC: power electronic loads with rated power greater than 75 W with p-PFC
- PE a-PFC: power electronic loads with rated power greater than 75 W with a-PFC

To compare the characteristics of these subcategories, different SMPS applications were measured, with results presented Figure 3.10. Additional details are given in Table 3.4. To allow for a direct comparison, the input current waveforms in Figure 3.10 have been normalised using (3.5) and (3.6):

$$I_{base} = \frac{P}{V_{rms} \times PF_1} \tag{3.5}$$

$$I_{pu} = \frac{I_A}{I_{base}} \tag{3.6}$$

where: P is the power drawn by the device, V_{rms} is the rms value of input supply voltage, PF_1 is the displacement power factor, I_{base} is the base current, I_A is the current in amperes and I_{pu} is the current in pu.

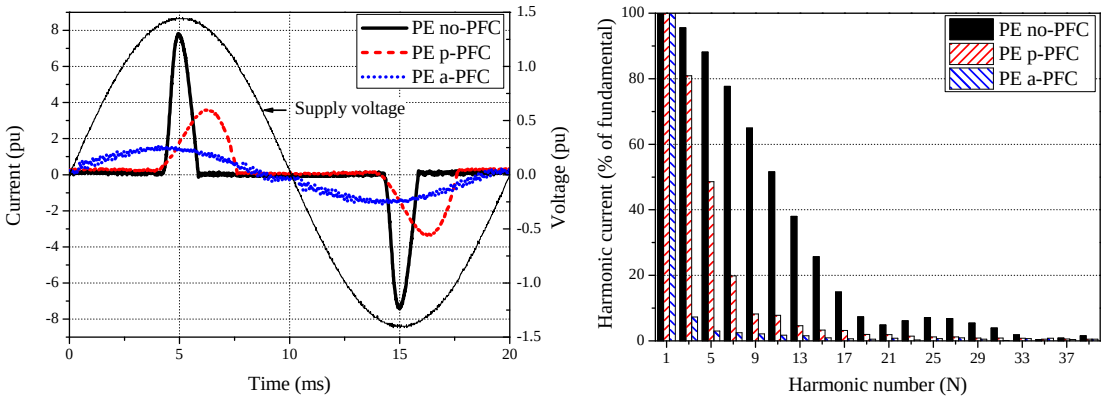

(a) input current waveforms (b) associated harmonic content

Figure 3.10: Comparison of input current waveforms of power electronics load subcategories.

Figure 3.10 clearly shows that PE no-PFC subcategory loads will have a current pulse of much greater magnitude than those with PFC. The sinusoidal current waveform of a-PFC devices will result in a comparatively lower peak current magnitude. Due to the additional components, the harmonic emissions of the PE p-PFC and PE a-PFC devices are much lower than that of PE no-PFC devices. The results in Table 3.4 clearly show the improvement in true power factor for devices with additional PFC components. Although the displacement power factor PF_1 will slightly reduce, the improvement in distortion power factor PF_d is significant.

Table 3.4: Comparison of selected electrical characteristics of power electronics subcategories.

Subcategory	Characteristic			
	PF	PF_1	PF_d	THD_I (%)
PE no-PFC	0.484	0.999	0.484	180.06
PE p-PFC	0.688	0.967	0.711	97.44
PE a-PFC	0.951	0.961	0.989	9.17

3.4 Modelling the power electronics load category

Detailed modelling of the circuits used in the power electronics load category requires specialised software, e.g. PSpice [19], which is not suitable for power system analysis. Furthermore, the high frequency switching of the dc-dc converter requires small simulation time-steps. The overall complexity of the circuit, coupled with the small simulation step, results in long simulation times. An example 'full circuit model' of a PE p-PFC device is shown in Figure 3.11.

Previous research, e.g. [18, 48, 49, 50], has shown that this full circuit model can be accurately represented by a simplified equivalent circuit model, which is shown in Figure 3.12. It should be noted that the equivalent circuit is used to model PE no-PFC and PE p-PFC subcategories in this thesis. Due to the performance of the a-PFC controller, which draws a sinusoidal current from the supply system, PE a-PFC load is modelled as a constant power load with unity displacement power factor.

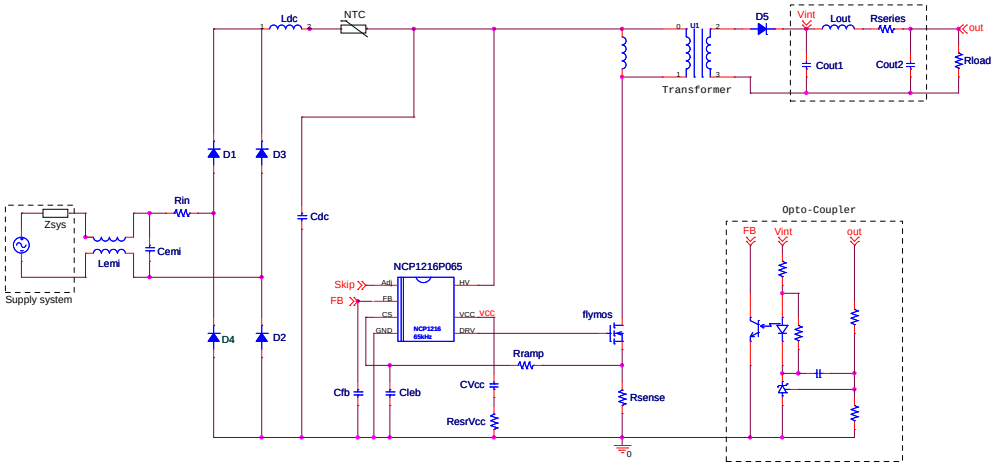

Figure 3.11: Detailed full circuit model of power electronics load with p-PFC [18, 64].

The equivalent circuit model consists of a DBR, dc link capacitor C_{dc}, input impedance $R + jX_L$ and an equivalent resistance r_{eq}. The input impedance (denoted R_{total} and L_{total}) represents the sum of all series impedances in the rectifier circuit (note: although the system impedance is in series, this is typically shared by multiple devices and is discussed further in Section 3.6). The EMI filter is represented by a single equivalent capacitor C_{EMI} and is normally neglected from the load model as its value is very small. However, this can influence the electrical characteristics for certain loading conditions, which are discussed later.

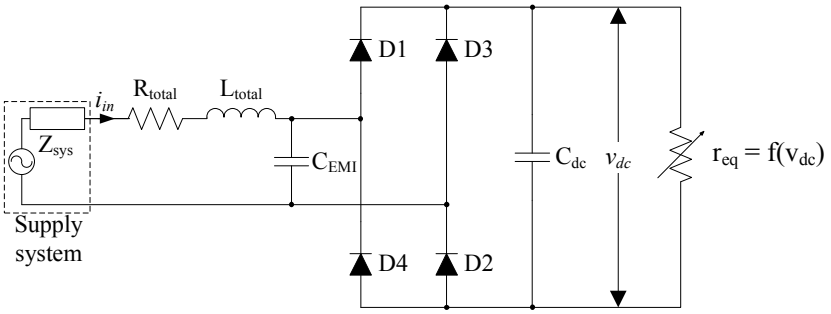

Figure 3.12: General equivalent circuit model of power electronics load without a-PFC.

The value of equivalent resistance is determined by an analytical expression which describes the behaviour of all components downstream of C_{dc}. The equivalent resistance is given as a function of the dc link voltage v_{dc}. In the power electronics load category, the equivalent resistance includes the dc-dc converter and the dc load itself. As the dc-dc converter supplies constant current and constant voltage to the dc load, the power drawn from the dc link is constant and does not change with variations in the ac supply voltage magnitude. Therefore, the equivalent resistance is defined as [18, 48]:

$$r_{eq} = \frac{v_{dc}^2}{P_{dc}} \tag{3.7}$$

Where: v_{dc} is the instantaneous value of dc link voltage and P_{dc} is dc power demand of the device.

If the power required by the device changes during the operation, then the value of P_{dc} in (3.7) should be updated accordingly. For example, the power drawn by computers will change based on the tasks performed by the processor (this is discussed further in Section 3.5.4).

3.4.1 Operation of equivalent circuit

Using the description of the equivalent circuit operation, discussed in Section 3.2.3, it is possible to define two general states of operation, determined by the state of charge of C_{dc}. When the magnitude of v_{rect} is greater than v_{dc}, C_{dc} will charge and the electronic dc load will draw current from the supply through the equivalent circuit components. As C_{dc} discharges through the connected electronic dc load, no current is drawn from the supply. The charging state is represented by an RLC-R circuit supplied by the rectified system voltage. The discharge circuit is represented by an RC discharge circuit. Both circuits are given in Figure 3.13.

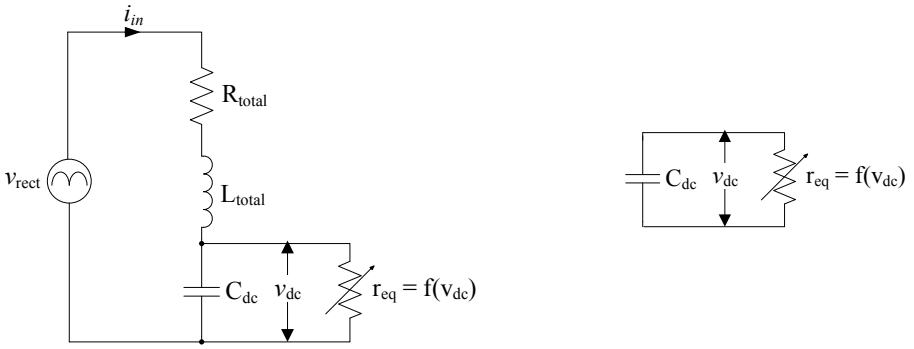

(a) charging state **(b)** discharging state

Figure 3.13: Circuit representation of the charging and discharging states of the equivalent circuit model.

The behaviour of these electrical circuits and corresponding input current waveforms can be represented analytically by considering the equivalent circuit for each state.

Discharging state

Operating conditions: $v_{dc} > v_{rect}$ and $i_{in} = 0$.

The current drawn from the supply is zero. The C_{dc} discharges through the equivalent load resistance following standard RC discharge equations. The resulting analytical expressions are:

$$v_{dc} = v_{start} e^{\frac{-t}{r_{eq} C_{dc}}} \tag{3.8}$$

$$i_{in} = 0 \tag{3.9}$$

where: v_{start} is the capacitor voltage at the start of the discharge period, v_{dc} is dc link voltage at time t, C_{dc} is the value of dc link capacitor, t is the pre-specified simulation time step and r_{eq} is as defined in (3.7).

Charging state

Operating conditions: $v_{dc} \leq v_{rect}$ and $i_{in} \neq 0$.

The power electronics load will draw current from the supply which is shaped by the input impedance and is also a function of the dc link voltage v_{dc}. This charging state can be represented by the following set of differential equations:

$$\begin{bmatrix} \frac{di_{in}}{dt} \\ \frac{dv_{dc}}{dt} \end{bmatrix} = \begin{bmatrix} \frac{R}{L} & \frac{1}{L} \\ \frac{1}{C_{dc}} & \frac{1}{C_{dc}r_{eq}} \end{bmatrix} \begin{bmatrix} i_{in} \\ v_{dc} \end{bmatrix} + \begin{bmatrix} \frac{1}{L} \\ 0 \end{bmatrix} v_{rect} \tag{3.10}$$

where: R is the previously used R_{total} and L is previously used L_{total}, and are used to simplify the presentation of the equations, C_{dc} is the value of dc link capacitor, v_{rect} is the rectified ac input voltage, i_{in} is the instantaneous input current, v_{dc} is the instantaneous value of dc link voltage and r_{eq} is as defined in 3.7.

This circuit can be solved using the trapezoidal integration technique, which is commonly used in circuit simulation software [19, 67, 72]:

$$x(t) = x(t-\Delta t) + \int_{t-\Delta t}^{t} [A(t)\,x(t) + B(t)\,g(t)]\,dt \tag{3.11}$$

Applying (3.11) to the differential equations (3.10) returns two recurrence relations (3.12) and (3.13). These can be programmed into any mathematical software and provide a flexible and transferrable tool for implementing the equivalent circuit model. The full mathematical derivation and simplification is given in Appendix B. The MATLAB implementation of the model is also included in Appendix C as an example.

$$\begin{aligned} i_{in}(n+1) = \frac{1}{\alpha}\big(&4C_{dc}i_{in}(n)LR_{eq} + \Delta t^2(-i_{in}(n)(R+R_{eq}) + v_s(n)) + \\ &2\Delta(i_{in}(n)(L - C_{dc}RR_{eq}) + C_{dc}R_{eq}(-2v_{dc}(n) + v_s(n+1) + v_s(n)))\big) \end{aligned} \tag{3.12}$$

$$\begin{aligned} v_{dc}(n+1) = \frac{1}{\alpha}\big(&4C_{dc}LR_{eq}v_{dc}(n) + 2\Delta t(2i_{in}(n)LR_{eq} - Lv_{dc}(n) + C_{dc}RR_{eq}v_{dc}(n)) + \\ &\Delta t^2(-Rv_{dc}(n) + R_{eq}(-v_{dc}(n) + v_s(n+1) + v_s(n)))\big) \end{aligned} \tag{3.13}$$

and:

$$\alpha = 4C_{dc}LR_{eq} + \Delta t^2(R+R_{eq}) + 2\Delta t(L + C_{dc}RR_{eq}) \tag{3.14}$$

where: Δt is the simulation time step, v_s is instantaneous supply voltage, n and $n+1$ denote two subsequent calculation steps with values of $i_{in}(n+1)$ and $v_{dc}(n+1)$ calculated from the (n) step values. All other parameters are as previously defined.

If required, the effect of the EMI filter can be included in the analytical model using (3.15). As this is connected in parallel to the supply system and the equivalent circuit, the two current waveforms will sum to provide the total input current waveform of the modelled device.

$$i_{EMI} = C_{EMI}\frac{dv_s}{dt} = C_{EMI}\frac{v_s(n+1) - v_s(n)}{\Delta t} \tag{3.15}$$

where: i_{EMI} is the current drawn by the EMI capacitor C_{EMI}. All other parameters are as previously defined.

3.4.2 Analytical model validation

As previously stated, the equivalent circuit model is a widely accepted representation of power electronics loads. In this section, results are presented to validate the developed analytical model against a set of measurements performed on one PE no-PFC device and one PE p-PFC device. The measurements were performed using a fully controllable voltage waveform generator, with THD value less than 0.5% [73]. The current and voltage signals were recorded at a resolution of 2000 samples per cycle.

PE no-PFC subcategory

The equivalent circuit model is adjusted with component values to represent the modelled PE no-PFC load. As shown in Figure 3.14, this power electronics subcategory has a sharp rise in the current waveform, as a result of low input impedance. The analytical model is able to reproduce this current waveform, and corresponding harmonic emissions. The expected range of values of the power electronics load categories are discussed in more detail in the following section.

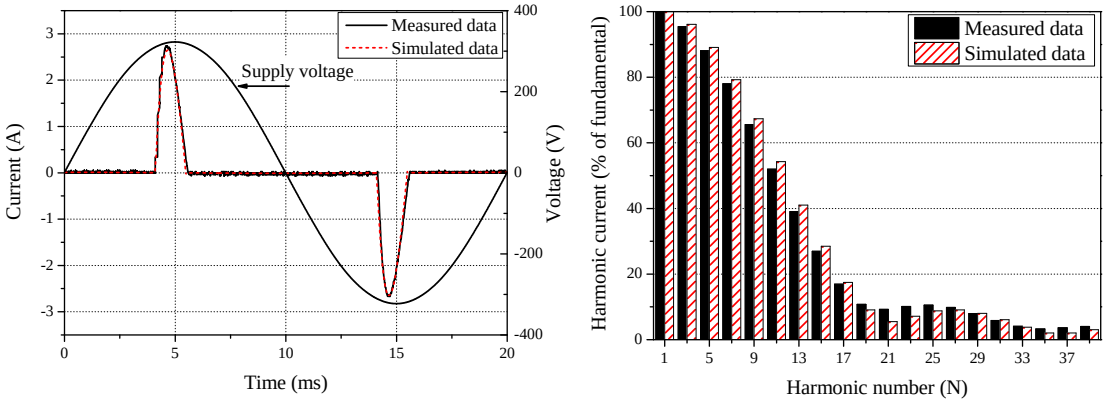

(a) input current waveform (b) associated harmonic content

Figure 3.14: Comparison of input current waveforms and associated harmonic content between the equivalent circuit PE no-PFC subcategory model and the measured data at 1 pu voltage.

Further validation of the analytical model is presented in Figure 3.15, which also shows how the electrical characteristics of the PE no-PFC load will change as a function of the supply voltage. To obtain these results, the magnitude of the supply voltage was increased in 0.05 pu steps from 0.8 pu to 1.2 pu and the models were allowed to run until steady conditions were achieved at each voltage level.

Although the typical operating voltage limits for the UK are ± 10% at MV and HV levels and +10/-6% at the LV level [74], this increased voltage range will allow more confidence in the developed models outwith the normal steady-state operational region of the power system. Furthermore, the increased voltage range allows for a better representation of the load characteristics at the steady-state boundaries.

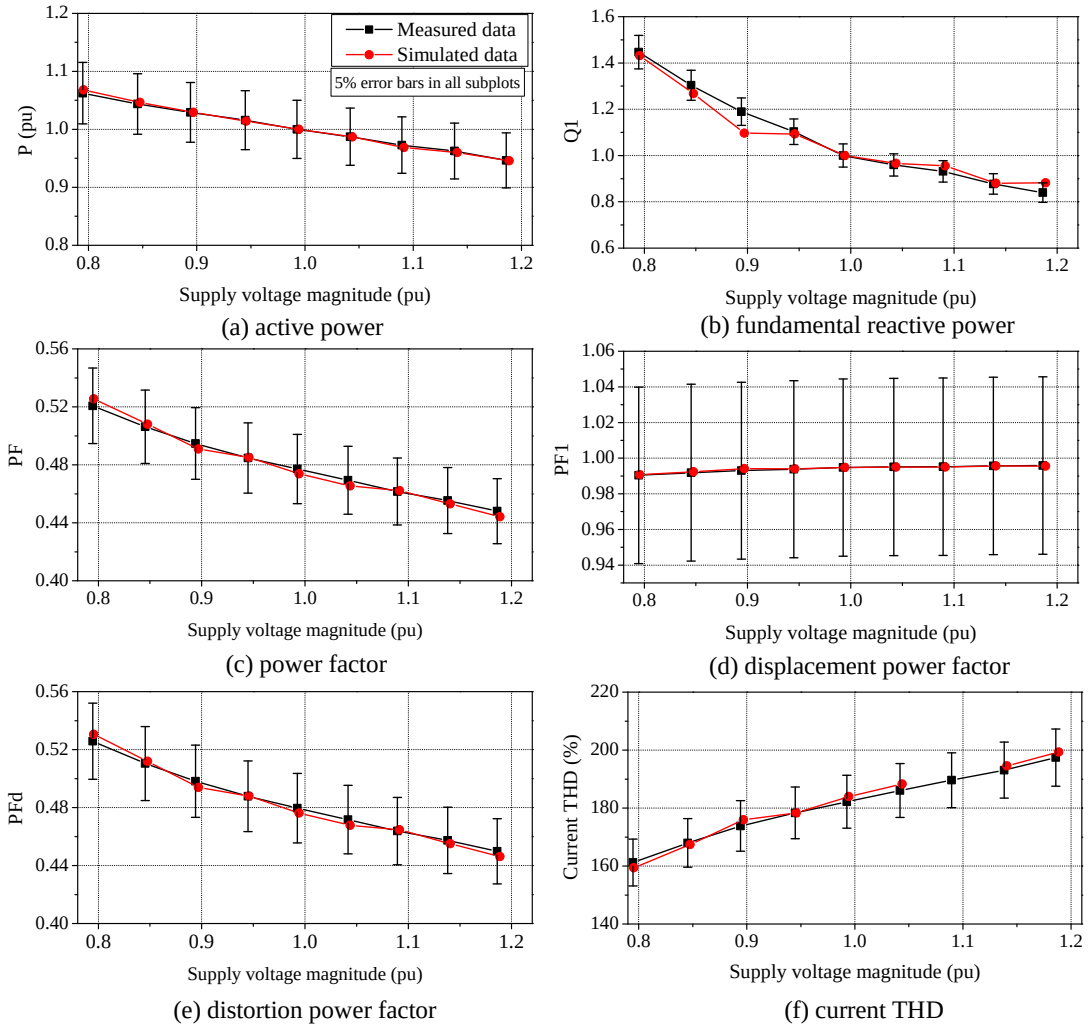

Figure 3.15: Comparison between the electrical characteristics of the equivalent circuit PE no - PFC subcategory model and the measured data.

This series of measurements was performed on an active device, and the active power demand of the equivalent circuit was adjusted to match the power drawn by the device at each voltage step, as this can vary depending on the operation performed by the device at the time of measurement. However, all other component values remain fixed for all simulations, as these cannot change in the actual device. Good matching between the simulated and measured data is observed, with the largest error recorded for the fundamental reactive power. However, it should be noted that the displacement power factor of the device is very close to unity. Therefore, the actual value of reactive power is very close to zero.

PE p-PFC subcategory

The equivalent circuit model is configured with typical values of components (which are discussed in the following section) to represent the measured PE p-PFC device. Again, the functionality of the analytical model is demonstrated by the good matching achieved for the input current between the analytical and equivalent circuit model, as shown in Figure 3.16. This validates the ability of the developed analytical model to represent both PE no-PFC and PE p-PFC subcategories.

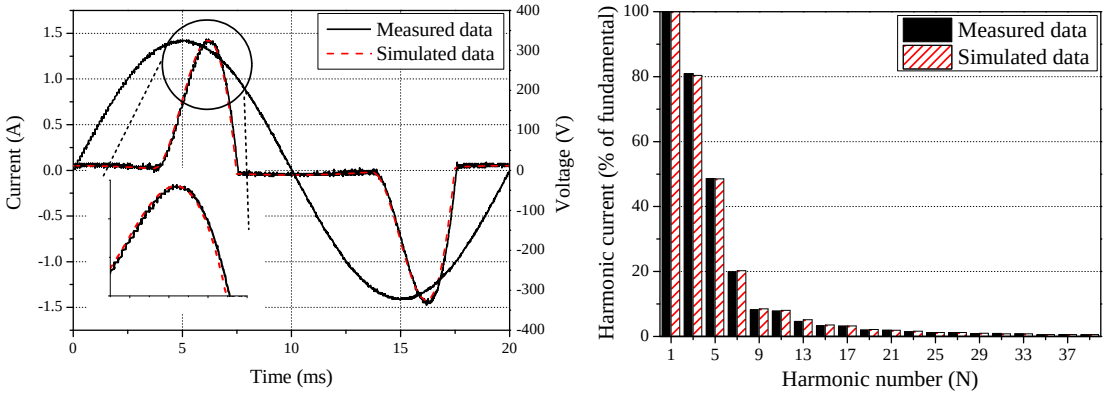

(a) input current waveforms (b) associated harmonic content

Figure 3.16: Comparison of input current waveforms and associated harmonic content between the equivalent circuit PE p-PFC subcategory model and the measured data at 1 pu voltage.

As with the PE no-PFC subcategory, further validation of the model is achieved by comparing against the measured data for the voltage range of 0.8 - 1.2 V_{pu}. The results of this are displayed in Figure 3.17 overleaf, and a similar accuracy is demonstrated by the model. In this case, the measured values are more representative of the expected behaviour of the power electronics load category, i.e. constant active power characteristic. This is a result of performing this series of measurements on a SMPS which had been removed from the electrical appliance. As such, this could be configured with a fixed value of resistance at the dc output to represent a fixed dc load. Therefore, any changes in the input characteristics of the SMPS are a result of operational changes in the device to variation in the supply voltage magnitude, and these are not masked by variations in the dc load (which are shown later in this chapter to have a significant impact on the electrical characteristics of the power electronics load).

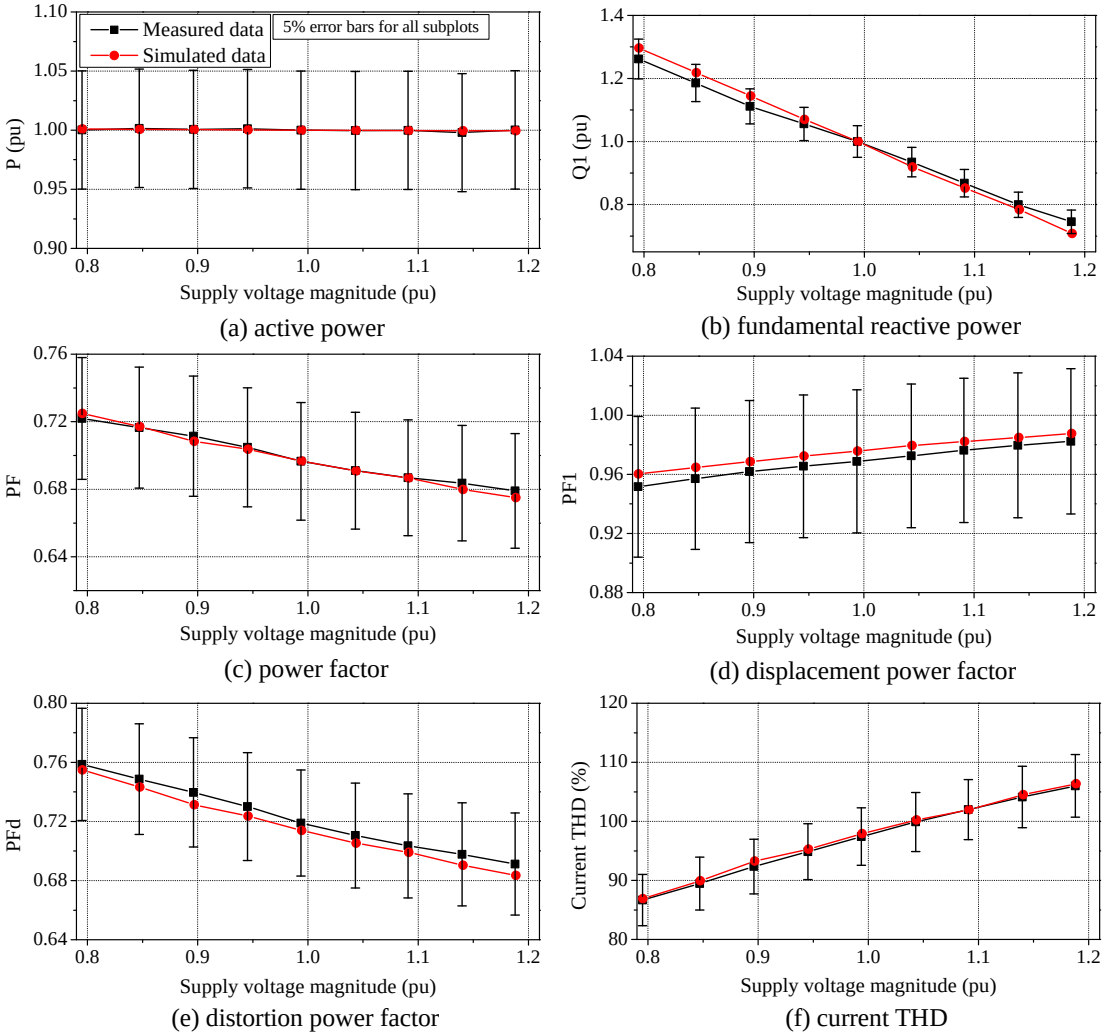

Figure 3.17: Comparison between the electrical characteristics of the equivalent circuit PE p -PFC subcategory model and the measured data.

The full range of characteristics for PE no-PFC (in Figure 3.15) and PE p-PFC subcategories above, clearly illustrate the similarities and differences between the device operations. Overall the trends of all characteristics are similar. As the supply voltage magnitude increases, the displacement power factor and current THD will increase for both subcategories. Conversely, the values of true and distortion power will reduce. Again, this is observed for both PE no-PFC and PE p-PFC subcategories.

The differences lie in the actual power factor values, with the addition of PFC inductor lowering the displacement power factor but raising the value of the distortion and true power factor in PE p-PFC loads. This discussion is continued in greater detail in the following section.

3.5 Generic model of power electronic loads

In order to represent the power electronics load category in power system studies, typical values of the equivalent circuit parameters must be determined. Due to slight variations in the circuit design and inherent manufacturing tolerances of the individual electrical components, it is not reasonable to assume a fixed value for each component. This will introduce variations in the input current of aggregate loads and the complex cancellation of harmonics in these waveforms should be fully included in the development of the aggregate load model.

In this section, a sensitivity analysis is performed using the expected range of parameter values for each component to assess their influence on the electrical characteristics of the load. These values will be used in the next section to develop aggregate load model representations of the power electronics load category. To test each component, a minimum, maximum and nominal value is presented based on measurement, inspection or consideration of the performance requirements of the SMPS. The other parameters are fixed constant to determine the influence of the component under test. These variations are then collated to show the boundaries of all considered electrical characteristics, which are compared against measured data to verify the range of model values.

3.5.1 Input resistance

The input resistance in the model represents the sum of all resistances in the conduction path. Although this will include several electronic components, the input resistance of the power electronics load category is dominated by the NTC thermistor used for inrush current protection, even during steady-state operation. Although resistors will typically have a tolerance of around $\pm 1\%$, in this thesis an increased range of $\pm 10\%$ is assumed for this component to allow for variations introduced by the NTC, such as differences in operating temperature and differences between NTC manufacturers.

From Figure 3.4, the value of this resistance is likely to lie between 1.5 - 2.25 Ω. The average value of NTC resistance is converted to a per-unit value, illustrated in (3.16) and (3.17) for the typical rated power (i.e. P_{rated} = 50 W) of PE no-PFC loads. The corresponding value for the PE p-PFC subcategory is 0.0085 pu (calculated for P_{rated} = 250 W).

$$R_{base} = \frac{V_{rms}^2}{P_{rated}} = \frac{230^2}{50} = 1058\Omega \tag{3.16}$$

$$R_{pu} = \frac{R_{\Omega}}{R_{base}} = \frac{1.8}{1058} = 0.0017\ pu \tag{3.17}$$

where: R_{base} is the base impedance, V_{rms} is the rms value of the supply voltage, P_{rated} is the rated power of the modelled SMPS, R_{Ω} is ohmic value of resistance and R_{pu} is the corresponding per-unit value.

As shown in Figure 3.18, this parameter does not have a significant effect on the input current waveform of PE no-PFC devices. Increasing the resistance will lower the current peak and slow the rate of charging of C_{dc}. A slightly wider current pulse is observed, to maintain the energy balance with the load, and the corresponding harmonic emissions are slightly reduced. However, the changes in the phase angle of the harmonic currents are negligible. The effect of these changes will slightly improve the true power factor, as a result of the lower current harmonics.

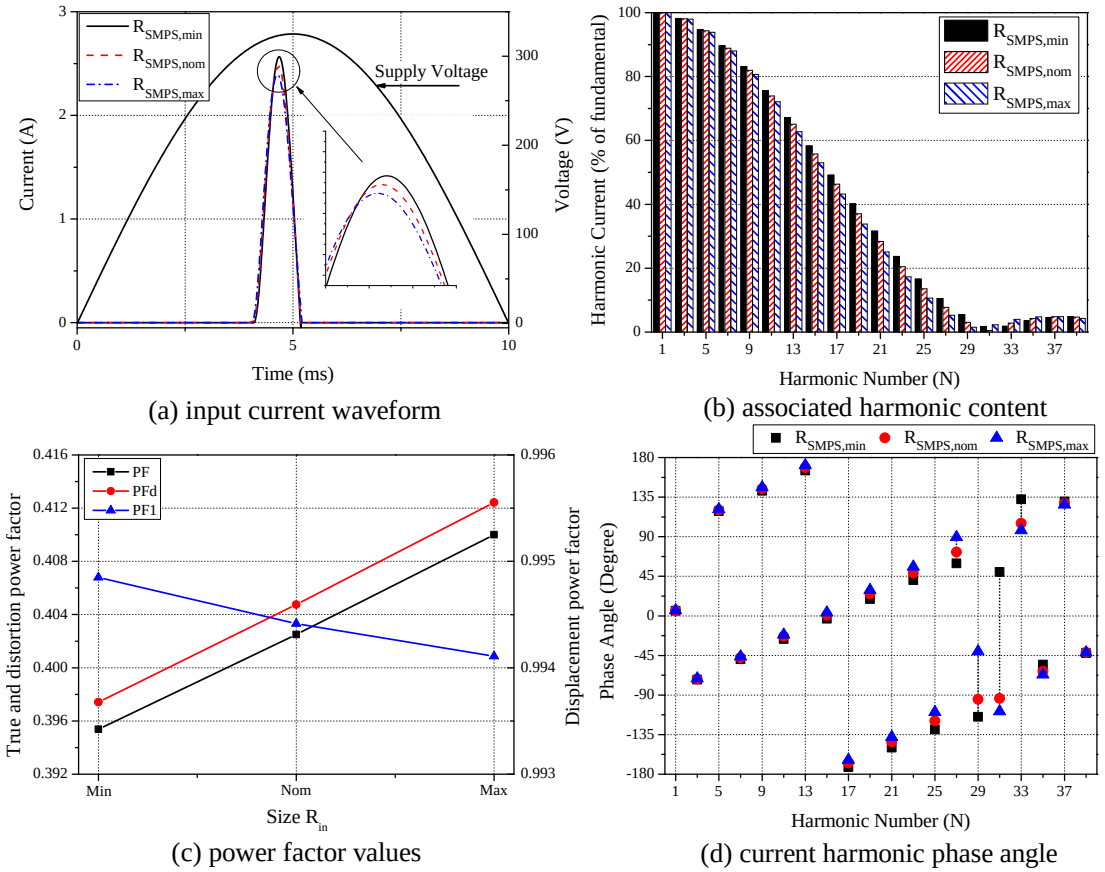

(a) input current waveform

(b) associated harmonic content

(c) power factor values

(d) current harmonic phase angle

Figure 3.18: Influence of input resistance on the input characteristics of the PE no-PFC subcategory.

There is even less variation observed in the PE p-PFC subcategory, with results of this study presented in Figure 3.19. Again, the larger value of resistance will reduce the peak current value, but this effect is insignificant. The reduced sensitivity is a result of the large inductance which dominates the input impedance in the conduction of PE p-PFC devices.

It is, therefore, possible to surmise that the contribution of this equivalent circuit model parameter on the steady-state electrical characteristics is minimal. Therefore, there is no need to improve upon the assumption with a more thorough investigation of the parameters (such as those presented for the other parameters in the subsequent sections).

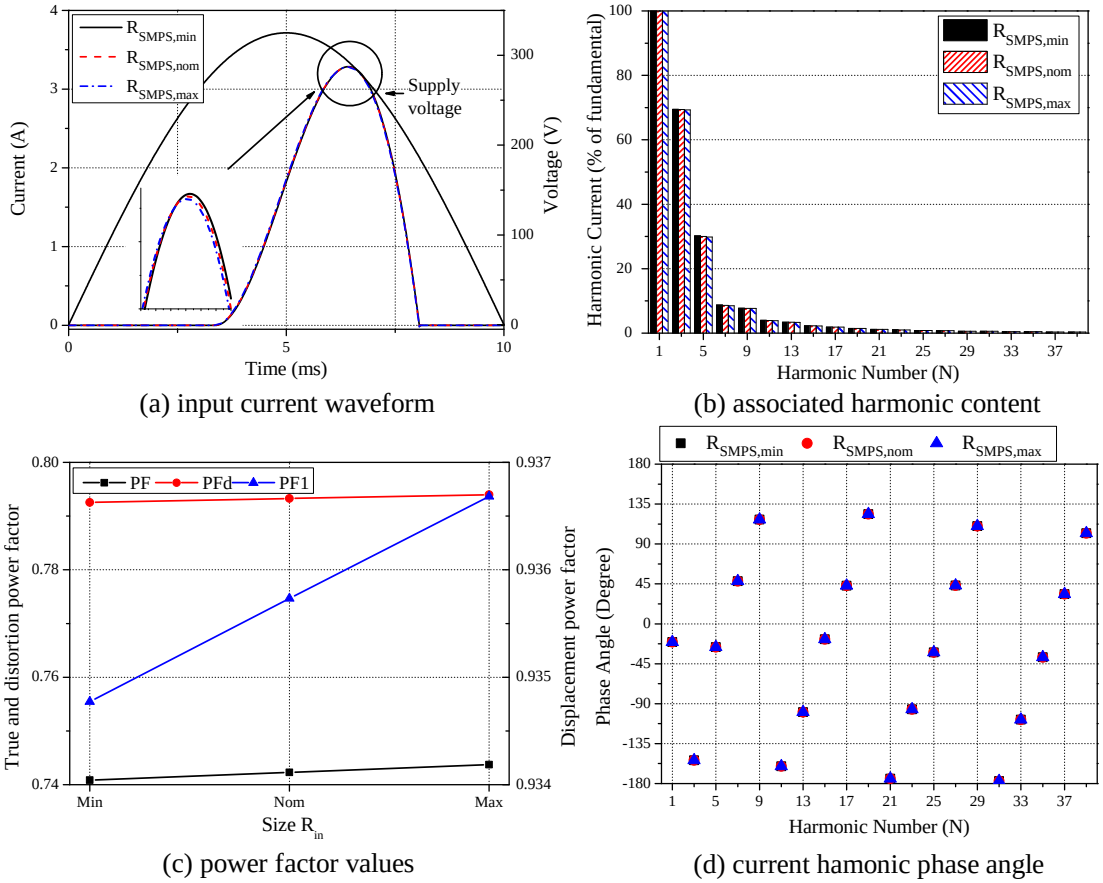

(a) input current waveform

(b) associated harmonic content

(c) power factor values

(d) current hamonic phase angle

Figure 3.19: Influence of input resistance on the input characteristics of the PE p-PFC subcategory.

3.5.2 DC link capacitance

The dc link capacitor C_{dc} in power electronics loads must be large enough to allow ride-through of a voltage interruption of up to 10ms [75]. However, if the voltage interruption starts just before C_{dc} is about to charge, then a 10ms interruption is actually a 20ms interruption. A common industry practice is, therefore, to select the value of C_{dc} to satisfy a hold-up time of 23ms, which represents the 20ms hold-up time plus an additional 'safety margin' [69].

In the previous research [18], the value of C_{dc} to satisfy this hold-up time requirement was established using a detailed full circuit model. These values are shown in Figure 3.20, with the shaded area representing the sizes of capacitor which will satisfy the 23ms hold up time as a function of rated power. Also included on this plot are several values of C_{dc} which have been obtained from measurement of actual devices and values taken from manufacturers data-sheets. The collected values cover many of the possible devices which are included in the power electronics load, covering the consumer electronics load type and the ICT load type. Despite the range of applications, there is a clear correlation between the rated power of the SMPS and the size of C_{dc}. This allows for the definition of a generic per-unit value for C_{dc}.

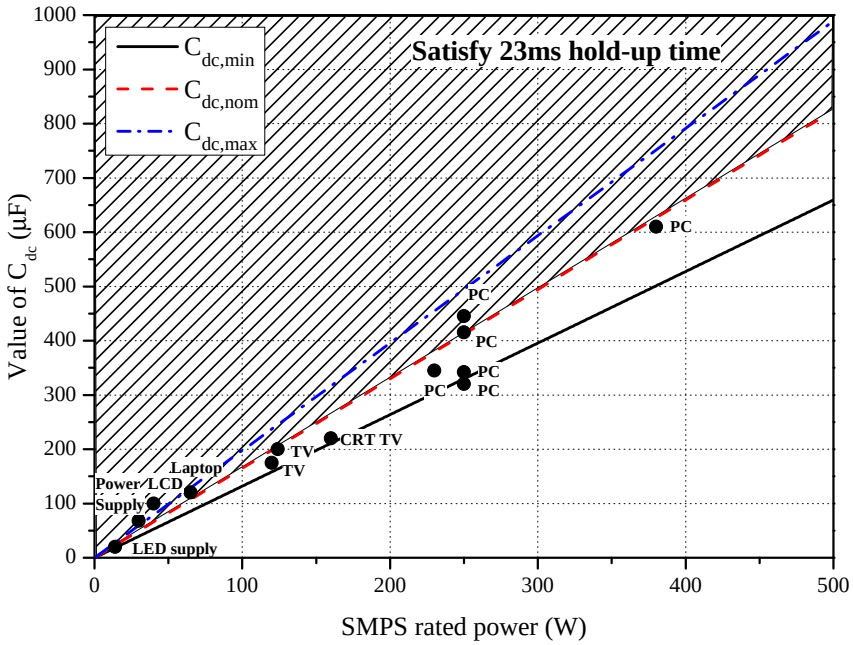

Figure 3.20: Range of typical C_{dc} values in power electronics load category, with $C_{dc,nom}$ values taken from [18].

Selecting one value from this curve (P_{rated} = 250 W and C_{dc} = 415 μF) allows for calculation of the corresponding per-unit reactance value of C_{dc}:

$$X_{C_{dc_{pu}}} = \frac{\frac{1}{\omega C_{dc}}}{\frac{V_{rms}^2}{P_{rated}}} = \frac{\frac{1}{415X10^{-6}\omega}}{\frac{230^2}{250}} \approx 0.036pu \tag{3.18}$$

where: V_{rms} is the rms value of supply voltage, P_{rated} is the rated power of the modelled SMPS and ω is the angular frequency of the supply voltage.

The actual values of capacitors in power electronics circuits may vary based on their manufacturing tolerance, which is typically ±20% for the electrolytic-type capacitors used in LV single-phase devices [76]. This tolerance is used to provide upper and lower boundaries for the C_{dc} range. These values are given in Table 3.5 and plotted on Figure 3.20. As all collected values of C_{dc} lie within these boundaries, this assumption seems reasonable.

Table 3.5: Assumed range of dc link capacitance tolerance values.

Model value	Capacitor size		σ	
	(μF)	(pu)	(μF)	(pu)
Min	334	0.045	±27.83	±0.54
Nom	417	0.036		
Max	501	0.030		

As the actual values of C_{dc} generally lie close to the nominal value, a normal distribution is taken for this parameter. For simulation purposes, the standard deviation σ is calculated by dividing the range of values, i.e. $C_{max} - C_{min}$, by six, to retain the characteristic six sigma shape of the normal distribution. This value is also included in Table 3.5.

Figures 3.21 and 3.22 show that for both subcategories of power electronics devices, increasing the size of C_{dc} will shift the current waveform slightly to right, as the larger capacitor is able to better regulate the dc link voltage. The harmonic content will marginally reduce as C_{dc} increases and the input current pulses widen. This effect can be attributed to the voltage drop across the input inductance, which will vary in proportion to the rate of change of current; effectively slowing the rate of charge for larger capacitor sizes. This will also be influenced by the value of the equivalent resistance as, in Chapter 4, the opposite effect is observed for CFLs.

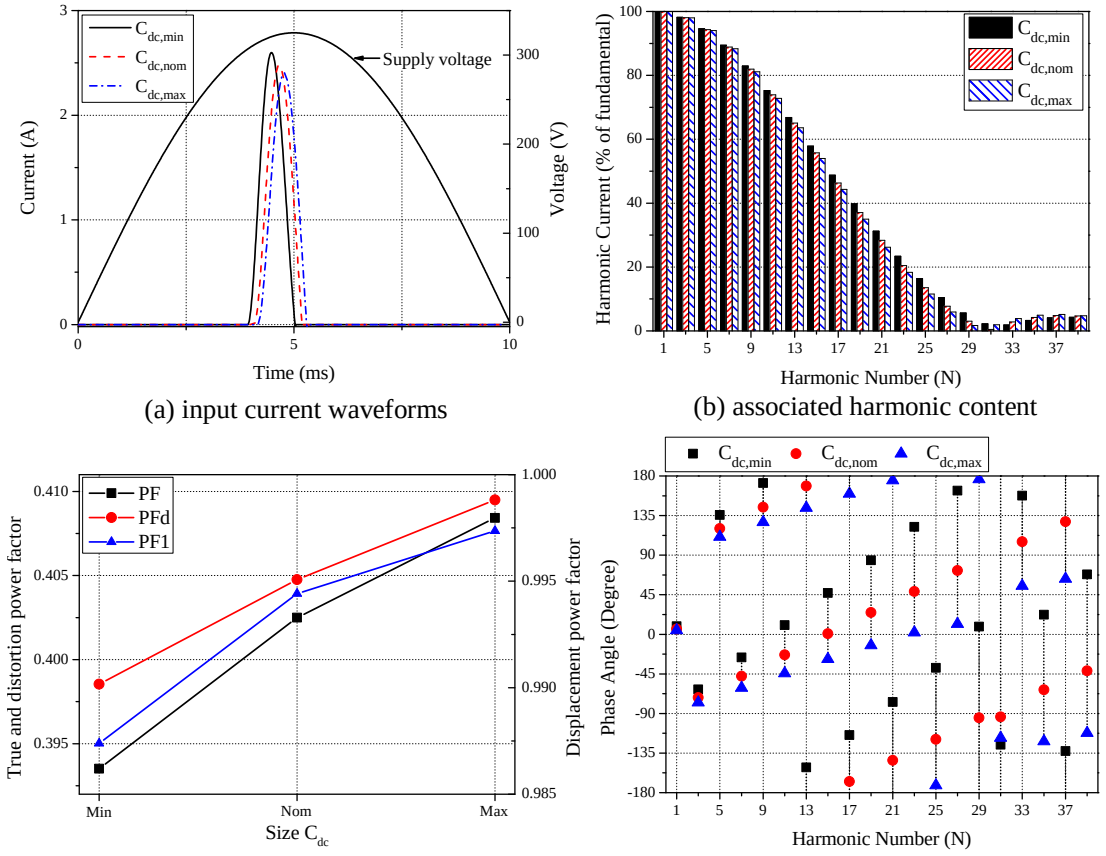

(a) input current waveforms

(b) associated harmonic content

(c) power factor values

(d) current harmonic phase angle

Figure 3.21: Influence of C_{dc} on the input characteristics of the PE no-PFC subcategory.

Although the effect on phase angle dispersion for PE p-PFC is very small, a visible difference is observed for PE no-PFC. This will result in increased levels of harmonic cancellation within aggregates of PE no-PFC devices. This dispersion is more pronounced for a change in C_{dc} than input resistance and will result in more cancellation within the aggregate load for variations of this parameter value.

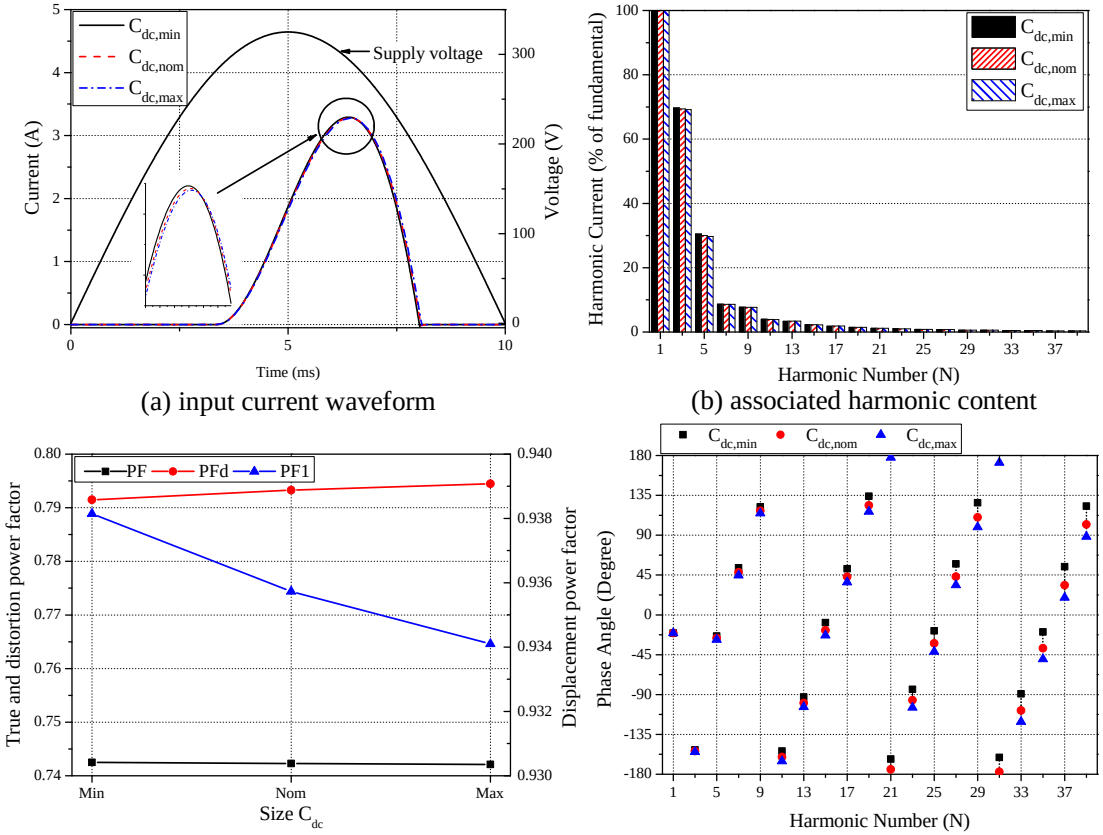

(a) input current waveform

(b) associated harmonic content

(c) power factor values

(d) current harmonic phase angle

Figure 3.22: Influence of C_{dc} on the input characteristics of the PE p-PFC subcategory.

3.5.3 Input inductance

As mentioned in Section 3.2.4, the value of input inductance is the biggest difference between the PE no-PFC and PE p-PFC subcategories. In the higher power PE p-PFC, the inductance of a typical device is dominated by the value of the PFC inductor L_{PFC} selected to satisfy harmonic legislation in [20]. However, for PE no-PFC the input impedance is considerably lower, as there is no PFC inductor in the conduction path. For this subcategory, the value of supply cable impedance (with typical values between R = 0.05-0.15 Ω and L = 0.01 - 0.03 mH [77]) will be the dominant inductance in the system. As the values of supply cable resistance are small in comparison with the input resistance, they can be neglected. For PE p-PFC, the impedance of the cables connecting the loads to the supply system can be ignored altogether due to the higher internal impedance of the SMPS circuit.

Accordingly, variation of this model parameter is only presented for PE p-PFC load. A minimum value of inductor size to satisfy the harmonic legislation in [20], was developed in previous research by configuring the model with typical circuit component values and adjusting the inductor size until the harmonic limits were just met. This was repeated for a number of rated powers. This minimum value is plotted in Figure 3.23, where the shaded area indicates

the values L_{PFC} which will satisfy the harmonic legislation. The influence of changing the size of C_{dc} is shown to have a negligible effect on this minimum value of inductance.

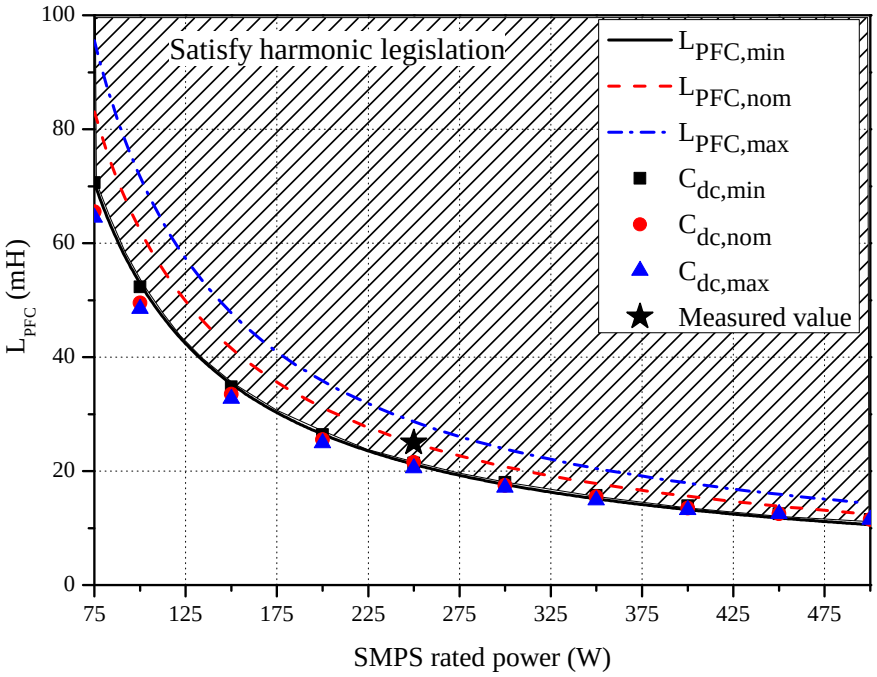

Figure 3.23: Assumed range of values of p-PFC inductors to satisfy harmonic limits in [20], with values for $L_{PFC,min}$ and $C_{dc,nom}$ taken from [18].

Figure 3.23 shows that, like the C_{dc}, the value of p-PFC inductors is a function of the rated power. This allows for a per-unit derivation of p-PFC inductance. The previous research estimated the value of L_{PFC} which would just satisfy the harmonic legislation. Therefore, this value is treated as the minimum value.

To create a range of values, typical inductor tolerances, between 10 % [78] and 15% [79], were applied. The measurement of the PFC inductor of an actual SMPS suggests that the 15% tolerance should be selected. The resulting per-unit reactance values are given in Table 3.6, which are calculated using equation (3.19) for one selected point (P_{rated} =250 W and L_{PFC} = 24.92 mH). Again, a normal distribution is assumed, with standard deviation calculated to retain the six sigma normal distribution.

$$X_{L_{PFC,pu}} = \frac{\omega L_{PFC}}{\frac{V_{rms}^2}{P_{rated}}} = \frac{\omega 24.92X10^{-3}}{\frac{230^2}{250}} \approx 0.0371 \tag{3.19}$$

where: V_{rms} is the rms value of supply voltage, P_{rated} is the rated power of the modelled SMPS and ω is the angular frequency of the supply voltage.

Table 3.6: Assumed range of PE p-PFC subcategory inductance tolerance values.

Model value	Inductor size		σ	
	(mH)	(pu)	(mH)	(pu)
Min	21.3	0.0312		
Nom	25	0.0371	±1.25	±0.00186
Max	28.8	0.0426		

The results of varying the inductor size in PE p-PFC devices are presented in Figure 3.24. These clearly show that the size of the PFC inductor has the most pronounced effect of all circuit components for this subcategory. Increasing the size of the PFC inductor will shift the input current waveform to further lag the input voltage, causing the load to become more inductive. This is confirmed by the values of the displacement power factor, which reduce as the inductor value increases. However, as shown previously, increasing the size of the inductor will reduce the harmonic content of the load and improve the true power factor. This parameter will also introduce significant phase angle dispersion, with the phase angle range increasing with harmonic number. Therefore, it can be expected that variations in this component value will introduce harmonic cancellation within the aggregate load.

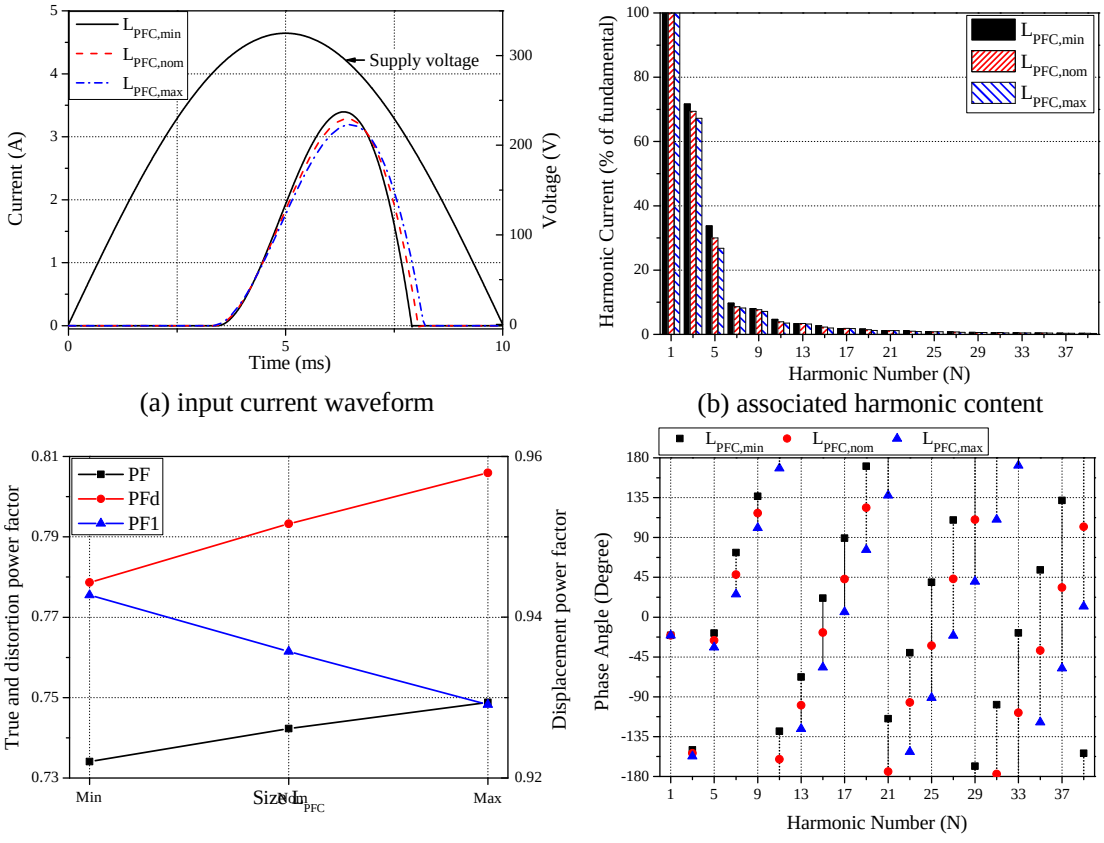

(a) input current waveform

(b) associated harmonic content

(c) power factor values

(d) current harmonic phase angle

Figure 3.24: Influence of L_{PFC} on the input characteristics of the PE p-PFC subcategory.

3.5.4 Power demand

The device rated power is the maximum power that the device can safely supply during normal operation. For the majority of applications, however, it is highly unlikely that the device will continuously provide this power. During normal operation, the power demand of the load will change based on the actual loading conditions at the dc output(s), which will be determined by the specific operation(s) being performed by the device. As these operations will change on a very short time scale, it is not practical to model such small variations for a power system load model. However, previous research has shown that the loading conditions of an adjustable speed drive (ASD) controlled induction motor will have significant influence on both the harmonic magnitude and phase angle [48]. Therefore, it is important to consider how loading conditions will influence the input current, and the associated electrical characteristics, of the power electronics load category.

To determine the range of loading conditions, several PCs and laptops of different ages and rated powers were measured while performing typical operations. The results of the power drawn, as a percentage of the device rated power, are shown in Figure 3.25. Although it was not always possible to maintain the highly loaded condition for a stable time to obtain measured data, it is expected that the devices will be heavily loaded during certain operations, e.g. playing high-resolution video, even if only for a short time.

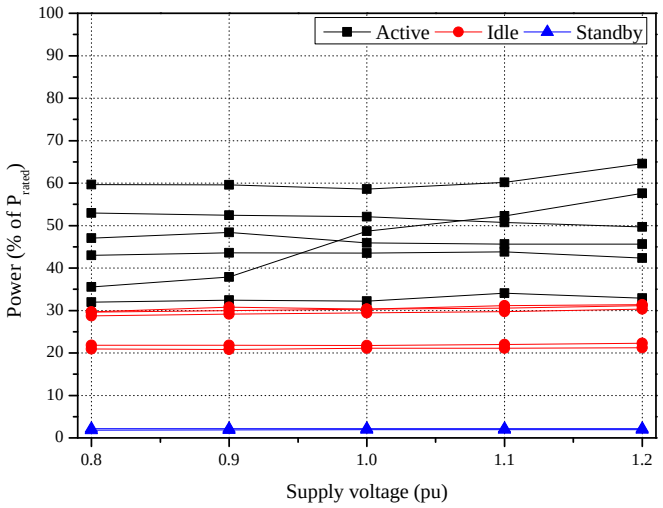

Figure 3.25: Measured variations in the power electronics dc load power demand for different loading conditions.

Although not shown in Figure 3.25, from available measurements, it was found that laptop chargers exhibit constant active power characteristics. The laptop charger will perform two functions, as it will have to charge the laptop battery while also supplying the electronic dc load. It is shown in Chapter 5, that EV battery chargers will have predominantly constant current active power characteristics, which suggests that the operation of laptop chargers is dominated by the circuits supplying the electronic dc load.

The measured results indicate that, during normal operations, the power electronics device is usually loaded to around 50% of the P_{rated} but will also vary within the entire possible range. Therefore, a normal distribution is taken for the dc load parameter, with a mean value of 50 %, as it is expected to vary close to 50% when the device is in use.

For both subcategories, the peak magnitude of the current pulses increase, and they will also become wider, as the power demand of the supplied load increases. This is intuitive, as more energy is drawn from the supply by the load. This effect is more pronounced for PE p-PFC loads. As shown in previous analysis, the wider current pulses will lower the harmonic content of the current waveform. Therefore, the variation of rated power will have a greater individual effect on harmonic content than any other single parameter of the equivalent circuit.

For PE no-PFC devices, increasing the dc power demand will shift the input current waveform to the left. This will cause the fundamental component of the current to be more out of phase with the fundamental component of the voltage, slightly lowering the displacement power factor and the device becomes more capacitive. However, the improvement in value of distortion power factor is more dramatic and acts to improve the true power factor.

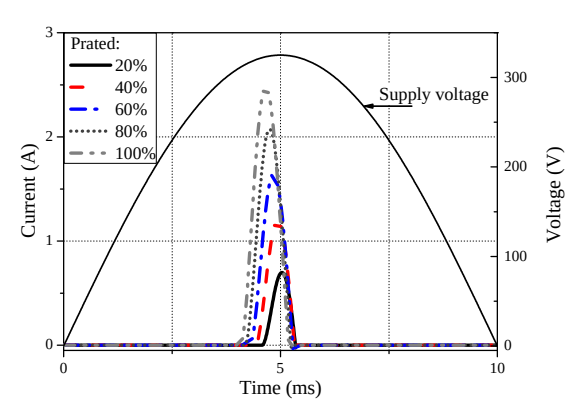

(a) input current waveform

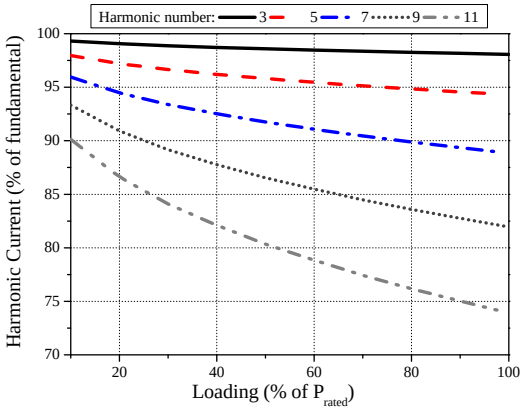

(b) associated harmonic content

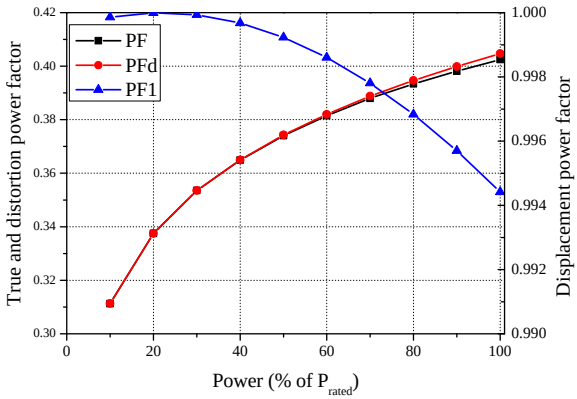

(c) power factor values

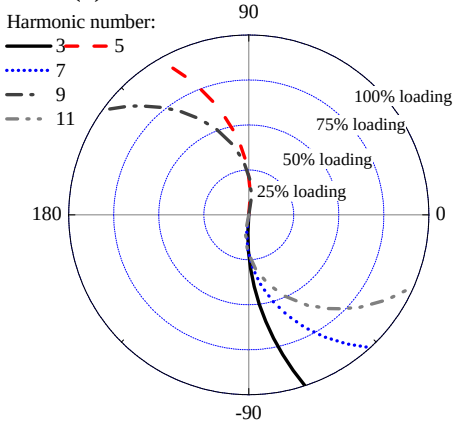

(d) current harmonic phase angle

Figure 3.26: Influence of P_{dc} on the input characteristics of the PE no-PFC subcategory.

Conversely, increasing the power demand of PE p-PFC devices will shift the input current waveform to the right, becoming more inductive. The shift in fundamental component of the current, and the corresponding reduction of displacement power factor, are more significant for this subcategory. This effect is observed at other harmonic frequencies, with increased ranges of harmonic phase angle dispersion for the PE p-PFC subcategory.

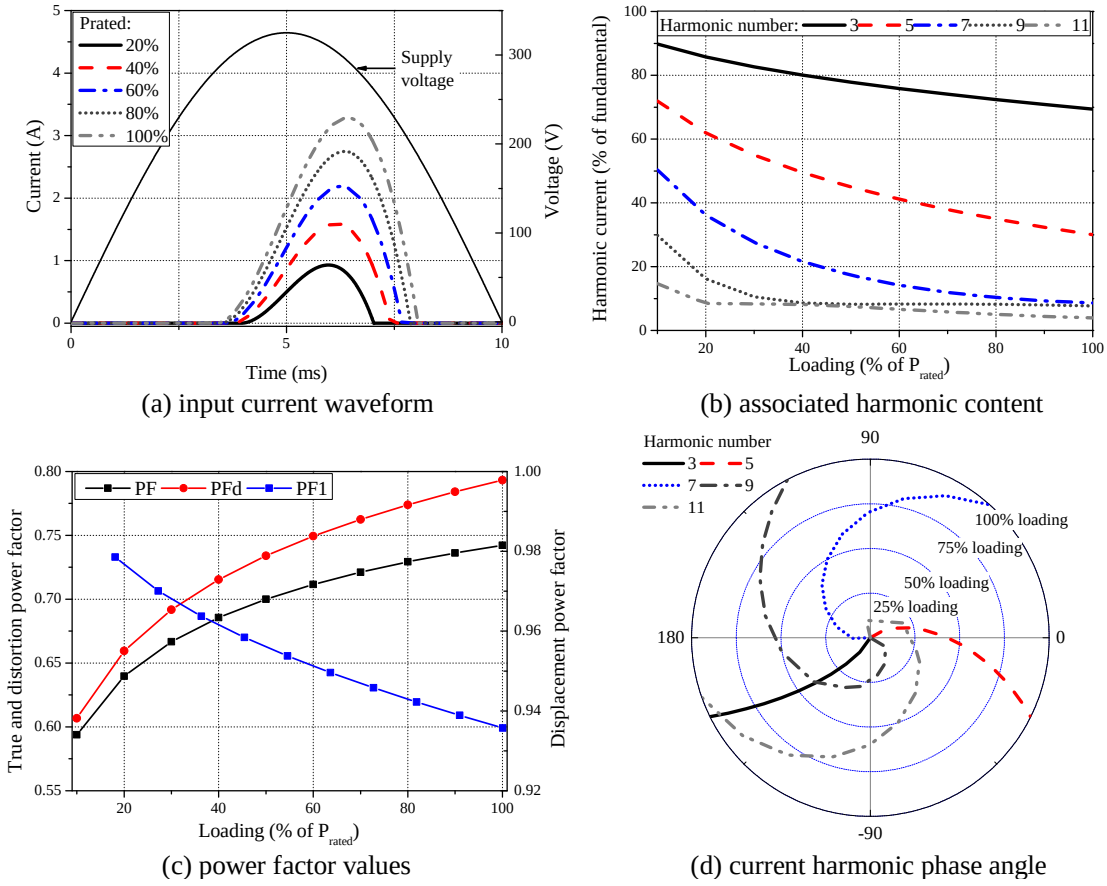

(a) input current waveform

(b) associated harmonic content

(c) power factor values

(d) current harmonic phase angle

Figure 3.27: Influence of P_{dc} on the input characteristics of the PE p-PFC subcategory.

3.5.5 Sensitivity of power electronics load models to parameter variation

The previous analysis has shown the expected sensitivities of the power electronics load category to variations in the circuit parameters. The input resistance will have the least influence on the input current harmonics, in terms of both magnitude and phase angle, for both identified subcategories. Changing the size of dc link capacitor will have only a small effect on the magnitude of the input current harmonics, but will result in some dispersion of the harmonic phase angles. This is particularly evident in the PE no-PFC subcategory, as the dc link capacitor will dominate input impedance, due to the lack of PFC inductor. In PE p-PFC devices, significant phase angle dispersion is introduced by varying the size of PFC inductor.

However, variation in the dc load power has been shown to have the biggest influence on the input current harmonics, as it will significantly change the input current waveform and, therefore, both the harmonic magnitude and phase angle. In reality, it is the combination of these effects that will influence the characteristics of the aggregate model.

This is calculated by setting-up the developed analytical model with the maximum, mean and minimum values for each circuit parameters and simulating all possible combinations of values. The maximum and minimum value of each electrical characteristic at every voltage step is extracted to define the upper and lower boundaries. The simulated boundary conditions are compared with a number of measurements, which are displayed as hollow circles, in Figures 3.28 and 3.29 for PE no-PFC and PE p-PFC subcategories, respectively. All measured data points lie within upper and lower limits, with only small errors visible at the maximum and minimum voltage setting, which verifies the defined parameter ranges.

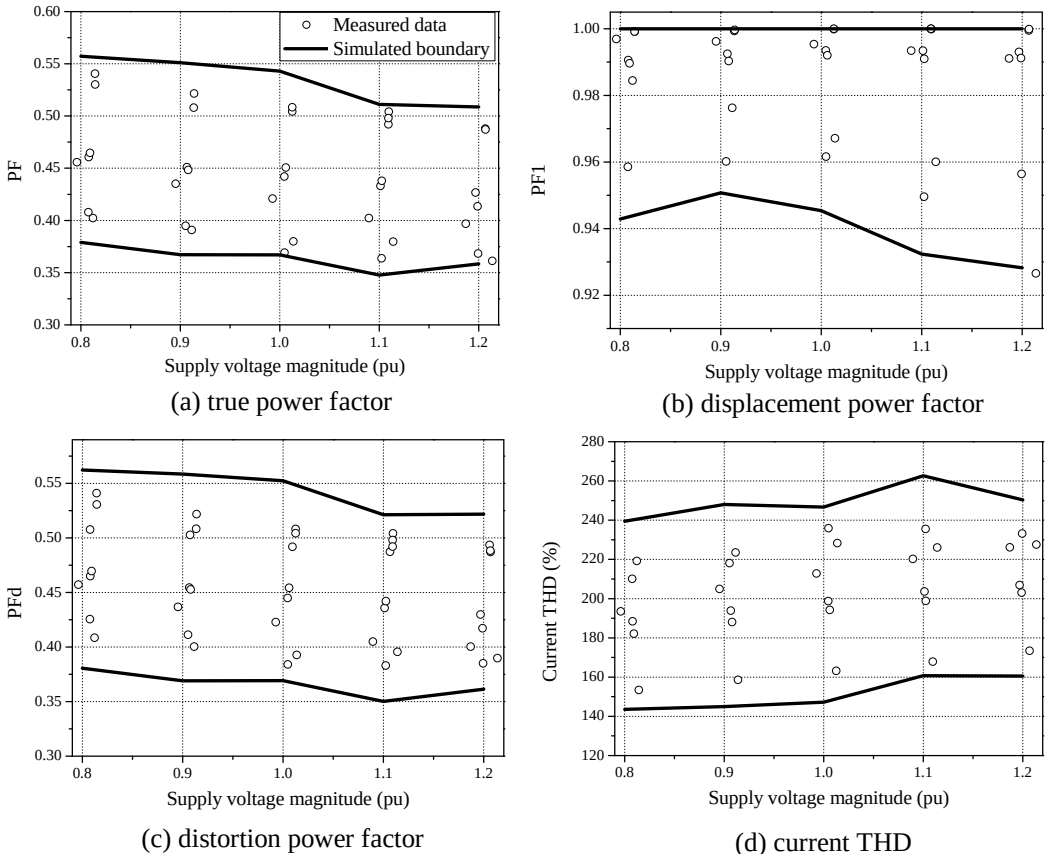

(a) true power factor

(b) displacement power factor

(c) distortion power factor

(d) current THD

Figure 3.28: Comparison between simulated operating boundaries and measured data for the PE no-PFC subcategory electrical characteristics.

Measured values for active and reactive power are not included as they were obtained from 'active', i.e. in-use, devices. This gives a more accurate representation of the range of device characteristics but, as it is not possible to set the device to perform the exact same operations when recording at each voltage level, the active and reactive powers cannot be normalised.

The measured devices include: TVs, laptops, PCs, monitors, audio/hi-fi equipment, DVD players, which have been measured in various modes of operation (i.e. active, idle and standby) where possible. Although the specific age of device is unknown, the sample size can be considered to be fairly representative of the devices which are used at the time of this research.

An arbitrary value of EMI filter capacitance C_{EMI} was included as this was visible in some of the measurements. Although the influence of this component is small during typical operations, it can have a more pronounced effect on the electrical characteristics for devices in idle or standby modes, especially if the voltage magnitude is higher than nominal. Previous analysis has shown that the current pulse magnitude will reduce when the power drawn by the device reduces. In this mode of operation, the shift introduced by the parallel connected C_{EMI} may be substantial. This effect is amplified if the supply voltage magnitude is higher than nominal, as the current drawn by the capacitor is proportional to the supply voltage magnitude.

The influence of this component is particularly evident in the data for PE p-PFC loads and is the cause of the high values of displacement power factor in Figure 3.29. Although the size of C_{EMI} has not been considered in extensive detail (as its influence is not visible in all devices), a typical value for PE no-PFC and PE p-PFC devices has been derived from the available measurements and is included in the final presentation of the power electronics model in Section 3.7.

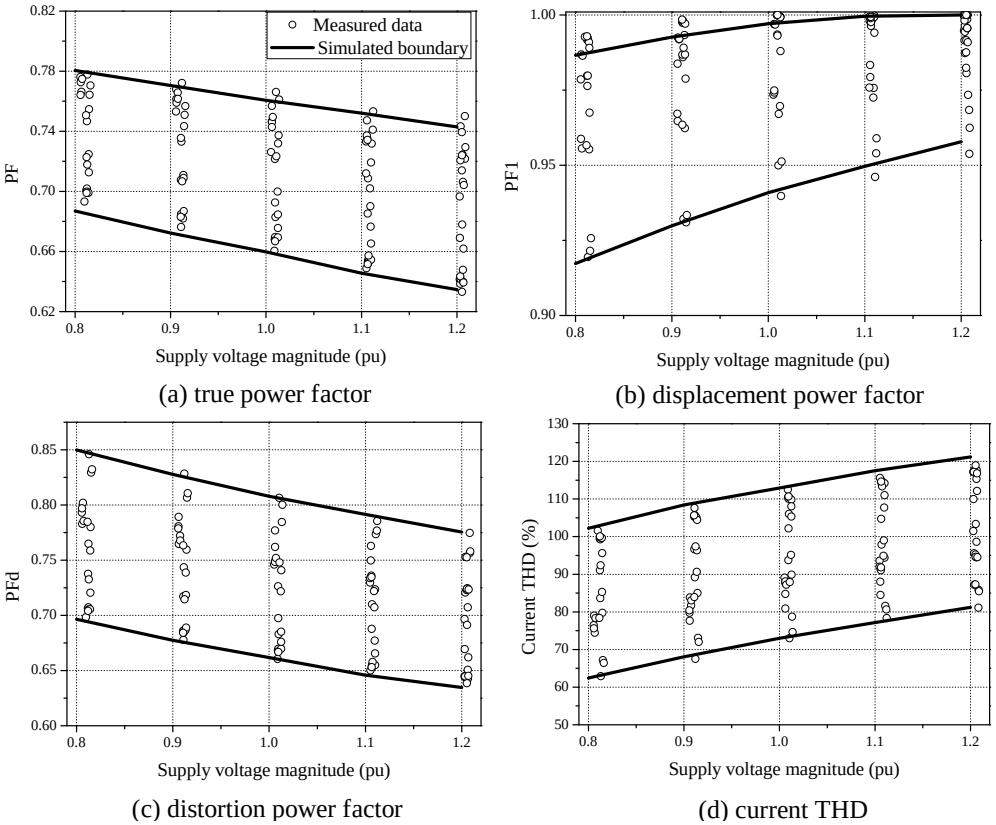

(a) true power factor

(b) displacement power factor

(c) distortion power factor

(d) current THD

Figure 3.29: Comparison between simulated operating boundaries and measured data for the PE p-PFC subcategory electrical characteristics.

3.6 Development of aggregate models of the power electronics load category

An aggregate power electronics load will contain a large number of devices operating with different circuit component values and loading conditions. This will impact on the aggregate load model, as the current waveforms of the individual loads within the aggregate will be slightly offset from each other, with differing harmonic currents. Previous research has shown that these harmonics will cancel, i.e. reduce, within the aggregate load and also distort the supply system voltage [48]. Therefore, both of these effects should be considered when developing the aggregate model representation.

In this thesis, these effects are included by taking into account the ranges of equivalent circuit component values and loading conditions introduced in the previous section. A large number of power electronics loads is simulated by allowing these model parameters to vary simultaneously within these defined ranges using the Monte Carlo simulation technique. The PE p-PFC and PE no-PFC subcategories are aggregated separately before investigating a mixed aggregate of all power electronics subcategories. The aggregate models are presented in two forms: as harmonic injections and as standard exponential and polynomial/ZIP interpretations.

In addition to these standard power system load model representations, the ability of the previously defined generic equivalent circuit models to reproduce the electrical characteristics of the aggregate load is shown. This is an important result for this research as it allows for the development of aggregate load models, which retain the relevant electrical characteristics, from only a few individual models.

3.6.1 System impedance

An accurate aggregate representation of non-linear loads should include the effect of harmonic attenuation, which is the term often used to describe the complex interactions between current harmonics and the supply system impedance Z_{sys} [48, 52]. When harmonic currents are injected from the load side, they will interact with the supply system impedance and distort the supply voltage at the point of common coupling. This, in turn, will normally reduce the harmonic current injections of the load.

The value of system impedance will vary throughout the UK network, but some guidance of expected values for LV residential customers is available in [80]. These values are used in this thesis and are presented in Table 3.7, along with an assumed minimum value taken from [18]. This minimum value is calculated as half of the nominal system impedance, therefore maintaining the same ratio between $Z_{sys,min}$:$Z_{sys,nom}$ and $Z_{sys,nom}$:$Z_{sys,max}$. Finally, the 'stiff grid' condition represents the infinite grid, with system impedance equal to zero.

Table 3.7: System impedance values [18, 80].

Value	System impedance (Ω)	R (Ω)	L (mH)
Min	0.12 + j0.11	0.12	0.35
Nom	0.25 + j0.23	0.25	0.73
Max	0.46 + j0.45	0.46	1.43
Stiff	0 + j0	0	0

3.6.2 Harmonic cancellation within the power electronics load category

Harmonic cancellation occurs due to phase angle dispersion between the same order harmonics produced by different harmonic sources, in this case the individual power electronics loads. The most comprehensive research in this area, consisting of a series of papers [48, 52, 77], was funded by EPRI and performed in the US. This research was performed prior to the introduction of harmonic legislation in the EU, i.e. pre-2001, and, as such, the published results may not be representative of the expected harmonic cancellation between the identified subcategories of modern power electronics loads and should be updated.

In this thesis, the harmonic diversity factor DF_h (refer to Section 2.3.3 for further details) is used to quantify the effect of harmonic cancellation. To calculate the DF_h, the power electronics load models were connected to a common system impedance, as shown in Figure 3.30. The number of loads was incrementally increased, and the DF_h recalculated for each new load configuration, until an asymptotic value was reached.

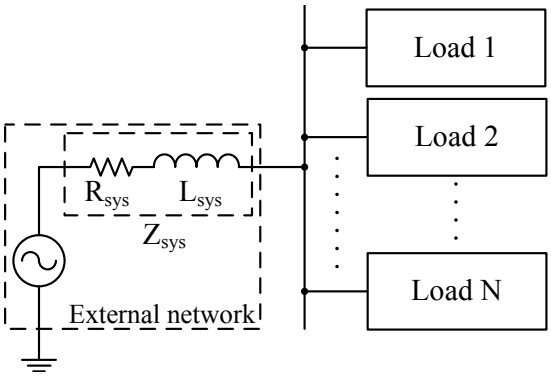

Figure 3.30: Single line equivalent of aggregate load connected to the low-voltage network.

The values of Z_{sys} in Table 3.7 will include both the impedance of the LV network and the single-phase service cable, which connects individual households to the LV network. The impedance of the service cable is high, so it is assumed to dominate the system impedance seen by individual household loads. Therefore, the system impedance values are shared by the different loads connected to the supply system, and the value is proportionally reduced to allow for a realistic representation of this system effect. A total of seven power electronics devices

per household was assumed, based on available device ownership statistics, e.g. [58], so the value of system impedance is proportionally reduced for every seven appliances.

Harmonic cancellation in PE no-PFC aggregate loads

The analysis presented in Section 3.5 has shown that the expected range of phase angle dispersion for this subcategory is quite small. Accordingly, the level of harmonic cancellation is expected to be quite low. This is confirmed by the simulation results presented in Figure 3.31, which compares the harmonic current magnitude of the aggregate load with the minimum, maximum and mean value recorded for the harmonic currents of the individual devices within the aggregate load for stiff grid conditions, i.e. ideal sinusoidal supply voltage. This also includes a comparison with the generic model value, which lies close to the mean value of individual PE no-PFC devices. This is expected as the generic model is defined as the mean value of all component value ranges (a larger simulation size would reduce the difference between these values). A more detailed comparison of the electrical characteristics of the generic model with the aggregate load is presented in Section 3.6.3.

The results indicate an increase in harmonic cancellation with increasing harmonic number, which is confirmed by the calculated diversity factor in Figure 3.32. Full results, which are included in Appendix D, confirm this trend until 1.5 kHz (I_h = 30), where the DF_h will vary between the range 0.8 - 0.9 when all harmonics are considered.

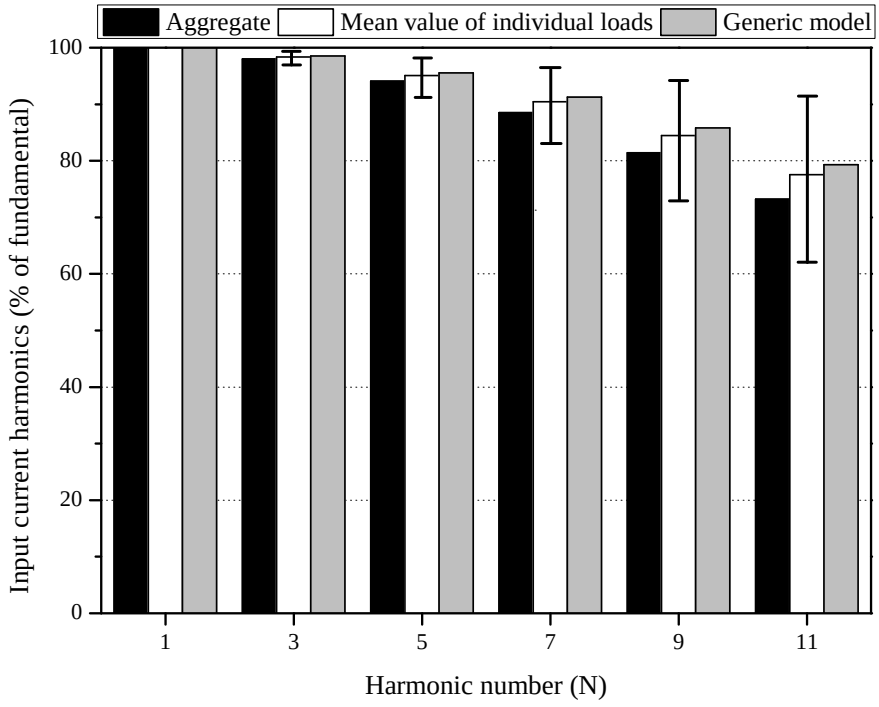

Figure 3.31: Comparison between the input current harmonics of aggregate load and individual loads for the PE no-PFC subcategory for stiff grid conditions.

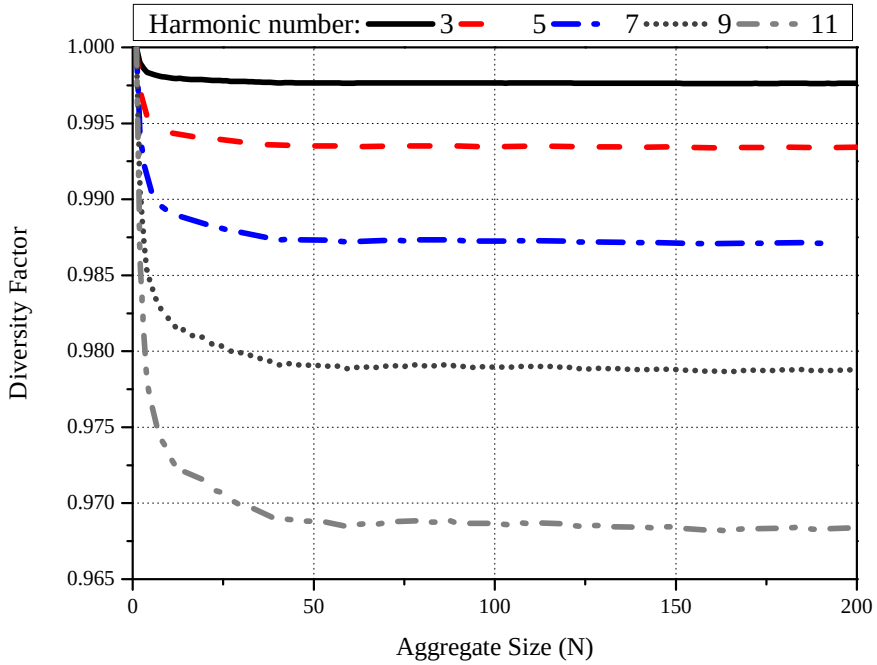

Figure 3.32: Diversity factor of the PE no-PFC subcategory for stiff grid conditions.

Harmonic cancellation in PE p-PFC aggregate loads

The previous analysis has shown that the expected harmonic phase angle dispersion is greater for this subcategory, as a result of the significant phase angle variation with changes in the dc power demand. Consequently, the range of input current harmonic phase angles is, generally, increased in this subcategory and greater cancellation is expected. A comparison of the aggregate and individual harmonic currents, with corresponding harmonic diversity factor values, are displayed in Figures 3.33 and 3.34. The calculated diversity factor values are much lower for this subcategory, clearly indicating greater harmonic cancellation.

It is interesting to observe that the DF_h is not as closely correlated to the harmonic order, as was the case for the PE no-PFC subcategory. For example, Figure 3.34 shows that DF_h for the 9^{th}order harmonic is lower than 11^{th} order harmonic. This is also reported in [48]. The cancellation is a result of the harmonic phase angle dispersion (see Figure 3.27), which shows that the phase angle dispersion for the 9^{th}order harmonic around the 50% dc load condition is between quadrant two and three, i.e. phase angle range of $\pm 180^o$, resulting in high cancellation.

Again, the harmonic currents of the generic model lie very close to the mean value. For this subcategory, the harmonic emissions of the generic model are only slightly higher than the aggregate model, as a result of the low level of harmonics within the current waveforms of the individual devices. Although the diversity factor shows a higher level of cancellation, this is expressed as a ratio which, when applied to the low starting value of the higher order harmonics, will actually result in small cancellation (in absolute terms).

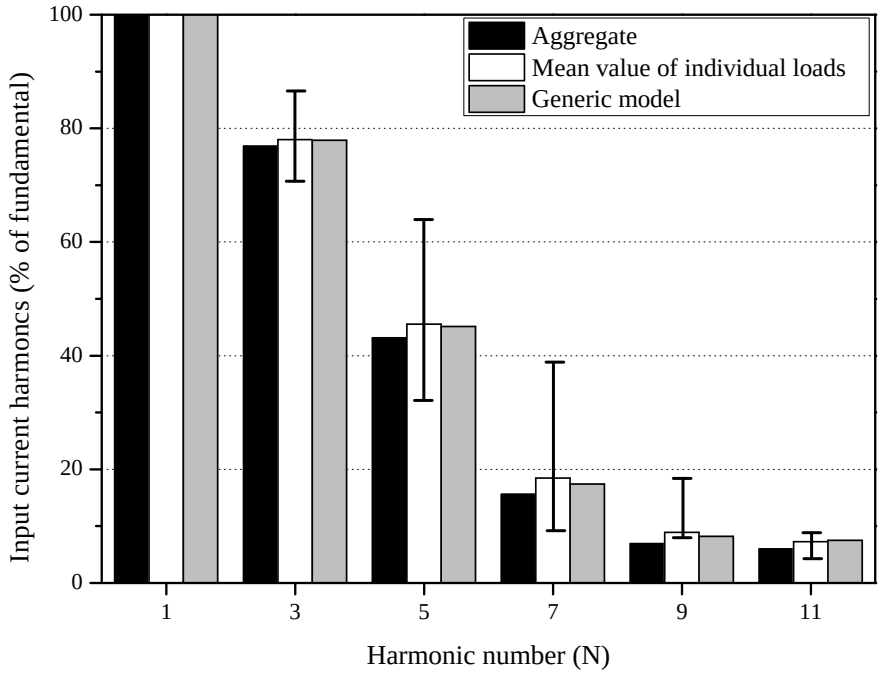

Figure 3.33: Comparison between the input current harmonics of aggregate load and individual loads for the PE p-PFC subcategory for stiff grid conditions.

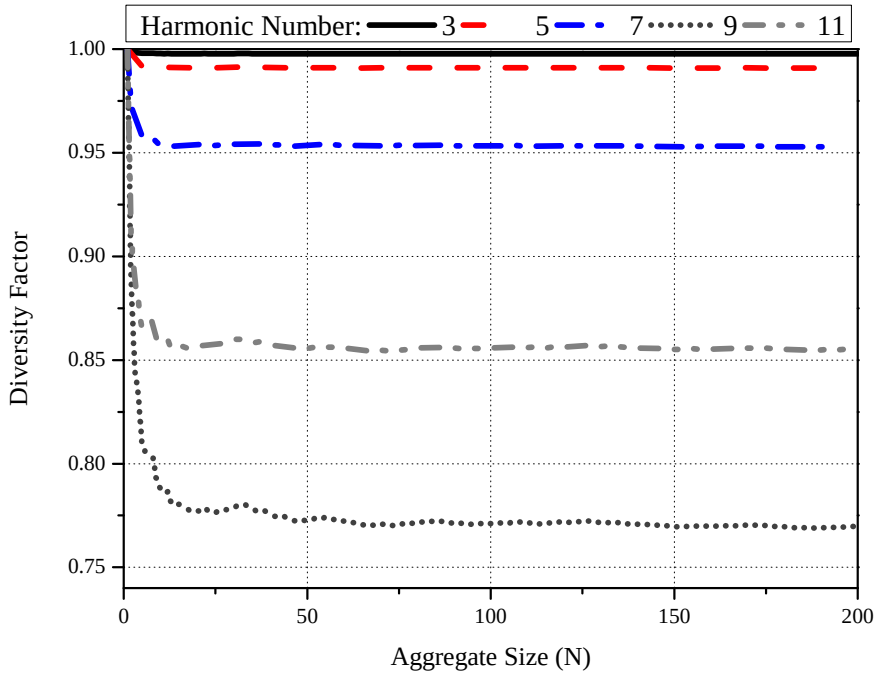

Figure 3.34: Diversity factor of the PE p-PFC subcategory for stiff grid conditions.

Harmonic cancellation of mixed PE aggregate loads

To calculate the diversity factor of the mixed PE aggregate load, the next connected load in the aggregate was alternated between PE no-PFC and PE p-PFC devices, i.e. if Load 1 was PE no-PFC, then Load 2 was PE p-PFC and so forth. In this chapter, a 50-50 composition was assumed to illustrate the effect of harmonic cancellation between subcategories. Clearly, the composition of the load will play a key part in the overall harmonic characteristics of the aggregate, and this is discussed further in Chapter 6 and Chapter 7.

Connecting the two subcategories to the same network will inherently increase the harmonic phase angle dispersion within the aggregate load. Accordingly, the level of harmonic cancellation should increase for this aggregate load scenario. This is confirmed in Figure 3.35, which displays the aggregate harmonic current magnitudes. The harmonic current of the aggregate load is significantly reduced in comparison to the mean value of the individual loads, and, for the 3^{rd}, 5^{th} and 7^{th} order, will have lower harmonic injections than either of the individual subcategories. The most significant cancellation is observed at harmonic order seven. Observing the phase angle dispersion due to dc load variation (Figures 3.26 and 3.27), the phase angle values are opposite for 50% mean value of dc load variation which will be a contributing factor to this phenomena. This effect is also preserved when using only the two generic models to represent the aggregate load.

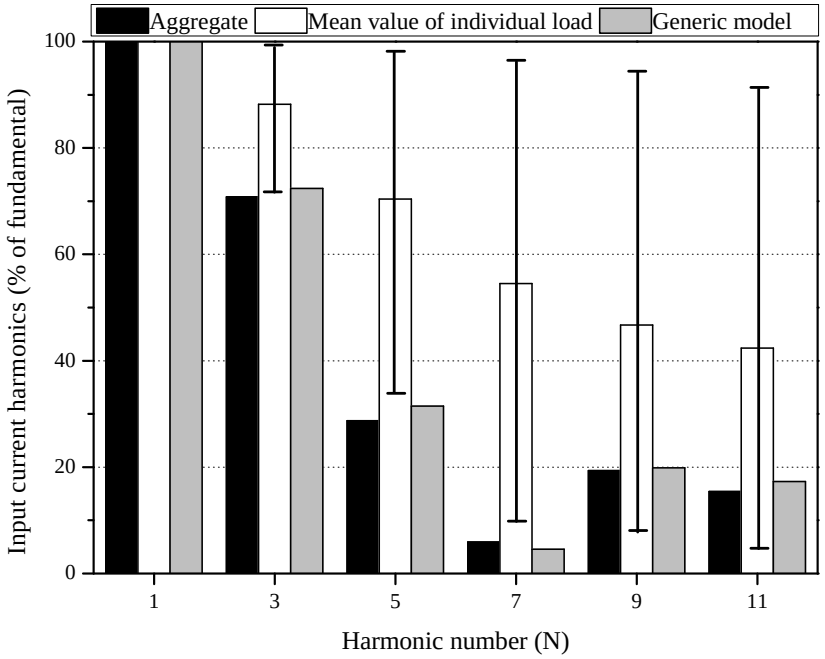

Figure 3.35: Comparison between the input current harmonics of a mixed aggregate of PE no-PFC and PE p-PFC subcategory loads for stiff grid conditions.

The identified harmonic cancellation is reflected in the calculated diversity factors, shown in Figure 3.36 for a mixed aggregate of low and high-power SMPS, which generally lie between

the diversity factors of same-type aggregates. However, cancellation of lower-order harmonics (3rd-9th) is more pronounced. This is clearly visible in the direct comparison of the calculated diversity factors for the first 15 harmonic orders for all three aggregations presented in Table 3.8. The diversity factors, of the same type and mixed type aggregate (up to and including the 39^{th} harmonic order) are included in Appendix D.

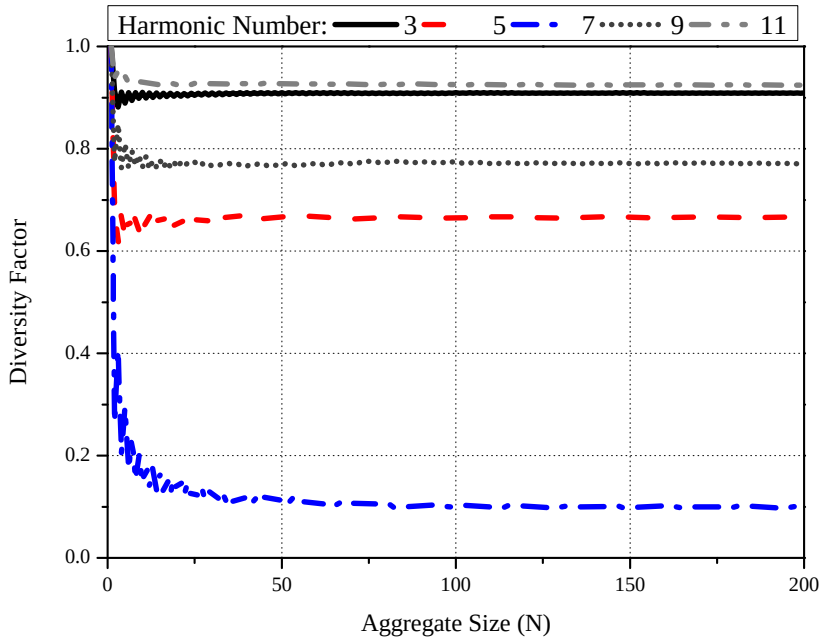

Figure 3.36: Diversity factor of mixed aggregate PE load.

Table 3.8 also includes the DF_h calculated for a computer aggregate load in [81]. There are some noticeable differences between the two sets of results which can be apportioned to the fact that the research in [81] was performed prior to the introduction of harmonic legislation in 2001. In [81], the computer and monitor are represented by one equivalent circuit model. While this analysis was suitable for the device characteristics at the time (i.e. with no harmonic legislation), the introduction of harmonic legislation in the EU has changed the electrical properties of these devices.

Table 3.8: Calculated diversity factor values for different power electronics aggregate loads.

Harmonic Number (N)	Diversity factor DF_h			
	PE no-PFC	PE p-PFC	Mixed aggregate	Ref. [81]
3	0.99763	0.99727	0.90869	0.98
5	0.99343	0.98846	0.66516	0.94
7	0.98714	0.9264	0.10072	0.86
9	0.97878	0.78415	0.77145	0.64
11	0.96837	0.85021	0.92453	0.88
13	0.95595	0.65227	0.71457	0.72
15	0.94156	0.63835	0.63704	0.56

Currently, the majority of desktop computers are PE p-PFC, while monitors are predominantly PE no-PFC, and the harmonic cancellation between these device cannot be accurately represented by a single circuit model. However, the analysis in this section has shown that this behaviour will be preserved using the two generic models presented in this thesis. Furthermore, the component values of equivalent circuit model selected in [81] are substantially different to the values used in this research. The mean value of PFC inductor reactance was only 0.5%, compared with 3.7% in this thesis, and the mean value of C_{dc} is 7%, compared to 3.6% used in this work. These differences can be attributed to the impact of harmonic legislation and performance requirements which will have influenced the design of power electronics equipment over the years. This shows that these results need to be updated for use in analysis in power systems within the EU.

Influence of system impedance on harmonic cancellation in the power electronics load category

Up until this point, the harmonic cancellation has been calculated for stiff grid conditions. However, this effect does not exist in isolation and should also include the interaction between the load harmonics and the supply system impedance to distort the supply system voltage. Accordingly, the analysis in this section will show how the harmonic attenuation will influence the harmonic emissions of the power electronics load category.

To simulate this effect, the previously developed load models are connected to a common system impedance (as described in Section 3.6.1) in the MATLAB Simulink SimPowerSystems toolbox [82]. The size of the aggregate load is set to 200 devices, as the previous results have shown that the asymptotic value is achieved for aggregate loads of this size. To allow for a direct comparison, the exact simulation model parameters used in the previous sections are used in the simulation models in this section.

When a same type aggregate load is connected to the supply system impedance, the harmonic currents will interact with the supply system impedance and act to distort the supply voltage waveform. This distorted voltage will then lower the harmonic currents injected by the load. This effect is observed in both PE no-PFC and PE p-PFC devices in Figures 3.37 and 3.38.

As the supply system impedance value increases, the magnitude of the current harmonics will reduce. However, this effect is more pronounced for PE no-PFC, Figure 3.37, than for PE p-PFC, Figure 3.38. Although the power drawn by the PE no-PFC devices is lower than PE p-PFC devices, there is more power drawn at the harmonic frequencies which will interact with the supply system impedance. Furthermore, as the input impedance of the PE no-PFC devices is low, it is very sensitive to voltage distortion caused by the supply system impedance. This is clearly displayed by the corresponding values of THD_I and THD_V (for all aggregate scenarios) in Table 3.9. The values in this table show that as the value of system impedance increases, the current THD will reduce while the voltage THD will increase. This clearly demonstrates

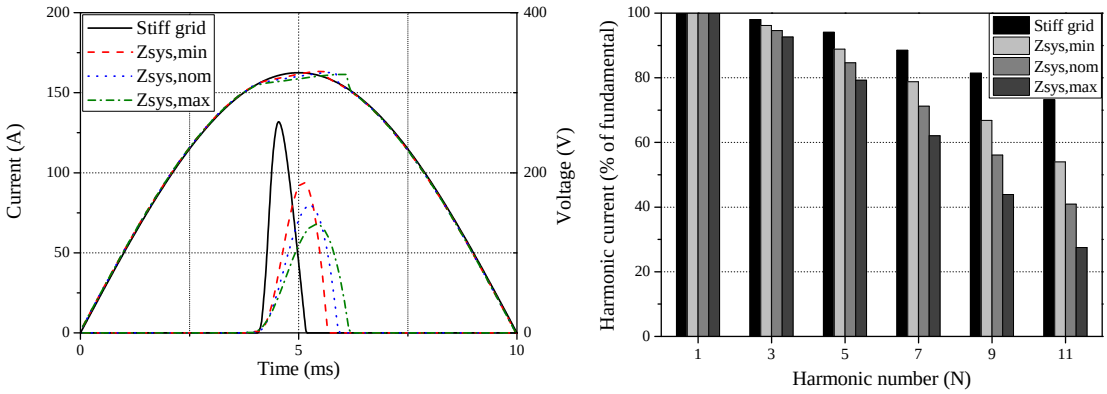

(a) input current waveform (b) associated harmonic content

Figure 3.37: Influence of system impedance values on harmonic cancellation in the PE no-PFC subcategory.

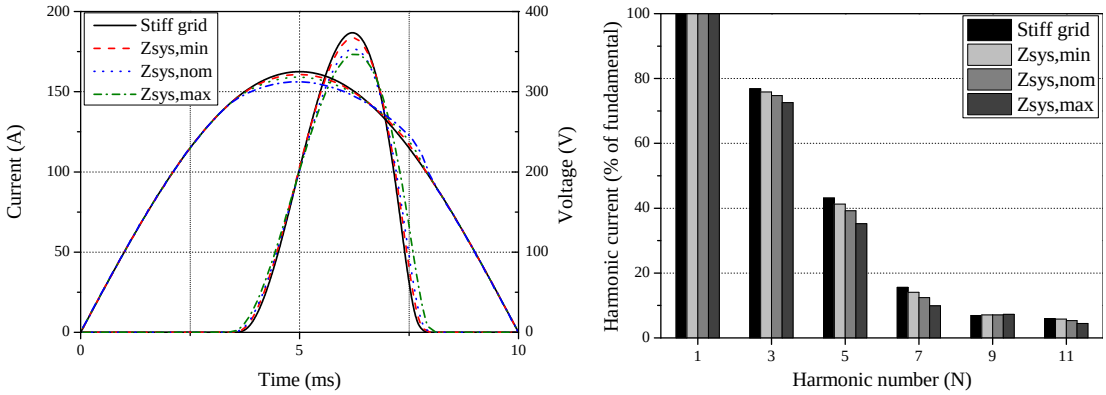

(a) input current waveform (b) associated harmonic current

Figure 3.38: Influence of system impedance values on harmonic cancellation in the PE p-PFC subcategory.

the self-compensating principal of harmonic attenuation. Although the PE p-PFC will result in higher levels of voltage distortion, the effect of this voltage distortion on the harmonic content of the current waveform is greatly reduced, in comparison to PE no-PFC devices. This is reflected by the change in input current shape, where the PE no-PFC input current waveform changes significantly for the different levels of supply voltage distortion, while only a slight change in PE p-PFC is recorded. Changes in the input current waveform will alter all electrical characteristics of the load, which is discussed in more detail in the following section.

When the two types of power electronics loads are connected to the same supply system as a mixed aggregate, the effect is more complicated. In addition to harmonic cancellation between the two devices, it has been shown that, in isolation, the two devices will cause different types of voltage distortion. The PE no-PFC devices will result in 'notching' type distortion of the supply voltage waveform, while PE p-PFC distortion will act to reduce the peak voltage and widen the voltage waveform.

Table 3.9: Voltage and current THD values for aggregate power electronics loads.

Aggregate Load	System impedance							
	Stiff		Min.		Nom.		Max.	
	THD_I (%)	THD_V (%)	THD_I (%)	THD_V (%)	THD_I (%)	THD_V (%)	THD_I (%)	THD_V (%)
PE no-PFC	230	-	184	0.59	165.47	0.97	148.04	1.51
PE p-PFC	90.07	-	88.09	0.70	85.88	1.40	81.79	2.63
Mixed	83.53	-	84.78	0.48	84.13	0.90	82	1.61

When these effects are combined, it will actually resolve to initially increase the overall harmonic content, i.e. THD, of the current waveform, in comparison to the stiff grid condition. This effect is attributed to the behaviour of PE no-PFC devices which will increase in THD_I when supplied with a typically distorted supply voltage, i.e. voltage distortion waveform which includes a mix of devices, which is demonstrated in more detail in the subsequent section. However, the expected correlation between THD_I and THD_V is observed as the supply system impedance increases from the minimum to the maximum value.

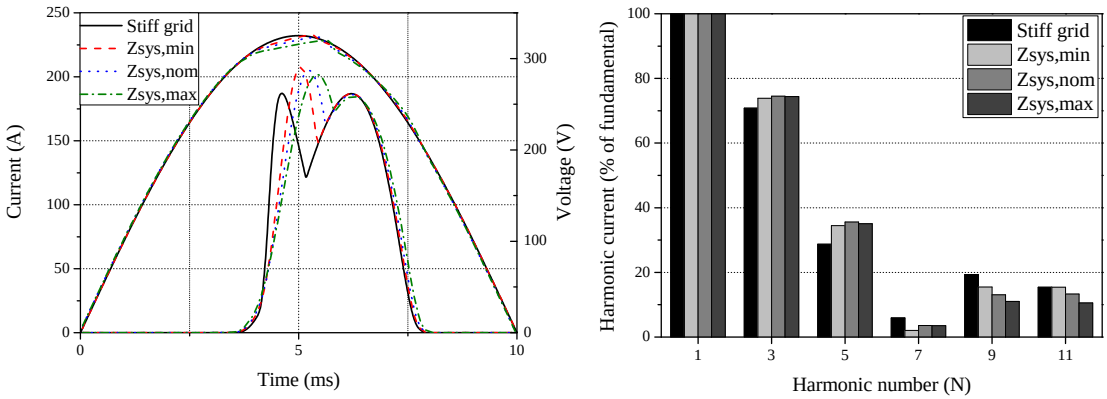

(a) input current waveform

(b) associated harmonic content

Figure 3.39: Influence of system impedance values on the harmonic cancellation of a mixed aggregate of power electronics loads.

The diversity factors and harmonic injections of all aggregate loads for the four values of system impedance are included in Appendix D. These can be directly implemented for use in harmonic power flow studies. However, it should be reiterated that the the equivalent circuit model and defined range of values is a far more powerful modelling tool and can be either directly connected in the power system analysis, to allow for full reproduction of input current waveform, or configured to produce a large number of individual devices, from which statistical processing can define the distribution of harmonic currents for use in more detailed harmonic power flow studies.

3.6.3 Electrical characteristics of aggregate power electronics load

The previous section has shown that the combined effect of harmonic cancellation and harmonic attenuation will change the input current drawn by the aggregate power electronics loads. This will cause changes in all electrical characteristics of the modelled load. In this section, these effects are quantified and used to present standard exponential and polynomial/ZIP load model implementations of power electronics loads. In addition to this, the ability of the generic model to preserve the considered electrical characteristics across the voltage range is tested.

The influence of the supply network on the aggregate electrical characteristics is included by comparing the aggregate load behaviour when supplied with an ideal sinusoidal waveform and with a distorted voltage waveform of THD_V 2.37%. The distorted voltage waveform (displayed in Figure 3.40) was measured within the Edinburgh LV network and was comparable to the voltage waveform measured at 'rural' and 'urban' areas and can, therefore, be considered representative of the typical voltage distortion levels of residential customers.

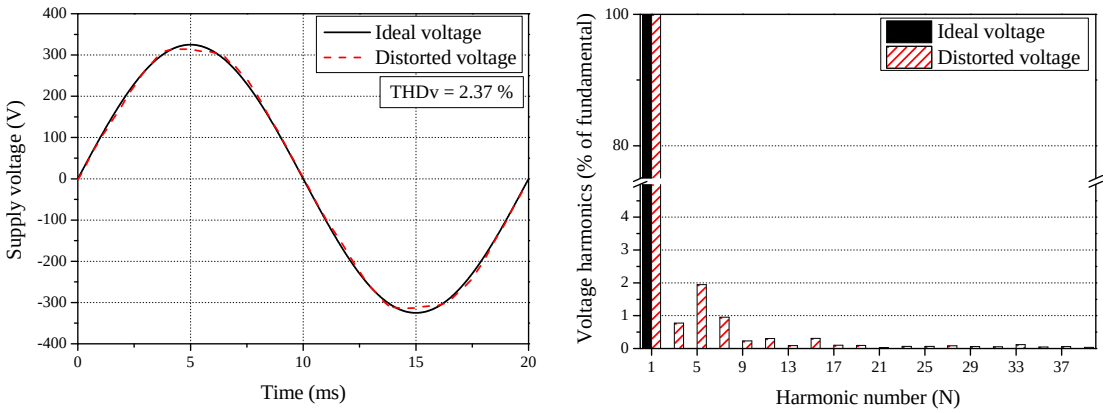

(a) input current waveform (b) associated harmonic content

Figure 3.40: Distorted supply system voltage waveform.

To calculate the aggregate electrical characteristics, the previously developed circuit models, component parameters and supply system connection were implemented for stiff grid and distorted supply conditions. Therefore, the harmonic cancellation effects are fully retained and included in the aggregate model development. As before, the two subcategories will be assessed individually before considering a mixed aggregate load.

Electrical characteristics of PE no-PFC aggregate load

A comparison between the individual PE no-PFC loads and the aggregation of these is presented in Figure 3.43 on Page 70. In this figure, the active and fundamental reactive power characteristics have been normalised to 1 pu for each device. Hence, there is there very little difference between the power characteristics of the generic model and the simulated aggregate. The biggest error is observed in the value of current THD and, consequently, in the the PF and PF_d values. The current THD of the generic model is approximately 20% higher than the aggregate result. However, in percentage terms, this is only around an 8% increase, which is reflected in the 8% error in PF_d. This is due to the result of accurate of cancellation within the aggregate load, which cannot be included in the simplified form of the generic model.

When the aggregate PE no-PFC load is supplied with distorted voltage waveform, the harmonic content of the load will actually increase (Figure 3.41). This effect was also noted in Figure 3.39 where it was shown that when PE no-PFC devices are supplied from a distorted voltage waveform, which has been distorted as a result of other non-linear loads, it can act to increase the harmonic emissions of the load. To explain this effect, analysis of the supply voltage and the dc link voltage, which will set the conduction periods of the loads, is required.

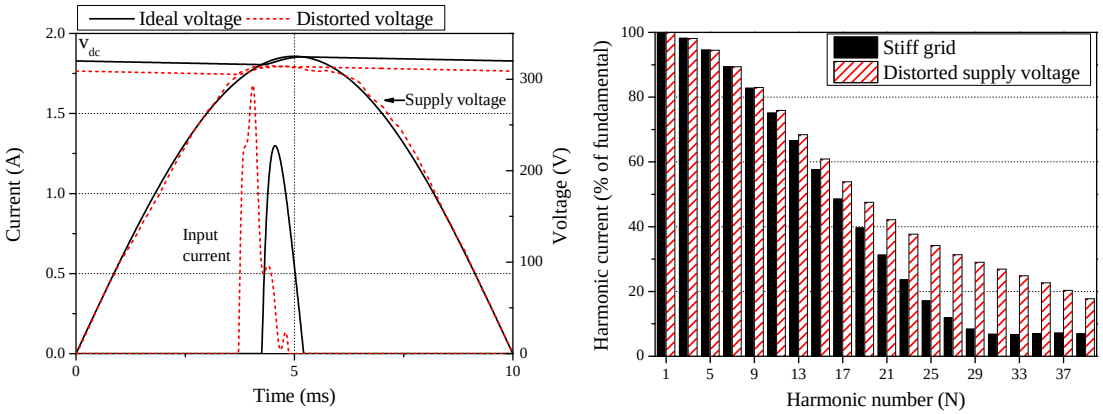

(a) input current waveform (b) associated harmonic current

Figure 3.41: Comparison of PE no-PFC aggregate load input current characteristics for stiff grid and distorted supply conditions.

In the close-up view of the dc link voltage and input current and supply voltage waveforms, presented in Figure 3.42, six points of interest are highlighted. At point '1', the dc link voltage falls below the (rectified) supply voltage and the dc link capacitor will charge, drawing current from the supply network and increasing v_{dc}. The input current will increase until point '2', when the gradient of the supply voltage will change. This results in an increased rate charge for the dc link capacitor, and corresponding input current, until the peak value at point '3'. The input current will reduce to point '4', when an increase in supply voltage will cause C_{dc} to charge again point '5'. The final charging current increase at point '6' completes the cycle. The increased charging rate until point '3', with narrower current pulse, is the principle reason for the higher harmonic content in the input current waveform.

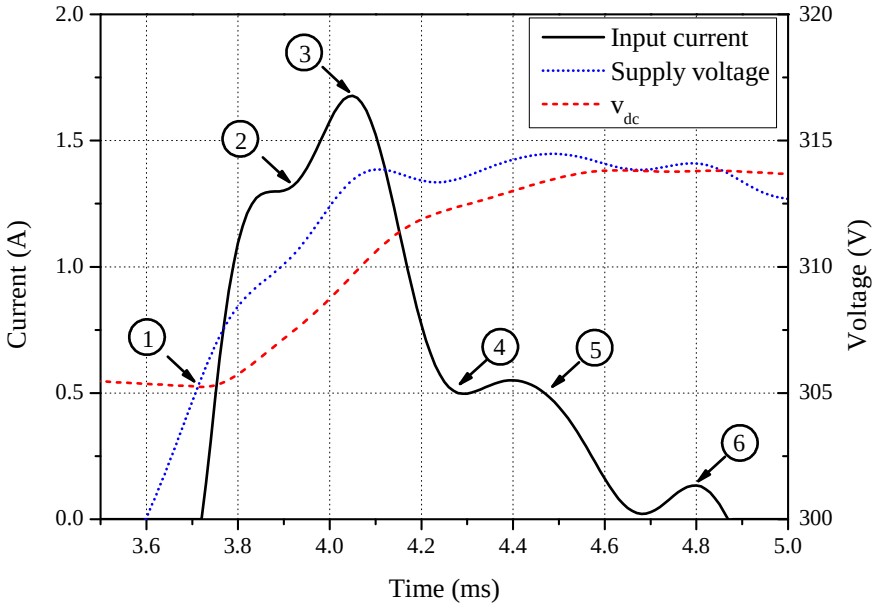

Figure 3.42: Close up view of the simulated dc link voltage waveform for the PE no-PFC subcategory with distorted supply conditions.

Furthermore, the waveform will shift to the left when supplied from distorted voltage, as shown in Figure 3.41, which will influence the value of the displacement power factor. As the flat-top voltage has a lower peak value, the dc link capacitor will, relatively speaking, charge sooner in the cycle. Therefore, the current fundamental is further displaced from the fundamental component of the voltage, i.e. it is more capacitive.

The influence of these effects on the electrical characteristics of the aggregate load are also illustrated in Figure 3.43, which offers a comparison between the aggregate characteristics supplied from stiff grid and distorted supply conditions.

The fundamental reactive power characteristics are more linear under distorted supply conditions. This is a consequence of the shift in displacement power factor between the two supply conditions. Although the gradient of the displacement power factor is similar for both supply conditions, the actual phase angle should be considered when quantifying the fundamental reactive power. As the displacement power factor is higher for ideal supply conditions, the phase angle between current and voltage fundamentals is smaller for this scenario. The rate of change of the sinusoid function increases for smaller angles, therefore the reactive power characteristic, which is governed by the sinusoidal component of the current (i.e. $Q_1 = V_1 I_1 sin(\theta_1)$, will experience a bigger change in values. Conversely, the reactive power characteristic for distorted supply is more linear as the 'angular rate of change' is slower.

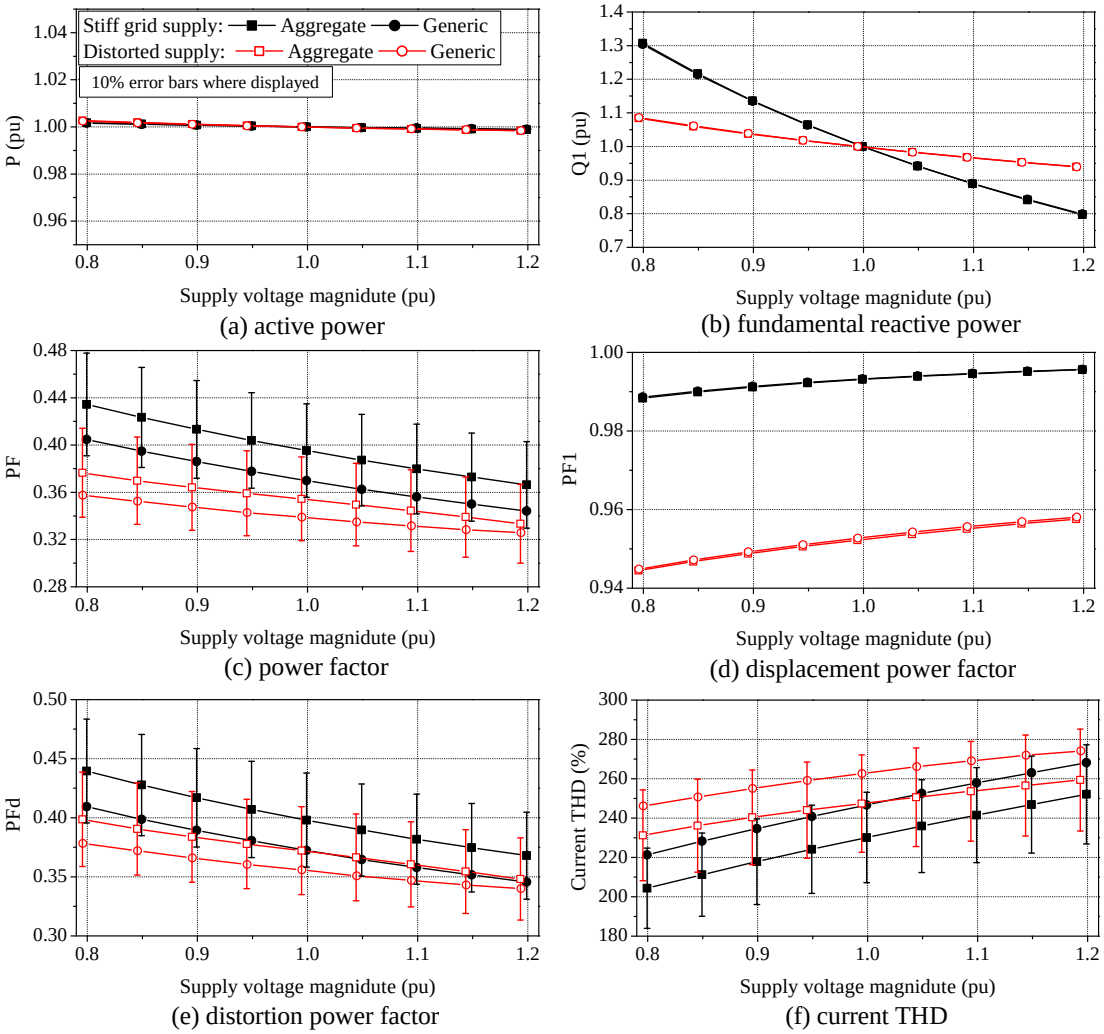

Figure 3.43: Comparison of electrical characteristics between aggregate and generic PE no-PFC load for stiff grid and distorted supply conditions.

Electrical characteristics of PE p-PFC aggregate load

Similar conclusions to the PE no-PFC devices can be drawn when comparing the electrical characteristics of individual PE p-PFC loads and an aggregation of these supplied from a stiff grid. Again, the effect of harmonic cancellation will lower the current THD and increase the overall characteristic of the aggregate load distortion power factor. The results of this analysis are displayed in Figure 3.44.

Although aggregation under stiff grid conditions returns similar trends to the PE no-PFC loads, the aggregate PE p-PFC load will behave differently under distorted supply conditions. As the flat-top voltage has a lower peak voltage, the dc link capacitor will start to charge sooner in the cycle and will have to charge longer, becoming more sinusoidal in shape. Therefore, for this PE subcategory, the harmonic content of the input current will reduce. This is shown in

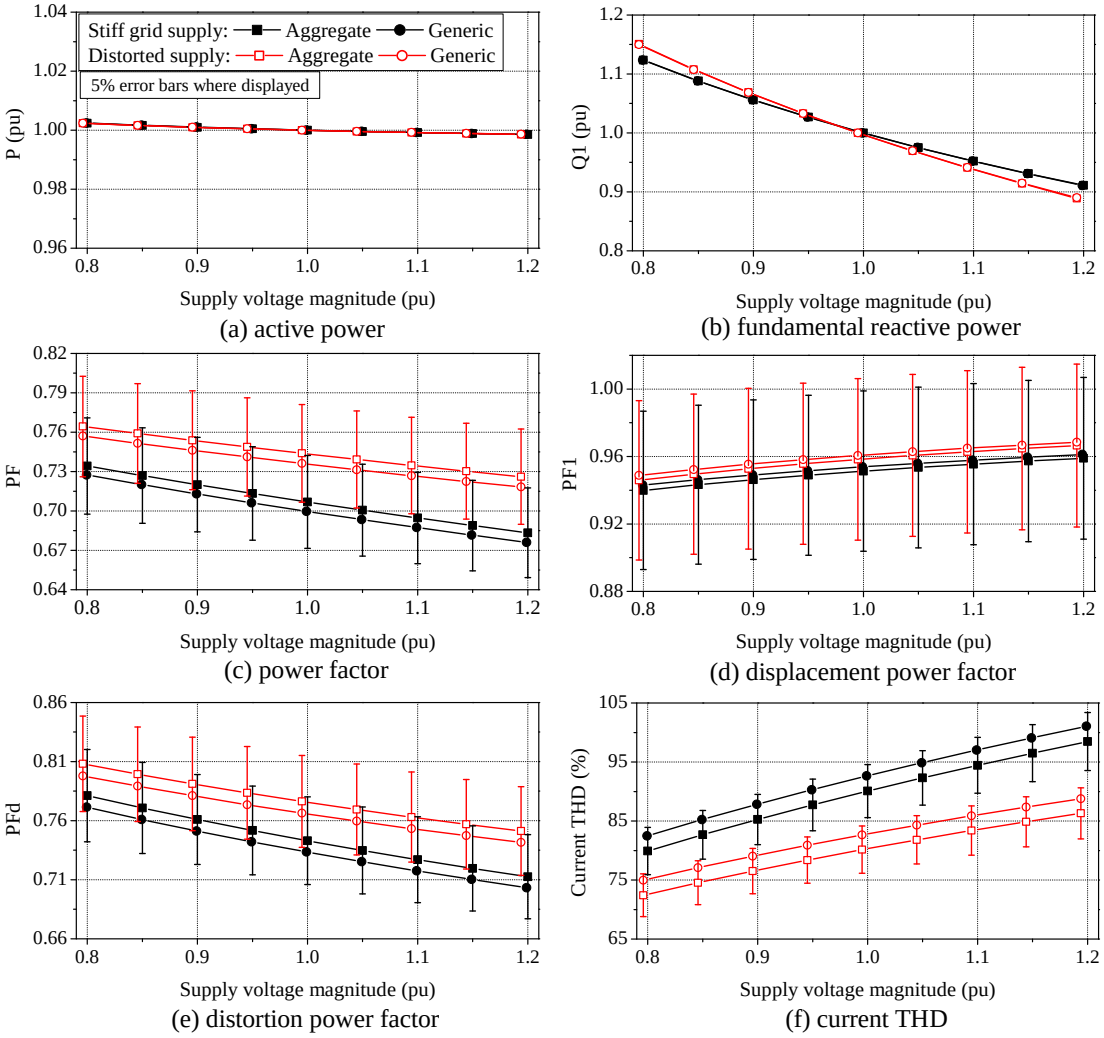

Figure 3.44: Comparison of electrical characteristics between aggregate and generic PE p-PFC load for stiff grid and distorted supply conditions.

Figure 3.45, with a comparison of electrical characteristics for stiff grid and distorted supply conditions in Figure 3.44.

The displacement power factor will actually marginally improve when supplied from a distorted voltage waveform. Therefore, the corresponding reactive power characteristics are more non-linear for this subcategory. This effect, in combination with the improved distortion power factor, will act to improve the true power factor.

Due to the lower harmonic current emissions of this subcategory, the error in current THD between the generic model and the simulated aggregate is reduced, and the resulting PF_d values are closer. Overall, better matching is observed between the generic model and the simulated aggregate.

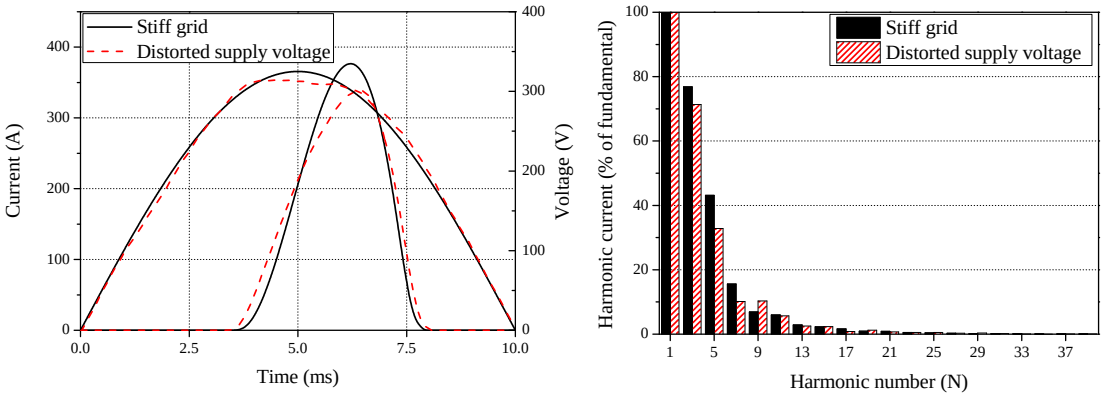

Figure 3.45: Comparison of PE p-PFC aggregate load input current characteristics for stiff grid and distorted supply conditions.

Electrical characteristics of mixed power electronics aggregate load

The results in Figure 3.39 confirm the complex nature of harmonic cancellation, both within the aggregate load and also by interaction with the supply impedance. When supplied from an already distorted voltage waveform, the total harmonic distortion of the aggregate load will reduce, resulting in an improvement in distortion power factor. The combined harmonic cancellation effect of the two subcategories will resolve to the highest aggregate distortion power factor. For stiff grid supply conditions, the aggregate displacement power factor value will lie between the two individual aggregates. This is because the fundamental current components will not shift significantly unless supplied from a distorted voltage waveform. When supplied in this configuration, the fundamental component of the current waveform will shift three degrees with respect to the fundamental component of the supply voltage which will slightly improve the aggregate displacement power factor.

When the two generic models are combined, which is more representative of the actual loading conditions found in LV networks, the largest error is 5% for current THD. The maximum resulting error in the corresponding power factors is 1.5%, for PF_d. The largest error in displacement power factor is less than 1%, with true power factor around 1%. This level of accuracy is retained for both ideal and distorted supply conditions.

This is an important result for this research as it shows that all electrical characteristics of the power electronics load category can be represented by using only two loads, with only a minimal error. This significantly simplifies the development of aggregate load models.

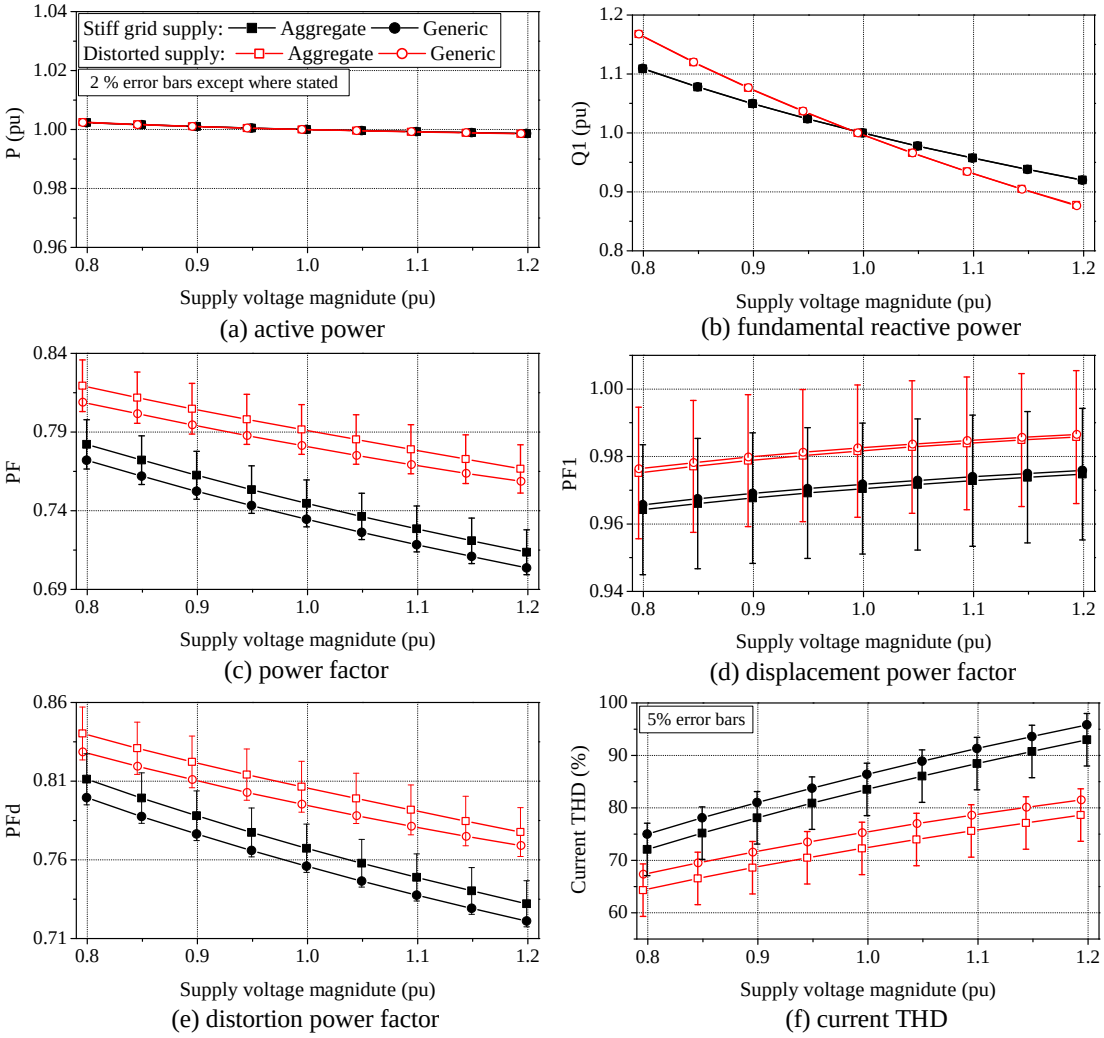

Figure 3.46: Comparison of electrical characteristics for mixed aggregate containing PE no-PFC and PE p-PFC load for stiff grid and distorted supply conditions.

3.7 Proposed power electronics load models

3.7.1 Generic equivalent circuit model values

The analysis in this chapter has defined the generic circuit model parameters for the power electronics load category, and used these to investigate the electrical characteristics of aggregate power electronics loads. The equivalent circuit model set-up with generic component values has been shown to accurately represent the electrical characteristics of the simulated aggregate power electronics loads. As previously discussed, this has the added functionality of reproducing the instantaneous input current waveform for a given supply voltage waveform, and allows for preservation of harmonic currents within the aggregate model. Therefore, the output of the generic circuit model can be converted into exponential or polynomial forms (as illustrated in the next section), or processed to obtain harmonic magnitude and phase angle information for use in harmonic studies (which are included in Appendix D).

The generic values and typical range of parameters are presented in Table 3.10. In this table, the values for PE no-PFC have been normalised to a base power of 50 W, while the PE p-PFC values have been normalised to a base power of 250 W.

Table 3.10: Proposed generic values for equivalent circuit model.

Parameter	Generic value (pu)	Distribution	
		Range	Notes
PE no-PFC			
$X_{C_{dc}}$	0.036	Normal	$\sigma = 0.54$
X_L	$6 \times^{-6}$	Uniform	min = $3 \times^{-6}$, max = $9 \times^{-6}$
R	0.0017	Uniform	min = 0.0015, max = 0.0019
$X_{C_{EMI}}$	18.8	-	-
PE p-PFC			
$X_{C_{dc}}$	0.036	Normal	$\sigma = 0.54$
$X_{L_{PFC}}$	0.037	Normal	$\sigma = 0.00186$
R	0.0085	Uniform	min = 0.0077, max = 0.0094
$X_{C_{EMI}}$	7.52	-	-

3.7.2 Exponential and polynomial load model interpretations

The electrical characteristics of the aggregate power electronics load subcategories simulated using the generic equivalent circuit in the previous section can be converted to standard exponential and polynomial/ZIP load model forms for implementation in standard power flow analysis software. This is achieved by applying a curve fitting routine to the calculated active and reactive power demands obtained during the voltage sweep analysis (e.g. the data in Figure 3.43(a) and (b)). The MATLAB curve fitting toolbox [83] was used to fit the exponential and polynomial/ZIP models to the simulated data. This implements a least squares curve fitting algorithm, which minimises the sum of the squares of model residuals, i.e. the difference between the observed data value and the value predicted by the model.

The proposed load model coefficients are shown in Table 3.11 for both exponential and polynomial/ZIP forms. For all reactive power load models, the R-squared error is unity, indicating the accuracy of both model forms. For the active power coefficient, the polynomial/ZIP R-squared error is unity, while the R-squared error for the exponential model is ≈ 0.99, which confirms the accuracy of both model forms for representing this load category.

As the loads are designed to deliver constant power to the connected dc load, the variations in this load characteristic between supply conditions are negligible. The most striking differences are in the reactive power characteristics of the loads, with the biggest change witnessed in PE no-PFC. Due to the large input impedance, PE p-PFC devices are similar for both supply conditions and display a reactive power characteristic which is approximately between constant current with a negative gradient and constant power. The characteristics of a-PFC are assumed

to be ideal. Note: if PE a-PFC is not ideal, then the exponential or polynomial/ZIP load model parameters can be used to represent the phase shift in the fundamental components for the voltage range.

The characteristics of a mixed aggregate of these non-linear loads is included for illustration purposes only as the aggregate load should be developed from the models of the individual load categories in conjunction with detailed statistical data on the contribution of each load category (or subcategory) to the aggregate load (this is discussed further in Chapters 6 and 7 which convert available load use statistics into the three PE subcategories).

Table 3.11: Proposed exponential and polynomial load models of the power electronics load category.

Supply	PF_1	Load model							
		Exponential		Polynomial/ZIP					
		n_p	n_q	Z_p	I_p	P_p	Z_q	I_q	P_q
PE no-PFC									
Ideal	0.99	-0.007	-1.21	0.008	-0.023	1.015	1.314	-3.889	3.574
Dist.	0.95	-0.011	-0.352	0.014	-0.038	1.025	0.297	-0.951	1.653
PE p-PFC									
Ideal	0.95	-0.009	-0.518	0.011	-0.032	1.02	0.436	-1.399	1.963
Dist.	0.96	-0.009	-0.628	0.012	-0.033	1.021	0.509	-1.661	2.151
PE a-PFC									
-	1	0	-	-	-	1	-	-	-
where: clean and dist. refer to previously shown stiff grid and distorted supply conditions.									

A comparison between the proposed models and the existing models identified in literature is presented in Figure 3.47. The active power characteristics of the proposed models, approximately constant power, are in agreement with the most recent references. The slight negative characteristic is a result of the current flow through the internal impedance and the associated active power losses, which is inversely proportional to the supply voltage. However, this effect is negligible as it is less than 0.5% at the upper and lower boundary of the considered voltage range.

There is a more noticeable difference in the reactive power characteristics. The two references that suggest a highly non-linear characteristic both have constant impedance active power characteristics which indicates that they are not representative of modern power system loads. Note: although reference [63] states a unity power factor, it has a reactive power characteristic of Z_q = 0.15 but the reported characteristics actually shows an increase in reactive power demand as supply voltage magnitude reduces, similar to the trend to shown by the proposed load model, which are not conveyed in the published model value.

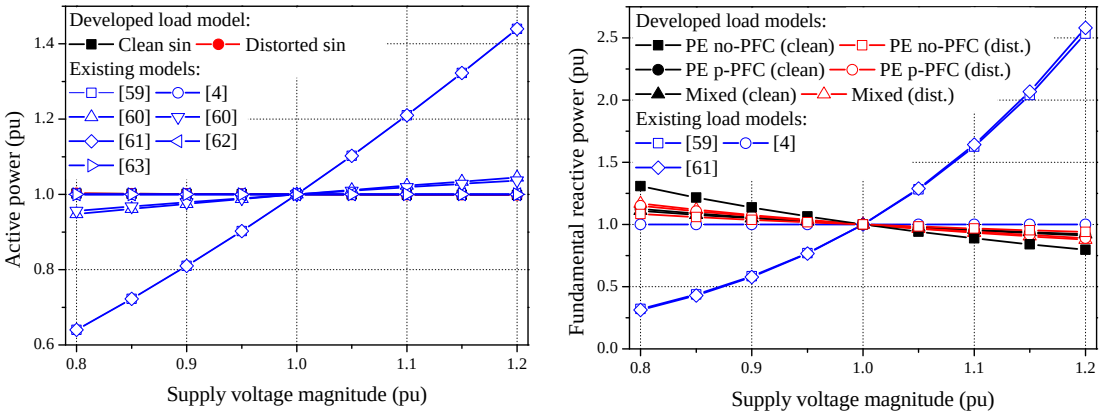

(a) active power (b) fundamental reactive power

Figure 3.47: Comparison between the developed load models and existing load models.

3.8 Conclusions

This chapter has presented a thorough consideration of the representation of modern power electronics loads for power system analysis. It has been shown that the assumption to model all power electronics loads with the same load model may be a source of error in simulation, as there are three distinct subcategories with significantly different electrical characteristics. These three subcategories are a direct consequence of the introduction of harmonic legislation in the EU in 2001, which requires all devices of rated power greater than 75 W to limit the harmonic current emissions. This is achieved by the addition of PFC circuits, which take one of two general forms: active or passive.

The electrical characteristics of the three PE subcategories have been discussed in detail and variations between same-type aggregates and mixed aggregates have been assessed using a range of load modelling techniques. The modelling approach began with a description and analytical derivation of the operation of an equivalent circuit model which can represent diode bridge rectifier loads. This is the standard form of many modern loads and provides a quick simulation tool which can be implemented in any mathematical software. Typical values of the equivalent circuit model components were introduced and validated to provide generic values, and the associated variations of each parameter.

Monte Carlo simulations of the developed analytical model were performed to investigate the harmonic cancellation within the power electronics aggregate load, with results also presented in the forms most widely used in power system analysis, i.e. exponential and polynomial form. However, it was shown that direct use of the generic models will introduce only a small error, between 1 - 1.5 % for all considered electrical characteristics, in comparison with the simulated results for the aggregate load. This approach allows for the inclusion of harmonic cancellation and attenuation in the aggregate models, which is not normally included in the development of power system load models. These topics have been shown to have a significant impact on the characteristics of the aggregate load and will be revisited in subsequent chapters of this thesis.

Chapter 4

Lighting load category

4.1 Introduction

Recent statistics estimate that approximately 19% of global electricity consumption is used for lighting [84]. The vast majority of this demand is from the residential and commercial load sectors, which contribute around 30% and 40%, respectively, to the total lighting demand. The corresponding UK figures estimate that the proportion of energy consumption by light sources ranges from 9%-20% of the total demand, with lighting contributing between 20% to 40% of the total demand in the residential and commercial load sectors [58]. As lighting technolologies are responsible for such a large proportion of demand, they should form a significant part of the load modelling effort.

The analysis presented in this thesis focuses on the residential load sector, where the two main lamp types currently in use are general incandescent lamps (GILs) and CFLs. Linear fluorescent lamps (LFLs), halogen incandescent lamps (HILs) and LED LSs are also currently used in the residential load sector, but in much smaller numbers. The same types of light sources are also found to varying levels in the other load load sectors, with high-intensity discharge (HID) lamps also used to light larger indoor areas and also for outdoor illumination.

The research in this chapter is driven by the overall trend in improving the energy efficiency of power system loads. In 1992, the EU passed a directive to introduce 'energy efficiency labels' for electrical appliances [85], which have been applied to a large number of appliances and lighting technologies. However, this did not enforce any performance requirements. This has since been addressed and measures taken to phase out use of GILs, which should have been fully banned by the end of 2012 [86]. This is implemented with respect to the 'energy efficiency labels', in which CFLs and LED LSs are rated as Class A (the best), while GILs are rated as Class E (Class G is the worst). In 2010, all 'clear bulb' light sources with rated power greater than or equal to 75 W were required to be Class C or above, essentially resulting in banning GILs of higher rated powers. This was to be extended to all 'clear bulb' light sources with rated power of 60 W and above in 2011 and, finally, all rated powers in 2012. Similar efforts exist in the US [87], and several other countries, which have either passed, or are considering, legislation to restrict or ban the sale of GILs. These actions clearly suggest that CFLs, and LED LSs in the future, will become increasingly dominant in the residential load sector.

This trend is confirmed by UK annual consumption statistics in Figure 4.1, which shows a reduction in the overall lighting demand, and a visible replacement of incandescent lamps with 'energy saving' light bulbs.

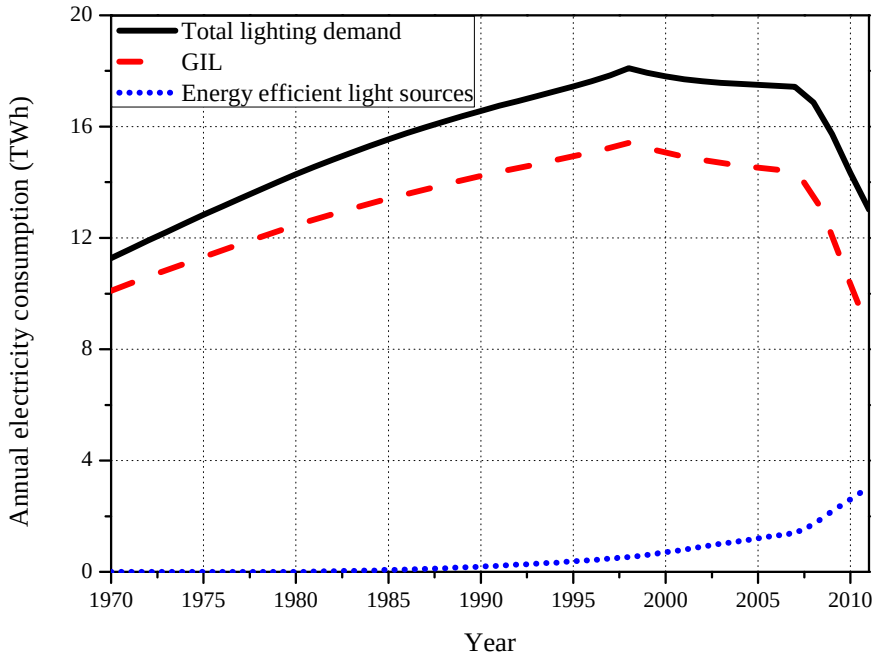

Figure 4.1: Consumption statistics of the UK residential sector lighting load [58].

Both CFLs and LED LSs include electronic control circuits which result in the devices having significantly different electrical characteristics to traditional GILs. As a result of these circuits, the energy efficient lamps are non-linear loads and will not only reduce the active power demand but will also alter reactive and harmonic power flows. To accurately assess the impact of the widespread use of these non-linear loads on the power system, the development of load models which are able to reproduce the necessary electrical characteristics, i.e. harmonic currents (in addition to the standard P-V/Q_1-V characteristics), are required.

This chapter begins with a brief overview of the lighting technologies which are currently employed in different load sectors, and the available load models in literature. The main section of this chapter focuses on the modelling of CFLs and will follow the general approach used to analyse and model the power electronics load category in the previous chapter. This begins with the description of the detailed full-circuit model and the reduction to the equivalent circuit model. Expected ranges of component values for the equivalent circuit model are then defined and a sensitivity analysis is performed to define the aggregate characteristics. Initial results on the modelling of LED LSs, which are still a developing technology, are also presented. The chapter concludes by comparing the electrical characteristics of present day and future lighting technologies, with respect to the operation and performance of the electrical power system.

4.2 Lighting technologies for different load sectors

Electric light sources are characterised by a range of features, including: operating life, efficacy and colour rendering index (CRI). Certain characteristics are desirable for particular applications, and in most cases standards/guidelines specify a required level of performance (e.g. CIBSE recommendations [88]). As a result of this, different types of light sources are found to be more prevalent in different load sectors.

In the residential load sector, GILs are still the dominant lighting technology because of their low cost and high CRI. As discussed previously, these are being replaced by energy efficient light sources with similar CRI performance but which offer increased lifetime and efficacy, albeit at the expense of increased cost. In the commercial load sector, the higher power outputs, efficacy and lifetime ratings ensure that LFLs are widely used to light large spaces economically. In the industrial load sector, LFLs are again found in large numbers and there is also a significant contribution from HID lamps, which generally offer the best efficacy and lifetime performance (although at a considerably lower CRI). These characteristics explain the widespread use of HID lamps for outdoor illumination.

An overview of the statistics is given in Table 4.1, where it is shown that GILs are LFLs are the most widely used lighting technologies.

Table 4.1: Contribution of lighting technologies as percentage of the total lighting demand in different load sectors, based on data in [58, 84].

Load sector	Lighting technology				
	GIL	LFL	CFL	HID	LED LS
Residential	66	9	23	-	< 1
Commercial	9-18	68-77	7-12	2-7	< 1
Industrial	1-2	62-67	< 1	31-37	< 1
Outdoor	-	-	-	100	-

4.2.1 Available lighting load models in literature

Existing load models offer some insight into the general characteristics of different lighting technologies, with a selection shown in Table 4.2 on Page 81. This table includes the existing models of all major lighting technologies, not just those which are found in the residential load sector. There is a general agreement on the characteristics of GIL, which have unity power factor and active power characteristics between constant current and constant impedance type. This is different to the constant impedance model which may be assumed due to the operation and is a result of the variation in filament temperature, and resistance, with changing supply voltage. The only available model for HILs indicates that these have similar electrical characteristics to GIL, which, due to similarities in operation, is expected.

The first observation which can be made on the available LFL, CFL and HID models, is that, with the odd exception, they will operate will a displacement power factor less than unity. Two proposed LFL models operate with unity power factor, which can be attributed to the use of electronic ballast circuits. However, the remaining LFL models will operate with a displacement power factor between 0.86 - 0.98. It should be noted that the more recent models of this lighting technology indicate a capacitive power factor, while the older models are inductive loads. The inductive variants have much greater non-linearities in the reactive power characteristics which are not displayed in the newer technologies. This is likely to be the result of technological improvements in ballast design over the past 20 - 30 years. Historically 'magnetic' ballasts, consisting of only a few passive electronic components, were used to supply LFLs. These have since been replaced with more sophisticated 'electronic' ballasts which are able to provide better regulation of tube current and voltage. The implications of this are considered in more detail when modelling the commercial load sector in Chapter 7.

Despite the differences in the reactive power characteristics, the majority of LFL models show an approximately constant current active power characteristic. This $P-V$ relationship is also evident in the CFL models, which are predominantly constant current. This relationship is also observed in the CFL Q_1-V characteristic. At the current time, there are no available load models for LED LS for use in power system analysis which can be attributed to their status as an emerging technology.

It is hard to draw any conclusions about the electrical characteristics of HID lamps, although both models indicate that the reactive power characteristics are highly non-linear. Furthermore, the definition of the available HID load models do not clearly state the modelled load type. The HID model proposed in [60] is defined only as 'representative of the largest fraction of residential/commercial/industrial' loads. However, as CFLs and LFLs are included as a different load model in [60], it can be assumed that this represents either high pressure sodium or metal halide HID lamps, as these are most extensively used for outdoor illumination and lighting large indoor areas. Similarly, the HID model in [39] is not fully classified.

As all of models are presented in either the exponential or polynomial load model form, they retain no information on the harmonics of the lighting technologies. Recently, there has been considerable effort in characterising the harmonic emissions of CFLs and their impact on power system operation, e.g. [89, 90, 91, 92, 93, 94, 95]. However, the majority of these present results from measurement campaigns or field studies, which clearly offer value and insight into the real world operation of these devices, but do not present values suitable for the load modelling methodologies applied in this research. It should be noted that several of these references, i.e. [91, 92, 93, 94], also include the connection of LED LSs in the analysis. This highlights the need for load models of both lighting technologies.

Table 4.2: Lighting load models identified in literature.

Ref.	Year.	PF_1	Exp. Model		Polynomial/ZIP Model					
			n_p	n_q	Z_p	I_p	P_p	Z_q	I_q	P_q
GIL										
[59]	1982	1	1.6	-	ns	ns	ns	ns	ns	ns
[4]	1993	1	1.55	-	ns	ns	ns	ns	ns	ns
[63]	2008	1	ns	ns	0.64	0.4	0	0	0	0
HIL										
[63]	2008	1	ns	-	0.66	0.39	0	-	-	-
LFL										
[59]	1982	0.91	1.7	5.0	ns	ns	ns	ns	ns	ns
		0.90	1.0	3.0	ns	ns	ns	ns	ns	ns
		1.00	1.0	4.6	ns	ns	ns	ns	ns	ns
[96]	1982	ns	0.96	7.38	ns	ns	ns	ns	ns	ns
[60]	1998	1.00	0.49	0.0	-2.48	5.46	-1.97	0.00	0.00	0.00
[60]	1998	0.98	0.38	1.43	-1.60	3.58	-0.98	0.79	-0.16	0.36
[39]	2002	0.96	ns	ns	-6.27	12.97	-5.69	8.16	-12.26	5.14
[63]	2008	0.86	ns	ns	0.35	0.72	-0.04	0.28	-0.9	0.03
[63]	2008	0.88	ns	ns	0.34	0.71	-0.03	0.20	-0.76	0.02
[63]	2008	0.93	ns	ns	-0.03	1.10	-0.05	0.32	-0.75	0.03
[63]	2008	0.94	ns	ns	0.06	0.97	-0.03	0.24	-0.6	0.02
CFL										
[60]	1998	0.99	0.95	0.31	0.14	0.77	0.09	-0.06	-0.34	-0.60
		0.97	1.03	0.46	0.16	0.79	0.05	0.18	-0.83	-35
[63]	2008	0.91	ns	ns	-0.42	1.50	-0.06	0.66	-1.16	0.06
[63]	2008	0.90	ns	ns	-0.28	1.35	-0.05	0.58	-1.11	0.05
[63]	2008	0.91	ns	ns	-0.30	1.36	-0.05	0.60	-1.08	0.04
HID										
[60]	1998	0.99	1.92	14.43	0.98	-0.03	0.06	29.84	-48.26	14.41
[39]	2002	0.96	ns	ns	0.28	0.38	0.34	2.52	-6.51	4.99

where: ns - not stated

4.3 Compact fluorescent lamps

As mentioned previously, the analysis presented in this thesis is primarily related to CFLs intended for use in residential lighting applications, i.e. for direct replacement of GILs. According to [97], the most common types of GILs used in the residential load sector are of rated powers 40 W, 60 W and 100 W, making up 46%, 46% and 8%, respectively, of estimated stock of GILs in the residential load sector. The current recommendation/trend is to replace 40 W, 60 W and 100 W GILs with 8 W, 11 W and 18 W CFLs, as they have similar values of total output lumens. However, it is shown that all measured CFLs with rated power less than or equal to 25 W have similar electrical characteristics.

4.3.1 Main components of a compact fluorescent lamp

A CFL is a low-pressure discharge lamp that consists of a glass tube coated with phosphors and wire electrodes. The tube, referred to hereafter as the compact fluorescent tube (CFT), is filled with an inert gas containing small amounts of mercury. When a current is supplied to the electrodes, a low intensity arc is created, ionising the mercury to emit photons in the ultraviolet wavelength region. The phosphors on the glass tube will absorb the ultraviolet radiation and emit photons in the visible light spectrum.

This process requires a high 'striking' voltage to initiate the discharge arc and then to reduce/limit the voltage and control the operation to provide a stable light output. This is achieved using a ballast circuit, with Figure 4.2 showing the typical CFL topology.

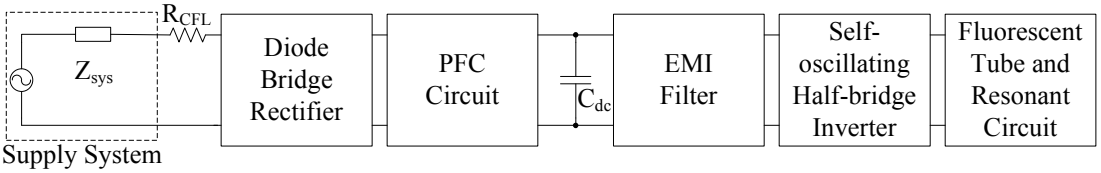

Figure 4.2: General block diagram of CFL electronic ballast and fluorescent tube.

Similar to the power electronics load category, it is not the aim of this thesis to accurately model the full circuit, but some appreciation of the main component blocks will provide more insight into the electrical characteristics of the CFL.

Input resistor

As discussed in Chapter 3, an NTC thermistor is the most common method for inrush current protection in consumer electronic devices. However, from inspection, CFLs usually do not contain an NTC thermistor. In order to protect the bridge rectifier from high inrush currents, a fixed value resistor R_{CFL} is more commonly used.

The presence of the fixed resistance in the bridge rectifier conduction path will result in extra losses, which are deemed as an acceptable trade-off in relation to the additional cost of including an NTC thermistor. The voltage drop on the resistor will also reduce the rate at which the dc link capacitor C_{dc} is charged, helping to reduce the harmonic content of the CFL input current.

Single-phase diode bridge rectifier

In order to convert a single-phase ac supply system voltage to a dc voltage, the front end of the CFL ballast circuit will incorporate an uncontrolled single-phase DBR. Similar to the power electronics load category, a 'smoothing' dc link capacitor C_{dc} is included to provide a dc voltage with a lower ripple component at the rectifier output. The details of this circuit operation can be found in Section 3.2.3.

Power factor correction circuit

Due to the non-linear nature of operation, the DBR circuit will draw input current rich in harmonics from the supply system. Harmonic current emissions in the EU are governed by legislation in [20], where lighting loads are designated as Class C equipment. The Class C limits, shown in Table 4.3, are defined based on the rated power of the device, with devices of rated power greater than 25 W having more stringent limits than lower power devices.

Table 4.3: Harmonic limits for the lighting load category, (Class C) loads given in [20].

Harmonic Number (N)	Class C load rated power		
	$\leq$ 25 W		$>$ 25 W
	Maximum permissible harmonic current		Maximum permissible harmonic current
	(mA/W)	(% of H_1)[1]	(% of H_1)
2	-	-	2
3	3.4	86	30*PF
5	1.9	61	10
7	1.0	-	7
9	0.5	-	5
11	0.35	-	3
$13 \leq n \leq 39$	3.85/n	-	3

where: PF is the true power factor

[1] Additional requirement of this limit is that the current waveform must reach 5% of its peak value before or at 60^o, has peak value before or at 65^o and does not fall to less than 5% of its peak value before or at 90^o (with respect to the supply voltage waveform).

At present, however, PFC circuits are not included in CFLs with rated power below 25 W, as the prescribed limits for their power factors and harmonic emissions can be satisfied by careful selection of the rectifier circuit component values. For devices with rated power greater than 25 W, PFC can be achieved using either passive or active PFC techniques. Of the two, passive PFC techniques are favoured in the competitive CFL market as they are a lower cost solution.

From available measurements, the most widely used PFC technique in CFLs is valley fill PFC. The basic operation principle of the valley fill technique is to increase the conduction period of the device, i.e. to widen the current pulse by extending the time for which current is drawn from the supply. This PFC technique requires only a few passive components and the functionality can be achieved using an additional capacitor and three additional diodes. The typical configuration of the valley fill PFC circuit is shown in Figure 4.3.

When the magnitude of the rectified system voltage v_{rect} is greater than the magnitude of the sum of the two capacitor voltages v_{dc}, current is drawn directly from the supply and valley fill capacitors $C_{dc,1}$ and $C_{dc,2}$ will charge through $D6$ to half the peak supply voltage, i.e. Vp/2. When v_{rect} is less than v_{dc}, $C_{dc,1}$ and $C_{dc,2}$ will discharge through D_5 and D_7 to supply the

load. As the Vp/2 occurs at approximately 30 degrees of the voltage waveform, there will be an extended (theoretical) charging period of 120 degrees around the peak voltage value. Several improvements to this basic circuit are proposed in literature, e.g. [98, 99].

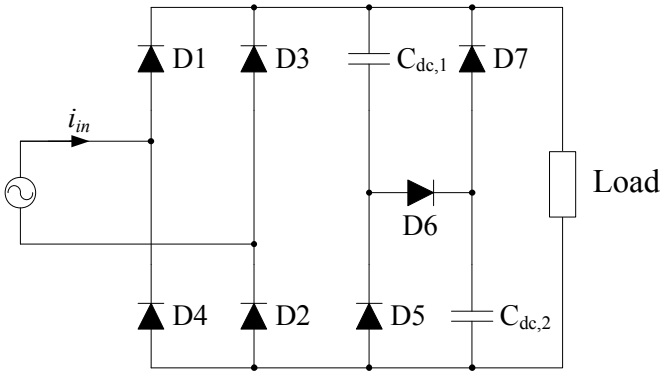

Figure 4.3: Typical configuration of the valley fill PFC circuit.

The measurements of an actual valley fill CFL (with rated power 30 W) are displayed in Figure 4.4, where the harmonic emissions are shown to satisfy the harmonic limits. The current waveform is approximately in phase with the voltage waveform, and the corresponding displacement power factor is close to unity. As the harmonic emissions are also relatively low, these devices operate with a high value of true power factor. A comparison between the different lighting technologies is presented in Section 4.9 and further electrical characteristics of the valley fill CFL are provided in Appendix E.

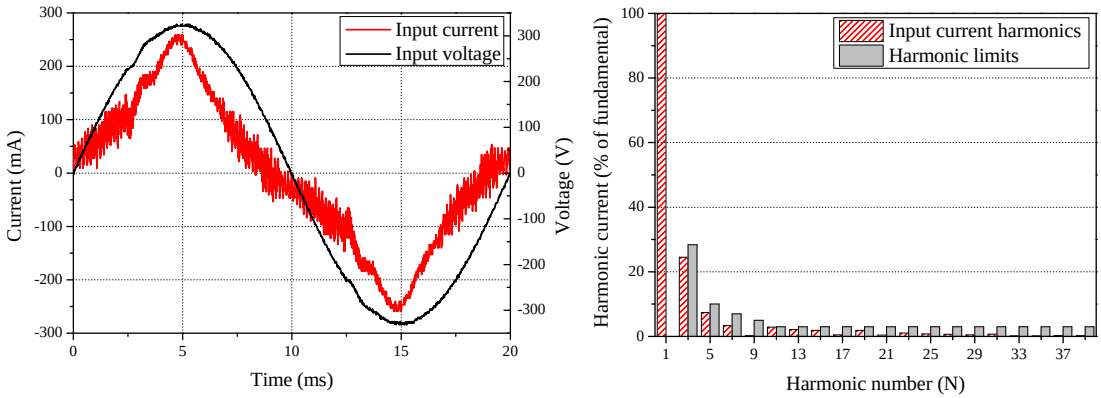

(a) input current waveform (b) associated harmonic content

Figure 4.4: Input current characteristics of the valley fill CFL.

This type of CFL is not expected to be widely used in the residential load sector, so they are not modelled in detail in thesis. However, standard exponential and polynomial/ZIP load model representations of the measured data are included in the final section of this chapter.

EMI filter circuit

CFL electronic ballasts include a bridge inverter, discussed further in the next section, to regulate the current/voltage at the tube terminals. The inverter will operate with a switching frequency typically around 40 - 45 kHz [100] and EMI suppression filters must be used to mitigate any EMI related problems. A typical CFL EMI filter is shown in the full circuit schematic in Figure 4.5, represented by components L_{EMI} and $C_{+,-}$ (which also form part of the half-bridge inverter circuit) [101]. However, similar to the power electronics load category, the EMI filter components are small and, therefore, do not have any significant influence on the CFL load models (in the considered frequency range).

Half-bridge inverter

To convert the dc waveform back to ac to operate the tube, a half-bridge inverter is utilised. This circuit will control the lamp operation at a high frequency, typically between 40 - 45 kHz, as this significantly improves the efficiency of the tube. According to [102], the vast majority of CFLs available in EU market incorporate a bridge inverter in a simple chopper topology, consisting of two semiconductor switches controlled by a driving circuit. Gate drive pulses for the inverter switches can be produced either using an IC, or a specifically designed self-oscillating circuit topology. Self-oscillating bridge inverters require only passive electrical components and are considerably cheaper than the IC-controlled ones and are almost always used in residential CFL applications. The IC-controlled electronic ballasts, however, can be found in larger numbers in LFL applications, as they can provide additional beneficial features (e.g. prolonged lifetime, detection of lamp failure, dimming, etc.).

Figure 4.5 shows a typical CFL circuit with a self-oscillating half-bridge inverter. The circuit incorporates a toroid, which, due to its non-linear saturation characteristic, allows the circuit to oscillate in the designed frequency range (further details on the inverter circuit operation can be found in [102]).

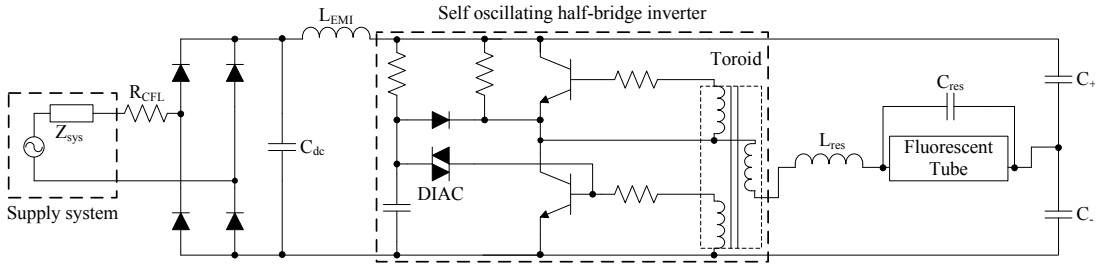

Figure 4.5: Schematic of typical modern CFL circuit with a self-oscillating ballast [18].

Resonant circuit

To initiate the conduction/discharge process in the fluorescent tube, a high 'striking' voltage, typically between 500 V and 1200 V [102], is required. The standard method of starting the lamp is to use a resonant circuit, where the tube acts as a resistance and forms an RLC resonant circuit with L_{res} and C_{res}. On start-up, the tube has a very high resistance and approximates an open circuit, and a lightly damped resonant circuit is formed by the series connection of L_{res} and C_{res}. The resonant operating conditions will influence a rapid increase of the voltage across C_{res}, until the striking voltage is achieved and the tube starts to conduct. After reaching steady state operating conditions, the tube effectively turns the resonant circuit into a series LR circuit.

4.4 Modelling of compact flourescent tube

As previously discussed, the CFT represents an open circuit until a sufficient striking voltage is applied to initiate the discharge process. The resulting ionisation of the CFT will result in the tube displaying a negative resistance characteristic, i.e. as current flow through the tube increases, the tube resistance reduces. This is clearly visible in Figure 4.6.

Although there has been a considerable amount of previous work on the analytical representation of fluorescent tubes (e.g. [103, 104, 105, 106, 107, 108, 109, 110, 111]) this was mainly related to the ballast design process and not for the purpose of power system load modelling. Various approaches have been used to model the fluorescent tubes used in CFLs and LFLs, with Table 4.4 giving an overview.

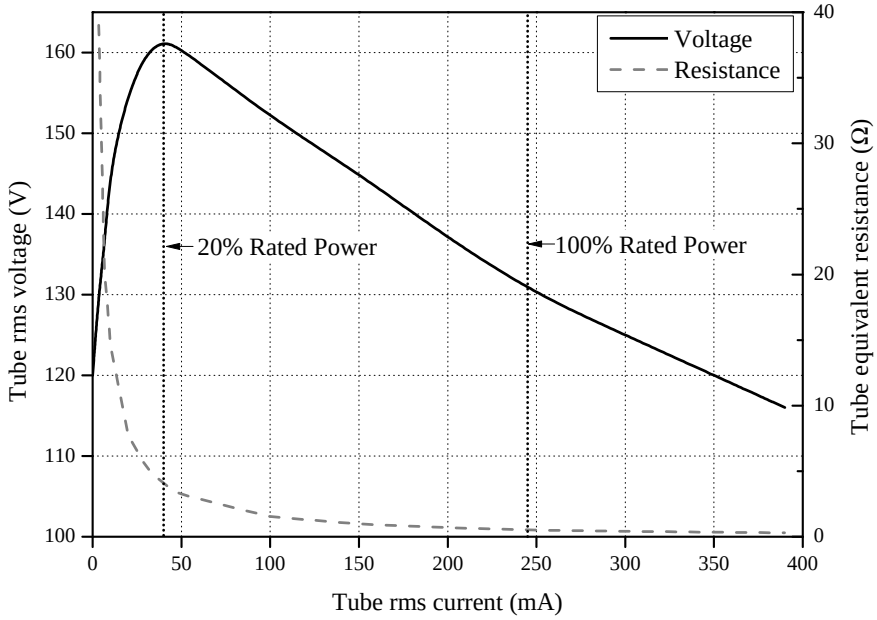

Figure 4.6: Measured V-I tube characteristics for a 32W T8 LFL [105].

Table 4.4: The LFL and CFL tube models identified in literature.

Ref	Type	Year	Tube model	Further information
[103]	LFL	1992	$v_T(t) = \left(\frac{V_{T,DC}^2}{P_T + P_{T0}}\right) i_T(t)$	$V_{T,DC}$ is the dc tube voltage, P_T is the average tube power, P_{T0} is the average tube power offset, i_T and v_T are the instantaneous tube current and voltage.
[103]	LFL	1992	$v_T(t) = A i_T(t) + B i_T^3(t)$	i_T and v_T are the instantaneous tube current and voltage. Coefficients $A, B = \alpha (P_T + \gamma)^{\beta}$ are calculated from measurements, where P_T is the average tube power and parameters α, β and γ determine curves for fitting coefficients.
[104]	CFL	1993	$V_T = \frac{1}{A + B I_T}$	I_T and V_T are the tube rms current and voltage. Coefficients A and B are calculated from measurements as constant values: A = 7.8e-3, B = 2.01e-5.
[105]	LFL	1995	$v_T(t) = \left(A + \frac{B}{I_T}\right) i_T(t)$	v_T and i_T are the instantaneous tube voltage and current. Coefficients $A = (V_{100} - V_{20}) / (I_{100} - I_{20})$ and $B = (V_{20} - I_{20}) A$ are calculated from measurements, where V_{100}, I_{100} are tube rms voltage and current at full power, while V_{20}, I_{20} are tube rms voltage and current at 20% rated power.
[106]	LFL	1998	$v_T(t) = A i_T(t) + (B i_T(t))^3$	i_T and v_T are the instantaneous tube current and voltage. Coefficients $A, B = \alpha_1 P_T^{-1} + \alpha_2 + \alpha_3 P_T + \alpha_4 P_T^2$ are calculated from measurements, where P_T is the average tube power and α_{1-4} are the Laurent series coefficients.
[107]	LFL	1999	$v_T(t) = \frac{A_0 + A_1 e^{-A_2 I_T} - A_3 e^{-A_4 I_T}}{I_T} \times i_t$	v_T and i_T are the instantaneous tube voltage and current, I_T is the rms lamp current. Coefficients A_{0-4} are calculated from measurements as constant values, based on the tube power.

[108]	LFL/CFL	2000	$R_T = \frac{A}{P_T^C} - B$	P_T is tube rated power; R_T is tube equivalent resistance. Coefficients A, B and C are constant and calculated from measurement of lamps with $P_T \leq 25$ W, average value for CFL: A = 2.83, B = 1.83. No value is given for C.
[109]	CFL	2003	$\ln(R_T) = A\ln(I_T) + B$	I_T is the tube rms current, R_T is tube equivalent resistance. Coefficients A and B are constant and calculated from measurements; 15 W: A = -1.34, B = 3.76; 20 W: A = -1.43, B = 3.69; 26W: A = -1.45, B = 3.96.
[110]	LFL	2005	$R_T = Ae^{BP_T} + Ce^{DP_T}$	P_T is tube power; R_T is tube equivalent resistance. Coefficients A-D are constant and calculated from measurements for 32 W lamp.
[111]	CFL	2007	$V_T = A_0 + A_1 e^{-A_2 I_T} - A_3 e^{-A_4 I_T}$	V_T and I_T are the tube rms voltage and current. Coefficients A_0-A_4 are constants and calculated from measurements: A_0 = 69, A_1 = 156, A_2 = 10, A_3 = 276, A_4 = 100

From the data in Table 4.4, there has clearly been a large interest in the modelling of fluorescent tubes. The majority of the existing models present relationships between instantaneous current and voltage, while some of the more recent references present only the equivalent resistance. There is a large variation in the form of the implemented functions, which include: linear relationships, e.g. [105], higher order quadratic equations, e.g. [103, 106], exponential functions [111] and natural logarithmic relationships [109]. Furthermore, several models present coefficients as a function of tube rated power, which suggests that there is a correlation between the two.

It should be noted that the tube models from the previous work in Table 4.4 are usually obtained after the tubes were removed from the ballasts and connected to a controllable high frequency voltage source. The tubes are then operated at different powers by adjusting the applied square-wave voltages. However, in CFLs, the tube and ballast are integrated, which clearly suggests that the CFT characteristics for developing the corresponding load model should be obtained without detaching the tube from the ballast.

4.4.1 Measured characteristics of modern CFTs

The fluorescent tube model presented in this thesis is obtained with the tube connected to its ballast, as this is the case in real CFL applications. For the range of variations of input ac supply voltage considered in the analysis (between 0.8 pu and 1.2 pu), the minimum tube power is around 70% of the lamp rated power, i.e. well above the operating region with pronounced non-linearity. Therefore, the CFT models developed in this thesis do not consider tube characteristics at low powers, as the ballast-controlled tube will not enter this region during normal operation. This method of tube characterisation results in the development of a simplified CFL model, as the tube will never enter certain operating regions if controlled by the integrated ballast circuit. Some of the previous research modelled the tubes in the operating region between 5% and 120% of their rated powers.

In the experimental results presented in this thesis, a fully controllable voltage source ([73], with THD $\leq$0.5%) is used to supply the ballasts connected to the CFT with voltage variations from 0.8 pu to 1.2 pu in 0.05 pu steps of the nominal 230 V, 50 Hz supply. A sample of the measured ballast circuit output, measured at the electrodes which connect the CFT to the ballast circuit, is available in Figure 4.7, from which several interesting observations can be made. First of all, the tube current and voltage characteristics have an operating cycle of 100 Hz, i.e. twice the supply frequency. During this cycle, the maximum value of tube current coincides with the minimum value of voltage. However, as the increase in current is much more pronounced than the change in the voltage waveform, the power drawn by the tube will exhibit variations across the operating cycle. With respect to the rated power of the lamp, the power drawn by the CFT will vary between approximately 0.74 pu to 1.14 pu, with operating points near A and D providing the lower values and B and C providing the higher power values.

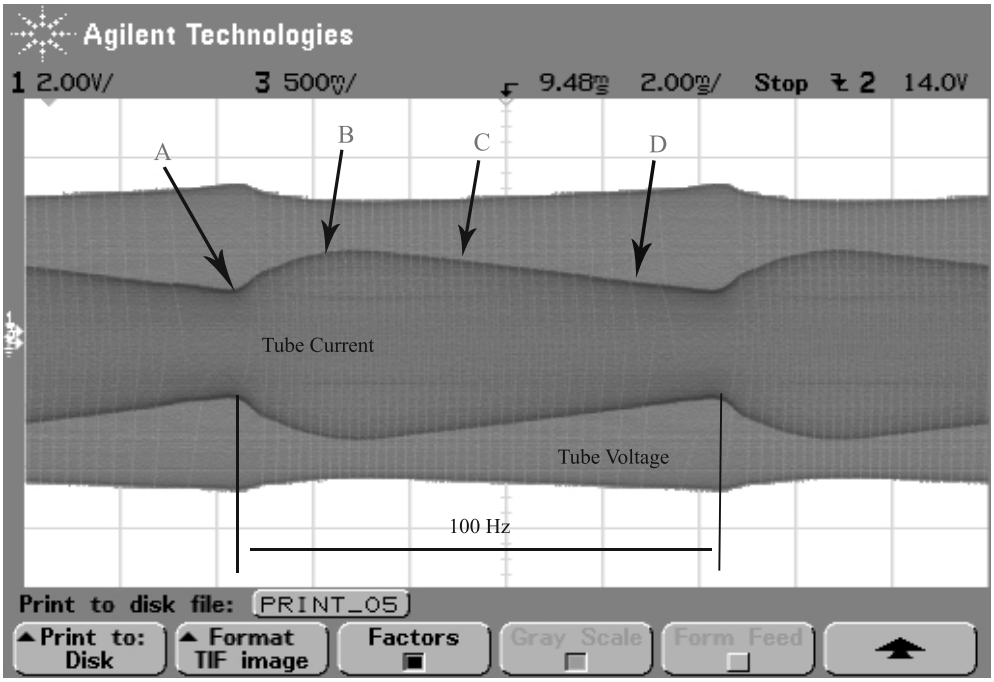

Figure 4.7: Measured instantaneous voltage and current at the terminals of an 11 W CFT [18].

The rms values of the tube voltage and current are calculated from the measured tube instantaneous current and voltage waveforms for the considered supply voltage conditions, with the tube rms voltage plotted as a function of tube rms current for lamps with rated power less than or equal to 25 W in Figure 4.8. The power demand of the tube will increase as the magnitude of the supply voltage increases.

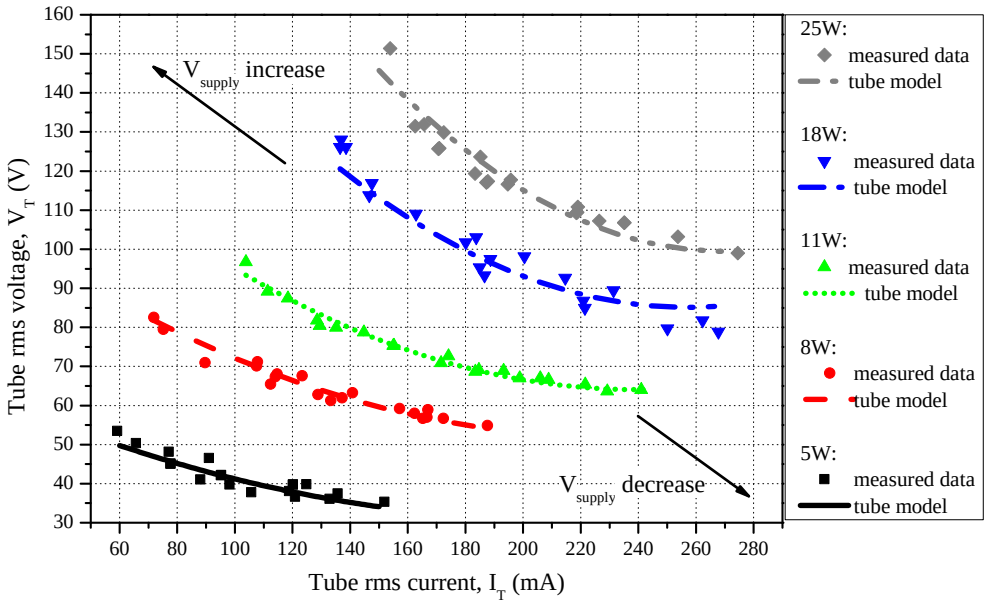

Figure 4.8: Measured V-I characteristics and models of different rated powers of CFTs.

4.4.2 Analytical formulation of CFT model

The data in Figure 4.8 shows that for the considered 0.8 pu to 1.2 pu range of input ac supply voltages, the V-I characteristics of the measured tubes still exhibit some non-linearity. Therefore, a new CFL steady state tube model was proposed in a simple quadratic form [18]:

$$V_T = AI_T^2 + BI_T + C \tag{4.1}$$

where: V_T, I_T are the tube rms voltage and current, and A, B and C are tube coefficients.

A 'least-square method' in MATLAB was used to fit the model given by (4.1) to the measured data, with values for coefficients A, B and C presented in Table 4.5. These results are shown in Figure 4.8, where results of the analytical CFT model are plotted with thick lines. The model is able to reproduce the characteristics of all measured tubes with rated power less than or equal to 25 W, which validates the model and also demonstrates that the electrical characteristics of CFTs in typical residential applications are comparable. This is illustrated in Figure 4.9, where the original values from Figure 4.8 have been normalised using the rms value of the tube current and voltage as measured at nominal supply voltage as the base values.

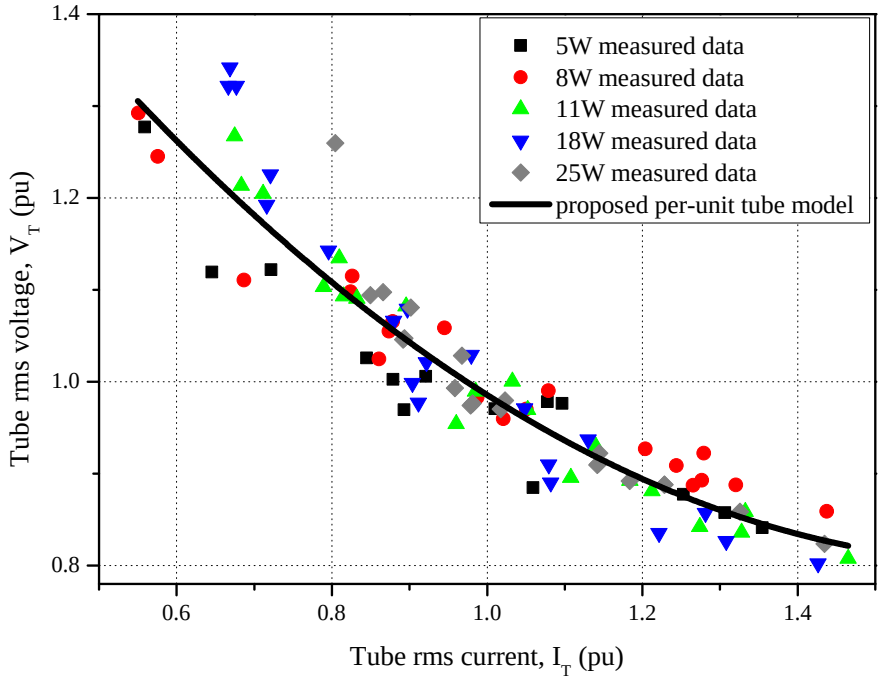

Figure 4.9: Normalized V-I characteristics and proposed generic pu CFL tube model.

This clearly indicates a relationship between the individual tube coefficients in (4.1) and the rated power. This relationship can be expressed by an algebraic equation with a single exponent. Although using this form will introduce an error in the tube model, this can be used to approximate the tube coefficients of CFTs not listed in Table 4.5.

Table 4.5: Coefficients of the proposed steady-state CFL tube model, with 8, 11 and 18 W values taken from [18].

CFL rated power	Coefficient		
	A	B	C
5	812	-335	69.5
8	1276	-550	114
11	1546	-744	154
18	2317	-1278	256.5
25	3292	-1727	328.5
Generic	$196P^{0.87}$	$-67P^{1.012}$	$16.46P^{0.9354}$
where: P is the CFL rated power in W.			

4.5 Equivalent circuit model of CFL load

The developed generic tube model can be combined with the detailed full circuit ballast model developed in previous research [18] to build a full circuit CFL model. This full circuit model may then be reduced to an equivalent circuit model by analysing the current and voltage characteristics at the dc link. This allows for the creation of an equivalent resistance which can be used directly in the equivalent circuit form, and the analytical model derivation (in Section 3.4.1).

The previously introduced form of the equivalent circuit model was separated into two regions based on the charging characteristics of the dc link capacitor. Therefore, a similar analysis is required for the CFL load category. A detailed discussion of these operating characteristics has been presented in the previous research, with further information available in [18], and is not repeated here. However, a brief summary is provided to offer insight into the final result of this conversion, which are ultimately presented in Figure 4.11.

The instantaneous dc link voltage and current waveforms are shown in Figure 4.10. From the envelope of v_{dc} it is clear that the current during the charging cycle is not constant, like the value during discharge. However, the oscillations in i_{dc} are not constant frequency and cannot be directly included in the equivalent representation. Instead, the cycle-by-cycle rms value of the current oscillations are calculated using a sliding rms calculation window. Comparing these rms values against the equivalent rms value of the dc link voltage, calculated for the specific current oscillation cycle, allows for the calculation of the equivalent resistance.

More detailed results are shown in Figure 4.11, which displays the change in equivalent resistance with variation in the supply voltage magnitude. There are two areas of interest in the equivalent resistance curve. The upper boundary of this curve, which displays an approximately linear function, is the period when C_{dc} is discharging. The lower boundary of the equivalent resistance represents the load characteristic when C_{dc} is charging from the supply system. Over the simulated voltage range, this section of the equivalent resistance curve does not exhibit a

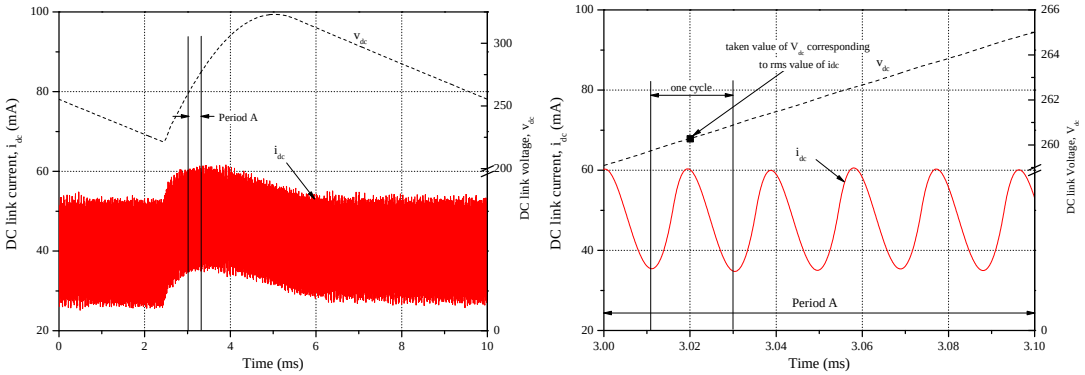

(a) full cycle **(b)** zoomed in plot

Figure 4.10: Simulated CFL dc link current and voltage waveforms [18].

linear relationship with v_{dc}, and the line will arc slightly. However, within each voltage step, the value is quite linear for the majority of this period. These two regions are connected by two transition stages, as the rectifier circuit moves from charging to discharging operation.

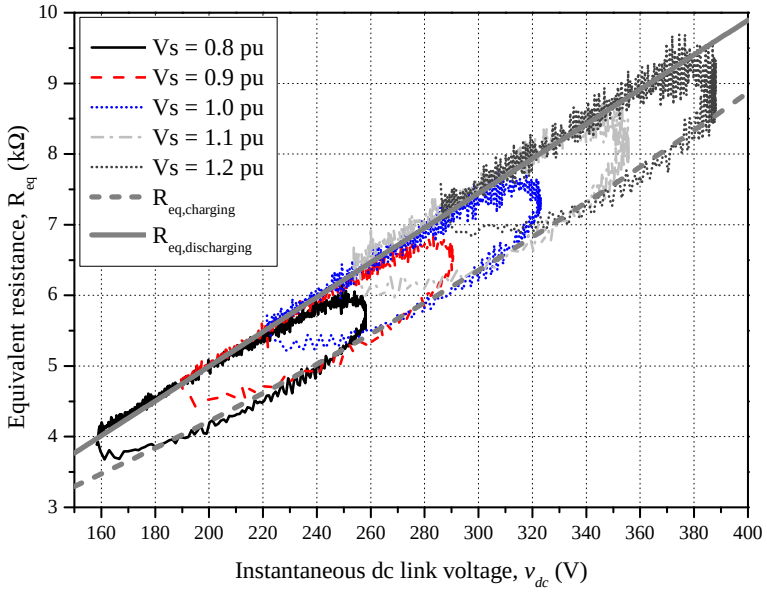

Figure 4.11: DC link characteristics and equivalent resistance of the generic CFL model.

These two regions can be represented as a set of two analytical functions for equivalent resistance. In order to provide an accurate representation of the two regions of interest, the transition data points are excluded from the curve fitting routine. A linear polynomial function is selected to represent the discharge period, while a quadratic function is selected to model the charging period. A higher order quadratic function was also fitted to the data, but will not improve the fit of this dataset. The results of this are plotted with the original simulated dataset in Figure 4.11, with values given in (4.2) and (4.3) overleaf.

$$R_{eq,charging} = 0.01928v_{dc}^2 + 11.69v_{dc} + 1110 \tag{4.2}$$

$$R_{eq,discharging} = 24.5v_{dc} + 94.29 \tag{4.3}$$

where: v_{dc} is the instantaneous dc link voltage and $R_{eq,charging}$ and $R_{eq,discharging}$ are the equivalent resistance during charging and discharging stage of the dc link capacitor.

Although the value of the second-order term is small, the value of the dc link voltage is high and this term cannot be neglected. However, this reflects the almost linear nature of the charging characteristic. Analysis of Figure 4.11 reveals that during both the charging and discharging cycles, the current at the dc link has two almost constant values. As it is during the charging stage of the cycle that the rectifier is drawing current from the supply, it is this stage that will determine the electrical characteristics for power system analysis. This suggests that the CFL load will present a constant current load to the power system, which is discussed further in the subsequent text.

4.5.1 Validation of CFL equivalent circuit model

The equivalent resistance developed in previous research is implemented in the analytical model developed for power electronics load category. The derivation of this model is discussed in Section 3.4.1 in the previous chapter and is not repeated here. The model is configured with values of a measured 11 W CFL to provide a comparison with measured data and the new formulation for the equivalent resistance. A comparison of the input current waveforms is presented in Figure 4.12 and it is observed that the analytical implementation of the equivalent circuit model is able to accurately reproduce the instantaneous input current waveform and associated harmonic content. As the voltage waveform of the controllable voltage supply was distorted, this was decomposed by Fourier transform into the harmonic frequencies, reconstructed and supplied to the analytical model, to allow for a fair comparison of the data.

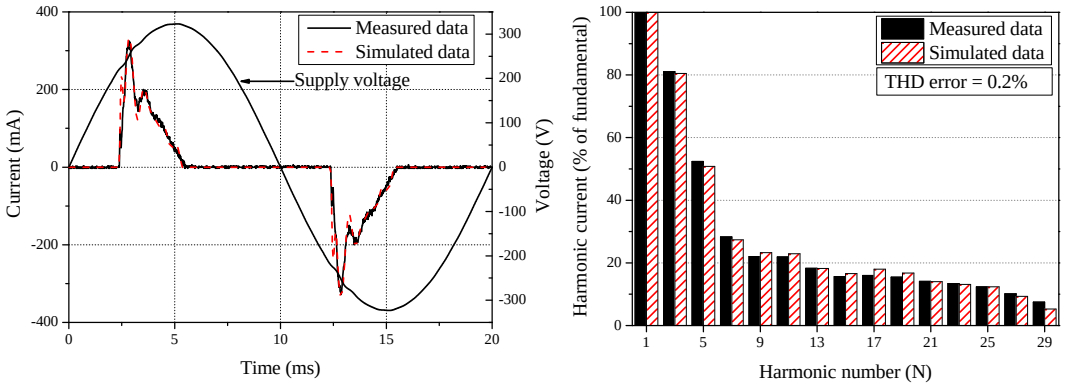

(a) input current waveform (b) associated harmonic content

Figure 4.12: Comparison of input current waveforms and associated harmonic content between the equivalent circuit CFL model and the measured data at 1 pu voltage.

A more detailed comparison of all electrical characteristics is presented in the accompanying Figure 4.13. This confirms the ability of the developed analytical model to retain the electrical characteristics of the measured CFL over the specified voltage range. A maximum error of 5% is observed towards the lower boundaries of the voltage range. This is deemed as an acceptable error in the simulation result as a small error is present in the developed full circuit model, and a further error will be introduced in the reduction of the full circuit model to the equivalent resistance.

However, the slight reduction in accuracy is far outweighed by the saving in simulation time. Due to accurate modelling of magnetic properties of the toroid and small simulation time-step required to capture the 45 kHz switching frequency, the full circuit model will take several tens of minutes to produce results. The simulation time for the analytical model is approximately 0.03s, even with a simulation time step of 10 μs. Therefore it is a much more powerful tool for the development of aggregate load models for power system analysis.

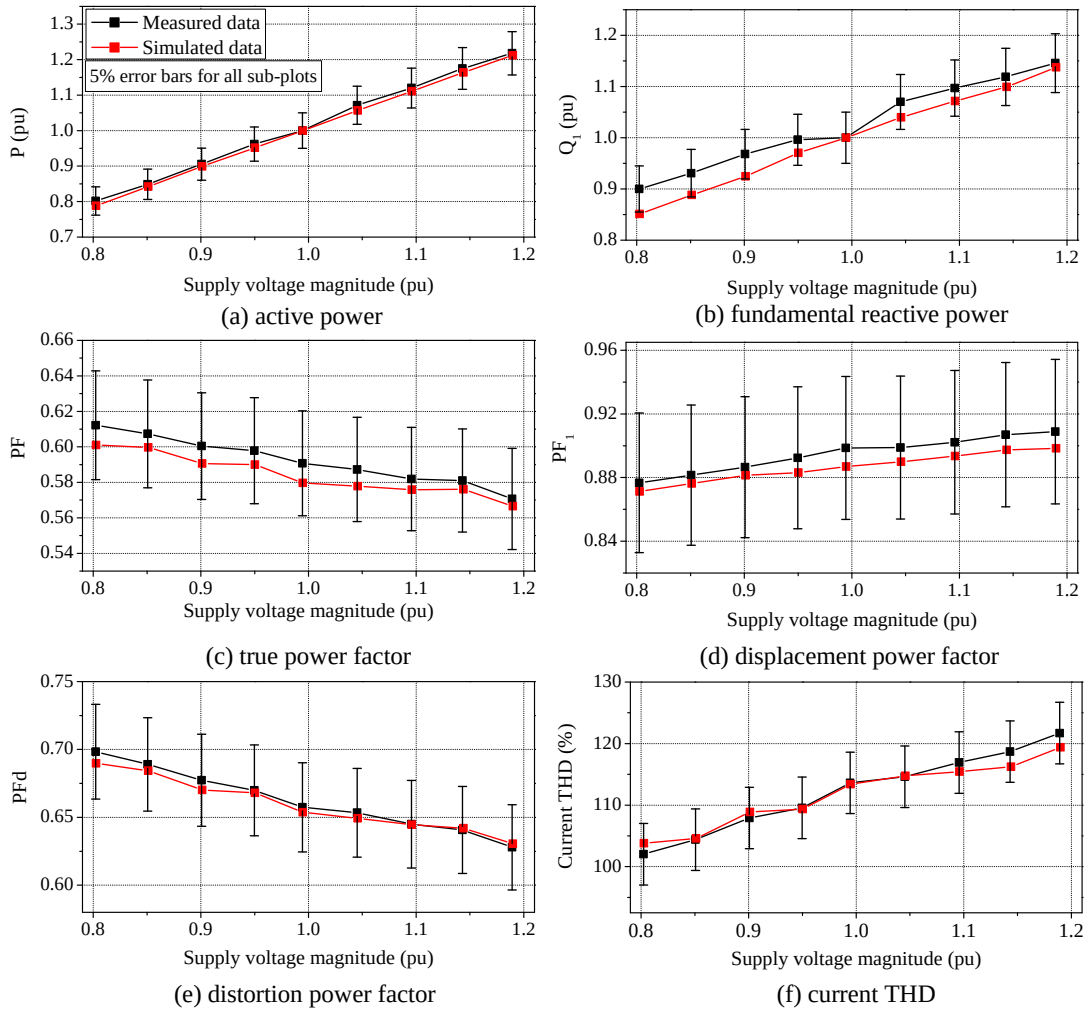

Figure 4.13: Comparison between the electrical characteristics of the equivalent circuit CFL model and the measured data.

The P-V characteristics confirm the constant current hypothesis which was displayed at the dc link. The (fundamental) reactive power characteristics are capacitive, which was also shown in the previous CFL models, and the characteristics of the measured lamp lie between constant power and constant current load types. A more detailed comparison with the CFL models developed in this research and the existing CFL models is presented in Section 4.10.

4.6 Generic model of CFLs

To model CFLs, typical values of the equivalent circuit parameters must be defined. The methodology applied in this section is similar to that presented for the power electronics load category, and begins by considering the individual influence of each component on the electrical characteristics of the modelled CFL. The possible ranges of component values are then combined to define the expected boundaries, which are verified against measured data.

This analysis uses measurements and inspection of CFL ballasts of rated power from 5 W to 25 W to illustrate the electrical characteristics of these loads are comparable. However, as CFLs of rated power 8 W, 11 W and 18 W are much more prevalent in the residential load sector, more emphasise is placed on these devices.

4.6.1 Input resistance

From the inspection of available CFL ballasts and measuring of R_{CFL}, it was found that typically 5 W, 8 W, 11 W, 18 W and 25 W CFLs have resistors of value 6 Ω, 9 Ω, 10 Ω, 15 Ω and 20 Ω, respectively. This suggests that the value of R_{CFL} is roughly correlated to the rated power of the CFL. MATLAB curve fitting routine is used to determine the relationship:

$$R_{CFL} = 2.868 + 0.6851 P_{CFL} \tag{4.4}$$

The same arbitrary range of plus minus 10% considered for the power electronics load category was again selected for this component in the equivalent CFL model. This accounts for resistor manufacturing tolerances and also design variations between different CFL manufacturers. As shown in Figure 4.14, this parameter does not have a significant effect on the input current waveform of a typical CFL. Reducing this value will increase the oscillation at the peak of the current waveform, but this is not reflected in a change in harmonic currents in the analysed harmonic frequency range. The corresponding changes in power factor values are also neglible.

This effect is due to the large value of the dc link capacitance, introduced in the following section, which will dominate the input impedance of the equivalent circuit during the charging cycle.

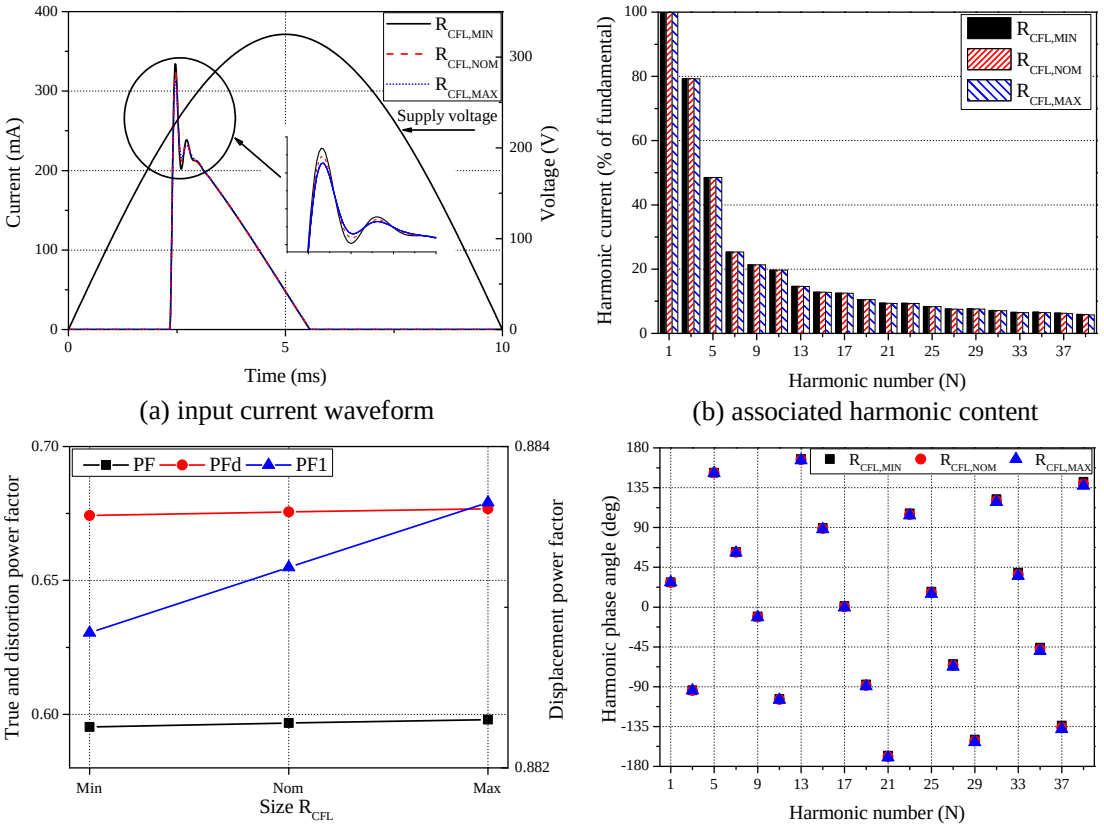

(a) input current waveform

(b) associated harmonic content

(c) power factor values

(d) current harmonic phase angle

Figure 4.14: Influence of R_{CFL} on the input characteristics of the generic CFL.

4.6.2 DC link capacitance

Previous analysis in [18] has shown that size of C_{dc} is selected as a trade-off between satisfying legislative harmonic limits, given in [20] and discussed in Section 4.3.1, and device performance. A smaller value of C_{dc} will stretch the input current waveform, i.e. it becomes more sinusoidal, lowering the harmonic content. However, a smaller value of C_{dc} will increase the ripple content of the dc link voltage which will place greater electrical stress on the CFT. These two considerations are used to define the upper and lower boundaries of C_{dc} shown in Figure 4.15, which were obtained using the detailed full circuit model in [18].

Although the values and ranges are shown to increase, the relative change is proportional to rated power of the CFL. This suggests that the selected value of C_{dc} can be correlated to the rated power of the lamp. After the extensive review of the available literature, several manufacturers' specifications and design data and inspection of a number of actual CFLs, it was found that the size of C_{dc} is directly related to the rated power of the CFL. For CFLs with rated powers from 5 W to 25 W, the typical values for C_{dc} are between 1 μF to 5.6 μF (ranging between 0.2 μF/W to 0.26 μF/W). The measured data are shown in Figure 4.15 as hollow circles.

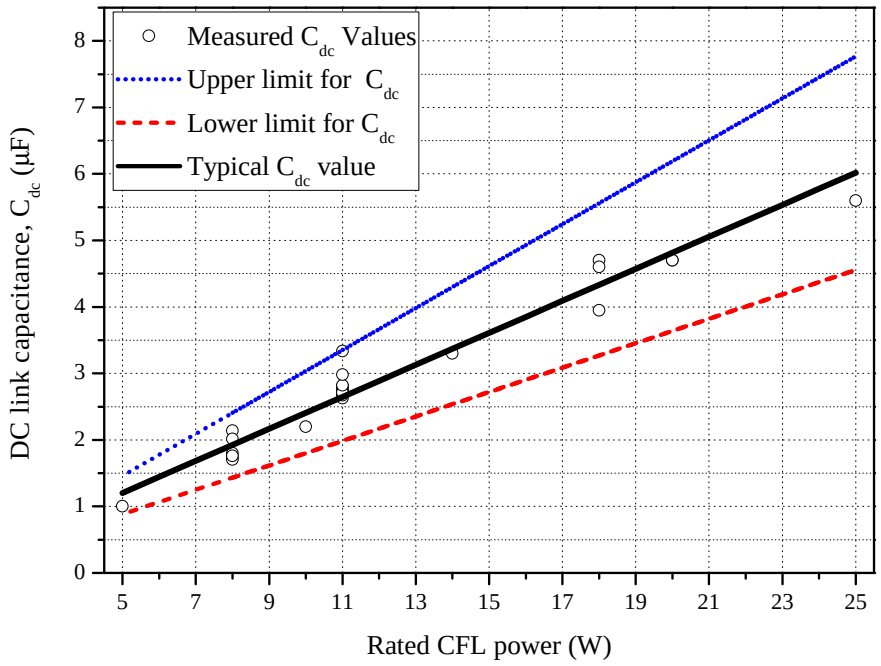

Figure 4.15: Two general limits and measured values of dc link capacitors for CFLs with rated powers less than or equal to 25 W.

All measured values lie within the predetermined boundaries. The linear line of best fit through the measured data is actually almost identical to the geometric mean of the two boundaries. Selecting one value from this curve (P_{CFL} = 11 W and C_{dc} = 2.67 μF), allows for the calculation of the corresponding per-unit value of C_{dc}:

$$X_{C_{dc}} = \frac{\frac{1}{\omega C_{dc}}}{\frac{V_{rms}^2}{P_{rated}}} = \frac{\frac{1}{\omega 2.67\times^{-6}}}{\frac{230^2}{11}} \approx 0.25pu \tag{4.5}$$

where: V_{rms} is the rms value of supply voltage, P_{rated} is the rated power of the modelled CFL and ω is the angular frequency of the supply voltage.

As with the power electronics load category, a range of plus/minus 20% is assumed for this parameter. This value is based on the manufacturing tolerance for the electrolytic-type capacitors which, from inspection, are universally used in CFLs found in the residential load sector. This tolerance is used to define the upper and lower boundaries for the C_{dc} range, which are displayed in Table 4.6. This proposed range is slightly narrower than that defined by the upper and lower boundaries in Figure 4.15, which stipulate the extreme limits of device operation. However, it is unlikely that significant numbers of CFLs will be designed to either of these specifications. As shown, the majority of values lie close to the mean value, which verifies this assumption. The fact that the majority of measured data points are clustered around the mean also suggests that a normal distribution is acceptable for representing the possible variations in the values of this component, and the standard deviation value is also included in Table 4.6.

Table 4.6: Assumed range of dc link capacitance tolerance values for CFL, illustrated by 11 W CFL.

Model value	Capacitor size		σ	
	(μF)	(pu)	(μF)	(pu)
Min	2.14	0.31	$\pm$ 0.18	$\pm$ 3.75
Nom	2.67	0.25		
Max	3.2	0.21		

The previous discussion of harmonic legislation and selection of C_{dc} for CFLs indicated that the size of dc link capacitor will have a significant influence on the harmonic emissions of CFLs. This is confirmed in Figure 4.16. It is clearly visible that even for the modest range, there is a significant change in harmonic magnitude and phase angle. As the size of C_{dc} increases the input current waveform will shift to the right, becoming more in-phase with the supply voltage. This is reflected in the corresponding increase in displacement power factor. However, the increasing harmonic content will act to reduce the true power factor of CFLs. It should be noted that for the considered range of C_{dc} values, the harmonic emissions are still within the harmonic legislation in [20].

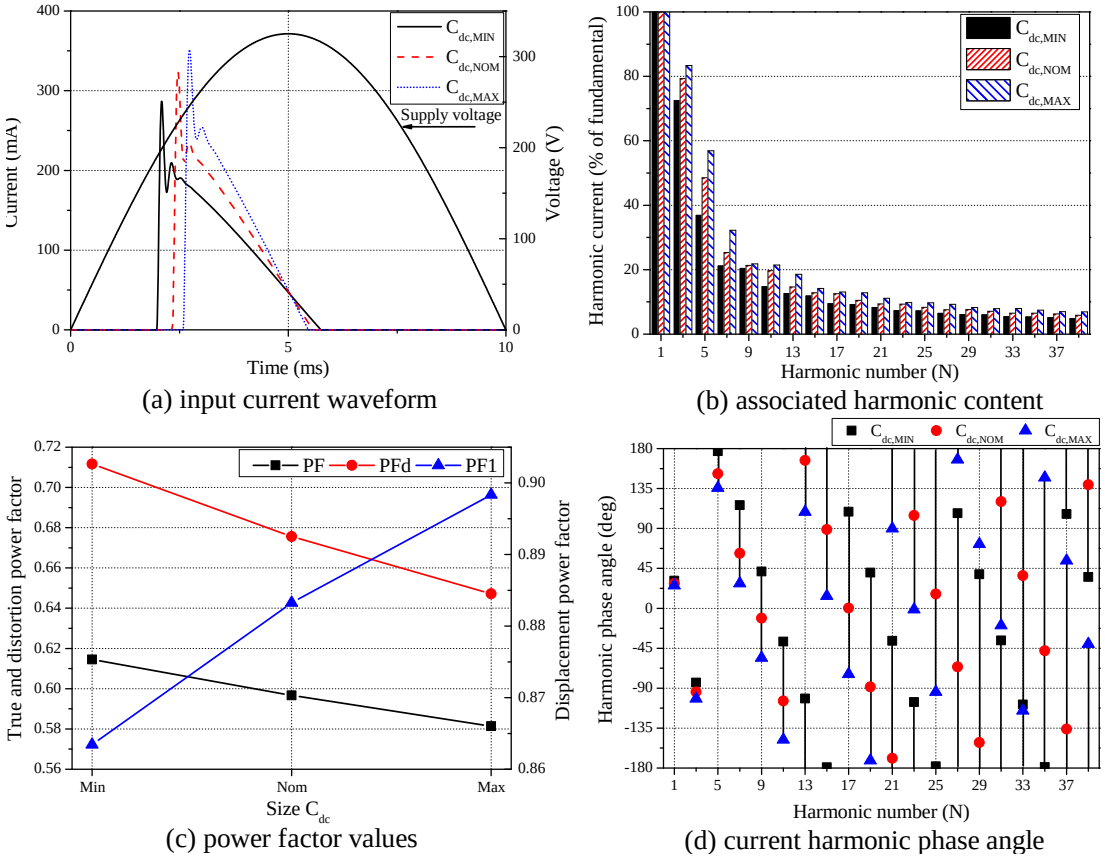

(a) input current waveform

(b) associated harmonic content

(c) power factor values

(d) current harmonic phase angle

Figure 4.16: Influence of C_{dc} on the input characteristics of the generic CFL.

4.6.3 Tube rated power

As shown previously, the power drawn by the CFT will vary during fundamental frequency voltage. This change is captured within the expression of equivalent resistance (4.2) - (4.3). However, there will also be variations in the tube rated power due to differences in the tube and the operating conditions of the ballast circuit. From measurements performed during the characterisation of the CFT, the average power drawn by the tube during the fundamental supply frequency cycle was found to vary between approximately 0.87-1.02 pu, with respect to the rated power of the CFL, at nominal supply voltage.

The impact of varying this parameter on the electrical characteristics of the generic CFL are shown in Figure 4.17. As the rated power of the tube/inverter circuit increases, the charging stage of the CFL will begin earlier in the supply voltage waveform. A higher rated power at the dc link will present a lower resistance and, as the dc link voltage value does not change, a higher current is drawn from the supply system. As the conduction period of the rectifier increases as the value of P_{tube} increases, the harmonic emissions of the input current waveform are reduced. There is some dispersion in the harmonic phase angles, but this is not as pronounced as for variations in C_{dc}.

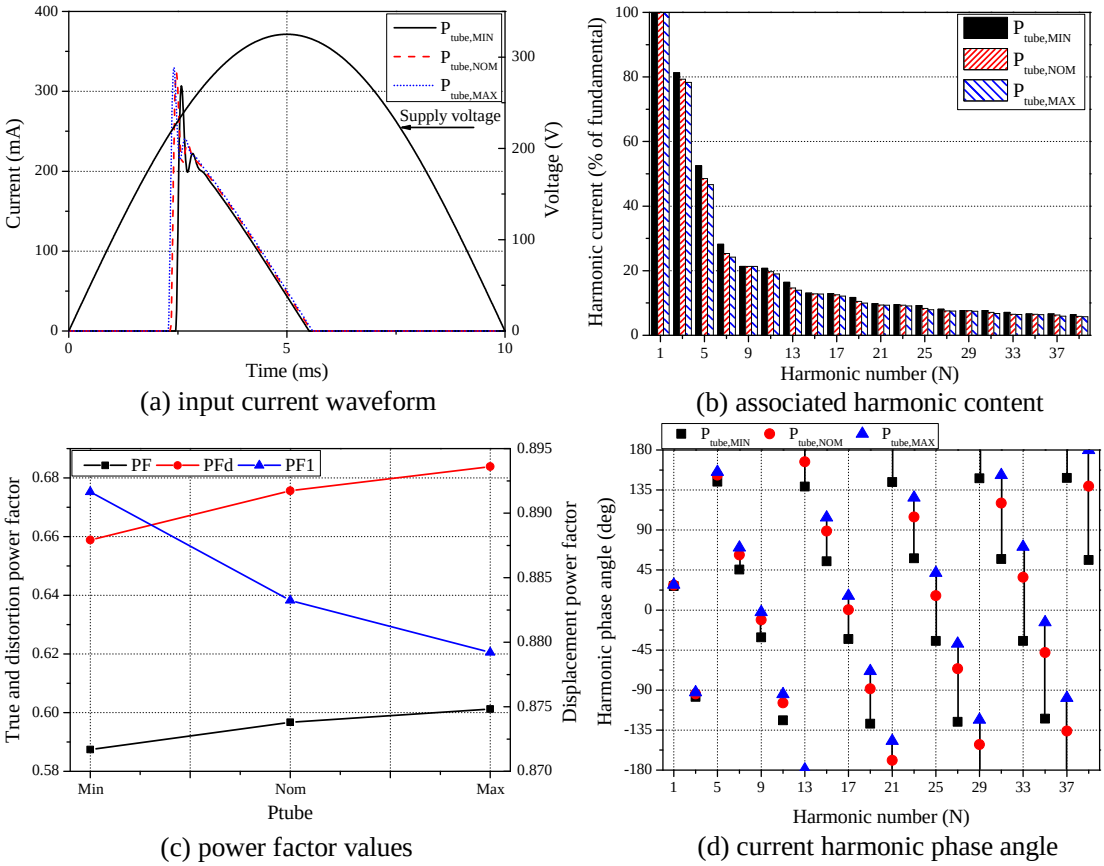

(a) input current waveform

(b) associated harmonic content

(c) power factor values

(d) current harmonic phase angle

Figure 4.17: Influence of P_{tube} on the input characteristics of the generic CFL.

4.6.4 Sensitivity of CFL load models to parameter variation

The previous analysis has investigated the influence of each equivalent circuit parameter on the input electrical characteristics of the CFL. The impact of the input resistance was shown to be negligible, similar to the power electronics load category. The component with the largest influence on the input characteristics is the dc link capacitor C_{dc}. As the capacitor value increases, the input current waveform will shift to the right, similar to the effect observed for the power electronics load category. However, in the case of CFLs, this will increase the harmonic currents as it reduces the conduction period of the device, therefore, a higher current pulse is required to transfer the required energy to the load. The other parameter in the CFL equivalent circuit (the power drawn by the bridge inverter/CFT) will have only a small influence on the electrical characteristics.

To confirm the range of parameters, the developed CFL model is compared against measurements of a number of actual CFLs. Similar to the analysis performed for the power electronics load category in Section 3.5.5, the CFL model is configured with the maximum, mean and minimum value of each parameter. All combinations are simulated to determine the corresponding maximum and minimum boundary of each electrical characteristic across the entire voltage range. Unlike the power electronics load category, the power drawn by individual CFLs is relatively constant during typical operating conditions (neglecting device start-up and deterioration due to aging effects), and the presented results can also include a comparison for the values of active and (fundamental) reactive power.

It should be noted that the measured CFLs were found to slightly distort the supply voltage waveform. To ensure that the comparison is as representative as possible, this waveform was decomposed into its sinusoidal components by Fourier transform and reconstructed for supplying to the model. This process was repeated for every measured CFL, although the THD levels were similar. Therefore, the simulated boundaries from the generic CFL model presented in Figure 4.18 are the result of the generic CFL model run with a number of distorted voltage waveforms.

From the results of this comparison, there are several interesting observations. Most importantly, all measured values, with only a few exceptions, lie within the simulated boundaries, thus verifying the proposed parameter value ranges. As Figure 4.18 includes measured data of 8 W, 11 W and 18 W CFLs, which are assumed to be the main CFLs used in the UK residential load sector, this suggests that the electrical characteristics of these CFLs are comparable. Although there are differences both within and between the different rated powers, this is an important result for the research as it allows for the use of the proposed generic CFL model to represent CFLs in this power range.

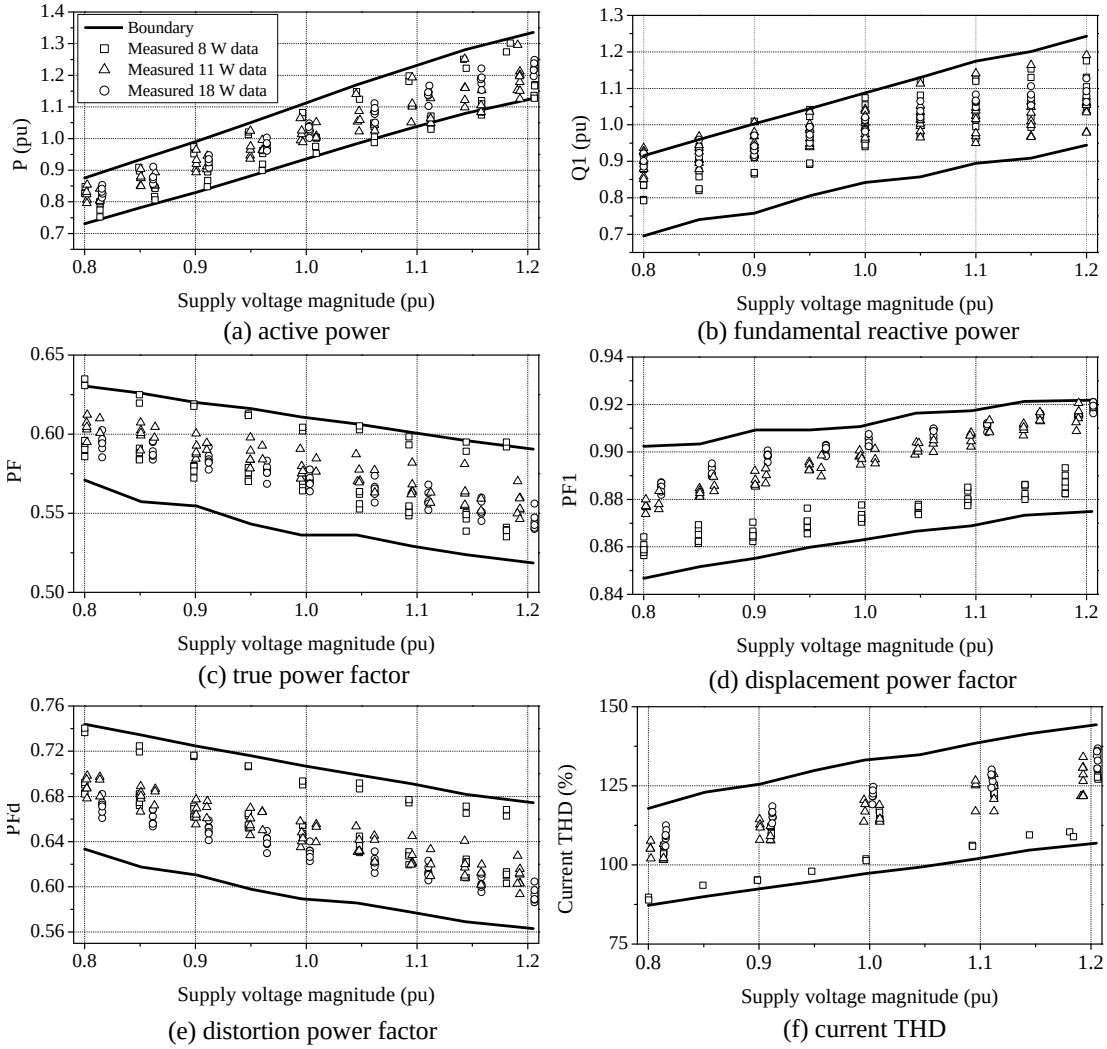

Figure 4.18: Comparison between simulated operating boundaries and measured data for the CFL electrical characteristics.

4.7 Development of aggregate models of the CFL load category

Although the developed generic models are able to represent the characteristics of the typical individual CFL, an aggregate load representation is required for large scale power system analysis. As CFLs are expected to become the most prominent non-linear load in the residential load sector, in terms of number of devices, accurate development of the aggregate load model should begin by consideration of the harmonic cancellation.

The analysis presented in this section will utilise the same techniques used in the analysis and development of aggregate power electronics load category models. This begins by quantifying the levels of harmonic cancellation within the aggregate load and investigating the effects of voltage distortion on the electrical characteristics of the CFL load. The aggregate models are presented as standard exponential and polynomial/ZIP load models, with the simulated

aggregate harmonic currents included in Appendix E. However, it is shown that, as with the power electronics load category, the generic CFL equivalent circuit model presented in the previous section is able to represent the aggregate to a good level of accuracy.

4.7.1 Harmonic cancellation within the CFL load category

It was shown in the previous chapter that there are significant levels of harmonic cancellation within the power electronics load category, due to harmonic phase angle dispersion. The diversity factor DF_h was introduced in Section 2.3.3 and used extensively in Section 3.6 to illustrate the harmonic cancellation in the power electronics load category. The DF_h is again selected to quantify the harmonic reduction within the CFL aggregate load.

This is analysed using a Monte Carlo simulation approach and allowing all equivalent circuit model components to vary independently within the previously defined ranges of values. The size of the CFL aggregate is increased until an asymptotic value of harmonic cancellation is obtained. The results presented in Figure 4.19 suggest moderate levels of harmonic cancellation within an aggregate load of CFLs, with all calculated diversity factor values included in Appendix E. These aggregate values have been obtained using the generic CFL model configured

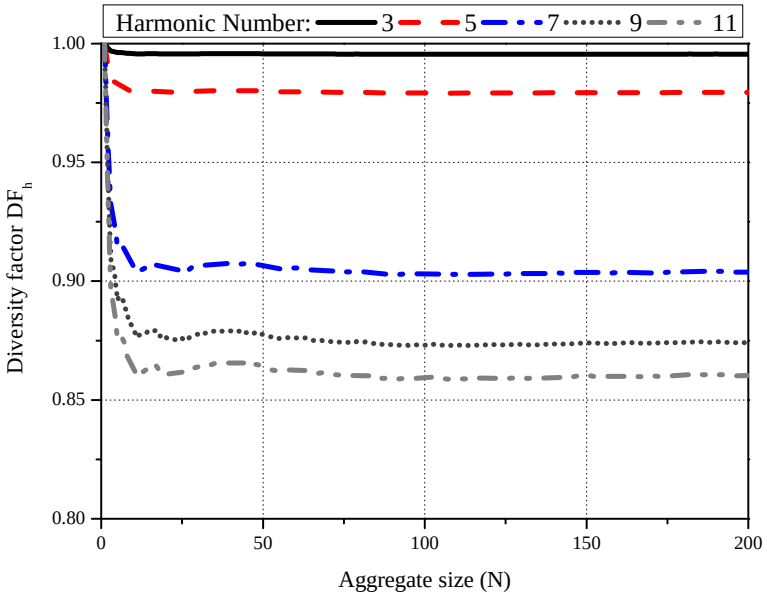

Figure 4.19: Diversity factor of generic CFL aggregate for stiff grid conditions.

for a given rated power, i.e. it does not contain the effect of harmonic cancellation between different rated powers of CFLs. The results in Figure 4.18 show that the values of individual CFLs of different rated powers will vary within the boundary conditions of the defined generic model values. Although it was shown in the previous chapter that the harmonic cancellation between subcategories of power electronics loads should be considered when representing the combined aggregate, the reduced variability between different types of CFLs indicates that the cancellation will not be significantly influenced by the composition of the aggregate load.

To test this hypothesis, a series of measurements have been performed on different CFL aggregate compositions, with the aggregate loads constructed to represent a typical household CFL load, which is assumed to be 8 CFLs, for a range of CFLs with different rated powers in differing proportions. This comparison is a blind study as the measurements have been supplied by [112] and are performed using CFLs purchased in Germany. A comparison between the measured harmonic currents at nominal supply voltage and the results of a number of simulations is presented in Figure 4.20, where the error bars indicate the maximum and minimum values recorded for each harmonic order during simulation.

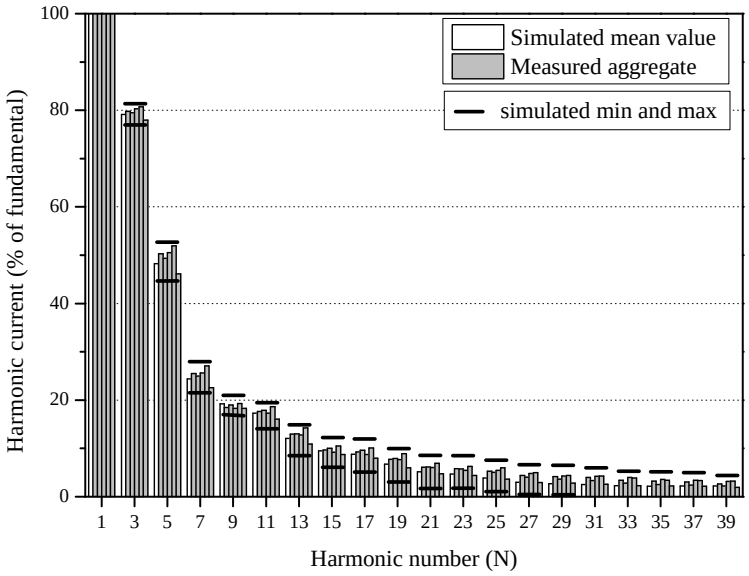

Figure 4.20: Comparison between results of simulated and measured CFL aggregates.

Two important conclusions are displayed in this set of results. First of all, the performance of the proposed generic CFL model and defined ranges of component values is again verified. The mean value obtained from simulations is very close to the measured data, and the minimum and maximum value of simulated data encompasses all measured data. Furthermore, the upper and lower values produced by simulation present a reasonable tolerance and are not excessively underestimating or overestimating the levels of harmonic cancellation within the aggregate. The second important finding is that the harmonic contents of the different measured aggregate CFL loads are very similar, which supports the earlier hypothesis that the level of harmonic cancellation is relatively insensitive to the actual composition of the CFL aggregate load.

Further experimental results are shown in Figure 4.21, which also presents a comparison between the generic CFL model and the simulated CFL aggregate consisting of the individual devices, i.e. the outcome of the Monte Carlo simulations. These values provide further validation of the ability of the developed CFL models to reproduce the electrical characteristics of actual devices. The simulated aggregate of the individual CFLs, denoted as 'simulated aggregate', intersects the measured data points, while the values obtained using the generic CFL model will introduce a maximum error of 5%.

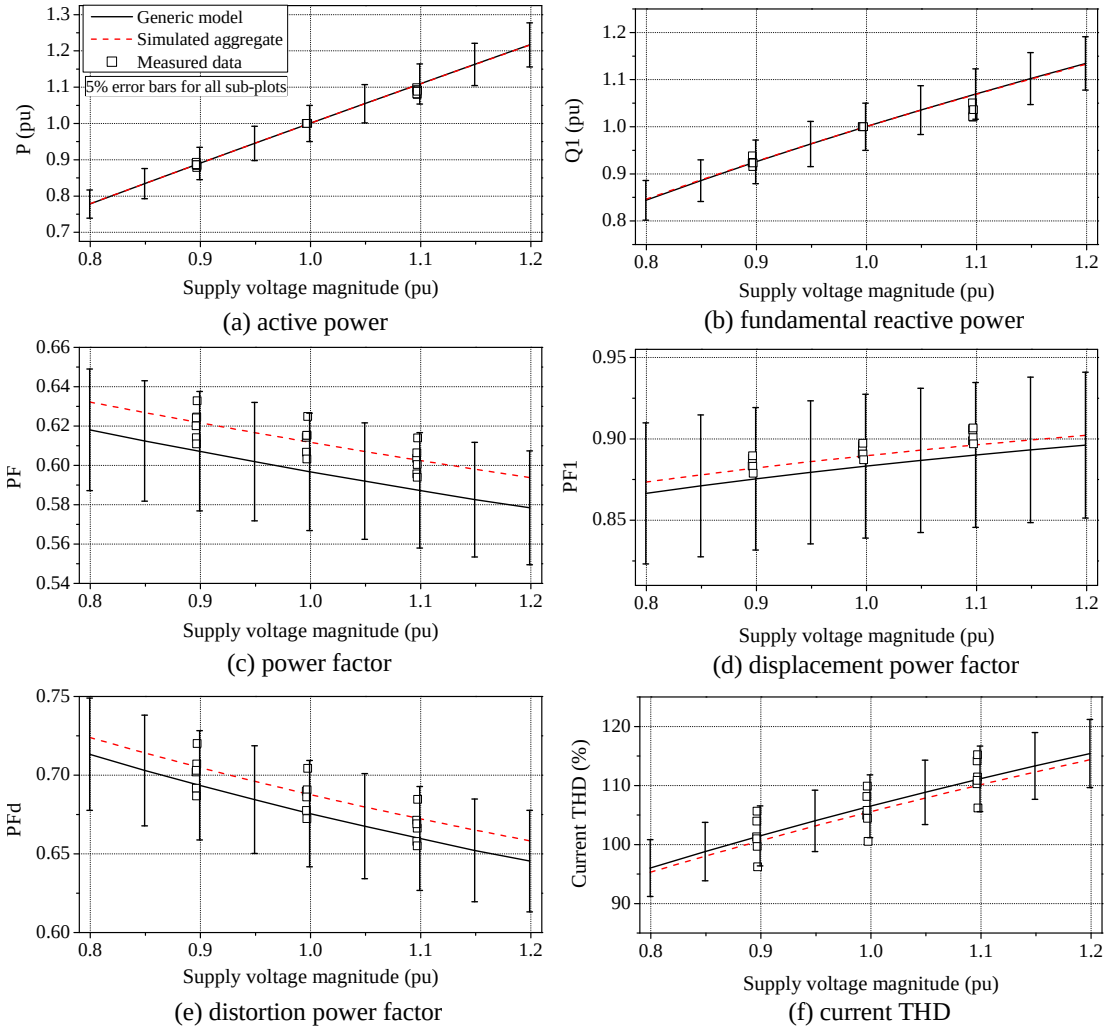

Figure 4.21: Comparison of electrical characteristics between results of simulated and measured CFL aggregates.

The final analysis required is to characterise the performance of the aggregate CFL load when supplied from distorted voltage waveform. A direct comparison of the electrical characteristics between ideal and distorted supply conditions is available in Figure 4.22. Similar to the PE no-PFC load, the current THD of the aggregate CFL load will increase when connected to distorted to supply conditions, with a shift in the fundamental also observed. However, the effects are less pronounced for this load category. The ability of the generic model to reproduce the aggregate load data to a good level of accuracy for the distorted voltage condition is also illustrated.

It should be noted that the motivation for this analysis is to demonstrate the development and functionality of the generic CFL model. The voltage distortion results do not include the effect of harmonic cancellation with other load categories, which are only included during the load model aggregation process. The impact of this is discussed further in Chapters 6 and 7.

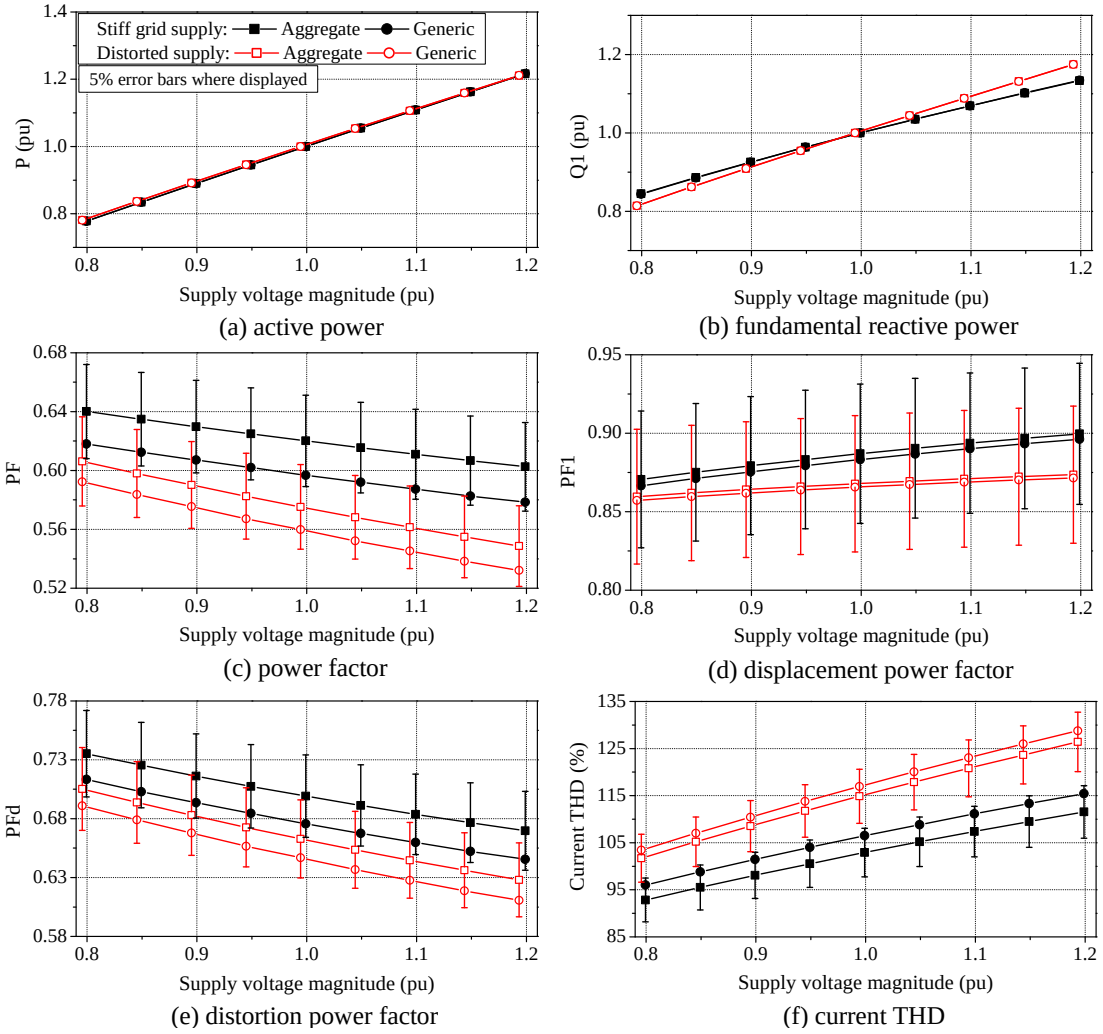

Figure 4.22: Comparison of electrical characteristics for aggregate CFL loads for stiff grid and distorted supply conditions.

4.8 LED light sources

Although CFLs are experiencing large market growth, the continual progress in developing more affordable and efficient LED LSs is expected to have a strong influence on the lighting market in the near future. By many, they are seen as the next generation of residential illumination and there is considerable support for this lighting technology. For example, the US Department of Energy is supporting a research programme to achieve an efficacy of 200 lm/W by 2025 (the most visible outlet being the L Prize®[113]) to help accelerate development of LED LSs. Current LED efficacy values range between 78 - 119 lm/W, while typical CFL values are around 70 lm/W [114]. Further benefits of LEDs include (expected) longer operational lifetime and no toxic materials (as mercury in CFLs).

The potential of LEDs lies in the flexibility of the technology. As well as GIL replacement (i.e. general illumination), several studies have investigated the use of LEDs for a range of applications. This includes: street lighting [115, 116], LFL replacement [117] and traffic signals [118, 119]. Although many driver circuits are presented in literature, e.g. [120, 121], there is a lack of information on the currently used technologies. Furthermore, no load models for residential LED LS applications are available in the existing literature.

During the initial period of this research, the only widely available LED LSs were lower-power variations, intended as a replacement for halogen spotlights. Although not suitable for GIL replacement/general illumination, these were modelled to gain some insight into the electrical characteristics of LED LSs. This initial work is supplemented by the analysis of measurements of higher power variations, which were available during the latter stages of the research (but which could not be comprehensively modelled due to time restrictions). However, the measurements show that, as the technology is still not mature and several variations exist, there is not yet enough knowledge to be able to identify typical electrical characteristics, or the corresponding generic circuits. Although a detailed circuit model is not presented, some simple static load models are proposed for higher-power LEDs from analysis of the electrical characteristics, which are not currently available in literature.

4.8.1 Main components of LED light sources

Compared to CFL/LFL electronic ballasts, the requirements of LED LS driver circuits are relatively straightforward. As LEDs are solid state technology, there is no need for high 'striking voltages' to initiate discharge ionisation. From the operational point of view, the only requirement for the LED LS driver circuit is to limit the operating current through the LEDs and keep it at approximately constant value (as the LED chain must be driven with constant current to ensure stable light output and maximise lifetime [122]).

From the inspection and measurement of available LED LSs, two general variants of driver circuit were observed. For the purpose of this research, these are labelled as 'low-power' and 'high-power' LED LS, with the block diagrams depicted in Figure 4.23.

Low-power LED light sources

Low-power LED LSs tend to sacrifice lifetime and performance by using cheap, and simple, driver circuits. These circuits contain very few components and the electrical conversion stages are shown in Figure 4.23(a). A thermistor is included as part of an input filter, reducing the current passing through the series LED chain during start-up and helping to protect from any inrush current drawn by the dc link capacitor. Due to space limitations, the rectification stage is achieved using a surface mounted IC chip. From examination of currently available driver circuits, the dc link capacitor may or may not be included. Including this component will improve performance and lifetime by reducing the dc link voltage ripple, which will result in smaller variations in the current supplied to the LED chain.

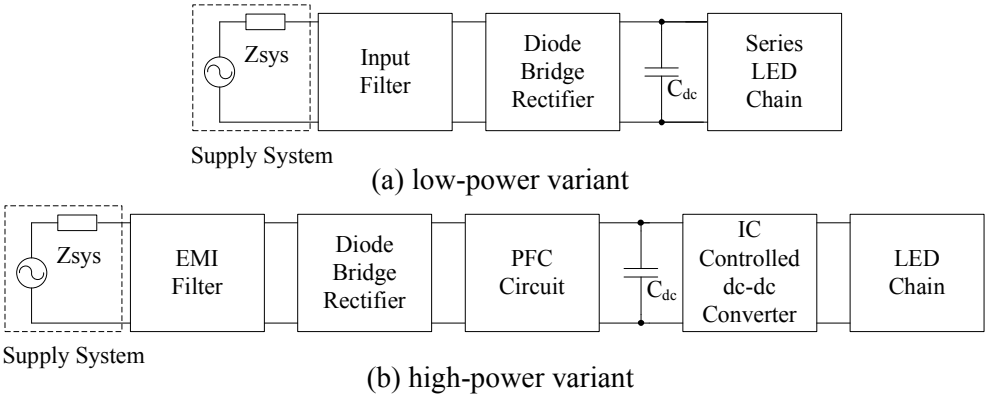

Figure 4.23: General block diagrams of LED LS.

High-power LED light sources

Higher-power LED LSs, intended for general illumination, offer improved illumination performance. This is achieved by more sophisticated driver circuits which are similar in structure to the SMPSs utilised in the power electronics load category and contain several ICs for control and regulation of LED LS performance.

As devices of this form will draw non-linear current from the supply system, they will include some form of PFC circuit to adhere to harmonic legislation. As discussed in Section 4.3.1, lighting loads are classified as Class C in harmonic legislation [20], with limits listed in Table 4.3. The form of PFC circuit used in higher-power LED LS is discussed in more detail in Section 4.8.4 later in this chapter.

4.8.2 LED model

LEDs are semiconductor devices that emit photons in the visible light spectrum and their operation is governed by standard diode mechanisms. The electrical characteristics of diodes are given by (4.6), which is often referred to as the diode equation. Although it is possible to incorporate more detailed factors into the modelling of LEDs, e.g. small signal analysis and thermal modelling [123, 124], from a load modelling point of view, the most important relationship is between the voltage and current. However, for the higher currents and powers in LEDs the ohmic losses in the device must be included [125]. Ohmic losses are present in all diodes due to the electric fields in the p-n regions [126]. The introduced voltage drop is proportional to the current through the LED and is not constant. Therefore, for LED representation, the standard diode equation (4.6) should be modified to include ohmic losses, given in (4.7).

$$I_F = I_0 \left[exp\left(\frac{qV_F}{nkT}\right) - 1 \right] = I_0 \left[exp\left(\frac{V_F}{nV_T}\right) - 1 \right] \tag{4.6}$$

where: I_F forward current, I_0 reverse saturation current, V_F forward voltage, V_T thermal voltage, q constant of electron charge ($1.62\text{x}10^{-19}$), n is the ideality factor, k is the Boltzmann constant ($1.3805\text{x}10^{-23}$) and T is the temperature.

$$I_F = I_0 \left[exp\left(\frac{V_a - IR_s}{nT} \right) - 1 \right] \tag{4.7}$$

where: V_a is the applied voltage, I is the current flowing through the LED and R_s is the internal resistance of the LED.

To accurately model LEDs, measurements were made on individual LEDs from LED LSs available for general sale in the UK market. A controllable DC source was used to increase the forward voltage in steps of 0.05 V, which was measured directly across the LED. The current through the LED was calculated by measuring the voltage drop across a series resistor. The measured data was then fitted to (4.7) using the MATLAB curve fitting toolbox. As shown in Figure 4.24, this simple model can accurately replicate the measured LED characteristics.

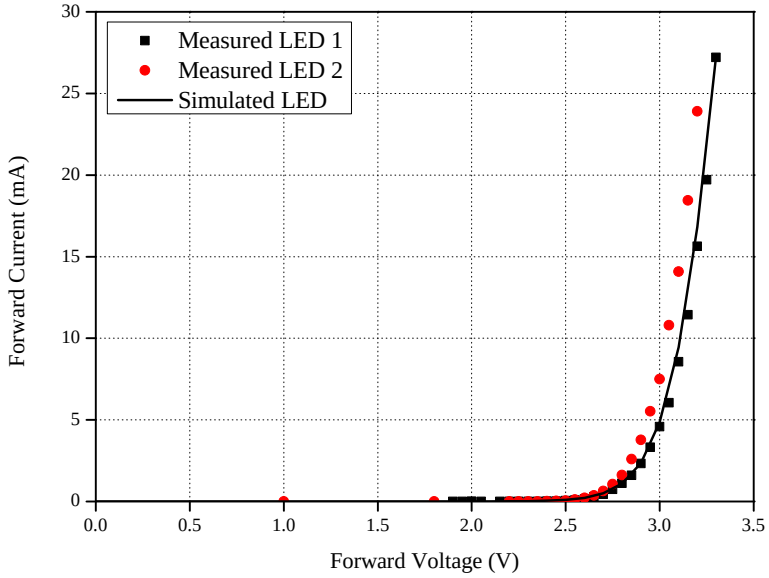

Figure 4.24: Comparison of PSpice implementation of LED model with measured data.

4.8.3 Modelling of low-power LED light sources

The full circuit model of the low-power LED LS is shown in Figure 4.25. As the circuit contains only a few components, the full circuit low-power LED LS model can be used for accurate and quick calculations; there is no need to equivalent any part of the circuit to reduce calculation/simulation time. The low-power LED LS model was developed in PSpice software [19] using standard components and a modified diode model to represent (4.7).

In order to validate the developed full circuit low-power LED LS model, low-power LED LSs were measured using a controllable voltage source [73]. The simulation results are compared with the corresponding measured data in Figure 4.26, where it can be clearly seen that there is a very good matching between the two sets of results. The high frequency noise is present in the measured results as these data were obtained using a fully controllable voltage source, whose sinusoidal voltage output is constructed/adjusted using a high frequency output inverter.

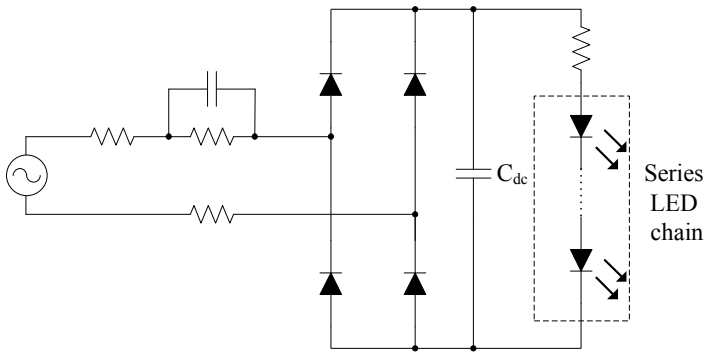

Figure 4.25: Full circuit schematic of low-power LED LS.

The almost sinusoidal nature of the current waveform results in low harmonic emission, well below the required limits (given in Table 4.3). However, there is a significant phase shift between the current and supply voltage waveforms, which are almost 90 degrees out of phase. The electrical characteristics are shown in more detail in Figure 4.27, which offers further validation of the developed model for all relevant electrical characteristics (active and reactive power demands, true, displacement and distortion power factors and current THD) across the input voltage range from 0.8 to 1.2 pu. Comparison between the simulated and measured data shows that all values lie within 5 % error boundaries, confirming the accuracy of the model.

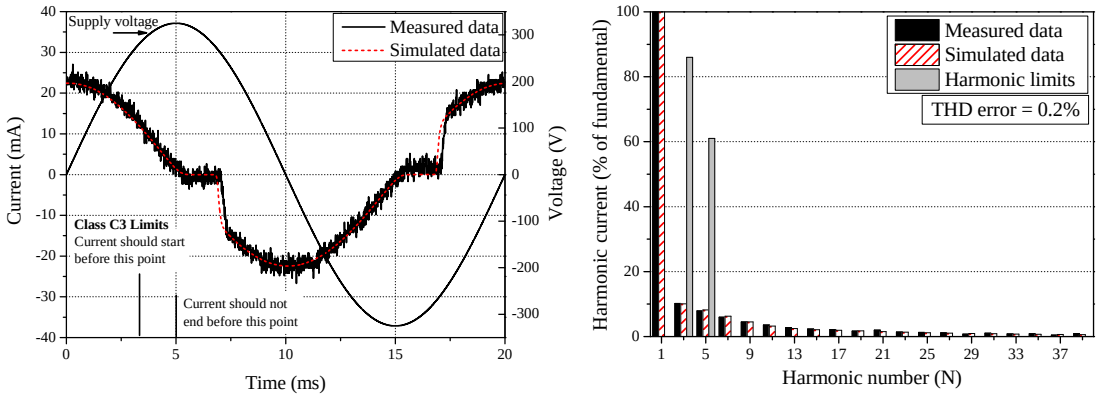

(a) input current waveform (b) associated harmonic content

Figure 4.26: Comparison of input current waveforms and associated harmonic content between the low-power LED LS model and the measured data at 1 pu voltage.

Although the active power demand $P-V$ characteristics of low-power LED LSs appear to be linear, they actual lie between constant current and constant impedance load types. The fundamental reactive power Q_1-V characteristics of low-power LED LSs, however, are almost purely quadratic, i.e. their reactive power characteristics can be closely described as constant impedance (i.e. constant capacitance) load type. It should be noted that low-power LED LSs operate with a very low leading power factor and act as the 'sources' of reactive power. As they are of low rated power, the amount of generated reactive power is not expected to be large enough to significantly alter the operation and performance of LV networks.

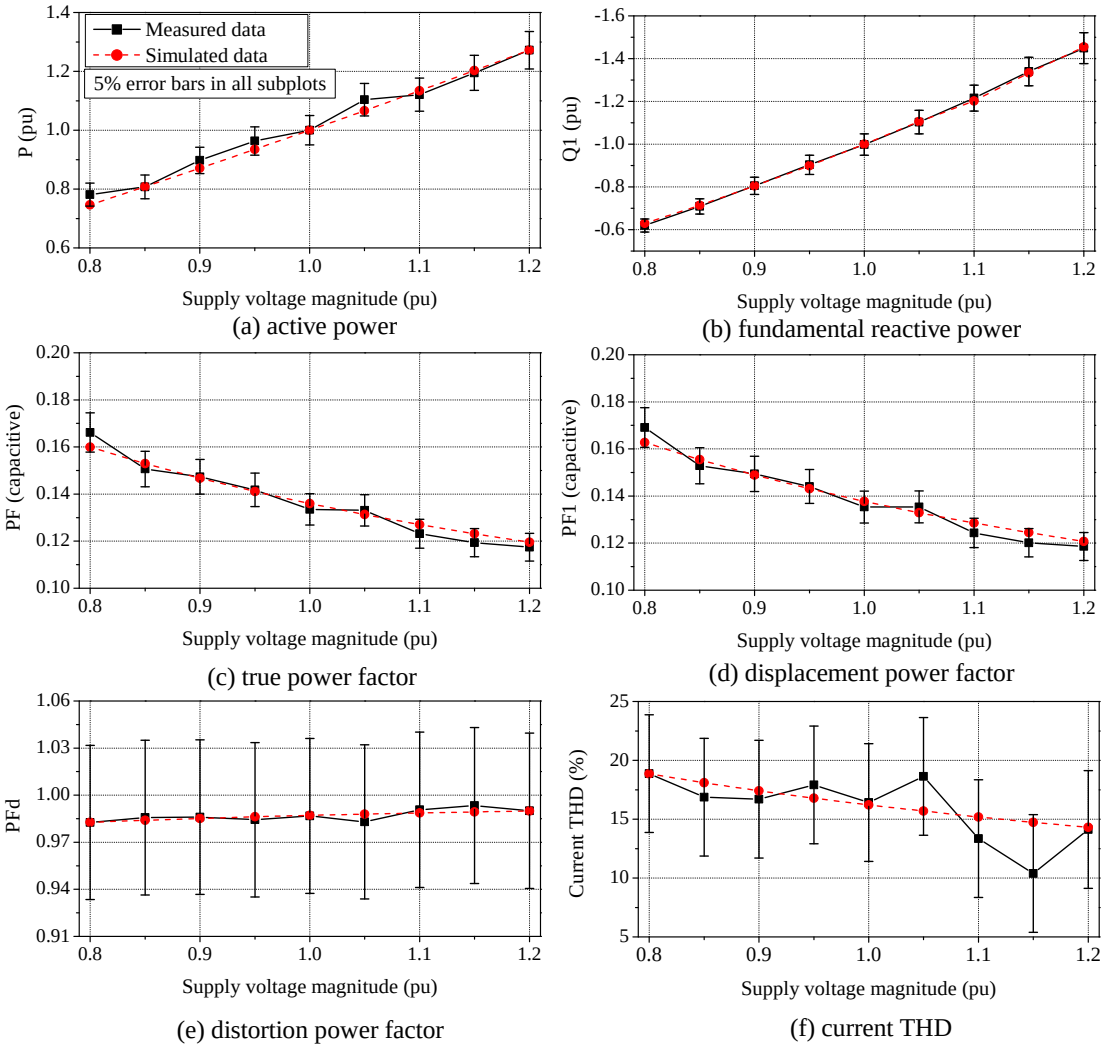

Figure 4.27: Comparison between the electrical characteristics of the low-power LED LS model and the measured data.

The true and displacement power factors of low-power LED LSs are both very low, as their capacitive nature introduces a large phase shift between the fundamental components of the input voltage and current. However, the almost sinusoidal nature of the current waveform results in a low current THD, and a high value of distortion power factor. Therefore, to reduce the complexity of aggregate load model representation, this load can be represented by the exponential and polynomial interpretations. Values of the developed low-power LED LS model are presented, along with all other lighting load models, in Section 4.10.

4.8.4 Electrical characteristics of high-power LED light sources

Over the duration of the research, a growing number of higher-power LED LSs became available in the mass market. Although there was not time to develop simulation models of these new LED LS variants, the electrical characteristics were analysed to identify possible generic circuits. Through a project collaboration with the Technical University of Dresden, a series of measurements of LED LSs were made available for analysis [127].

These measurements allowed the identification of typical input current waveforms for higher power LED LS and also the development of simple exponential and polynomial/ZIP representations of this load category, providing some insight into the electrical characteristics. These 'typical waveforms' are shown in Figure 4.28, where the current has been normalised using the method described in Chapter 3. The rated power of the high-power LED LS are as follows: HP LED 1 = 4 W, HP LED 2 = 5 W, HP LED 3 = 7 W, HP LED 4 = 9 W, where abbreviation HP (high-power) is used for display purposes.

HP LED 1, 2 and 3 have a similar input current waveform shape to that of a low-power CFL. However, the harmonic content of HP LED 1 and 3 are much lower, as the waveforms are wider and, therefore, more 'sinusoidal' in nature. It is also interesting to observe that HP LED 1 has significantly different phase characteristics. The input current waveform of HP LED 4, the highest power LED, clearly exhibits signs of an additional PFC circuit. The wider current pulse waveform is indicative of the valley-fill PFC circuit described in Section 4.3.1.

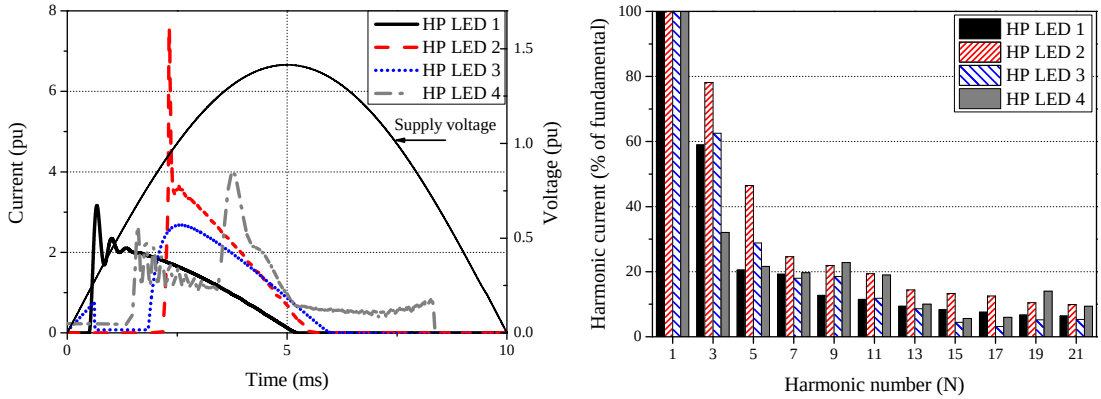

(a) input current waveform (b) associated harmonic content

Figure 4.28: Comparison of instantaneous input current waveform and associated harmonic content of measured high-power LED LS.

The full electrical characteristics of higher-power LED LSs are presented in Figure 4.29. These characteristics are presented for a reduced range of supply voltage, 0.9 to 1.1 V_{pu}, which makes the interpretation more difficult. Even from this small sample, there is a significant spread in the electrical characteristics. The active power demand characteristics vary from approximately constant power (HP LED 2 and 4), to approximately constant current (HP LED 3) to approximately constant impedance (HP LED 1). Variations in the reactive power characteristics range from negative gradient constant current to a fourth power exponential.

The true power factor values follow the same trend, a general decrease with increasing supply voltage. However, the displacement power factor will decrease for HP LED 1 and 4, with HP LED 3 being approximately constant, while HP LED 2 shows a slight increase. The distortion power factor will increase for HP LED 1, but all other variants exhibit a similar reduction in value.

These ranges of electrical characteristics confirm the previous assertion that there is not yet a typical high power LED LS circuit available for load model development. In lieu of this, the exponential and polynomial/ZIP interpretation of the measured data are presented in the final section of this chapter, in Table 4.11, with harmonic currents available in Appendix E. The high current THD values suggest that this load category should be represented by detailed circuit-based models when further information is available to fully characterise the electrical characteristics. This is discussed as an area of further work in Chapter 8.

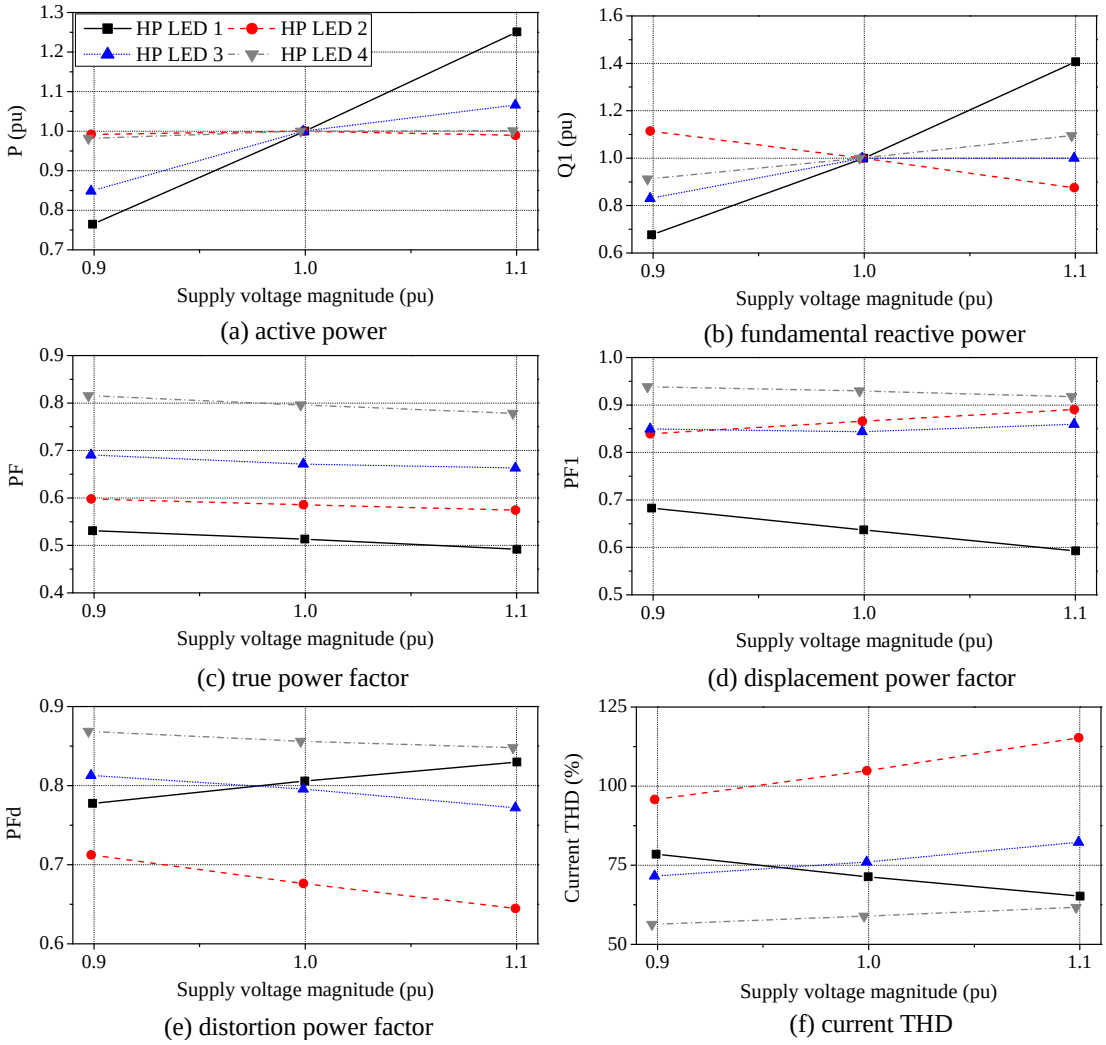

Figure 4.29: Comparison of the electrical characteristics of measured high-power LED LS.

4.9 Comparison of lighting technologies

The main aim of this chapter was to model the CFLs currently used in residential applications, which has been discussed at length. Initial results of the characterisation of LED LSs which are likely to supersede CFLS have been included to complement this. These two technologies are brought together in this section, which presents a brief discussion on the differing electrical characteristics, and their potential impact on the operation and performance of power systems.

It has been shown that the electrical characteristics of the most widely used CFLs, i.e. with rated power less than or equal to 25W, are similar. These are capacitive loads with very high levels of current THD. Higher power CFLs, in the form of valley fill PFC, offer reduced harmonic emissions but they are not widely used in the residential load sector.

Between the two CFL loads, the active power characteristics, which are influenced by the operation of the load served by the ballast circuit, i.e. the CFT, are very similar. However, the reactive power characteristics of the lower power CFL are between constant power and constant current, while the higher power CFL is between constant current and constant impedance. This difference can be attributed to the additional capacitance in the rectifier circuit of the valley-fill PFC CFL. The true power factor is much higher due to the improved distortion power factor, but the displacement power factor is also improved.

The displacement power factor values of the higher power LED LSs are generally comparable with the corresponding data for CFLs. This suggests that the substitution of the CFLs with LED LSs in the near future may not have a significant impact on the active and reactive characteristics of the residential load sector. Furthermore, as the current THD values are similar between CFLs and the measured LED LSs, there is not expected to be a significant change in harmonic emissions from the aggregate load as a result of this replacement. This hypothesis agrees with the observations put forth in [93].

4.10 Proposed energy efficient lighting load models

4.10.1 Generic equivalent circuit model values

The developed generic component values for the equivalent circuit model are presented in Table 4.7. The equivalent circuit model may be configured to represent a generic CFL, i.e. by using the values given in column two. Alternatively, this can be used to model a large number of individual CFLs by allowing each component to vary within the defined ranges.

Table 4.7: Proposed generic values for CFL equivalent circuit model.

Parameter	Generic value (pu)	Distribution	
		Range	Notes
$X_{C_{dc}}$	0.25	Normal	σ = 3.75
R	2.16e-3	Uniform	min = 1.87e-3, max = 2.38e-3
$Ptube$	1	Uniform	min = 0.87, max = 1.02

4.10.2 Exponential and polynomial load model interpretations

The exponential and polynomial/ZIP load models of the aggregate CFLs, for both clean and distorted supply voltage conditions, are given in Table 4.8. Tables 4.9, 4.10 and 4.11 show the equivalent values for individual valley-fill CFLs, low-power LED LSs and high-power LED LSs, respectively. These models may be implemented directly for use in power system analysis.

The presented coefficient values for CFLs are in general agreement with the existing models (given in Table 4.2). However, as discussed throughout this thesis, the models developed in this research are able to retain additional information on the load electrical characteristics, and can be used to provide more detailed analysis. Therefore, the harmonic injections of all modelled, and measured, energy efficient lighting loads are included in Appendix E, to provide a more complete set of load characteristics.

Table 4.8: Proposed exponential and polynomial/ZIP load models for CFL load category.

Supply	PF_1	Load model							
		Exponential		Polynomial/ZIP					
		n_p	n_q	Z_p	I_p	P_p	Z_q	I_q	P_q
clean	0.89	1.09	0.72	0.10	0.90	0	0.27	-1.26	-0.01
dist.	0.87	1.08	0.90	0.08	0.92	0	0.14	-1.18	0.04
where: clean and dist. refer to stiff grid and distorted supply conditions.									

Table 4.9: Exponential and polynomial interpretations of measured valley-fill PFC CFL.

PF_1	Load model							
	Exponential		Polynomial/ZIP					
	n_p	n_q	Z_P	I_P	P_P	Z_Q	I_Q	P_Q
0.94	0.95	1.76	0.01	0.93	0.068	-1.74	1.75	-1.01

Table 4.10: Exponential and polynomial interpretations of developed low-power LED LS model.

PF_1	Load model							
	Exponential		Polynomial/ZIP					
	n_p	n_q	Z_P	I_P	P_P	Z_Q	I_Q	P_Q
0.137	1.32	2.06	0.23	0.85	-0.08	-1.05	0.04	0.01

Table 4.11: Exponential and polynomial interpretations of measured high-power LED LS.

LED (N)	PF_1	Load model							
		Exponential		Polynomial/ZIP					
		n_p	n_q	Z_p	I_p	P_p	Z_q	I_q	P_q
1	0.64	2.40	3.59	0.79	0.82	-0.62	4.12	-4.59	1.48
2	0.87	-0.01	-1.14	-0.92	1.84	0.09	-0.49	-0.22	1.70
3	0.84	1.07	0.83	-4.24	9.56	-4.32	-8.48	17.8	-8.31
4	0.93	0.10	0.91	-0.86	1.82	0.04	0.39	0.14	0.48

4.11 Conclusions

This chapter has primarily focussed on modelling the electrical characteristics of the main rated powers of CFLs currently used in the residential load sector, and has shown that the variations between these can be represented by defining only one set of generic equivalent circuit model parameters. The expected range of values for individual CFLs has been verified against measured data for both individual CFLs and also aggregates of these. The aggregate measurements were obtained for a number of different combinations of CFLs, and, as the harmonic emissions are similar, suggests that the aggregate electrical characteristics are relatively insensitive to the actual composition. The functionality of the equivalent circuit model was shown to reproduce the measured aggregate data when configured to simulate an aggregate of individual devices, using the previously defined range of values, and also when set to run as the one generic CFL. As could be expected, running multiple individual devices was shown to produce a better match, as it allows for better representation of the effects of harmonic cancellation within the aggregate. However, as the level of harmonic cancellation within the CFL aggregate is relatively low, the use of the generic CFL results in less than a 5% error for both clean and distorted supply conditions. Therefore, this generic model can be used for the modelling of aggregate loads with confidence.

This analysis was accompanied by a more general discussion of the electrical characteristics of LED LSs, which are expected to become to become more widespread in the residential load sector. Although this technology is still developing, a series of measurements of currently available lamps indicate several similarities between the LED LSs suitable for general illumination and the CFLs which they may replace. Although time was not available to develop circuit-based models for these higher power LED LSs, the measurements have been converted into standard load model representations for use in power system analysis.

Chapter 5

Electric vehicle battery chargers

5.1 Introduction

Recent statistics estimate that the road transport sector contributes almost 15% of the EUs total greenhouse gas (GHG) emissions [128]. Despite efforts to reduce global CO_2 emissions, which have helped to reduce the contributions from other sectors, and the improving efficiency of road transport vehicles, GHG emissions from the road transport sector is steadily increasing as the number of vehicles on the roads continues to rise. EVs and plug-in hybrid EVs (PHEVs) are considered by many as a crucial step in lowering GHG emissions, while simultaneously reducing the dependency on diminishing oil resources.

To support the uptake of EV technologies, many countries around the world, including the US and China [129], have set EV penetration targets. There are various incentives, ranging from tax exemption to government grants, put in place to help meet these targets. For example, the UK government is currently offering a grant of up to £5,000 to support individual purchases of EVs, which has recently been extended to 2015 [130]. Meanwhile, the Scottish government has pledged £2.6 million funding to support the installation of home charging points and public charging points throughout the road network.

These government targets and incentives, coupled with the growing uncertainty and rising cost of oil resources, suggests that EVs may be introduced in large numbers in the near future. Although there are operational differences, EVs and PHEVs are grouped together as EVs for the purpose of load modelling in this thesis, as they will both require connection to the electrical power system. This will introduce a significant amount of new load in the power supply system as the batteries in EVs must be charged prior to use. Currently available EVs contain an on-board battery charger to allow charging by connection to the single-phase LV supply, and this will present a major challenge for the operation of LV networks, as the widespread introduction of EV charger loads will cause changes in power flows, voltage profiles, harmonic emissions and overall network performance.

Commercially available EVs will also have a 'fast charge' option, which requires connection to either a three-phase supply or a dedicated dc charging station. As the analysis in this thesis is primarily concerned with the modelling of the residential load sector and associated LV

network loads, dc 'fast charging' units are neglected from the analysis. However, it is possible to include the installation of a three-phase charging point within the low-voltage network, which will offer a faster charging time and this charging scenario is included.

In this chapter, simple EV battery charger load models are developed using the load modelling approach presented in the previous two chapters. The models are based on measurements of a number of currently available EV applications, focussing on those which are likely to be prevalent in LV residential networks. Due to the commercial sensitivity of the measurements, no manufacturer information is included.

5.1.1 Previous work on the representation of EV battery chargers for power system analysis

Despite being a relatively new load type, there has been a considerable amount of research associated with EV battery charging. While this highlights the importance of this research area to the power engineering community, there is very little guidance on the representation of EV battery chargers from a load modelling viewpoint.

The majority of previous research has focussed on assessing the potential impact on power quality, e.g. [131, 132], whether the increased load can be handled by the power system, e.g. [133, 134], and optimised charging scenarios, e.g. [135, 136, 137]. The load models used in this research are often not fully specified or are based on idealised charging characteristics. A summary of this work is given in Table 5.1. In addition to the EV battery charger models developed for use in power system analysis, there has been a multitude of references addressing the design of EV battery chargers. Review paper [138] offers a comprehensive overview of the large number of different solutions available in literature.

Table 5.1: Sample of the previous work in the EV battery charger research area.

Ref.	Year	Type of Study	EV load model
[131]	1998	Power quality	Harmonic magnitude
[132]	2003	Power quality	Not declared
[133]	2010	Impact assessment	P_{rated}=3.5 kW,PF_1=1, constant current
[134]	2010	Impact assessment	P_{rated}=3.68 kVA,PF_1=0.95
[135]	2011	Smart charging	Not declared
[136]	2011	Smart charging	Not declared
[137]	2012	Smart charging	P_{rated}=3.5 kW,PF_1=1, constant current

For the existing research, the applied EV battery charger models are presented in only one load model form, and can, therefore only be used for specific types of power system analysis (as indicated in Table 5.1). The modelling philosophy of the research in this thesis is to provide a flexible load representation which can be used for a range of power system analysis, i.e. by reproduction of input current waveforms. Accordingly, the models developed should begin by assessing and characterising the EV battery charger instantaneous input current waveforms.

5.2 Currently available electric vehicle applications

There are a number of EV applications currently available on the market, ranging from mopeds and scooters, to cars of various sizes, to buses and freight/transport vehicles. As this research is concerned with the modelling of the residential load sector, only moped/scooter and car EV applications are considered, as these are most likely to be connected to the LV residential network. For the remainder of this thesis, electric moped/scooters are referred to as low-power EVs, and electric/hybrid cars are defined as high-power EVs.

Obviously, the rated power of the electric motor and the required battery size will increase with the size of the EV application, and this will have a direct impact on the input characteristics of the EV battery charger. This is confirmed by a series of measurements, supplied by [112], of the input current waveforms for a number of currently available EVs. The measured input current waveforms, which have been normalised using the method described in Chapter 3, and the corresponding harmonic content are presented in Figure 5.1, where the measured EV battery chargers have been grouped into 5 distinct types. More details are included in Table 5.2, which compares the active and (fundamental) reactive power, power factor and THD values.

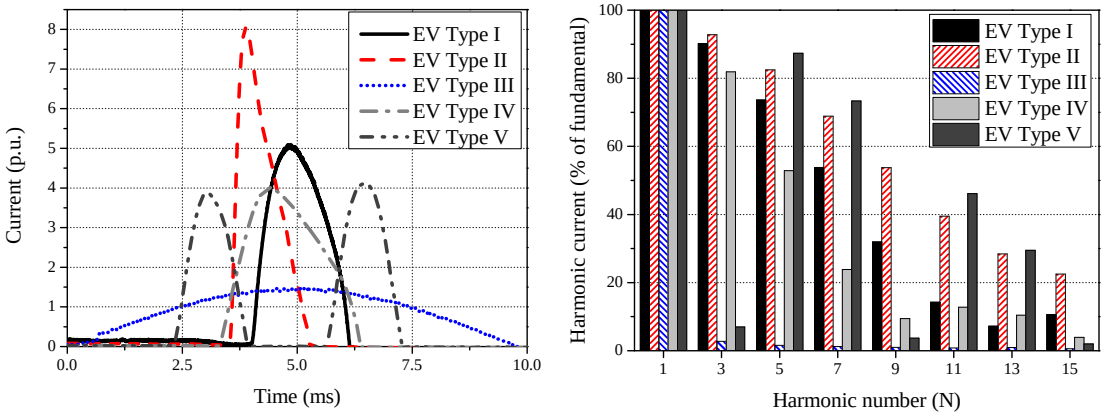

(a) input current waveforms (b) associated harmonic content

Figure 5.1: Measured input current characteristics of EV battery chargers for a range of EV applications, measurements from [112].

All measured EV battery chargers have very high displacement power factors (> 0.99). However, the true power factors for EV Type I, II, IV and V are low, due to the very high harmonic content of the input current waveforms. A more general classification is provided in Table 5.3. In this Table, EV Type I and II are defined as low-power, while EV Type III, IV and V are shown to be high-power EV applications.

The differences in characteristics of the measured EV battery chargers suggest that the specific type of EV being charged should be carefully considered when constructing scenarios for power system analysis. The type of EV will also define the electrical connection, the active and reactive power demand of the charger and the duration of the charging cycle.

Table 5.2: Electrical characteristics of the measured EV battery chargers.

EV Type	Characteristic						
	P (kW)	Q_1 (VAr)	PF	PF_1	PF_d	THD_I %	THD_V %
I	0.11	13.24	0.582	0.993	0.586	134.641	2.28
II	0.12	35.30	0.492	0.958	0.514	166.42	0.14
III	2.18	69.71	0.998	0.999	0.999	3.96	1.88
IV	2.19	194.75	0.682	0.996	0.685	102.33	2.62
V	2.18	86.91	0.624	0.999	0.624	127.49	1.71
Note: values for EV Type V are per-phase quantities.							

Table 5.3: Classification of measured EV battery chargers, based on data in [138, 139, 140, 141].

Characteristic	EV Type				
	Low-power		High-power		
	I	II	III	IV	V
	Bicycle	Moped	Car	Car	Car
Rated Power (kW)	0.07-0.11	0.1-0.42	2-3.5	2-3.5	6.5-11
Connection	1-phase	1-phase	1-phase	1-phase	3-phase
Battery Type	Li-ion	Li-ion	Li-ion	Li-ion	Li-ion
Capacity (kWh)	0.22-0.33	0.72-3.6	10-55	10-55	10-55

5.3 General EV battery charger topology

The main purpose of the EV battery charger is to provide a regulated dc supply to charge the EV battery. To achieve this, all commercially available EVs have an on-board charger for connection to the single-phase LV supply system. The maximum current drawn from an individual single-phase circuit connected to the LV network is normally limited to between 13 and 16 A, which creates an upper limit on the charging current supplied to the EV battery. This results in long charge cycles, typically between 4 - 8 hours, under normal charging conditions.

It is possible to reduce the duration of the charging cycle by connecting to the three-phase supply, or by connecting to a higher dc charging voltage, i.e. to an off-board charging station. This 'fast charging' condition requires special charging equipment, e.g. charging station, which are not currently widespread in the UK. However, the requirements of both on-board and off-board chargers are identical: they must provide regulated dc supply voltage and current while monitoring key battery parameters, e.g. temperature and state of charge (SOC), to ensure maximum performance whilst maintaining safety. Although the EV charger is a complex electrical system, it can be broken down into only a few circuit blocks by identifying the key electrical conversions required. As the principle of operation is similar, it is assumed in this thesis that the typical EV battery charger has the same basic structure and component blocks as the power electronics load category. The generic block diagram is shown in Figure 5.2. The uni-

directional EV battery charger circuits presented in [138] are of similar topologies, validating this assumption.

It is possible that the DBR shown in Figure 5.2 will be substituted for an active front-end rectifier. An active rectifier has a similar topology to the DBR but will utilise insulated gate bipolar transistors (IGBTs) in place of standard diodes. This configuration is capable of operating with unity power factor and allows for bi-directional power flow, i.e. allowing EVs to supply energy back into the grid, referred to as vehicle-to-grid (V2G), to provide ancillary services to the power system.

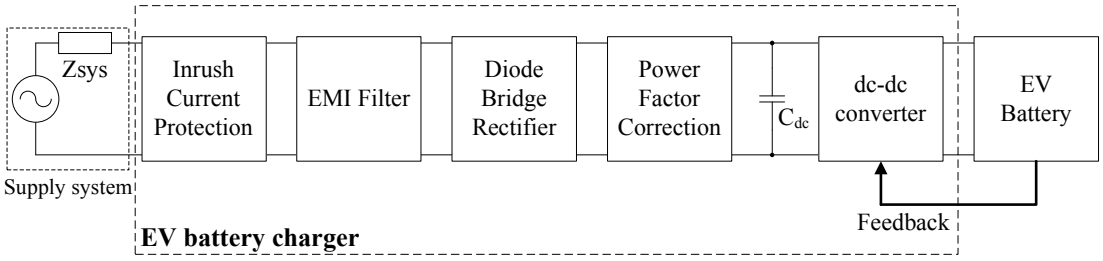

Figure 5.2: General block diagram of a typical EV battery charger circuit for normal single-phase charging conditions.

The key operational differences between the power electronics load category and the EV charger are a result of the charging requirements of the EV battery. Therefore, the electrical performance of the EV charger is slightly different, resulting in different electrical characteristics of the load. However, as the function of many of the component blocks does not change from the power electronics load category (described in Chapter 3), they are not discussed in this section.

5.3.1 Power factor correction

As discussed in Chapters 3 and 4, all loads connected to the LV supply system must adhere to harmonic legislation in order to limit the harmonic emissions into the power supply system. To provide the regulated dc supply voltage during the charging cycle, EV battery chargers must rectify the ac supply voltage, a process which inherently draws input current rich in harmonics. Chapters 3 and 4 discussed several methods, by passive and active PFC techniques, which may be applied to reduce the harmonic content of current drawn by non-linear loads.

Due to the large rated power of many EV battery chargers, the corresponding harmonic emissions may have significant impact on the performance of both the local power supply system and the wider network. However, as EV battery chargers are a relatively new load, there is very little guidance available on harmonic emission limits. The current harmonic requirements for on-board EV battery chargers are defined in [142], while harmonic limits of charging stations are defined in [143]. Both EV battery charger standards cite harmonics requirements in [20], while chargers with higher current values (> 16 A) have to adhere to legislation in [21]. It is likely that these standards will be superseded by specific EV harmonic legislation.

In the existing harmonic legislation [20], EVs can be classified as either Class A loads or Class D loads. Class A loads include balanced three-phase equipment and household appliances (excluding those considered as Class D loads). Class D loads are specified as being less than or equal to 600 W but is reserved for equipment which may have a pronounced effect on the power supply, as defined by the following factors:

- large number of pieces of equipment in use
- expected duration of use
- simultaneity of use
- power consumption

Currently, Class D loads only include PCs and TVs. EV battery chargers will satisfy all listed factors, but many EV charger applications are of rated power greater than 600 W. Therefore, it is unclear which limit will be applicable to EV battery chargers and both are considered in this analysis. Class D limits are shown in Column 1 of Table 5.4, with Class A limits in the second column. Note: there are two limits for Class D loads, with the second limit being equal to the Class A limits.

Table 5.4: Existing harmonic limits for EV battery chargers with input current less than 16 A, as given in [20].

Harmonic number (N)	Class D limits: Maximum permissible harmonic current (mA/W)	Class A & D limits: Maximum permissible harmonic current (A)
3	3.40	2.30
5	1.90	1.14
7	1.00	0.77
9	0.50	0.40
11	0.35	0.33
13	0.30	0.21
$15 \leq N \leq 39$	$\frac{3.85}{N}$	$\frac{2.25}{N}$

From the measured harmonic spectra shown in Figure 5.1, some of the harmonic currents are pronounced and are likely to result in the circulation of large harmonic emissions in the power system. The exception is EV Type III, which has very small harmonic injections as a result of either a controlled front-end rectifier or a-PFC stage. A comparison between EV Type I, II, IV and V harmonic currents and the existing harmonic limits is displayed in Figure 5.3.

EV Type I and II both breach Class D limits but are still comfortably within the required Class A limits. The harmonic currents of EV Type IV will violate both Class A and D limits up until the 15^{th} harmonic order. Similarly, EV Type V will breach the lower order harmonics. The only difference is that EV Type V is a three-phase connection so has very small harmonic injections at the triplen harmonics (harmonics occurring at frequencies at multiples of three of

the fundamental frequency). It is interesting to observe that two of the high-power EV battery chargers (Type IV and V) are shown to breach the existing harmonic legislation.

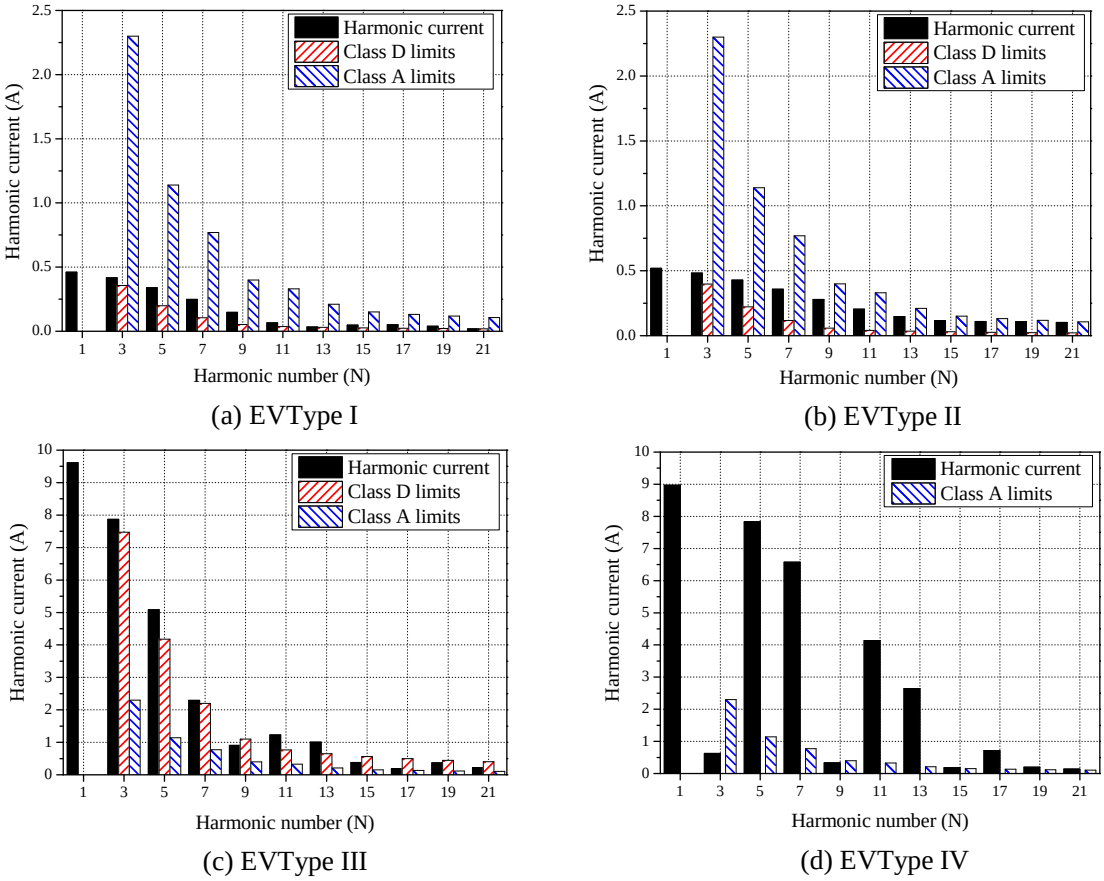

(a) EVType I

(b) EVType II

(c) EVType III

(d) EVType IV

Figure 5.3: Comparison between harmonic emissions of measured EV battery chargers and existing harmonic legislation given in [20].

5.3.2 DC-DC converter

The EV battery is a complex electrochemical system which is sensitive to overcurrent and overvoltage conditions during the charging cycle. Therefore, similar to the power electronics load category, a controlled dc-dc converter is included after the rectification stage, to isolate the EV battery from fluctuations in the ac voltage supply and to regulate the dc supply voltage.

Unlike the operation of the dc-dc converters found in the power electronics load category, which acts to maintain the fixed voltage levels required by the dc load while supplying the necessary load current, the dc-dc converter of an EV battery charger will have two distinct modes of operation to satisfy the EV battery charging requirements. The battery charging system will provide constant current (CC) followed by constant voltage (CV) charging conditions, which is often referred to as constant current-constant voltage (CC-CV) charging. This is a consequence of the battery characteristics and is discussed further in the next section. As shown in

previous chapters, it is the functionality of the dc-dc converter, rather than the specific electrical components/configuration, which will determine the behaviour at the ac input.

5.3.3 EV battery

As the battery serves as the load of the charger, it will have a significant influence on the electrical characteristics and behaviour of the charger. Batteries are electrochemical systems which convert chemical energy into electrical energy during the discharge cycle, i.e when connected to an electrical load. Rechargeable batteries, such as those required in EV applications, can also convert electrical energy into chemical energy during a charging cycle.

The EV battery pack will consist of a number of electrochemical cells connected in series and parallel to achieve the desired characteristics and electrical performance. Different cell chemistries have different electrical properties and characteristics, which need to be carefully selected to satisfy the performance requirements of the application. As the EV battery pack supplies power to the electric motor during vehicle propulsion, high energy and power densities are the most desirable characteristics of EV battery technology. High energy density essentially allows for more power to be stored in the same area, while high power density allows for a larger amount of power to be transferred quickly.

Of all the currently available rechargeable battery technologies, lithium ion (Li-ion) has the most suitable electrical properties for EV applications. Lithium is the lightest metal, allowing for a high energy density and making it particularly suited for mobile applications. However, pure (metallic) lithium is highly unstable so Li-ion is used to improve the safety of the battery. A comparison between Li-ion and the other main comparative rechargeable battery technologies is presented in Table 5.5. There are several variants of Li-ion battery technology, e.g. lithium-iron-phosphate, which will all offer slight variations on the performance characteristics listed in Table 5.5 , but this is not relevant to the research presented in this thesis.

Table 5.5: Comparison of main battery technologies [144].

Characteristic	Battery Type		
	Lead acid	NiMH	Li-ion
Cell voltage (V)	2	1.2	3.2-3.6
Energy density (Wh/kg)	30-40	50-80	100-200
Power density (W/kg)	100-200	100-500	500-8000
Max. Discharge rate (C)	6 - 10	15	100
Charge efficiency (%)	60-80	70-90	$\approx$100
Self discharge (%/month)	3-4	30	2-3
Cycle life (N)	600-900	$>$1000	2000
where: NiMH is Nickel-Metal Hydride			

A Li-ion cell has a higher potential than other technologies and a higher discharge rate, allowing for higher power density. It also has low losses during charging, very little self-discharge and

increased lifetime (i.e. number of discharge cycles). The main disadvantage of using Li-ion batteries is that extra safety circuits are required to protect the battery during the charge and discharge cycles. Overcharging and overdischarging will reduce battery lifetime and performance, and may even result in thermal runaway (damage due to overheating). This additional manufacturing cost is deemed acceptable as a trade-off against the improved performance.

The recommended typical charging cycle of Li-ion batteries is shown in Figure 5.4. During Stage 1 (CC), the battery is charged with constant dc current. When the cell is charging, the current flow will cause the cell voltage to increase, i.e. there is a decrease of the internal impedance of the battery. When the cell voltage reaches the upper threshold, the dc-dc converter operation will change to maintain the voltage at this level. In Stage 2 (CV), the voltage is maintained at this level while the charging current is gradually reduced to fully charge the battery. The charge cycle is terminated when the charging current reaches a lower threshold. Comparing the dc battery current and voltage characteristics with the ac input active power characteristics of the charger (Figure 5.4(b), it is clear that EV battery charging characteristics dominate the active power demand of the battery charger during charging operation and should form a significant part of the modelling effort.

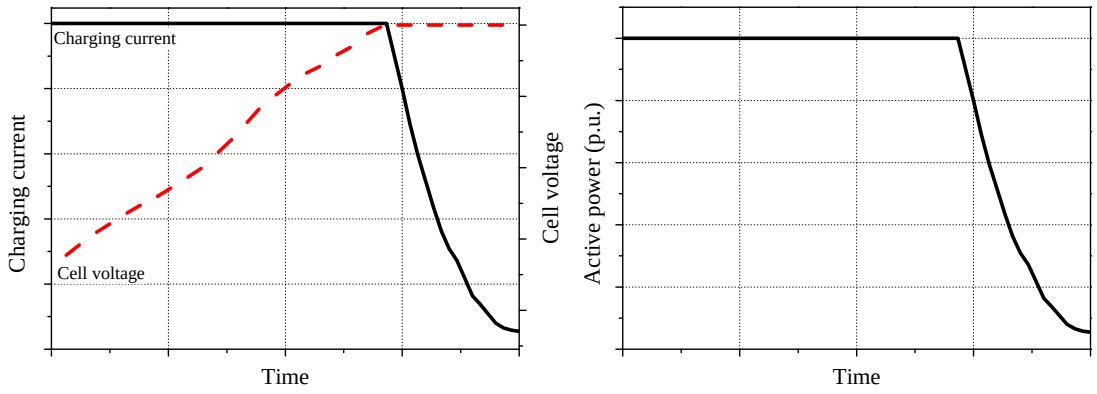

(a) battery dc current and voltage **(b)** battery charger input active power

Figure 5.4: Typical Li-ion battery charging characteristics.

5.4 Modelling of the EV battery

A Li-ion battery back is constructed from a collection of individual Li-ion cells. Each Li-ion cell contains three main components: an anode (negative electrode), a cathode (positive electrode) and an electrolyte. The electrolyte is an electrical insulator but ionic conductor, i.e. it separates the two electrodes but allows ion charge transfer between the two. During the charge cycle, positive lithium ions will transfer from the cathode to the anode. During the discharge cycle, the positive lithium ions transfer back to the cathode, with negative electrons supplied to the connected load to maintain the charge balance. The charge transfer will create a depletion layer which will dictate the battery impedances. A thorough overview of the electrochemical

processes within the L-ion battery is not required for this research but is available in many references, e.g. [145].

As the EV battery has the major influence of the power demanded by the EV charger, accurate representation of this is crucial to the modelling effort of the EV charger load type. There are three main approaches adopted for the modelling of batteries: electrochemical models, e.g. [146], artificial neural network models, e.g. [147], and electrical equivalent circuit models (EECM), e.g. [148, 149, 150, 151, 152, 153].

Although all approaches have been shown to accurately represent the electrical characteristics of Li-ion battery packs, EECM has obvious advantages for use in load modelling research. Circuit-based models use combinations of standard electrical components and can be implemented in a wide range of softwares. There is also a reduced need to fully understand the complex electrochemical interactions and transfer mechanisms within the Li-ion cells. The models proposed in literature vary in complexity, with a selection shown in Figure 5.5. As expected, the performance of the model improves for more sophisticated models forms, from around 80% to just over 90% (using a goodness of fit criterion) [150].

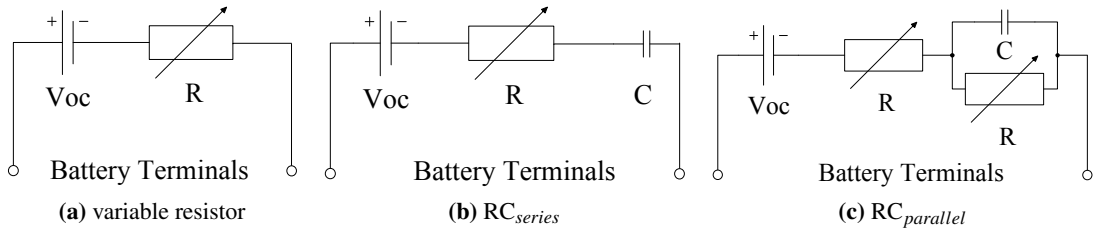

Figure 5.5: Sample of the EV Li-ion battery models proposed in literature [150].

To develop an EECM, the impedance of the battery is measured across the input terminals. For representation by a variable resistor, only the real component of the impedance can be included. This approach has been shown to match the EV battery characteristics with reasonable accuracy, but more advanced models can consider both the magnitude and phase of the battery impedance to improve the model performance.

Although it is not the objective of this work to fully characterise EV batteries, research performed in collaboration with [154] is used to identify the key steps in a modelling approach which may be used to develop detailed EECM battery models for future research. This level of modelling detail is beyond the requirements of the modelling approach in this thesis, therefore, the simple equivalent resistance model of the EV battery is also presented. The required level of modelling detail is determined by the type of analysis. For example, more accurate representation of battery impedances will provide greater insight into the overall charging and discharging efficiency of the EV battery system, which should be considered when analysing the use of EV battery charger operation when connected to the network.

5.4.1 Complex impedance model of Li-ion battery

Electrochemical impedance spectroscopy (EIS) is a widely used technique in the analysis of battery technology. The main advantages of using this approach is that it is a non destructive technique and the data obtained can be readily converted to an EECM form. EIS equipment is used to apply a small ac excitation potential, typically between 1 - 10mV [145], of increasing frequency to an electrochemical cell. Measuring the ac current will give both the magnitude and phase angle of the cell impedance, i.e. the real and imaginary components. The cell impedance is normally non-linear, so it is possible to obtain impedance information at different harmonic frequencies by applying Fourier transform theory.

The series of EIS measurements performed in [154] are presented here to illustrate the complexity of the Li-ion battery characteristics and the use of EIS and EECM to represent these characteristics. The Li-ion battery under test was a commercially available Li-ion battery with capacity of 2150 mAh (the data sheet is included in Appendix F). Although this battery is not suitable for use in EV applications, the results in this section highlight the ability of the EIS technique in the development of a Li-ion battery model. The model developed in [154] is shown in Figure 5.6.

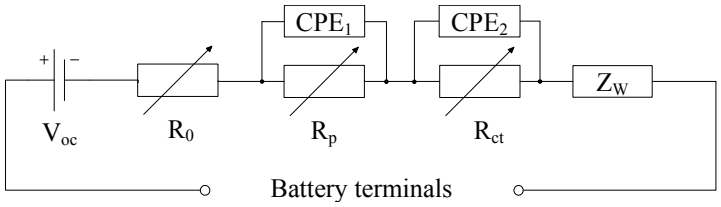

Figure 5.6: EECM Li-ion battery model [154].

Every element in the model has a physical significance. The internal resistances are modelled by element R_0, while R_P and R_{ct} resistance represent the electrode degradation and charge transfer. The *CPE* blocks are constant phase elements, which correspond to the electrochemical double layer (EDL - an accumulation of charge on either side of a depletion region, analogous to the electrical behaviour of a capacitor) at each electrode. The Warburg impedance Z_w defines the ion diffusion process due to the migration of ions from areas of high concentration to low concentration, to achieve uniform distribution. Each of these elements has a mathematical representation and can be expressed analytically, as shown in (5.1). This allows for the model to be implemented in a larger range of modelling softwares.

$$Z = R_0 + \frac{R_P Y_{0_1}^{-1} (j\omega)^{-n1}}{R_P + Y_{0_1}^{-1} (j\omega)^{-n1}} + \frac{R_{ct} Y_{0_2}^{-1} (j\omega)^{-n2}}{R_{ct} + Y_{0_2}^{-1} (j\omega)^{-n2}} + \left(O\sqrt{j\omega} coth\left(B\sqrt{j\omega} \right) \right)^{-1} \tag{5.1}$$

where: R_0 is the ohmic resistance, R_P is the passivation film resistance, R_{ct} charge transfer resistance, Y_{O1} capacitance of CPE_1, Y_{O2} capacitance of CPE_2, n_1 empirical exponent of CPE_1, n_2 empirical exponent of CPE_2, O capacitance of diffusion impedance, B diffusion coefficient.

A publicly available electrochemical modelling software, available from [155], performs a fitting algorithm to return values of the chosen model form to the given input data. The results in Figure 5.7 illustrate this approach and confirms the ability of the chosen model form to match the measured Li-ion impedance data.

The Nyquist plot in Figure 5.7 shows the complex nature of the battery impedance over the measured frequency range and clearly identifies the impedance of the effects discussed previously. As the battery impedance is capacitive in nature, the imaginary impedance component takes a negative sign. The EDL layer is not the ideal semi-circle which would be expected of a parallel RC circuit. This blurred semi-circle is due to the superposition of the impedance characteristics of both electrodes.

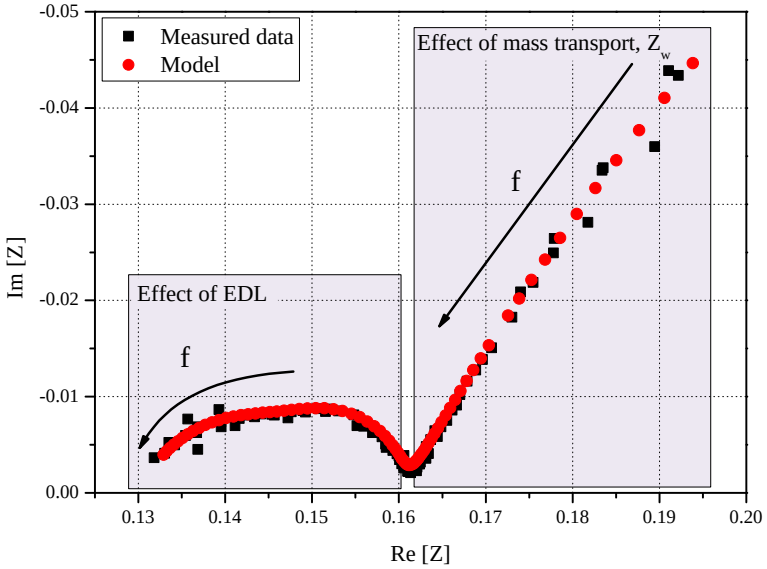

Figure 5.7: Comparison between measured and simulated impedance results for Li-ion cell with SOC = 60% (unregulated temperature), data from [154].

Sensitivity analysis of the cell impedance for different SOC and temperature conditions indicates some interesting results. The real and reactive component of the cell impedance will generally reduce as SOC increases. However, this mainly influences the low frequency characteristics, i.e. changes in the mass transport characteristic. Due to the high switching frequency of the dc-dc converter in the EV battery charger, it can be expected that the equivalent resistance of the EV battery will remain approximately constant during the charging cycle (discussed in the following section).

More pronounced variations are observed for changes in operating temperature. As the ambient temperature is reduced, the internal impedance of the cell will increase significantly. From the Nyquist plot in Figure 5.8(b), this will influence both high and low frequency components of the battery impedance. The wider arc at the higher frequencies indicates increased losses at the electrode EDL, which may also accelerate wear of electrode material. To put this in context of power system analysis, this suggests that the power demand of the EV battery may be sensitive to ambient temperature conditions, i.e. introducing seasonal variations into the load model.

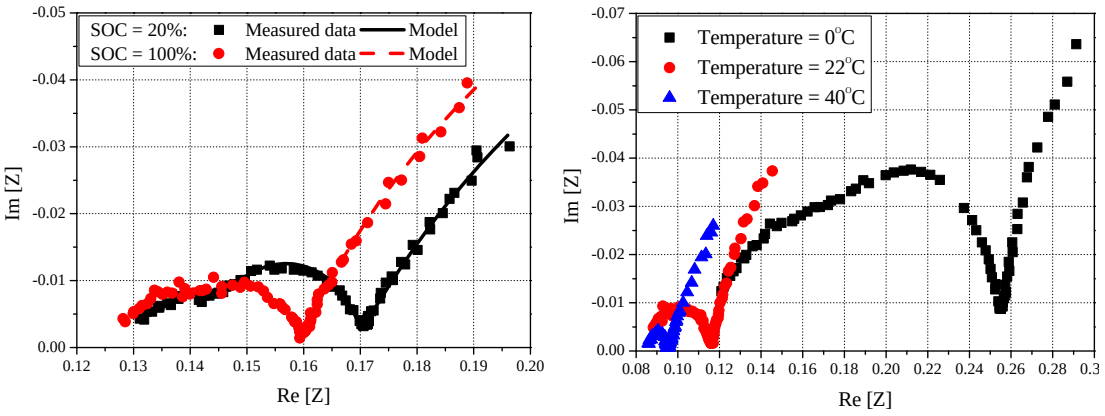

(a) change in SOC (unregulated temperature) (b) change in temperature, SOC = 70%

Figure 5.8: Comparison between measured and simulated Li-ion battery data for various operating conditions [154].

5.4.2 Equivalent resistance model of Li-ion battery

Although the Li-ion battery model presented in the previous section is able to provide an accurate representation of the measured data, the form of the model is too detailed for large scale power systems analysis. The simplified equivalent circuit model introduced in the preceding chapters is suitable for the development of load models and requires only an analytical representation of the dc link characteristics.

The performance of the EV battery will determine the electrical behaviour of the dc-dc converter and the dc link electrical characteristics. DC battery measurements are hard to obtain for EV battery chargers as these systems are integrated into the design of the car and the access is limited due to the high voltages and currents found there. One example of the output of an actual Li-ion EV battery charger from literature is shown in Figure 5.9(a) [156]. The equivalent battery resistance $r_{eq,batt}$, which has been calculated from the values of $v_{dc,batt}$ and $i_{dc,batt}$, is approximately constant for the majority of the charge cycle, with a fast increase at the end of the charge cycle when the charging current magnitude rapidly decreases.

The data presented in [156] is not in agreement with measurements obtained from the same type of EV battery charger during this research. The measured data was obtained by connecting digital voltage and current meters at the output of the on-board charger and recording at five minute intervals. The results are shown in Figure 5.9, which also shows the ac input active power and the dc power delivered to the battery during the charging cycle, as calculated from the measurements. For the measured data, both quantities are approximately constant. The small variations are due to changes in the supply voltage magnitude during the charging cycle, as the EV battery charger was supplied from actual LV distribution network. The resulting efficiency of this load, calculated as the ratio of power delivered to the battery to the power drawn by the charger, was found to be approximately 80% throughout the charging cycle.

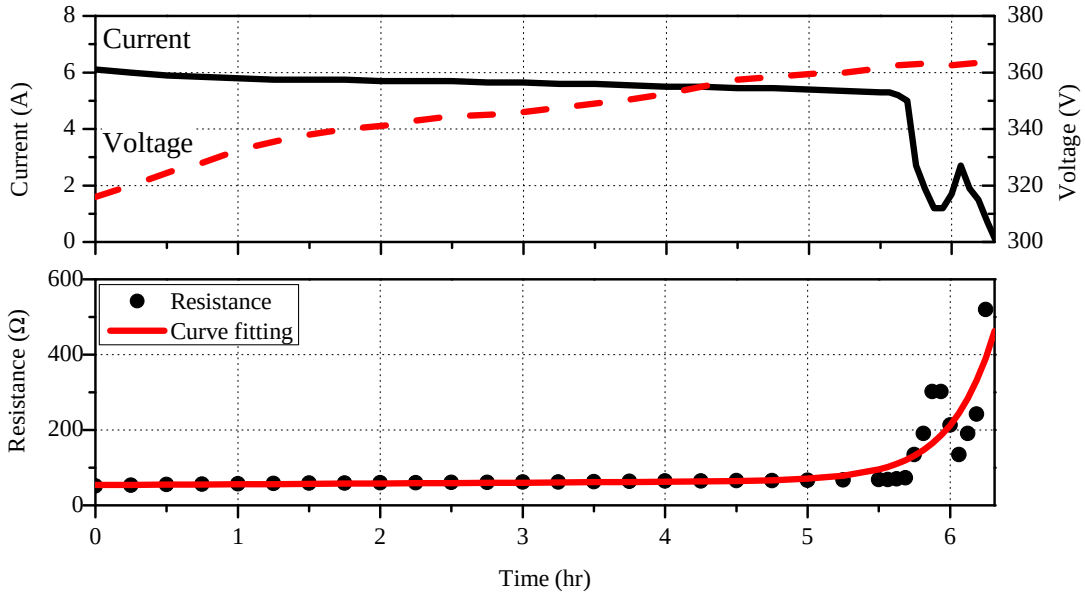

(a) data from [156]

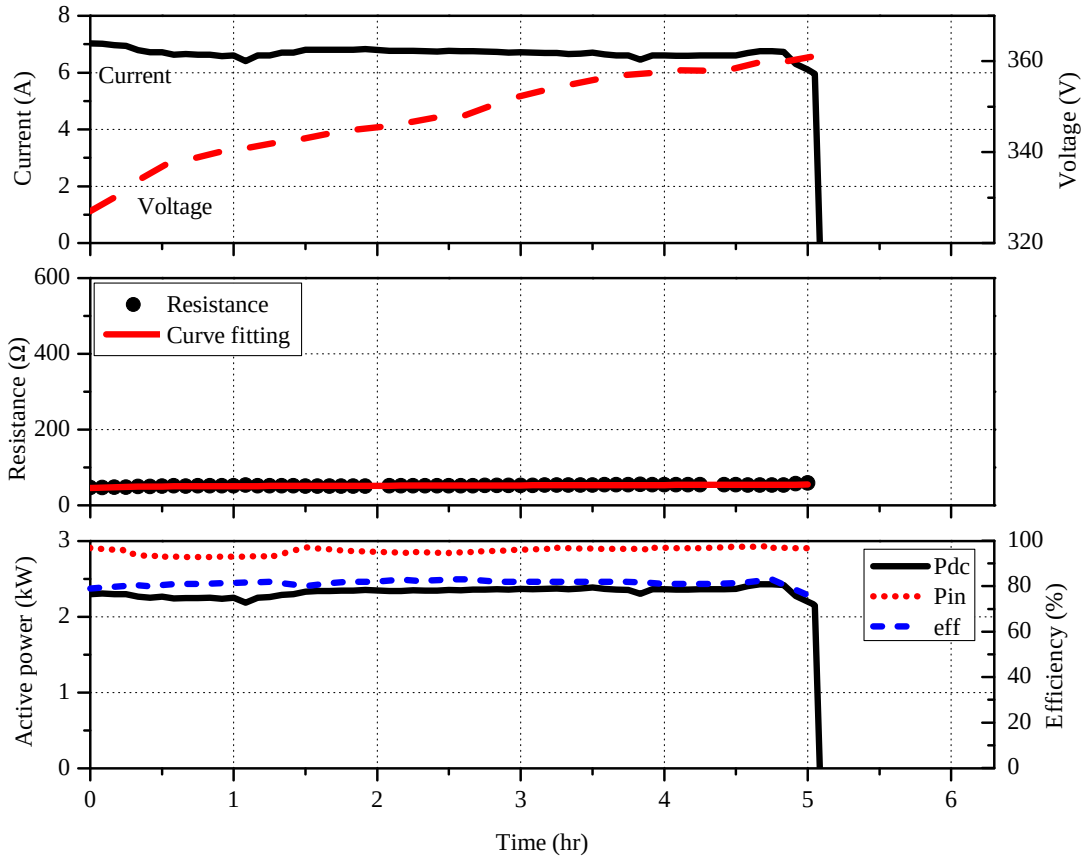

(b) measured

Figure 5.9: Comparison of measured and literature values for dc charging characteristics of Li-ion EV battery charger.

A comparison of the two datasets in Figure 5.9 highlights several differences. The duration of the measured charging cycle is shorter than the literature data by approximately one hour. This can be explained by the higher charging current magnitude for measured data, by approximately one ampere. The most significant difference is that the period of constant voltage charging is much shorter (which was observed for multiple tests), leading to a constant equivalent resistance characteristic for a given input ac supply. The result that battery resistance will not noticeably change during the charge cycle, i.e. as a function of battery SOC, is in agreement with the findings in the previous section. However, the current supplied to the EV battery will vary in proportion to the magnitude of the supply voltage, while the dc voltage level is regulated. An example result is presented in Figure 5.10, which was recorded during the constant current stage of the charging cycle.

The values have been normalised to the rms value of current and voltage for rated supply voltage to allow for a clearer description of the correlation between the current at the battery terminals and the supply voltage magnitude. As limited measured data is available, the trend is approximated as linear for the calculation of an equivalent resistance. This simplification is adequate for the development of steady-state load models, as the non-linearity is observed for supply voltage magnitude below 0.95 pu, which indicates that it is linear during the allowable voltage range (i.e. +10/-6 %). While it is shown later in this thesis that this approximation is able to reproduce the electrical characteristics of EV battery charger load, additional measurements should be performed to fully characterise this behaviour (this is discussed in more detail in the further work section in Chapter 8).

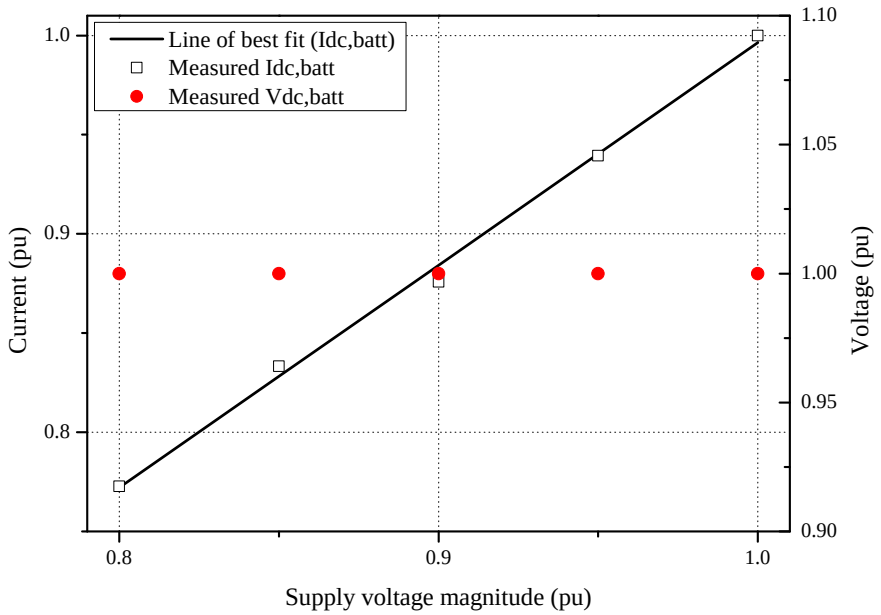

Figure 5.10: Measured EV battery charger dc characteristics for changing ac supply voltage magnitude.

This corresponds to a negative resistance characteristic at the charger output terminals, which can be represented as an equivalent dc link resistance for use in the equivalent circuit model. As the uncontrolled rectifier circuit cannot regulate dc link voltage v_{dc}, which will vary in proportion to the supply voltage magnitude, the negative resistance characteristic will resolve to a constant current representation (at the dc link), i.e:

$$r_{dc} \uparrow = \frac{v_{dc} \downarrow}{i_{dc}} \Rightarrow i_{dc} = \frac{v_{dc} \downarrow}{r_{dc} \uparrow} \approx k \tag{5.2}$$

By modifying the analytical model developed in Chapter 3, the equivalent dc link resistance for constant current load can be developed. The analytical model was configured with values to represent a typical non-linear load and the rms value of dc link current at rated supply voltage was extracted. This current value was then substituted for the equivalent resistance, thus obtaining a constant current load at the dc link. A sweep of the supply voltage was then performed to simulate the influence of this constant dc current on the dc link voltage, from which the equivalent resistance is calculated. The per-unit value of equivalent resistance is calculated as:

$$r_{eq,pu} = 0.006 v_{dc} - 0.01 \tag{5.3}$$

This per-unit value can be converted using the base impedance to any rated power. This expression assumes that there is no change between CC-CV charging states and allows for the creation of a simplified model. It would be possible to extend the functionality to model the resistance as a function of SOC by including a simple counter to update the SOC based on the initial SOC, the charging current and the charging time.

5.5 Modelling of EV battery charger loads

The EV battery charger is a sophisticated power electronic system. In addition to the primary function of supplying regulated dc output to the EV battery, it is required to monitor SOC, temperature and the possible occurrence of faults. Modelling this level of detail and functionality is not required for typical power system load analysis. In this section, the use of the equivalent circuit model and the approach that has been successfully applied for modelling other types of modern non-linear loads, i.e. power electronic loads in Chapter 3 and energy efficient lighting in Chapter 4, is applied to the modelling of EV battery chargers. The generic structure of the equivalent EV battery charger is shown in Figure 5.11.

The measurements presented in Section 5.2 are used as the basis for the analysis in this section. The tests were performed by charging the EV battery using the on-board charging equipment supplied with the EVs connected to a LV distribution network. In this way, the measurement

set-up represents the actual charging conditions. These measurements have been supplemented by measurements obtained from testing of EVs available in the UK at the time of this research. However, it should be noted that voltage sweep measurements could not be performed for EV Type I, II, IV and V so a more detailed discussion of the electrical characteristics of these chargers is not possible.

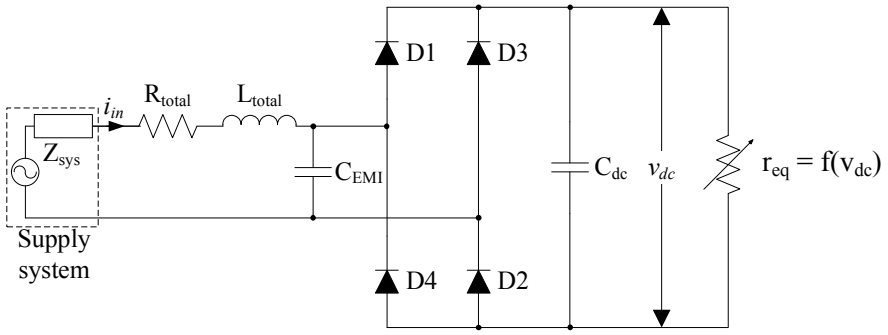

Figure 5.11: General equivalent circuit model of single-phase EV battery charger without a-PFC.

As the majority of measurements used in this analysis were performed by colleagues in Germany [112], access to the EV battery charger circuit was not possible for EV Type I, II, IV and V. In order to obtain the required equivalent circuit model component values, an 'exhaustive search' algorithm was written in MATLAB, using the previously developed analytical model for the power electronics load category (which was updated to include the equivalent resistance function for EV battery chargers). The MATLAB script was configured with estimated ranges for each circuit component, which were based on experience gained in the previous chapters, and then used for simulation of all possible combinations of values within the defined ranges. For each combination, the electrical characteristics (P, Q_1, PF, PF_1, PF_d and THD_I) for the simulated data were compared against the measured data. The model parameters obtained with the best fit to the measured data were then selected. The best fit criterion is simply defined as the minimum sum of percentage errors δ obtained for all parameters, i.e:

$$FIT = min(P_\delta + Q_{1,\delta} + PF_\delta + PF_{1,\delta} + PF_{d,\delta} + THD_{I,\delta}) \tag{5.4}$$

where:

$$\delta = \frac{|measured - simulated|}{|measured|} \times 100 \tag{5.5}$$

As the tested EV battery chargers were measured when connected to the LV distribution network, the supply voltage waveforms were generally found to contain voltage harmonics. Therefore, for each individual EV battery charger, the voltage waveform was decomposed by Fourier transform in MATLAB. This was then reconstructed from the sinusoidal functions at the measured frequencies and supplied to the equivalent circuit model for simulation to allow for a fairer comparison between the simulated and measured data.

5.5.1 EV Type I

Observing the input current waveform of EV Type I, the shape is generally similar to that of the PE no-PFC, although the harmonic content is considerably lower. From the current waveform, the sharp rise of the current pulse indicates a low value of input inductance. The results of the model fitting algorithm validate this presumption, with values for all model parameters given at the end of this section in Table 5.7.

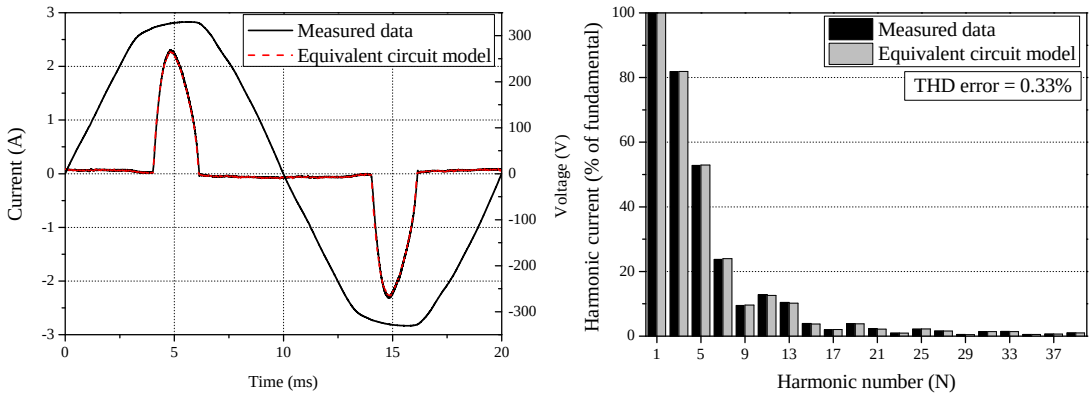

(a) input current waveform (b) associated harmonic content

Figure 5.12: Comparison of input current waveforms and associated harmonic content between the EV Type I model and the measured data at 1 pu voltage.

5.5.2 EV Type II

A good matching between the measured data and the equivalent circuit model for EV Type II is shown in Figure 5.13. The almost triangular current pulse is comparable to the triangular current waveform of CFL loads (see Chapter 4). However, the conduction period is shifted slightly to the right of the voltage waveform period, and the conduction period is smaller than CFLs. This suggests that the dc link voltage is better regulated, which indicates a larger dc link capacitor and a smaller input impedance which does not reduce the rate of charge. The resulting harmonic emissions are higher than the other low-power EV battery charger (EV Type I), .

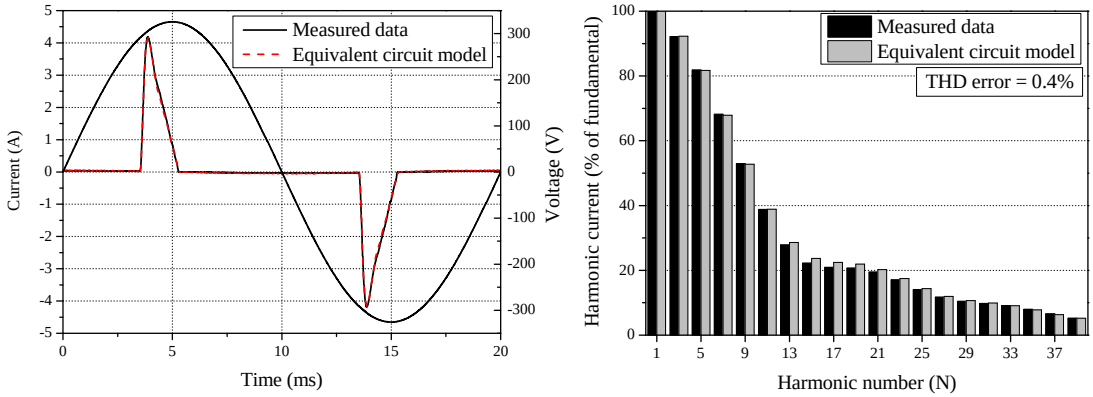

(a) input current waveform (b) associated harmonic content

Figure 5.13: Comparison of input current waveforms and associated harmonic content between the EV Type II model and the measured data at 1 pu voltage.

5.5.3 EV Type III

As EV Type III contains a-PFC, or a controlled front-end rectifier, the harmonic emissions are significantly lower than the measured battery chargers of the other EV types. Similar to the PE a-PFC load, this type of EV battery charger can be modelled as a continuous current waveform, with the active and (fundamental) reactive power demands, and corresponding phase shift, set by traditional (i.e. exponential/polynomial) load models.

Two different EVs from major manufacturers' were measured, denoted Type III-A and Type III-B, respectively. The input current waveforms and corresponding harmonic emissions at rated supply voltage are displayed in Figures 5.14 and 5.15. The input current waveforms of the EV battery chargers are very similar in shape, and this is reflected in the harmonic emissions. Although both sets of measurements were performed for SOC approximately equal to 50%, the peak current value of EV Type III-A is slightly higher than the EV Type III-B, which will result in a higher power demand. The harmonic currents are slightly higher than those measured with 'clean' supply (cf. Figure 5.1), they are still well within the required limits and significantly lower than any other type of measured EV battery charger.

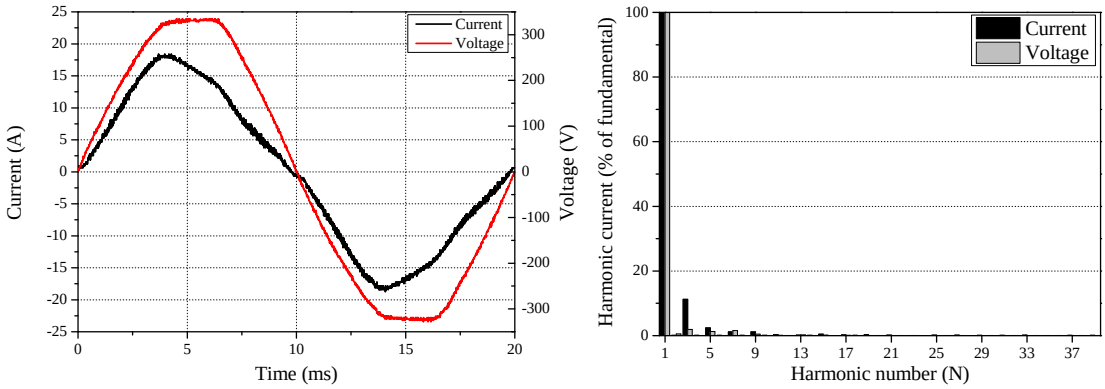

(a) input current waveform (b) associated harmonic content

Figure 5.14: Measured input current waveforms of EV Type III-A battery charger.

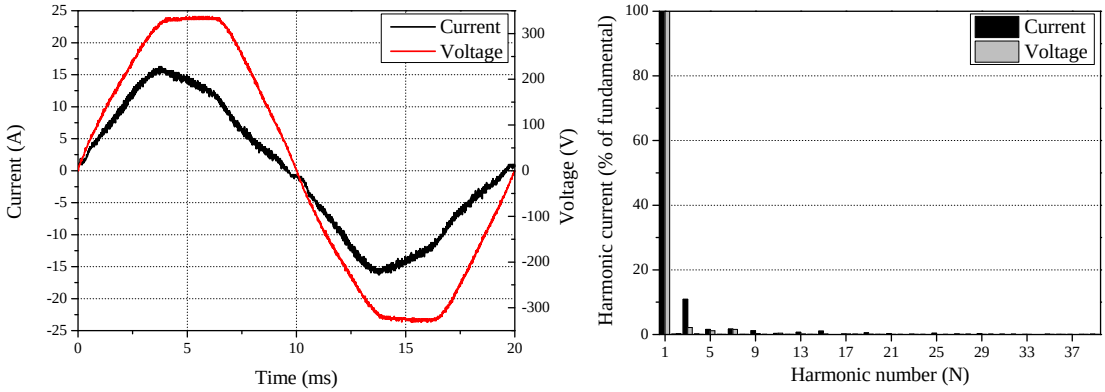

(a) input current waveform (b) associated harmonic content

Figure 5.15: Measured input current waveforms of EV Type III-B battery charger.

To develop the exponential and polynomial load models, the supply voltage magnitude to the EV battery charger was varied between 0.8 pu to 1.2 pu of nominal, in 0.05 pu steps. At each voltage magnitude, the load was allowed to achieve steady-state before the data was recorded. To allow for a more accurate model development, the measurements were performed for approximately the same SOC (around 50%) by discharging the EV battery between measurements. During the experiment, the EV battery charger turned off above a certain voltage magnitude, between 1.15 to 1.2 pu, which is evidence of the protection systems operation.

From the trends of $P-V$ and Q_1-V shown in Figure 5.16 and 5.17, the characteristics of both EV Type III are similar. Results from the MATLAB curve fitting routine are also displayed in Figures 5.16 and 5.17, with coefficient values given in Table 5.6. From the characteristics, both EV Type III battery chargers are behaving close to a constant current load for active power and between constant current and constant impedance for reactive power. For EV Type III-A, serious distortion of the supply voltage (> 5%) occured around 1.15 V_{pu}, which significantly altered the current drawn by the charger. This is clearly visible in the reactive power characteristics in Figure 5.17. Accordingly this data was omitted from the load model development.

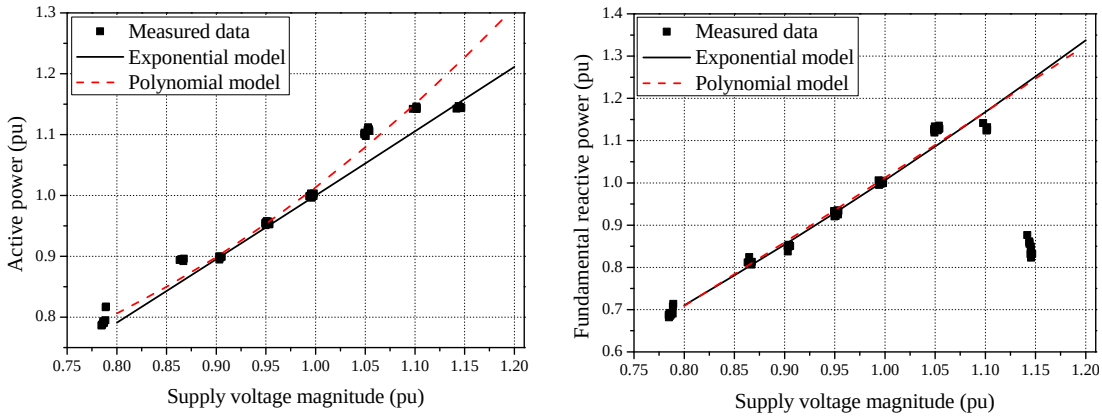

(a) active power (b) fundamental reactive power

Figure 5.16: Measured characteristics of EV Type III-A.

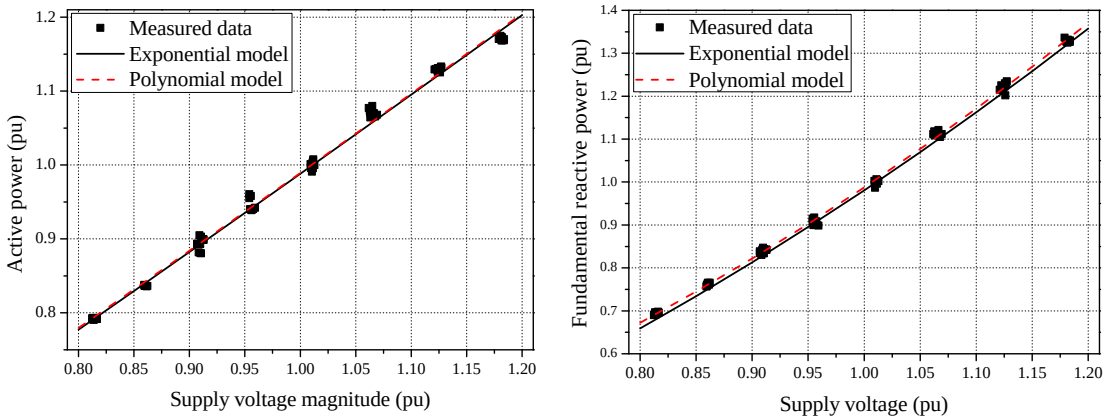

(a) active power (b) fundamental reactive power

Figure 5.17: Measured characteristics of EV Type III-B.

The power demand of both chargers is similar (2.3-2.75 kW) at rated voltage, which is approximately 66-79% of the rated power of the chargers presented in Table 5.1. This is a significant difference in power demand, which may influence results of network analysis. The values measured for the displacement power factor (at rated voltage) are within the bounds of the existing models. However, as the gradient of the $P-V$ and Q_1-V characteristics are different, this displacement power factor will change with supply voltage, and should be included in simulations. This data is included, along with all other electrical characteristics, in Appendix G.

Table 5.6: Proposed exponential and polynomial load models of EV Type III battery charger.

Type	PF_1	Load model							
		Exponential		Polynomial/ZIP					
		n_p	n_q	Z_p	I_p	P_p	Z_q	I_q	P_q
A	0.992	1.051	1.561	0.01	0.99	0.00	0.127	1.281	-0.402
B	0.983	1.077	1.782	0.075	0.926	0.0	0.861	0.0622	0.0842

The measurements of these EV battery chargers demonstrate how the electrical characteristics of the EV battery chargers vary across the entire voltage range. To validate the approximation of the equivalent resistance (defined in (5.3)), the equivalent circuit is configured with appropriate component values to represent the active and (fundamental) reactive power demand of the measured EV Type III battery charger at rated supply voltage. Although the equivalent circuit will draw a discontinuous current waveform from the supply system, the active power and fundamental reactive power (i.e. displacement power factor) characteristics can still be compared against the corresponding measured values. From the results displayed in Figure 5.18, the proposed equivalent resistance is able to predict the P-V and Q_1-V characteristics of the measured chargers with a good level of accuracy. All measured data points lie within five percent of the simulated values for the entire voltage range. This shows that only a small error is introduced by the simplified approach to r_{eq} modelling.

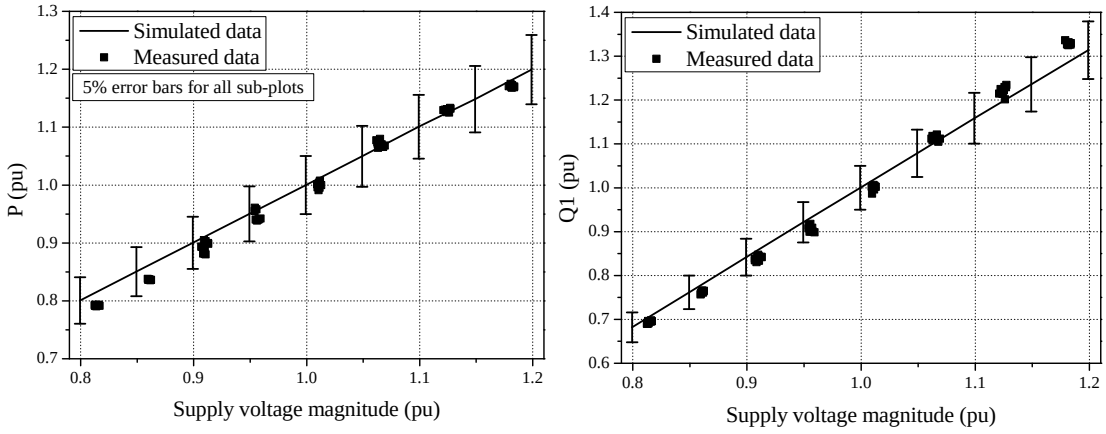

(a) active power (b) fundamental reactive power

Figure 5.18: Comparison between results of the equivalent circuit model and the measured data for EV Type III.

5.5.4 EV Type IV

For high-power EV Type IV, the harmonic emissions are not comparable to any of the previously encountered loads. The waveform does not exhibit the (almost) sinusoidal characteristics of a-PFC and is not characteristic of a p-PFC device, due to the relatively sharp rise of the current pulses. As this EV battery charger has been shown to breach the existing harmonic legislation (Figure 5.3), it is unlikely that this circuit will be suitable for widespread use. However, from the comparison between simulated and measured data, shown in Figure 5.19, the equivalent circuit is able to replicate the input current waveform of this EV battery charger.

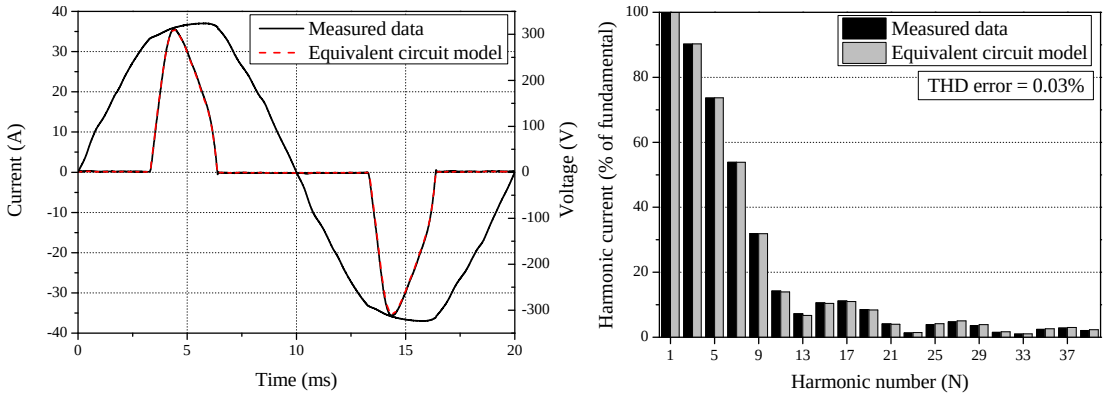

(a) input current waveform (b) associated harmonic content

Figure 5.19: Comparison of input current waveforms and associated harmonic content between the EV Type IV model and the measured data at 1 pu voltage.

5.5.5 EV Type V

EV Type V charger is connected to the three-phase supply and has an input current waveform which is significantly different to all other EV chargers. The charger is operating in discontinuous current conduction mode, which is a result of the low value of input impedance. If the input impedance was larger, the current flowing in the conduction path would not fall to zero and the input current would be continuous. Although three-phase loads are not common in UK residential areas, it is possible to install a special three-phase connection for EV chargers. The operation of the three-phase rectifier, given in Figure 5.20, is similar to the single-phase variant.

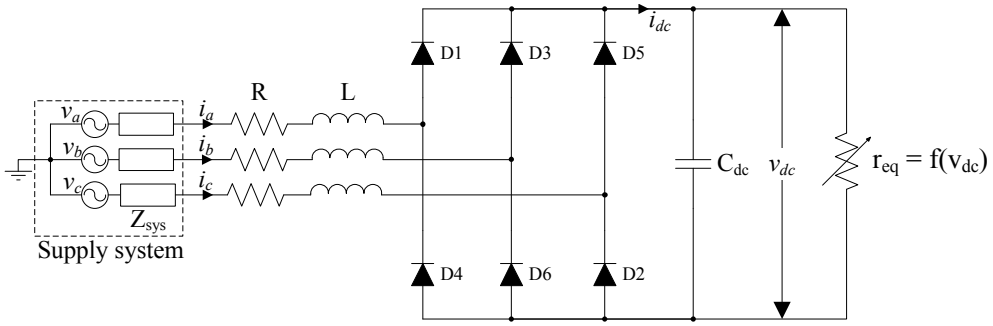

Figure 5.20: General equivalent circuit model of three-phase power electronics rectifier load.

The principle difference in operation lies in the conduction times of the diodes. As with the single-phase circuit, the current will flow through one diode from the top group of diodes (D_1, D_3 and D_5) and one diode from the bottom group (D_4, D_6 and D_2). In the top group, the diode with the highest potential $v_{supply,max}$ at the anode will conduct; in the bottom group, the diode with it's cathode at the lowest potential $v_{supply,min}$ will conduct. In this configuration, each diode will conduct for 120 degrees and there are three conduction pairs per cycle, which is clearly demonstrated in Figure 5.21.

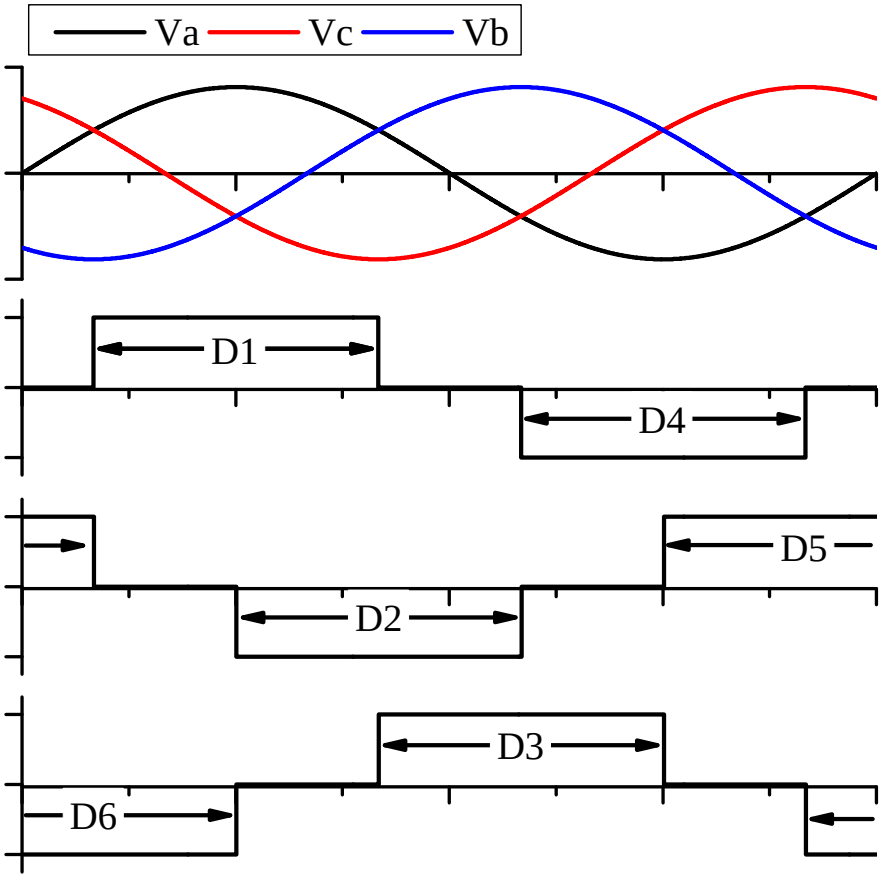

Figure 5.21: Illustration of diode conduction periods in a three-phase diode bridge rectifier.

The three-phase analytical model is developed by modifying the single-phase model. Each phase will have charging and discharging stages, which are based on the single-phase equivalent circuits in Figure 5.22. Therefore, the differential equations which describe the circuit operation are identical to the single-phase equivalent circuit model. Details of these equations, and their solution as an analytical representation, was presented in Section 3.4.1 and is not repeated here.

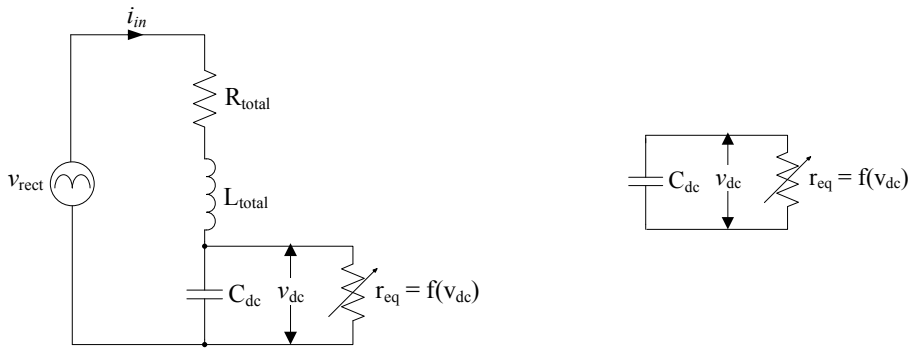

(a) charging state **(b)** discharging state

Figure 5.22: Single-phase circuit representation of the charging and discharging states of the three-phase equivalent circuit model.

The transition between the charging and discharging stages is identical to the single-phase circuit. When v_{dc} is less than v_{rect}, the dc link capacitor C_{dc} will charge through the circuit impedance. As the C_{dc} charges, the dc link voltage will rise and eventually exceed the value of v_{rect}. When v_{dc} is greater than v_{rect}, the C_{dc} will discharge through the connected dc load. This will cause v_{dc} to fall, and the cycle is repeated. However, in this configuration, the input impedance per phase is the summation of the two conducting phases. Also, the rectified voltage v_{rect} is the absoute value of the line voltage, i.e.:

$$v_{rect} = v_{supply,max} - v_{supply,min} = max\{|v_{ab}|, |v_{ac}|, |v_{bc}|\} \tag{5.6}$$

To implement this model, the single-phase analytical script is extended to identify which phases are conducting, using the simple logic rules:

$$i_a = \begin{cases} +ve, & \text{if } D_1 \text{ is conducting} \\ -ve, & \text{if } D_4 \text{ is conducting} \\ 0, & \text{if } D_1 \text{ and } D_4 \text{ not conducting} \end{cases} \tag{5.7}$$

$$i_b = \begin{cases} +ve, & \text{if } D_3 \text{ is conducting} \\ -ve, & \text{if } D_6 \text{ is conducting} \\ 0, & \text{if } D_3 \text{ and } D_6 \text{ not conducting} \end{cases} \tag{5.8}$$

$$i_c = \begin{cases} +ve, & \text{if } D_5 \text{ is conducting} \\ -ve, & \text{if } D_2 \text{ is conducting} \\ 0, & \text{if } D_5 \text{ and } D_2 \text{ not conducting} \end{cases} \tag{5.9}$$

The full MATLAB script for this is included in Appendix C. The ability of the developed three-phase model to reproduce the input characteristics of EV Type V is presented in Figure 5.23.

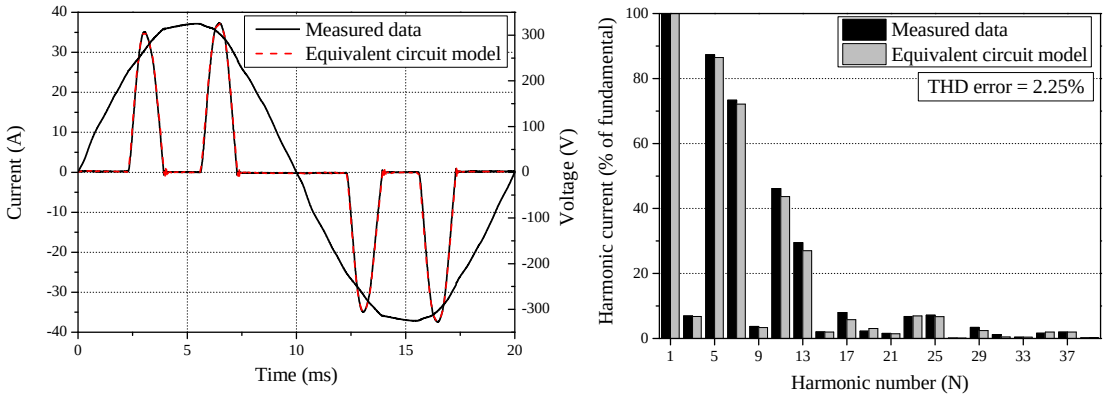

(a) input current waveform (b) associated harmonic content

Figure 5.23: Comparison of input current waveforms and associated harmonic content between the EV Type V model and the measured data at 1 pu voltage.

In this model, the value of dc link capacitor is of smaller size than for the single-phase rectifier of similar power. This is because the dc link capacitor will be charged six times per fundamental frequency cycle in the three-phase connection, as opposed to two times in the single-phase connection. Therefore, the dc link voltage ripple is reduced for three-phase connection. This smaller value of C_{dc} is shown in the model values returned by the MATLAB search algorithm.

5.5.6 Equivalent circuit component values for EV battery charger models

The values of all EV battery charger types discussed in the previous section are included in Table 5.7. As the rated power of the EV battery chargers is unknown, these per-unit values have been calculated using the rms voltage and the power demand of the load during test.

Table 5.7: EV battery charger equivalent circuit model component values.

Parameter (pu)	EV Type			
	I	II	IV	V
$X_{C_{dc}}$	0.0258	0.0834	0.0796	0.447
$X_{C_{emi}}$	9.198	12.58	90.26	601
$X_{L_{total}}$	3.17e-6	6.83e-5	601e-4	7.72e-4
R_{total}	0.0049	0.0028	0.0179	0.0356

These values present a new source of information for modelling of EV battery charger loads. When taken in conjunction with the exponential and polynomial load model values proposed in Table 5.6, this provides more detailed information on the modelling of EV battery charger load. At the moment, the penetration levels of different types of EVs is uncertain. This set of load models covers a wide range of applications, which may be combined using available statistics to build specific load models to represent the particular loading conditions. This could not be addressed within the timescale of this research, but suggestions for this are presented in the following section.

5.6 Aggregate modelling of EV battery chargers

Similar to the analysis of the power electronics and energy efficient lighting load categories, the development of EV battery charger load models presented in this chapter started by considering the electrical characteristics of individual devices. For use in large scale power system analysis, these models must be extended to represent larger number of devices as it is not practical to model every individual EV battery charger. The methodologies presented in Chapters 3 and 4 have demonstrated how the variations between a large number of individual loads can be quantified, and represented using the equivalent circuit model. To produce the same analysis for EV battery chargers will require access to large measurement databases, which are unlikely to be available due to the commercial sensitivity of the information.

Of particular importance to the modelling of EV battery chargers is the battery SOC, as this will dictate the required charging duration. In addition to this, it is also suggested in literature that, due to the two stage charger operation, the power demand of the charger will change depending if it is operating in CC or CV mode. This could have a significant impact on the results of power system studies and should be properly represented. In ideal operating conditions, the power demand of the charger was shown to reduce during the CV stage of the charging cycle. As this corresponds to the higher values of SOC, it is likely that this will account for a large proportion of the aggregate EV battery charger load (i.e. 'top up' charging). However, a series of measurements on two actual EV battery chargers, connected to a typical LV distribution network, has shown that the duration of this stage may be significantly reduced. These measurements have shown that the power demand of the EV battery charger is approximately constant for the entire duration of the charging cycle. The implications of this are that assuming a reduction in EV battery charger demand during the final stages of the charging cycle will lead to an underestimation of the impact on the power system, which, in turn, will result in overly optimistic predictions on the level of EV load which can be supplied. This should be clarified by a widespread measurement campaign in future research.

In current power systems, the penetration of EVs is low and it is, therefore, difficult to predict the characteristics of the aggregate EV battery charger load. However, as the EV battery chargers developed in this chapter cover a range of EV applications and variants of battery charger topologies, this allows for the assessment of a large number of potential scenarios. The contribution of each EV Type can be weighted to reflect the modelled aggregate load and combined with the models presented in the other chapters of this thesis to build aggregate models to analyse specific scenarios. As the models can reproduce the instantaneous input current waveforms of the EV battery chargers, an aggregation of these will also include the effects of harmonic cancellation and provides a powerful tool for power system analysis.

5.7 EV batteries as distributed energy storage

Currently available EVs allow for uni-directional flow of power, from ac supply to the EV battery. However, there is potential for EVs to allow for power flow back into the grid, i.e. acting as energy storage, to provide network support. This reversal of power flow from EVs is widely referred to as V2G. Although not presented as a topic of research in thesis, this could prove to be an important feature of EV load.

As EV batteries are connected directly to the LV network, they are ideally located to offer local support services in V2G applications. Acting as local energy storage units, EVs may help to provide balance between intermittent renewable energy sources or offer peak load shaving. However, using EV batteries for energy storage and local support services will increase the number, and depth, of charge/discharge cycles. This will impact the lifetime and charge efficiency of the EV battery pack. As this is the most expensive component in the EV, this should be considered in detail. This analysis is beyond the scope of the simple equivalent resistance model used power system load models, but can be achieved by extension of the initial work on the development of an EECM of the EV battery.

5.8 Conclusions

The work presented in this chapter adds EV battery chargers as a new load to the existing load library. This is an important result as EV battery chargers may represent a significant proportion of power system demand in the future. A series of measurements was analysed to differentiate between the chargers for different EV applications, from which five distinct types of EV battery charger were identified. After consideration of the electrical behaviour of the EV battery pack, it was demonstrated that the equivalent circuit model, and corresponding analytical interpretation introduced in the previous chapters, could be applied to accurately model the measured EV battery chargers.

As access to the EV battery charger circuits was restricted, an 'exhaustive search' algorithm was developed in MATLAB software to identify values of load model parameters for all charger types. Knowledge of the equivalent circuit model was used to define ranges of values for each component, and the returned values are reasonable for the shape of the input current waveforms. However, two charger types required the use of different modelling techniques.

EV Type III had an almost sinusoidal input current waveform, indicative of a-PFC or active front end rectifier, and can be represented using traditional exponential and polynomial interpretations. From the developed models, the active power characteristics are close to constant current type and the reactive power characteristics are between constant current and constant impedance types. For three-phase charger Type V, it was necessary to modify the previously developed single-phase analytical model to the corresponding three-phase operation. This functionality has been explained within the chapter, and all developed models have been shown to accurately reproduce the measured data.

Chapter 6

Aggregation methodology

6.1 Introduction

The previous chapters have discussed the characteristics and models of individual and aggregate groups of modern non-linear loads. The developed load models are intended for use in a component-based aggregation procedure, which is described in this chapter. This is an important stage in the load development process, as the typically required form of aggregate power system loads is to represent groups of customers with one set of load model parameters. These customer groups are normally defined with respect to certain characteristics and the most common approach is to cluster customers by the performed activities. In this thesis, these groups are referred to as load sectors, with the most common load sectors defined as: residential, commercial and industrial.

The aggregation methodology presented in this chapter combines the previously developed load category generic models to produce the aggregate load models required for power system analysis. The modelling approach offers several advantages over traditional load modelling practices as it is able to retain the short and long-term temporal variations in load characteristics, which are not readily available in existing literature. This is particularly important for the analysis of modern power systems, with an increasing penetration of distributed, time-varying generation and the possible introduction of DSM functionalities and EV battery charging.

Furthermore, as the aggregation methodology is able to reproduce the input current waveforms of the aggregate load for a given supply voltage, it is able to provide more information on the electrical characteristics of the load. In this chapter, standard static load models (i.e. exponential and polynomial) are used to present the results of the aggregation methodology, as they are still the most widely used load model forms for both steady-state and dynamic power system analysis (see Sections 2.3.1 and 2.3.2). However, the power factor values and current THD are also shown, with further implementations of the modelling approach and its application to a range of power system analysis provided in the following chapter.

The UK residential load sector is used to illustrate all stages of the aggregation methodology in this chapter. This uses a range of publicly available datasets to develop the aggregate load model, allowing the methodology to be applied wherever similar datasets are available.

6.2 Aggregate load sector models

Traditionally, load models have been developed at MV and HV levels for use in the analysis of centralised generation systems. At this level, the use of a single lumped generic model is a reasonable approximation, as the large number of customers will mask the naturally occurring variations in the load characteristics when representing such large sections of the network. The most commonly applied load representation was based on the overall characteristics, with constant (voltage independent) power loads being widely applied, as a result of the operation of OLTC transformers which will act to maintain a stable supply voltage. A more detailed approach would consider generic models of typically classified load sectors, e.g. residential, commercial, agricultural and industrial [157].

In available statistical data and government level reports, e.g. [58, 84], load sectors are used to group and represent customers with similar end-use activities. This results in inherent similarities in the power demands and electrical characteristics of load sectors. The residential load sector can be defined as dwellings, whose sole purpose is to provide residency to the occupants. The commercial load sector consists of public, private and voluntary establishments and businesses, which are generally aimed at providing a specific service to the public. The commercial load sector does not include manufacturing activities, which are classified as industrial load sector. The industrial load sector also includes fabrication, material processing and similar activities. Technical literature also adopts similar load sector classification for the development of aggregate load models, e.g. [4, 42, 62].

As the specific industrial processes at different sites are usually not comparable, it is generally not possible to define generic load models for the industrial load sector. It is more common to build a specific load model for large industrial customers, and assume a mix of motors and lighting for smaller industrial customers [62, 158]. However, aggregate load models for the residential and commercial sector are more widely available for use in power system analysis, with a sample of the available load sector models shown in Table 6.1.

The existing models present one set of load model parameters for each characteristic loading condition, i.e. maximum, minimum and year average, and confirm that the electrical characteristics of the load sectors are strongly influenced by the location and time of year, both of which influence the composition of the load. As the load composition will also change within the diurnal cycle, they may also change the electrical characteristics of the load. These short-term variations are not captured by the existing load models.

Table 6.1: Residential and commercial load sector load models identified in literature.

Ref	Year	Loc.	Sector	Subsector	Voltage level (kV)	Time of year	Model form	PF_1	Model parameter values
[96]	1982	US	Res.	ns	ns	S	Exp.	ns	n_p= 1.132, n_q= 1.79, k_{pf}= 0.348, k_{qf}= -1.62
			Com.	ns	ns	S	Exp.	ns	n_p= 0.664, n_q= 4.01, k_{pf}= 0.9824, k_{qf}= -11.3
[1]	1994	ns	Res	ns	ns	S	Exp.	0.9	n_p= 1.2, n_q= 2.9, k_{pf}= 0.8, k_{qf}= -2.2
						W	Exp.	0.99	n_p=1.5, n_q=3.2, k_{pf}=1.0, k_{qf}=-1.5
			Com.	ns	ns	S	Exp.	0.85	n_p= 0.99, n_q= 3.5, k_{pf}= 1.2, k_{qf}= -1.6
						W	Exp.	0.9	n_p= 1.3, n_q= 3.1, k_{pf}= 1.5, k_{qf}= -1.1
[62]	2004	US	Res.	ns	21	ns	ZIP	0.85	Z_p= 0.29, I_p= 0.1, P_p= 0.61 Z_q= 3.22, I_q= -4.53,P_q= 2.31
			Com.	ns	21	ns	ZIP	0.82	Z_p= 0.21, I_p= 0.15,P_p= 0.64 Z_q= 3.2, I_q= -4.5, P_q= 2.3
[55]	2008	Serbia	Res.	HU	10	S	Exp.	ns	n_p= 1.572, n_q= 4.101
						W	Exp.	ns	n_p= 1.761, n_q= 3.656
						Y	Exp.	ns	n_p= 1.629, n_q= 3.968

Where: Loc. - location, Res. - residential, Com. - commercial, HU - highly urban, S - summer, W - winter, Y - year average
ns - not stated, Exp. - exponential load model, ZIP. - polynomial load model, PF_1 is the displacement power factor and load model coefficients n_p, n_q, k_{pf}, k_{qf}, Z_p, I_p, P_p, Z_q, I_q, P_q are as defined in Chapter 2.

6.2.1 Residential subsectors

As the size of the aggregate load decreases, i.e. as the point of analysis moves from high to low-voltage, the influence of individual loads becomes more pronounced. At the lower voltage levels, the aggregate load models will be more sensitive to variations in end-use activities, building size, location and network configurations of the represented load/network. These factors effectively divide one load sector into several subsectors. This is confirmed in a number of studies and measuring campaigns, e.g. [96, 159, 160, 161, 162, 163]. In this chapter, the residential load sector is used to illustrate the aggregation methodology, and some consideration is given to the possible variations within this load sector.

Although the purpose of every residential dwelling is identical and, generally, the individual loads used there will be similar, it is possible to divide this sector into four subsectors based on the location, size and type of dwelling. The location and size will determine the network conditions, e.g. network strength, transformer rating and cable/overhead line length, and also the load density. Although small technological variations can be expected, it is these two factors which play the biggest role in the classification of the residential subsectors.

The level of street/outdoor lighting will also be influenced by the location and differences will also exist in terms of the size of renewable/distributed generation that is likely to be located in close proximity to the residential areas. The effect of MG can also be included in the aggregation methodology and is considered in more detail in Chapter 7. Based on these general characteristics and parameters, the residential load sector can be divided into the following subsectors: highly-urban, urban, suburban and rural.

Highly-urban residential load subsector

This subsector is represented by flat-type dwellings, usually found in large cities, in multi-storey and high-rise buildings and it is characterised by highly concentrated power demand. Three-phase motors may be used for elevators, pumps and central air-conditioning (AC) systems, which are usually not present in other residential subsectors. The number of rooms per dwelling is expected to be lower than in other subsectors, and there will be additional interior lighting load for illumination of communal areas. Dedicated public/street lighting is also greater than in other subsectors, due to the presence of parking spaces and higher required lighting levels in metropolitan areas.

Urban residential load subsector

This subsector consists of house-type dwellings, ranging from one to few-storey buildings, located in city urban areas and it is characterised by medium to high concentration of power. As the average number of residents and rooms per household is greater than in the highly-urban subsector, higher power demands per household may occur. The public/street lighting in this sector is slightly reduced in comparison with the highly-urban subsector.

Suburban residential load subsector

This subsector is similar to the urban subsector, representing individual house dwellings located in city suburban areas and towns in close proximity to big cities. The load mix is similar to the urban subsector but the contribution from public/street lighting is likely to be slightly reduced. It is further characterised by medium power density.

Rural residential load subsector

House-type dwellings in this subsector are one to few-storey buildings, located in more remote areas. Power density is low and some (smaller) three-phase motors may be used for agricultural works. Another notable difference is that no public/street lighting is present. Furthermore, the connection of larger DG is possible in this subsector.

Network classification

In addition to differences in load composition, there will be significant differences in the LV network supplying the loads. In the UK, LV networks are connected to the distribution network by 11/0.4 kV secondary distribution transformers. The typical network layout features several three-phase trunk feeders that supply a number of lateral spurs, to which customers are connected by single-phase service cables. The location of the network and the supplied customers will determine the specific characteristics of the network. In highly-urban and urban areas, both the three-phase trunk feeder and single-phase service cable are underground cables. In suburban areas, the three-phase trunk feeder is overhead line type, while the service cable may be either underground or overhead connection. In rural areas, overhead lines are exclusively used for all network connections. In addition to this, the supplied load density, which reduces proportionally from highly-urban to rural networks, will determine the length of the feeders and the rating of the transformer, with shorter cable lengths and higher rated transformers in areas with larger loads. The shorter cable length will ensure that the voltage drop across the feeder impedance does not breach the stipulated limits of 400/230 (+10%/-6%) V.

6.3 Aggregation methodology overview

The analysis presented in this thesis has shown that modern loads often contain sophisticated control circuits and, therefore, impose additional requirements for load modelling. The load control circuits may have significant impact on the performance of both the local electricity network and power supply system as a whole in a range of areas, e.g. power flow, voltage stability, harmonic propagation, voltage distortion and voltage fluctuations etc. Therefore, newly developed load models should be able to represent all relevant load characteristics, and allow for the extraction of specific characteristics for the required power system analysis.

The aggregation methodology is developed with respect to the following key requirements, which are considered important for building improved and more detailed aggregate load models for the analysis of existing and future electricity networks:

- Models should allow for aggregation to a range of voltage levels. While many future engineering challenges will be more focussed on the distribution networks than before, there will still be changes/impacts at the transmission level. Therefore, it should be possible to transform the aggregate load model from LV to HV levels, to allow for tracing the effects of changes in the LV network load/operation, e.g. through DSM actions, and related interactions through the wider power system.
- They should be able to correctly represent time varying demands, as the connected load will exhibit short-term (e.g. hourly, daily), medium-term (e.g. seasonal) and long-term (e.g. changes in load technology) variations. As the load mix changes, the aggregate load model will also change. Table 6.1 shows that some variations have been considered in the aggregate load models developed by previous research. Additionally, this will allow for better correlation with local generation, which will also exhibit short, medium and long-term variations. In future networks, this may include embedded LV MG and MV DG, which should also be included in any higher voltage load model.
- It should allow for easy integration of new load types/categories, e.g. EV battery chargers, and be easy to modify/update to analyse expected changes in load mix and technological modifications, e.g. higher penetration of energy efficient loads or reduction in rated power in power electronics harmonic legislation from 75 W to 50 W [20].

An overview of the aggregation methodology is illustrated in Figure 6.1. This also includes the connection of LV MG, which is discussed in the following chapter. Three sets of input data are required to fully represent each component within the methodology. To model the aggregate load: measured, estimated or simulated load demand curves, statistical or simulated decomposition of load mix and generic load models of the load components are required. The equivalent data for the network model is: the network configuration, typical component values and the component models. The methodology combines these datasets to develop the aggregate MV load model and can be divided into the following main stages.

For the measured or estimated demand curves, the corresponding load mix of the modelled load sector is identified. This should include both short-term (i.e. half-hourly/hourly) and medium to long-term (weekly to yearly) variations in active and reactive power demands of the considered load sector. Next, the load mix is converted into the main load categories, based on the general electrical characteristics of the equipment and devices within the aggregate load. The identified load categories are then represented using the corresponding generic load models, which, based on their contributions to the total active power demand of the modelled load sector, are combined to create the LV aggregate load model. The aggregate LV load model is then connected to the corresponding MV/LV network configuration, where the supply voltage magnitude is varied, in order to identify changes in the input current waveform, and associated/required electrical characteristics. This information is used for the formulation of the aggregate MV load model.

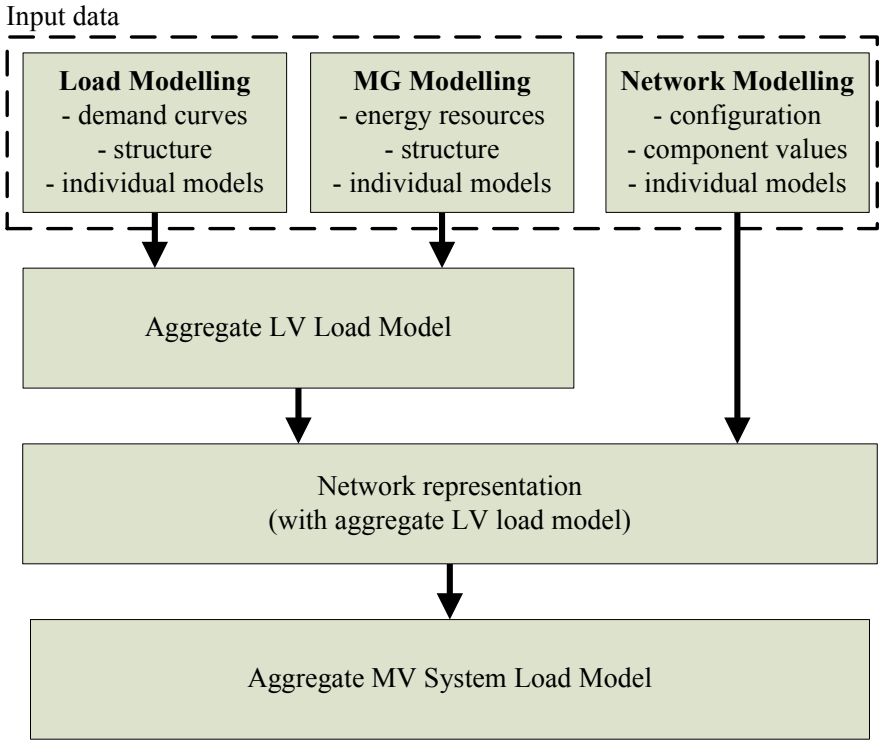

Figure 6.1: Overview of the aggregation methodology.

6.4 Load modelling

The first step of the aggregation methodology is to identify the load structure and load composition of the modelled load sector or subsector. Three sets of data are required: load curves (detailing how active/reactive power demands vary over the considered time period), and statistical information on the contributions of different load types to the total demand. This data is then converted into the load composition as represented by the previously defined load categories. This is illustrated in this section using the UK residential load sector, but the method may be applied to any similar datasets.

6.4.1 Load demand curves

This data may be available in government reports, e.g. [17], from research bodies, e.g. [160, 161, 162, 164, 165, 166], meaurement campaigns by utilities/network operators/research bodies, e.g. [167], or can be developed from techniques and methodologies in existing literature, e.g. [159, 163, 168].

To illustrate the methodology, typical aggregate load curves of the UK residential load sector given in [17] are shown in Figure 6.2. This represents the overall UK residential sector demand. However, as the urban subsector accounts for more than 50% of residential demand, this subsector can be considered representative of the overall UK residential sector demand.

The curves for the three characteristic loading conditions illustrate the short and long-term temporal variations in power demand. Between the three curves, the general profile is similar as user behaviour will not significantly vary throughout the year. The recorded seasonal variations are a result of changing contributions from physically-based loads, i.e. loads which respond to changes in the ambient conditions (through user response or internal thermostatic controls). Therefore, it is likely to expect increased/reduced contribution from lighting and electric space and water heating during the winter/summer seasons, respectively.

Available load demand curves will, generally, only provide information on the changes in active power demand, and a fixed power factor, typically around 0.95 - 0.98 (inductive), is often assumed for modelling purposes. The (fundamental) reactive power demands, which are represented by the displacement power factor PF_1 in Figure 6.2, are actually an output of the load modelling process. For aggregate loads, this presentation of reactive power characteristics is more intuitive than a normalised plot. Overall, the displacement power factor value will increase as active power demand increases, which can be attributed to the increased use of resistive loads. An additional effect is observed when the lighting demand includes CFLs, as their capacitive nature will act to compensate the inductive loads within the aggregate demand.

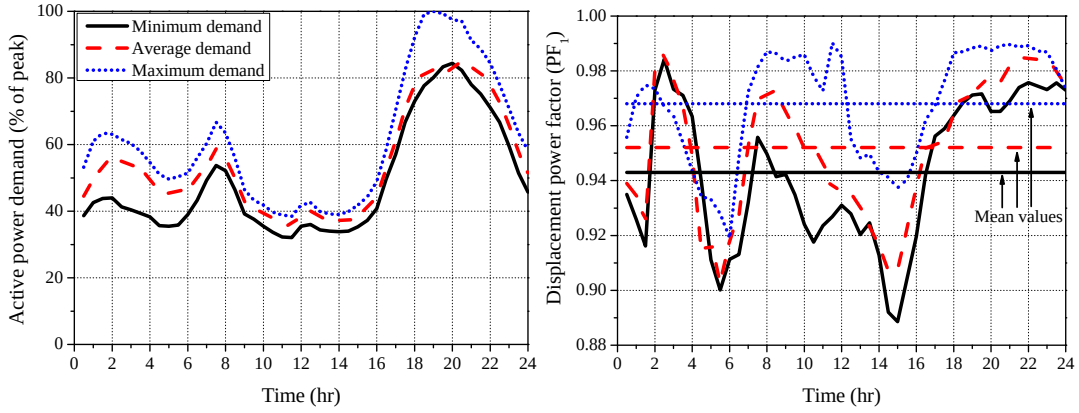

(a) active power [17] **(b)** displacement power factor

Figure 6.2: Typical aggregate daily load demand curves for the UK residential load sector for three characteristic loading conditions.

6.4.2 Load structure

Information on load structure/composition is available from a wide range of sources, with many of the previous references, e.g. [17, 159, 160, 161, 162, 163, 165, 166, 168], also including this information. There are also several attempts in literature to decompose the aggregate load using power system measurements. One common approach is to use the active and reactive power response to staged dynamic tests to determine the load composition, examples include [39, 42, 62]. In these examples, the OLTC transformer is used to initiate a staged voltage drop

and the active and reactive power responses are measured. The typical responses of the main loads within the aggregate are then used to determine the percentage contribution of each. This method has been shown to provide a reasonable estimate of the load composition. Another method, proposed in [169], is to analyse the network current flow to identify the composition. However, as shown in the previous chapters of this thesis, the effects of harmonic cancellation and attenuation make it difficult to obtain accurate results with this method.

Figure 6.3 (shown overleaf) plotted using the data given in [17], illustrates how the load curve for the UK residential load can be decomposed into the corresponding load mixes. In this figure, the electrical devices and equipment found in the residential load sector are divided into the following types of loads: consumer electronics (CE) and ICT equipment; cooking load; 'wet' load; 'cold' load; direct and storage domestic hot water (DHW) load; direct, storage and top-up space heating load; and lighting load. These are the most widely used load types for characterising residential load sector demand.

6.4.3 Conversion of load type to load category

Due to the large number of possible load variants within the residential load sector, it is not possible to directly convert the load types into the aggregate load model. An intermediate stage is required to convert from the load type mix (Figure 6.3) into the categories of load models which have been presented in the previous chapters of this thesis.

All types of electrical equipment and devices found in the residential load sector can be divided into one of five general load categories:

1. Power electronics load
2. Resistive loads
3. Energy efficient light sources (CFL and LED LS)
4. Single-phase and three-phase directly-connected motors
5. Drive-controlled motors, i.e. ASD loads

As discussed in Chapters 3 and 4, harmonic legislation [20] and technology/circuit topology variations in equipment design effectively introduced subcategories within some of the general load categories. Figure 6.4 on page 154 shows the general load categories and subcategories commonly found in the residential load sector (Note: These load categories/subcategories also represent the corresponding loads in other load sectors, e.g. commercial or industrial, and the shown motor variations are applicable for all possible motor connections, i.e. single/three-phase directly connected and single/three-phase drive controlled motors).

Chapters 3 and 4 have discussed in detail the subcategories within the power electronics and energy efficient lighting load categories. To complete the description of the load categories, a brief overview of the motor load categories is required.

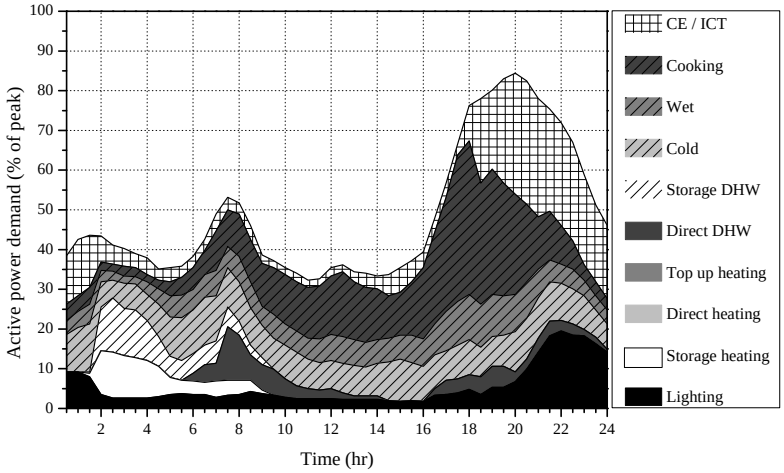

(a) minimum loading conditions

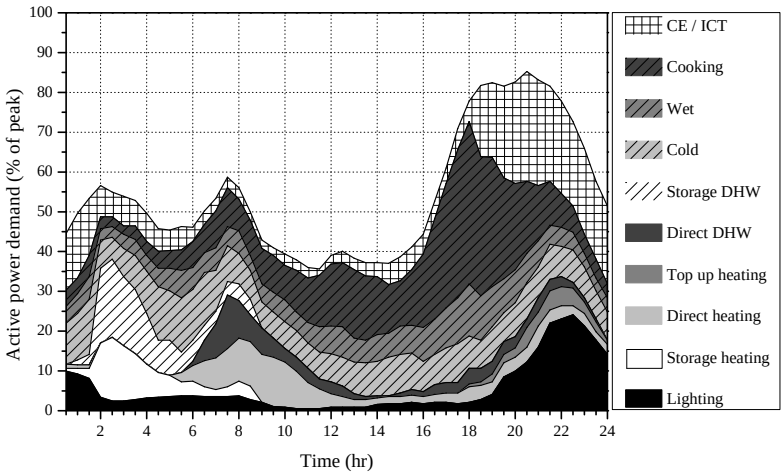

(b) average loading conditions

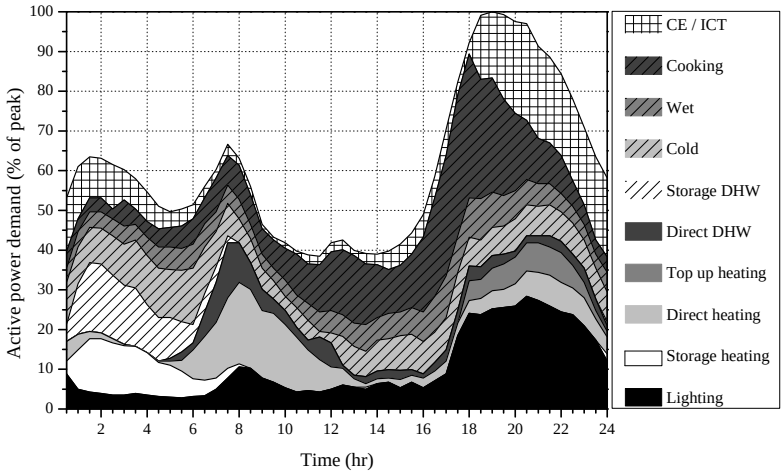

(c) maximum loading conditions

Figure 6.3: Decomposition of the UK residential load sector into load types for three characteristic loading conditions, using information in [17].

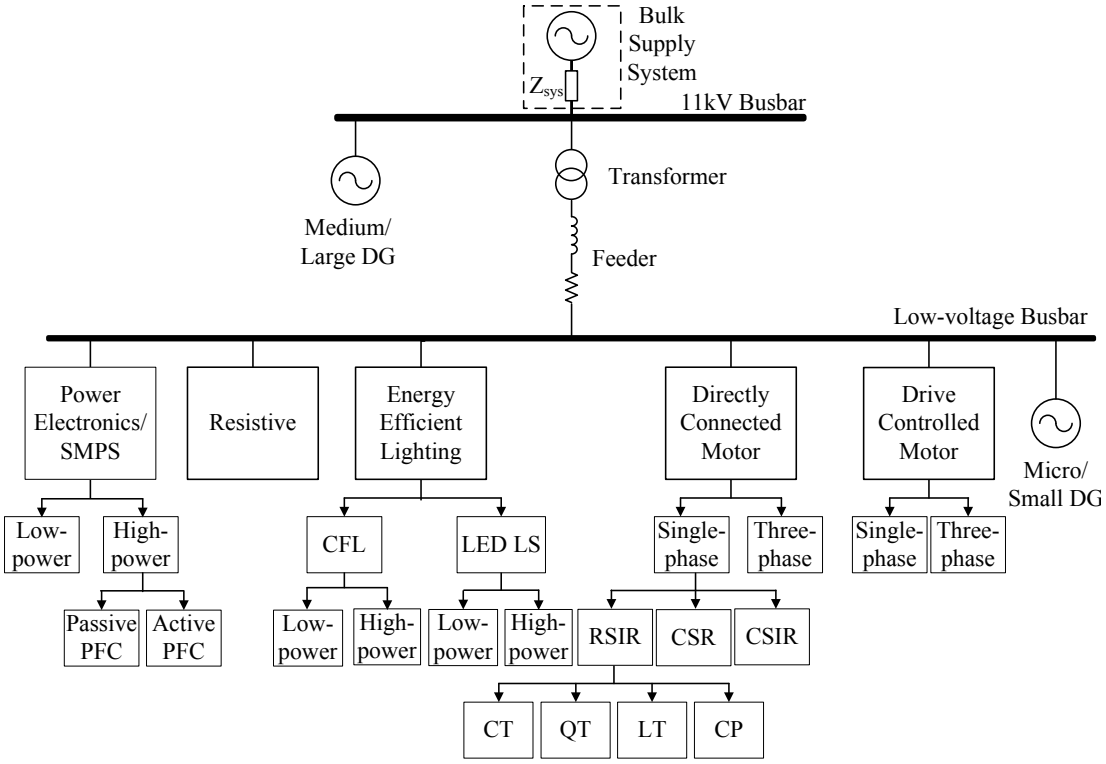

Figure 6.4: Main load categories and subcategories in the residential load sector.

Motor load overview

IMs are responsible for a large portion of the annual electricity consumption and significant effort has been dedicated to developing load models for a range of power system studies. Accordingly, there is no need to develop new models for the load aggregation methodology presented in this thesis.

There are various ways to categorise IMs. In this research, they are defined with respect to their electrical connection and also to the mechanical load. With respect to the electrical connection, the motors are designated as either single-phase or three-phase. In the UK residential load sector, SPIM are by far the most dominant technology. SPIMs are actually two-phase IMs, as a motor with a single winding cannot develop rotating magnetic field to start. Thus, an auxiliary winding is used to develop starting torque. The most common types of SPIM are: split-phase, capacitor start and capacitor start-capacitor run.

The split-phase SPIM is the most simple form as there are no additional electrical components required. In this configuration, the SPIM is equipped with unsymmetrical stator windings. The auxiliary stator winding is disconnected once the motor reaches a certain speed. This may also be referred to as 'resistive start-inductor run' (RSIR) SPIM. When higher starting torque is required, a capacitor can be placed in series with the auxiliary winding. This capacitor can be switched out once the motor has reached a certain speed or not, leading to two variants, de-

fined as 'capacitor start-inductor run' (CSIR) and 'capacitor start-capacitor run' (CSR) SPIM. For steady-state operating conditions, as considered in the research in this thesis, there is no difference between RSIR and CSIR SPIM.

The directly connected variants are generally used in applications such as refrigerators, washing machines and clothes dryers [41]. It is possible to have drive-controlled SPIM but they normally utilise a single-phase front-end rectifier with a three-phase inverter controlling a three-phase IM. These are not widespread within the UK residential load sector, but their use is expected to increase in the future. Further details of these motors is presented in the development of the commercial load sector model in Chapter 7.

The final distinction between motor types is the mechanical load on the rotor shaft. These are normally grouped into three general types: variable torque (VT) loads, constant torque (CT) and constant mechanical power (CP) loads [170, 171]. Variable torques may be divided into quadratic (QT) and linear torque (LT), depending if torque is directly proportional to the motor speed or to the square of the motor speed. Examples of variable torque loads include centrifugal pumps and fans. Constant torque loads include compressors, conveyors and traction drives. For constant mechanical power loads, the torque varies inversely to the motor speed, and examples of this load are grinders and winders. Figure 6.5 shows these characteristics, with a more comprehensive overview of motor load torque and the specific applications available in [170].

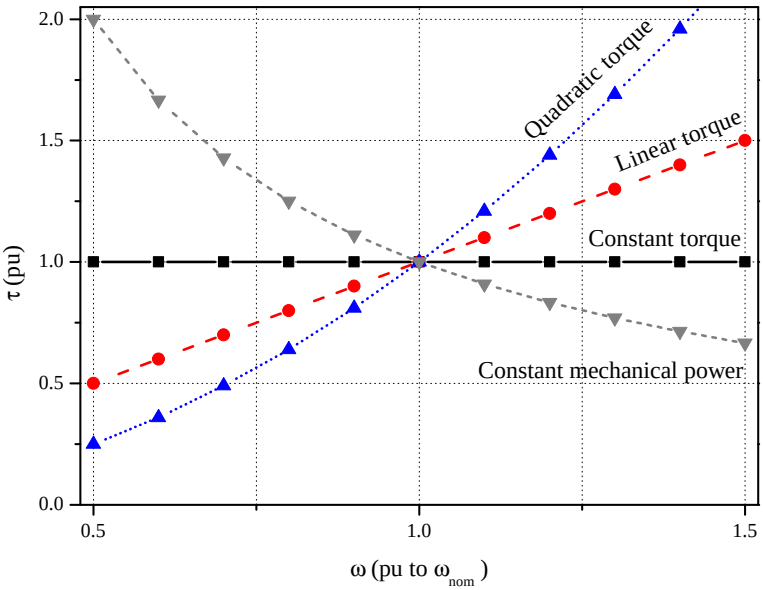

Figure 6.5: Types of mechanical torque.

The types of motors utilised for the major residential applications is considered in more detail in the following sections, and the corresponding load models are given in Table 6.3 on Page 162. As they draw a continuous current waveform from the supply system, they are represented by the polynomial/ZIP model during the aggregation process.

Conversion of residential lighting load type into corresponding load categories

As discussed in Chapter 4, the widely advocated phase-out of incandescent bulbs has increased the contribution of the energy efficient lighting load category in the residential load sector, and will further increase the contribution of these loads in the future. CFLs are the most developed technology in this sector, and are currently responsible for around 23% of the total UK domestic lighting demand [58].

According to [172], the most common types of GILs used in the UK residential sector are of rated powers 40 W, 60 W and 100 W, making up 46%, 46% and 8%, respectively, of the estimated stock of GILs in residential load sector. The current recommendation/trend is to replace 40 W, 60 W and 100 W GILs with 8 W, 11 W and 18 W CFLs, respectively, as they have similar values of total output lumens. Although LED LSs have recently been introduced to the mass market, their cost is still high so their expected current contribution is negligible. However, this is expected to increase in the future.

Figure 6.6 shows the conversion of the lighting load type into the correct load categories. In this process, HIL are grouped together with traditional incandescent lamps, as the available measurements of typical rated powers indicate similar electrical characteristics.

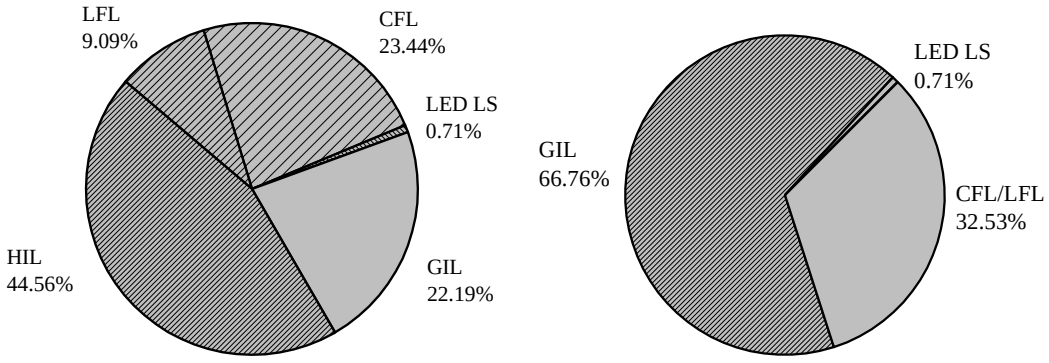

(a) by load type [58] **(b)** by load category

Figure 6.6: Conversion of lighting load type demand into the corresponding load categories and subcategories.

Conversion of residential space and water heating load type into corresponding load categories

The main principle of operation of electrical space and water heating load is a resistive heating element which heats the surrounding air or water. There are two possible variants of this type of load type, however, the load category is the same for both. The heating element in storage space and water heaters will typically be rated between 2-6 kW and used in conjunction with off-peak energy tariffs, i.e. Economy 7. Direct space and water heaters, which includes electric showers, generally have a higher rated power, between 2- 9 kW. Although the rated power will vary between direct and storage heaters, this information is not required for aggregate load modelling and this entire load type demand may be represented by the resistive load category.

Conversion of residential 'cold' load type into corresponding load categories

'Cold' load covers all types of refrigerators and freezers. These are typically divided into: refrigerators (14%), fridge-freezers (58%), upright-freezers (18%) and chest-freezers (10%), with the contribution to the total 'cold' load demand given in parentheses [58]. These devices operate by circulating a refrigerant which absorbs heat from within the device and expends this via external heat exchange pipes. This cycle requires the refrigerant to change state, i.e. from gas to liquid and liquid to gas, which is achieved by a compressor and an expansion valve. The electrical demand is a result of the SPIM used to drive the compressor. This will cycle on and off as a result of thermostatic control to maintain the desired temperature, with the typical cycle lasting around 45min (with a duty ratio of approximately 0.33, i.e. 15 min 'on', followed by 30 min 'off'). However, for the representations of aggregate loads, as proposed in thesis, these variations will cancel over a large aggregate load and present a constant base load.

As the compressors used in such devices do not require high starting or running torque, it is expected that 100% of this load uses RSIR SPIMs. The motor load is a reciprocating compressor which behaves as a constant torque mechanical load [170]. Although the different temperatures of fridges and freezers will require different sizes, and therefore, rated powers, of SPIM compressors, this information is not required for the analysis of aggregate loads. However, this data is required for the development of individual household load models and is discussed further in the last chapter of this thesis.

Conversion of residential 'wet' load type into corresponding load categories

'Wet' load consists of: dishwashers (22%), tumble-dryers (31%), washer-dryers (16%) and washing machines (30%) [58]. During the typical operating cycle of these devices, given in Figure 6.7, multiple operations are performed by these loads. In the case of the washing machines, tumble-dryers and washer-dryers, the device will have a resistive heating element, with high rated power, to heat the water or air to the required temperature, and a motor to rotate the drum. Similarly, dishwashers will have a resistive heating element to heat the water and a motor to drive a fan to produce a rotating spray of water for the cleaning process. Additionally, washing machines, washer-dryers and dishwashers will have a pump to draw water into the appliance and also to flush water out. The different stages are clearly visible in the operating cycles.

Due to high running torque requirements to agitate and rotate the drum, tumble-dryers, washer-dryers and washing machines are expected to utilise CSR SPIMs, while dishwashers will use RSIR SPIMs. The motor loads will operate with constant torque [170]. Even though the washing machine and washer-dryer will typically have two stages of spin speed, the torque conditions are approximately constant for the entire wash cycle which accounts for around 90% of the standard operation. The centrifugal pump commonly used in domestic appliances will present a quadratic torque load to the motor [170, 173].

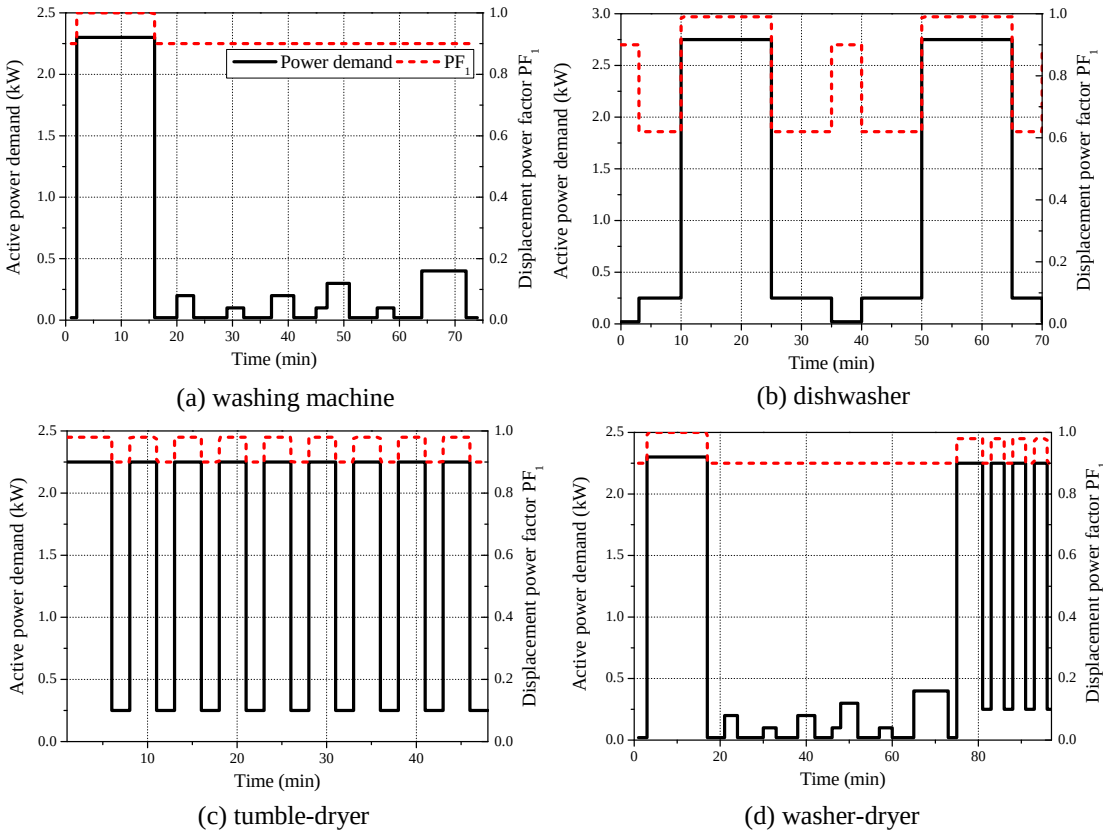

(a) washing machine (b) dishwasher

(c) tumble-dryer (d) washer-dryer

Figure 6.7: Typical operating cycles of 'wet' load devices, active power data taken from [166].

For the development of the aggregate model, the total overall effect of these cycles is required. Therefore, each operation of the segment of operating cycle is divided into the electrical loads and used to calculate the contribution of each load category to the total operating cycle demand. However, from the data in Figure 6.7, it is clear that the resistive element will dominate the electrical characteristics of the aggregate 'wet' load representation. This calculation is shown in Table 6.2. In this table, motor refers to the SPIM driving the main process, i.e. the CSR SPIM driving drum rotation in washing machines, washer-dryers and tumble-dryers and the RSIR SPIM driving the fan rotation in dishwashers.

Table 6.2: Calculation of aggregate 'wet' load characteristics.

Load.	Contribution to power demand					
	Resistive		Motor		Pump	
	(kWh)	(%)	(kWh)	(%)	(kWh)	(%)
WM	0.54	83	0.1	15	0.01	2
TD	1	83	0.2	17	-	-
WD	0.97	82	0.01	1	0.2	17
DW	1.25	85	0.21	14	.005	1

The data in Table 6.2 is combined with the overall contribution of each load type to the total 'wet' load demand to convert from the load types into the load categories, in Figure 6.8.

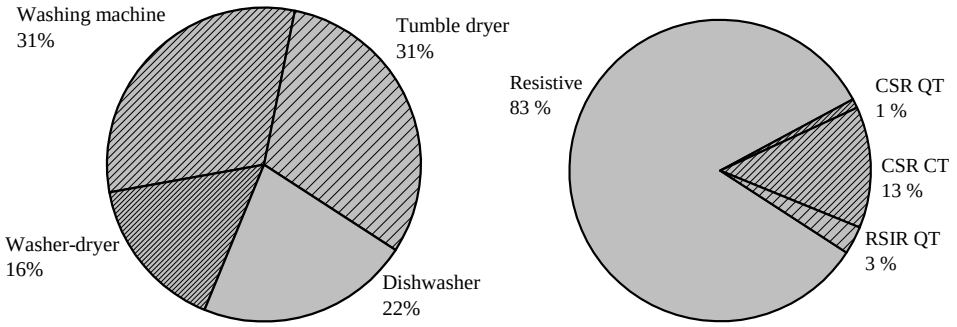

(a) by load type [58] **(b)** by load category

Figure 6.8: Conversion of 'wet' load type demand into the corresponding load categories and subcategories.

Conversion of residential cooking load type into corresponding load categories

Cooking loads can be divided into five general types: ovens, hobs, kettles, microwaves and small appliances. In the UK, the primary energy source for the main cooking loads, i.e. ovens and hobs, is gas, which is responsible for around 57 % of cooking energy. However, due to the high rated power of electric cooking appliances, typically between 2 - 3 kW for ovens, hobs and kettles and 0.6 - 1.2 kW for microwaves, there is still a considerable demand from electric cooking in the residential load sector.

Electric ovens, hobs and kettles all include a heating element, which can be modelled as a resistive load. Despite the difference in operation, measurements of induction cookers have a very high displacement power factor, greater than 0.99, which indicates that there is no need to make a distinction between the different types [127]. The more complex operation of microwaves requires the rectification of the supply voltage and is assumed to be PE p-PFC load category. These rules are applied to convert the cooking load type into the corresponding load categories, shown in Figure 6.9.

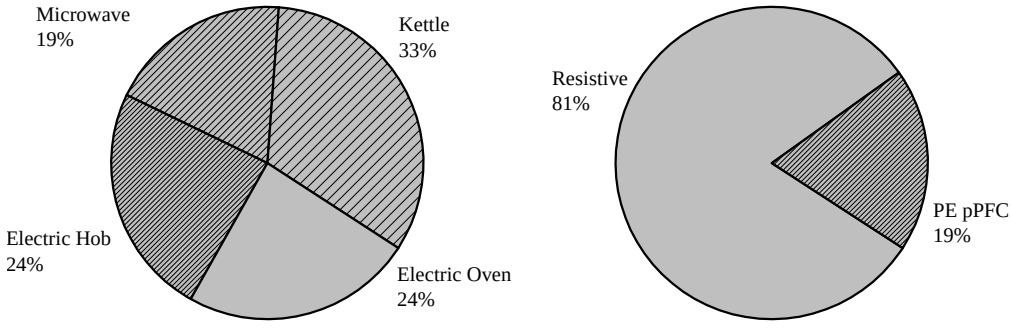

(a) by load type [58] **(b)** by load category

Figure 6.9: Conversion of cooking load type into the corresponding load categories and subcategories.

Conversion of residential consumer electronics load type into corresponding load categories

The consumer electronics loads include a large number of different load types, highlighting how the load model aggregation process is simplified by defining load categories. TVs, VCR/DVD players, set-top boxes and all variants of power supplies are classified as consumer electronics. Out with TVs, it can be assumed that all devices are of rated power less than or equal to 75 W and are modelled by PE no-PFC. However, TV load requires more careful consideration.

In the UK, households will typically have more than one TV set: one larger in size and with higher rated power, classed as the primary TV, and a smaller one, with lower rated power, classed as the secondary TV. Furthermore, this load type features several different technologies, most notably: plasma, LCD/LED and CRT. Rear projectors (RP) may also be found in the residential load sector, but they are responsible for only a fraction of demand and can be omitted from further analysis. The percentage contribution of different types of TV sets to the total UK consumption of all TV loads is shown in Figure 6.10.

Secondary TVs are all classed as low-power devices, i.e. their rated power is less than 75 W, exempting them from harmonic legislation requirements stipulated in [20]. Accordingly, they are assumed to have no PFC circuit (marked as PE no-PFC in Figure 6.10(b). Around 15% of CRT and LCD/LED TVs are considered to be secondary TVs [174]. Primary TVs are classed as high-power devices, with rated power greater than 75 W, and they must satisfy harmonic legislation in [20]. Therefore, primary TVs will feature some form of PFC circuit. Due to the falling cost of power electronics, more sophisticated a-PFC units are expected to be present in newer technologies, e.g. LCD, while p-PFC is expected to be utilised in older technologies, e.g. plasma and CRT TVs. This information is used for processing data from Figure 6.10(a), resulting in the representation of all types of TV loads using only the three general load subcategories introduced in Chapter 3. This data is displayed in Figure 6.10(b).

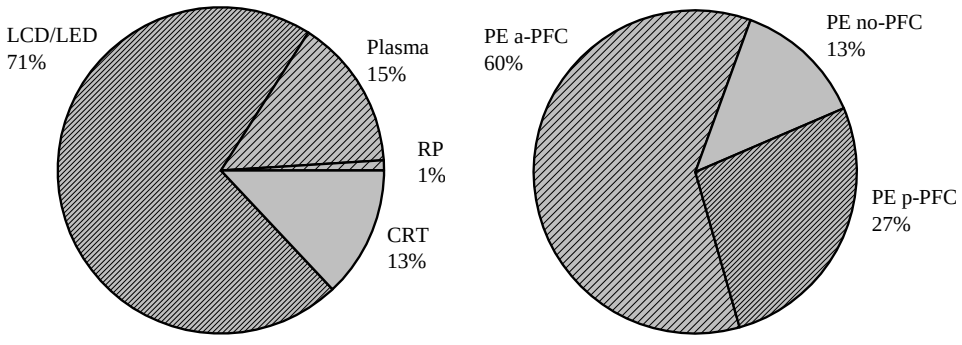

(a) by load type [174] **(b)** by load category

Figure 6.10: Conversion of TV load type into the corresponding load categories and subcategories.

The overall characteristics of the consumer electronics load are presented in Figure 6.11.

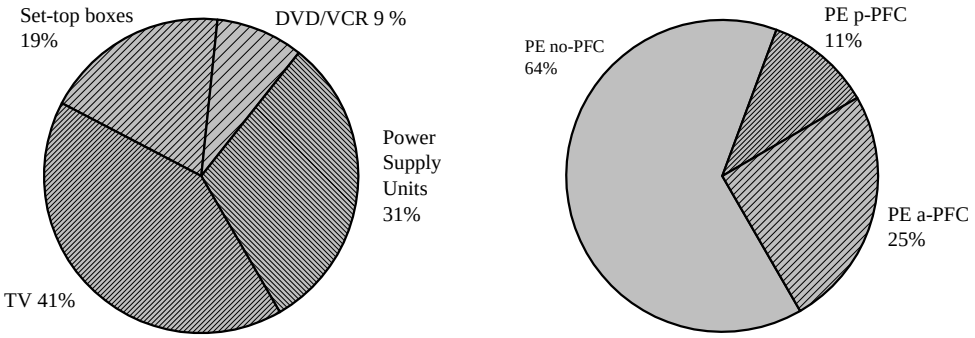

(a) by load type [174] **(b)** by load category

Figure 6.11: Conversion of consumer electronics loads into the corresponding load categories and subcategories.

Conversion of residential information and communication technology load type into corresponding load categories

ICT load includes the following devices: PCs, monitors, laptops, printers and multifunction devices (MFDs). Typically, the rated power of monitors used in the residential load sector is less than or equal to 75 W, and they are assumed as PE no-PFC load category. A series of measurements suggest that currently available desktops are high-power SMPS, with 85% having PE p-PFC characteristics and 15% as PE a-PFC. Printers were found to display approximately resistive load type behaviour. From a number of measurements performed on laptop battery chargers, with age ranging from one to six years old, it was found that the predominant technology was PE no-PFC (56%), with PE p-PFC contibuting 19% and PE a-PFC 25% to this load type consumption. This data is applied to convert the ICT loads into the appropriate load categories, Figure 6.12.

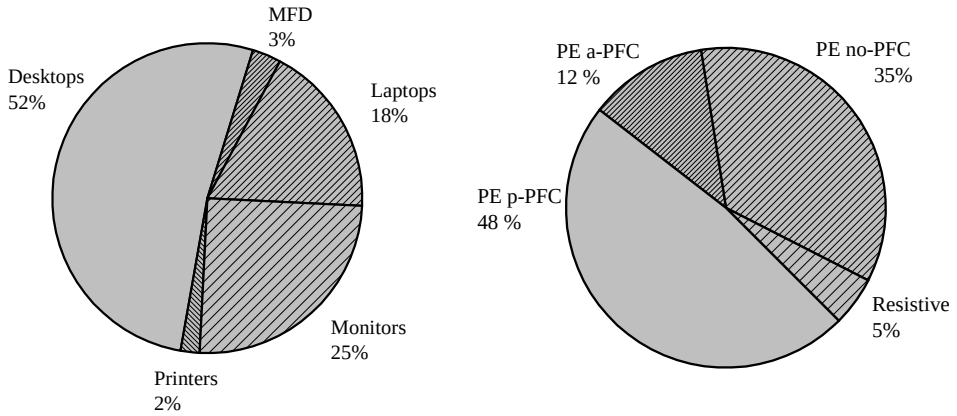

(a) by load type **(b)** by load category

Figure 6.12: Conversion of ICT load types into the corresponding load categories and subcategories.

6.4.4 Aggregate load composition by load categories

Following the conversion procedure outlined in the previous section, the aggregate demand profile (Figure 6.3) is converted into the corresponding load categories and subcategories. The result of this process is displayed in Figure 6.13 overleaf. The most striking observation is the dominance of resistive load in the aggregate demand, which follows the usage of storage space and water heaters during the night-time (00:00 - 04:00), the morning use of cooking and electric shower loads (06:00 - 09:00) and evening cooking loads (16:00 - 20:00). As previously discussed, this will increase for maximum loading conditions due to increased use of electric space and water heating. The contribution of the power electronics load categories will increase in the evening, as a result of the use of entertainment appliances. In this load category, PE no-PFC has the biggest share of the demand, followed by PE p-PFC and PE a-PFC. Of the motor categories, only RSIR_{QT} and CSR_{CT} have any meaningful influence on the demand.

6.4.5 Individual load models

Once the load profile has been converted into the corresponding load categories and subcategories, generic models of each load category are required to build the aggregate load model. The power electronics and lighting load categories are represented by the circuit-based generic load models introduced in the previous chapters of this thesis. The remaining load categories currently found in the UK residential load sector will draw continuous input current from the supply system. For steady-state analysis, they can be accurately modelled using the standard exponential or polynomial/ZIP form. This will retain the correct P-V and Q_1-V characteristics, while the power factor is used to set the phase angle shift between supply voltage and current waveforms. Table 6.3 includes the load model coefficients of these continuous current loads.

As discussed in Chapter 4, GILs are not ideal resistive loads and will have active power characteristics between constant current and constant impedance load types. The active power characteristics of all motor loads will tend towards constant power, while the reactive power characteristics will tend towards constant reactance. The displacement power factor of CSR motor is improved in comparison with the RSIR motor as a result of the run capacitor.

Table 6.3: Load model parameters of linear loads.

Ref.	Load	PF_1	Exp. Model		Polynomial/ZIP Model					
			n_p	n_q	Z_p	I_p	P_p	Z_q	I_q	P_q
[4]	GIL	1	1.55	-	0.43	0.69	-0.12	-	-	-
[18]	RSIR SPIM_{CT}	0.62	0.06	1.92	0.63	-1.20	1.57	1.4	-0.91	0.5
[18]	RSIR SPIM_{QT}	0.62	0.30	1.92	0.10	0.10	0.80	1.4	-0.91	0.5
[18]	CSR SPIM_{CT}	0.9	0.38	1.68	0.50	-0.62	1.11	1.54	-1.4	0.89
[18]	CSR SPIM_{QT}	0.9	0.53	1.68	0.22	0.08	0.69	1.54	-1.4	0.89
-	Resistive	1	2	-	1	0	0	-	-	-

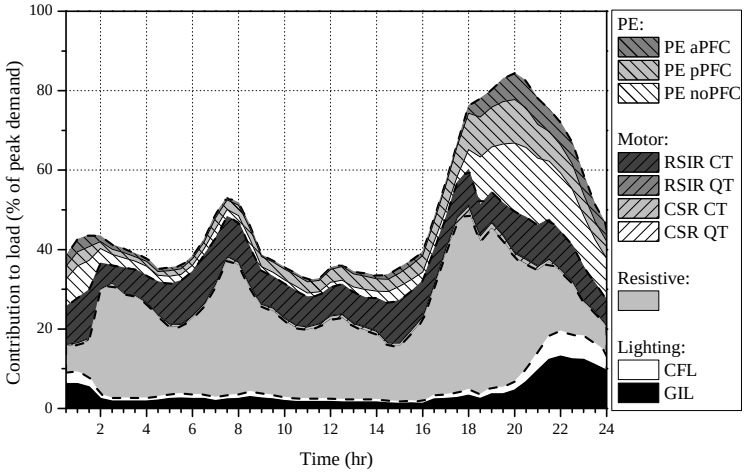

(a) minimum loading conditions

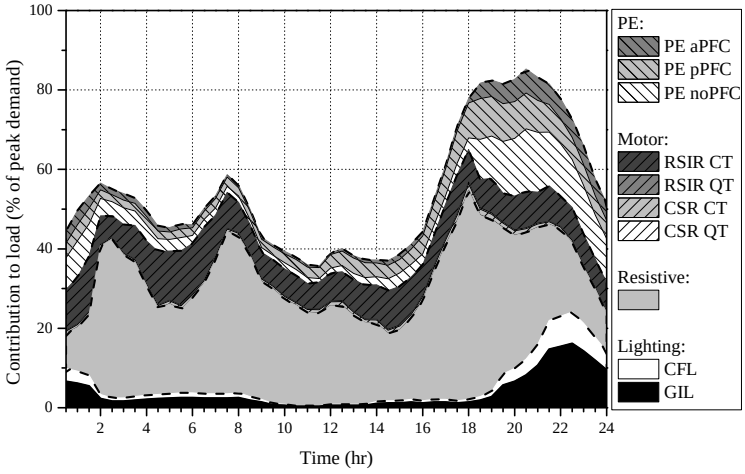

(b) average loading conditions

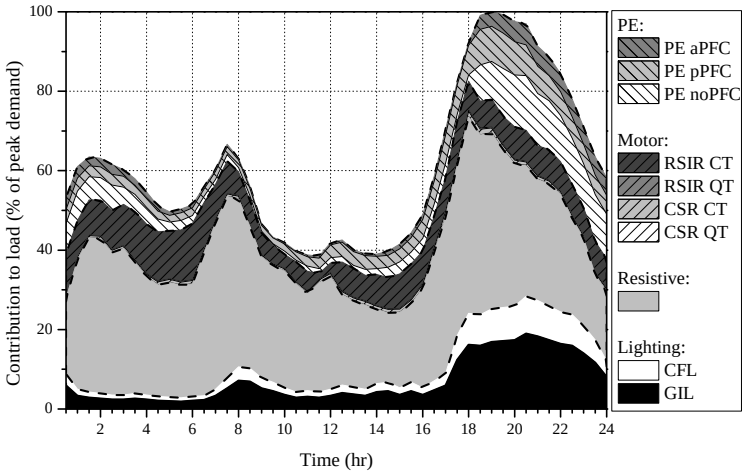

(c) maximum loading conditions

Figure 6.13: Decomposition of the UK residential load sector into load categories and subcategories for three characteristic loading conditions.

6.4.6 Low-voltage aggregate load characteristics

For connection to the network model, the LV aggregate load model must be prepared in a suitable form. This is achieved by summation of the current waveforms of the individual load categories to build the aggregate current waveform (Figure 6.14). As the generic models have shown to be able to represent the aggregate load characteristics of the individual load categories with only a small error, they can be used directly. Using the generic models reduces the required computation time and offers an improvement over existing load models for two main reasons. Firstly, harmonic legislation has had a significant effect on the design and electrical characteristics of modern loads, effectively making some existing load models obsolete. Secondly, the assessment of harmonic emission and propagation should be a standard part of analysis of modern networks, and that information should be provided by newly developed load models.

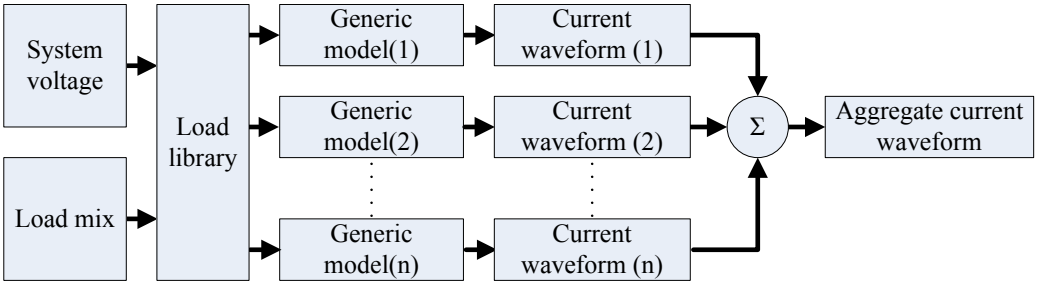

Figure 6.14: LV load aggregation process based on component-based generic load models.

As the developed load models are voltage dependent, it is possible to extract the electrical characteristics of the load by performing a voltage sweep. Although this does not include the effect of the network supplying the load (discussed in the next section), and cannot be implemented directly in power system analysis, it does serve to illustrate the temporal variations in load characteristics. To illustrate this, the active and reactive power demand of the UK residential load sector example are calculated for each voltage step and the exponential load model coefficients are extracted and displayed in Figure 6.15. The exponential form is selected to display the results as only one coefficient is required to describe the load characteristics. All exponential and polynomial/ZIP load model coefficients are included in Appendix H.

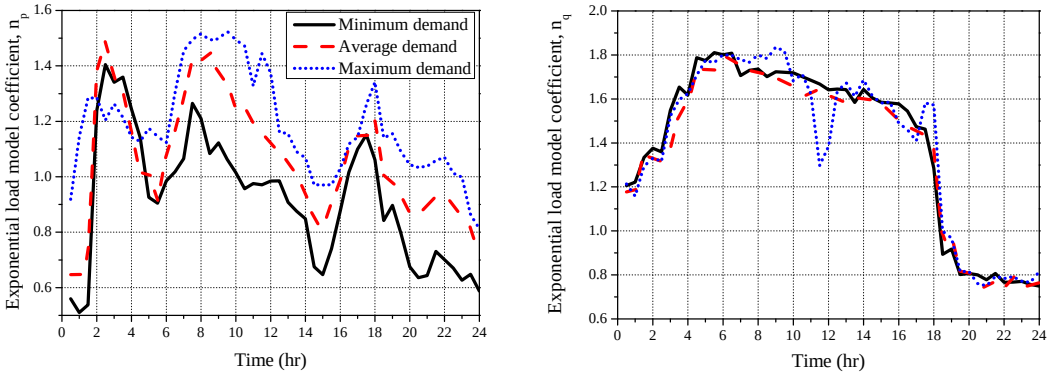

(a) active power (b) fundamental reactive power

Figure 6.15: Variation in aggregate LV load model represented by the exponential form.

There are several worthy comments on the results in Figure 6.15. The general trend in the diurnal cycle is similar for all loading conditions. As the resistive load is dominant, it is intuitive to use this as a reference point when describing the changes in the active load model coefficient. For a clear analysis, the day is divided into four regions: night-time (00:00 - 06:00), morning (06:00 - 10:00), daytime (10:00 - 16:00) and evening (16:00 - 00:00).

The active power coefficient will have a large value during night-time periods as a result of the connected storage space and water heating load. This value is actually lower during the maximum loading condition, as, although more resistive heating is required, the increased contribution of the lighting load during winter months will act to reduce the coefficient value of the aggregate load model. A similar peak value in load model coefficient is observed in the morning period as a result of some resistive cooking and electric shower loads. The active power load model parameter value is higher for the average and maximum loading conditions due to the increased resistive space heating load. During the daytime, the value of active power coefficient will decrease as the number of active occupants, and, hence, loads reduces and the load characteristics will tend towards the base load value. During the evening period, the initial characteristic is dominated by large resistive cooking loads. This is followed by a period where the use of power electronics loads and lighting will act to lower the load model parameter value.

The variation in the reactive power characteristics between the different loading conditions is almost negligible. This is because the most significant changes between loading conditions are a result of the electric space and water heating load, which will have very little influence on the reactive power characteristics of the load. During the night-time, the reactive power characteristics will steadily increase as the contribution of the power electronics load category reduces. The maximum value lies between the reactive power characteristics of the motor load (i.e. 1.68 - 1.92), which serves as the main reactive power demand in the residential load sector. In the evening period, the value of n_q will reduce significantly as the contribution of power electronics and lighting load category increases. This is mainly attributed to the CFL and PE p-PFC subcategories, as they have more linear reactive power characteristics than SPIM. Although there is a notable active power demand by PE no-PFC during this period, it has very little influence on the reactive power characteristics (due to the very high displacement power factor, its contribution to the reactive demand is very small).

The presentation of results in the exponential (and polynomial/ZIP, which are included in the Appendix) allows for the implementation of the developed load models in the most widely used power system analysis softwares. However, it is been emphasised throughout this thesis that the methodology pursued in the research will enable more information on the electrical characteristics to be retained during the aggregation process. To illustrate this, Figure 6.16 presents the changes in the true, displacement and distortion power factor and the current THD for the modelled set of aggregate load curves. Note: the displacement power factor is identical to that in Figure 6.2 and is included again to improve the comparison of characteristics.

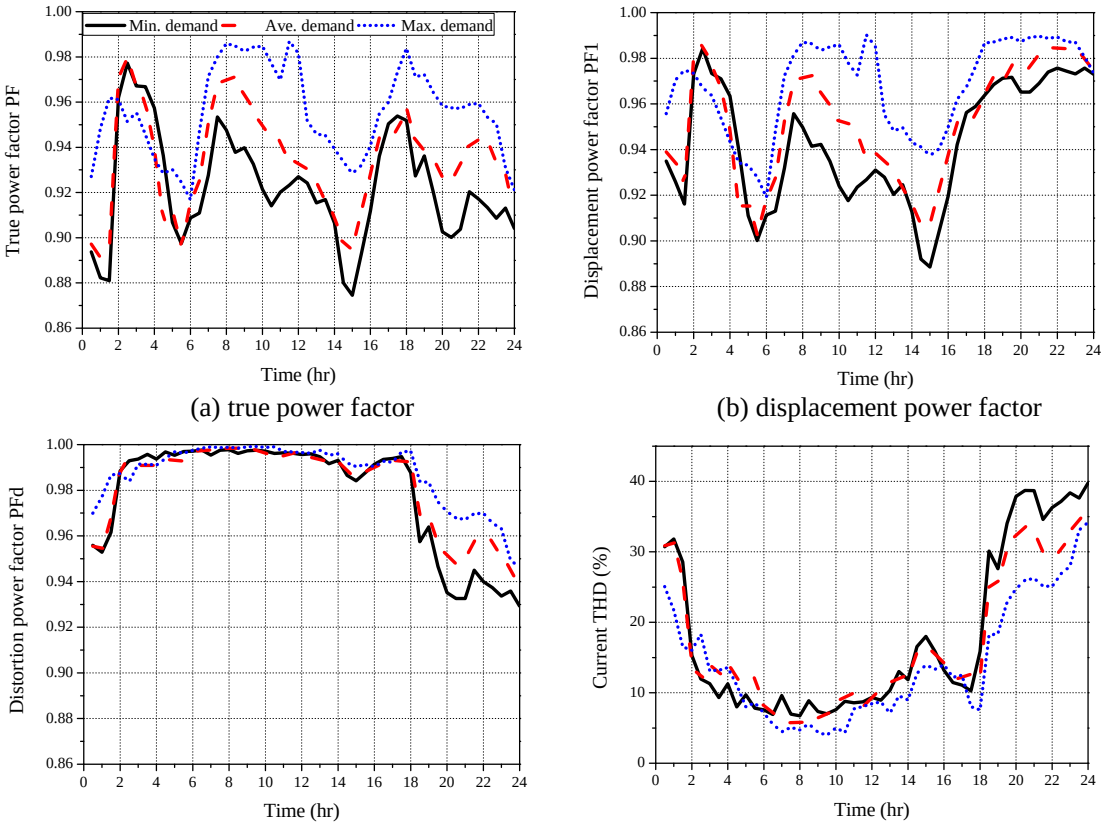

(a) true power factor

(b) displacement power factor

(c) distortion power factor

(d) current THD

Figure 6.16: Variation in the electrical characteristics of the aggregate LV load model.

This extra information is a direct result of representing the individual load categories (and subcategories) by their generic equivalent circuit models in the aggregation procedure, to build the instantaneous current waveform of the aggregate load. Processing this waveform allows for the extraction of electrical characteristics shown above and clearly demonstrates the value of the load modelling approach. These results show that the distortion power factor of the aggregate load is very high for the majority of the day, which can be attributed to the fact that the majority of the connected load is linear. The value of PF_d will reduce during the evening period as a result of the increased use of entertainment and lighting loads, which both contain loads with high harmonic emissions. This effect is not as pronounced during winter loading conditions as the higher lighting demand will introduce additional linear (GIL) and non-linear (CFL) loads, and there will be increased levels of harmonic cancellation. As PF_d is related to the inverse value of harmonic emissions, the opposite trend is displayed in the THD_I plot.

The current THD of the aggregate load is significantly lower than the current THD of the load categories, which shows further harmonic cancellation between the load categories. These results are obtained from stiff grid conditions (i.e. with zero value of system impedance and no harmonic attenuation), but the effect of this on the aggregate model characteristics is discussed in the next chapter.

6.5 Network modelling

After the LV aggregate load model has been developed, it must be connected to the supply network for power system analysis. For aggregate load model representation at the MV level, this requires accurate representation of the LV network up to and including the secondary distribution transformer. Accordingly, at this stage in the methodology, data on the network components and configuration is introduced. As the LV network configuration is a complex electrical system, techniques are introduced which allow for the representation of this as a single equivalent impedance. This significantly simplifies the analysis and allows for quick transformation of the LV load model to the MV level.

6.5.1 Network configuration

The schematic of the generic UK urban LV distribution network is shown in Figure 6.17. This type of network is the most common configuration in the UK which makes it suitable for demonstrating the aggregation methodology. Network component values are included in Tables 6.4 and 6.5 overleaf.

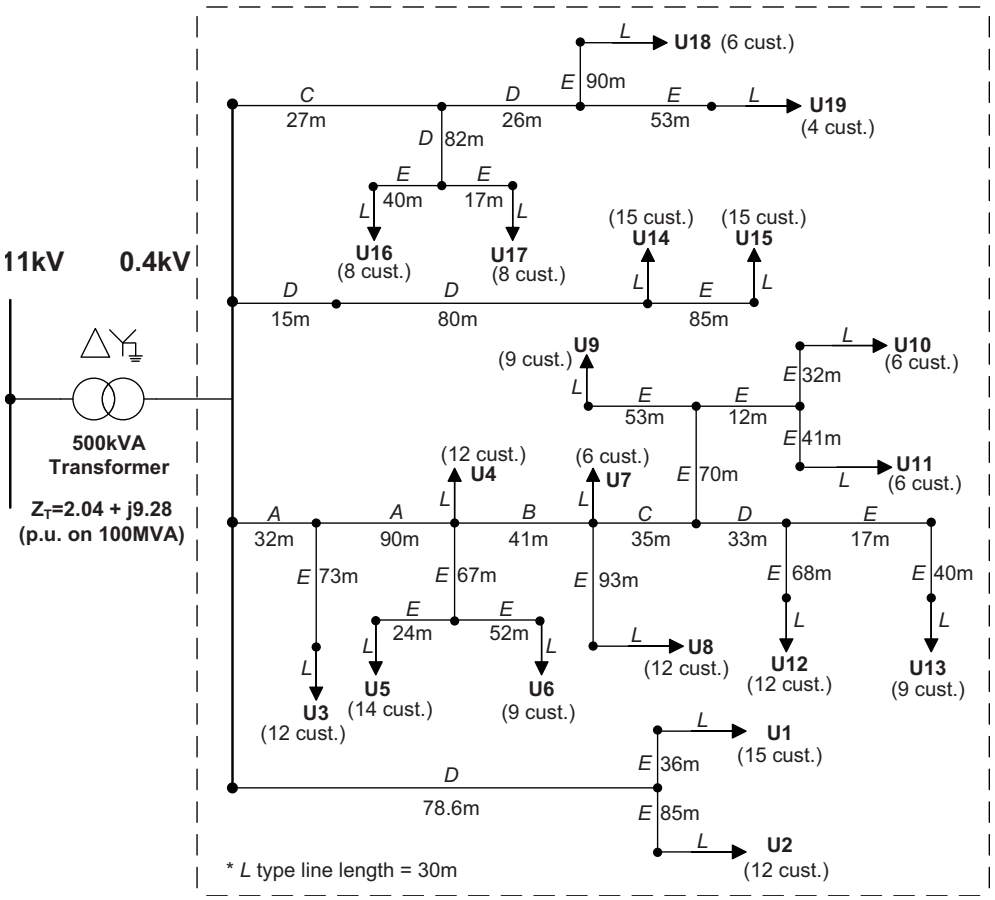

Figure 6.17: Generic UK urban LV distribution network [175].

The network has four three-phase trunk feeders which serve a total of 190 LV customers, i.e. individual households. The loads are represented as 19 load clusters, designated from U_1 to U_{19}. The customers within these groups are connected to the three-phase trunk feeder by single-phase service cable (Type *L* in Figure 6.17 and Table 6.4). The network is inherently unbalanced due to the number of supplied customers.

6.5.2 Network component values

The component values of the modelled LV network are given in Table 6.4, with the corresponding data for the secondary distribution transformer given in Table 6.5. Due to the urban location, all network cables are underground connection. Therefore, they have slightly lower impedance values than the overhead equivalent. Furthermore, due to the relatively high load density, the length of all conductors is short to ensure that the voltage regulation does not breach performance specifications, i.e. +10/-6%. The rating, and cross sectional area, of the conductors will decrease along the length of radial feeders, resulting in increasing impedance values.

Table 6.4: Generic UK urban LV distribution network component values [175].

Id.	Type	CSA (mm^2)	Impedance					I_{max} (A)
			Positive seq.		Neutral	Negative seq.		
			R	X	R	R	X	
			Ω/km					
A	UG	300	0.100	0.073	0.1268	0.593	0.042	465
B	UG	185	0.163	0.074	0.168	0.656	0.05	355
C	UG	120	0.253	0.071	0.253	1.012	0.047	280
D	UG	95	0.320	0.0975	0.320	1.280	0.051	245
E	UG	70	0.443	0.076	0.443	1.772	0.052	205
L	UG	35	0.851	0.041	0.9	3.404	0.03	120
Where: UG - underground cable and CSA is the cross sectional area.								

Table 6.5: Generic UK urban secondary distribution transformer values [175].

Voltage (kV)	Rating X_T (MVA)	Connection	Tap range	Impedance (%)	Model	
					R	X
					p.u. to X_T	
11/0.4	500	Dyn11	± 5 %	4.75	0.01	0.046

6.5.3 Network aggregation

For the purpose of investigating the aggregate load model characteristics, the level of detail afforded by the LV network in Figure 6.17 is not necessary. This network may be reduced to a single-line equivalent impedance Z_{eq}, Figure 6.18, by applying the methodology described in [176]. This established technique can be summarised in two steps:

1. Calculate the equivalent impedance at every load location in the network. This is the summation of all impedances up to the network location, and can include multiple customers at the same bus. This is expressed by (6.1).
2. Determine the overall network impedance by summing all equivalent impedances calculated in Step 1. This step is described by the equation in (6.2).

$$Z_{location}(i) = \sum_{n=1}^{N} Z_{customer}(n) \tag{6.1}$$

$$Z_{eq} = R_{eq} + jX_{eq} = \sum_{i=1}^{I} Z_{location}(i) \tag{6.2}$$

where: $Z_{customer}(n)$ is the network impedance up to customer n at location i, $Z_{location}$ is the sum of all customer impedances at location i, N is the number of customers, I is the number of network locations and Z_{eq}, R_{eq} and X_{eq} are the equivalent impedance, resistance and reactance.

Applying this to the generic urban network gives the equivalent network impedance, with original values derived in [28]:

$$Z_{eq,urban} = R_{eq,urban} + jX_{eq,urban} = 0.0063 + j0.0017\Omega \tag{6.3}$$

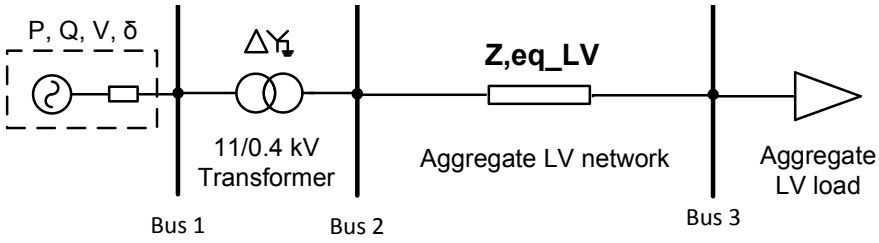

Figure 6.18: Equivalent network configuration.

In order to validate the equivalent network impedance for load modelling use, a comparison of the MV characteristics (i.e. at Bus 1 - Figure 6.18) using the detailed network and the equivalent network must be performed. For this analysis, the detailed LV network is populated with load models which are able to simulate the stochastic variations which characterise individual households. These models have been developed in research undertaken following the PhD period and do not require detailed explanation in this thesis, as its only purpose to this research is to validate the network aggregation methodology, i.e. to allow for the connection of the

aggregate LV load model to an equivalent network impedance. Further details of the load modelling approach for individual households is available in [177].

As this is an important stage in the process, and it is the direct comparison of two sets of load model parameters (rather than the actual values of the load model parameters) that is of interest, the more detailed polynomial/ZIP representation of load is used to display the results. The values in Figure 6.19 confirm the ability of the equivalent network impedance to retain the performance of the detailed network model. This is an important result for this research as it allows for the direct connection of an aggregate LV load model to the equivalent network impedance, which significantly reduces the modelling effort without introducing an error.

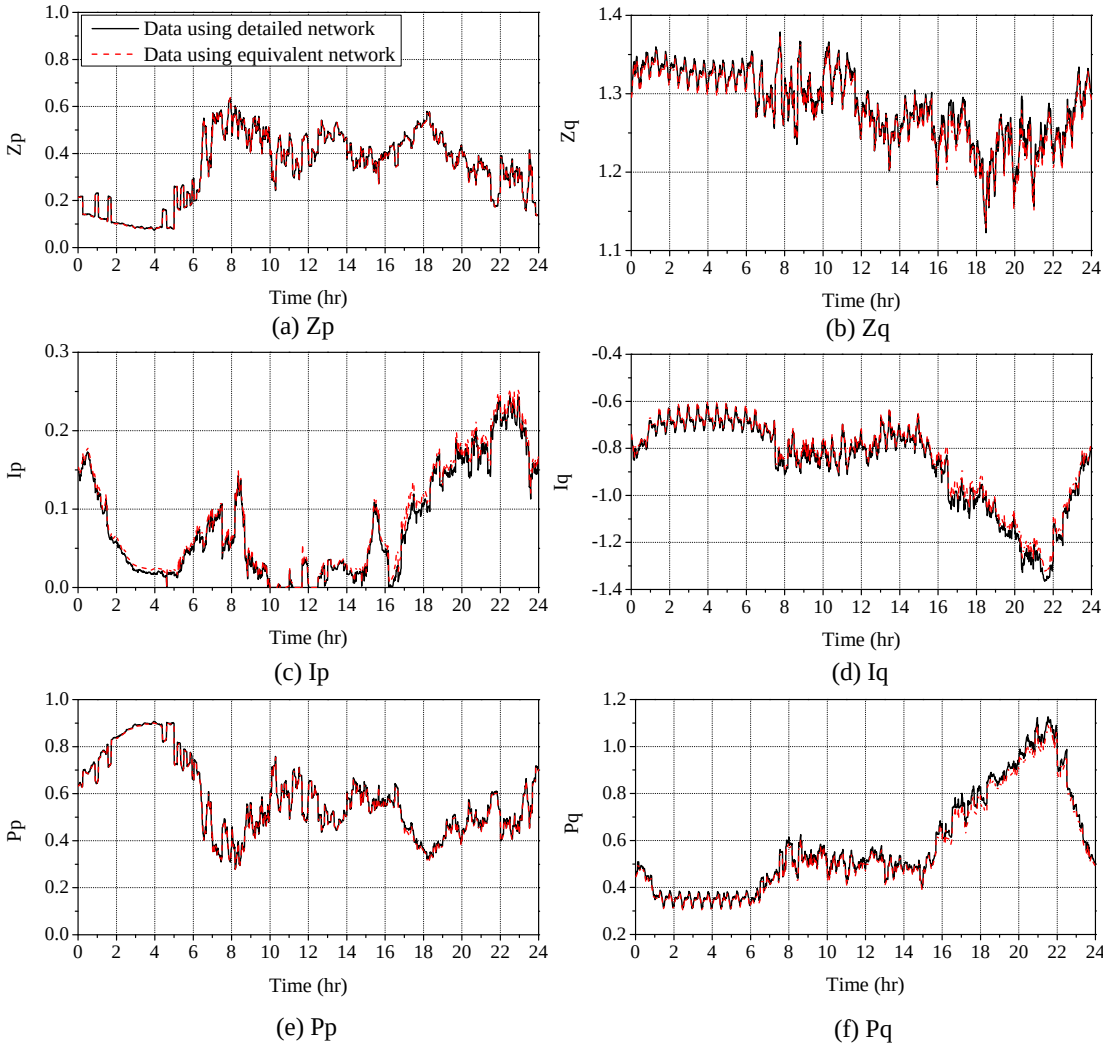

Figure 6.19: Comparison of example MV polynomial/ZIP load model coefficients obtained using detailed and equivalent network models.

6.5.4 Network influence on load model parameters

When developing the MV load model, the electrical behaviour of the load will be a combination of the load and the network. As current flows through the network impedances, the corresponding changes in active and reactive power flows are attributed to the network elements. For steady-state analysis, the current flow in the network, and, therefore, the aggregate MV model, is influenced by the connected LV load. For dynamic analysis, which is not considered in this thesis, the network effect will be more complex due to the operation of the various control devices, e.g. OLTC transformers.

To illustrate the effect of the network on the load model as the point of reference moves from LV to MV, a simple case study is presented. In the following examples, the reactive power characteristics of the load models are used to demonstrate the network contribution to the MV load model as the changes are more pronounced for reactive power than active power, due to the large reactance of the secondary distribution transformer. A voltage sweep is performed at the MV side and the values of reactive power at Bus 1, 2 and 3 (as denoted in Figure 6.18) are recorded, with the network influence being obtained as the difference between the values recorded at Bus 1 and Bus 3.

The most simple scenario is if the load is constant impedance type. In this case, the whole system (network plus load) will also behave as the constant impedance type of the load. This is shown in Figure 6.20(a), with additional values for all considered load scenarios included in Table 6.6. If the LV load is constant current type ($n_p = n_q = 1$), the current in the network is constant and, as the network components have a constant impedance, the network behaves as constant power type ($n_p = n_q = 0$). As the aggregate MV model includes both the influence of the network and the LV load, the corresponding exponential coefficient will lie between 0 and 1, depending on the percentage contribution of network and load to the total demand. If the LV load is constant power, the network current is inversely proportional to the network voltage and the network components behave similar to constant impedance type with negative exponents/characteristics (i.e. n_p and $n_q \approx -2$) as larger than 1 pu currents will be demanded by the constant power load type for supply voltages lower than 1 pu, resulting in an increase of network losses. Therefore, the resulting MV load model will have exponent between 0 and -2.

Table 6.6: Values for example of network influence on the aggregate MV load model.

Bus	Connected load			
	Z	I	P	Mixed
1	2.00	0.84	-0.56	0.79
N	2.00	0.00	-2.37	-0.12
3	2.00	1.00	0.00	1.00

where: N represents the combined effect of the supply network and transformer.

When the LV load is composed as a mix of the three general load types, as is often the case in reality (and as shown in this thesis), the network components will behave as a mixture of constant impedance (with positive and negative characteristics) and constant power types. Therefore, when a mixed LV aggregate load is connected, the effect of the network components is to generally reduce the values of the exponential coefficients of the MV aggregate load model. In this example, the mixed load is taken with an equal contribution of the three load types. Therefore, the aggregate LV characteristic is effectively that of the constant current load. However, the values in Table 6.6 shows that the network influence is not the same as for constant current loading condition, and the aggregate MV load model coefficient value is also lower for the mixed load scenario.

This analysis is extended to the developed aggregate LV load model in the following section.

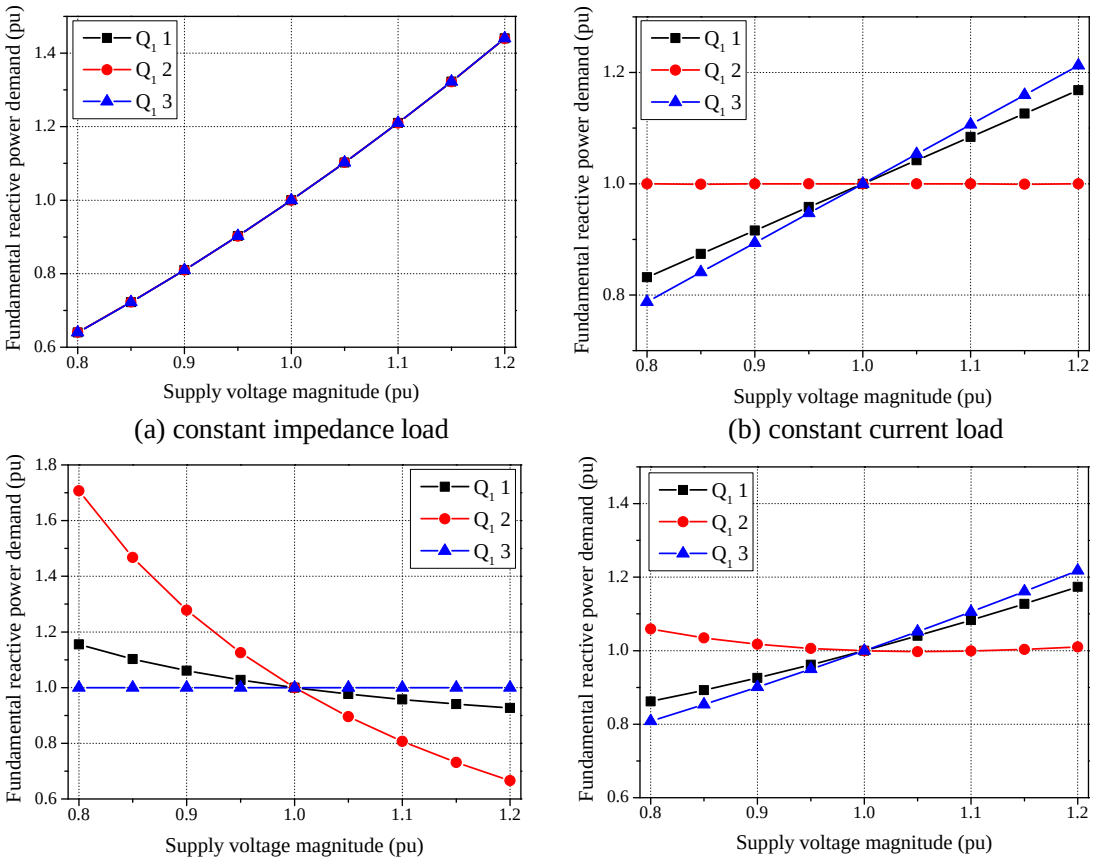

Figure 6.20: Network influence on MV aggregate load characteristics.

6.6 Medium-voltage aggregate load model

After the LV aggregate load model is connected to the aggregate network model, the MV load model is obtained by using the supply transformer to instigate a step change in voltage. This approach is similar to the method used to develop measurement-based load models [55]. A comparison between the aggregate LV and MV load characteristics is shown in Figure 6.22 overleaf, with model values included in Appendix H.

The influence of the network is clearly visible on the MV load representation, where a reduction in model exponential coefficient values at the higher voltage level is observed. As expected, the effect on reactive power coefficient is more pronounced because of a relatively large reactance of the network components (primarily the reactance of the supply 11/0.4 kV transformer). The effect on active power coefficient is small, as the resistive/active power losses in the network are low in comparison with the active power demand. The effect on the reactive power coefficient is more noticeable as the network demand increases, i.e. from minimum to maximum loading conditions. This is a result of higher current flow through the 11/0.4 kV transformer, which increases the influence of the network on the aggregate load model coefficient.

The network influence will also reduce the displacement power factor of the load, as viewed from the MV level, which is illustrated in Figure 6.21 for maximum loading conditions. This effect is attributed to the reactance of secondary distribution transformer and is most pronounced during the evening peaks. The MV displacement power factor values for all loading conditions are included in Appendix H.

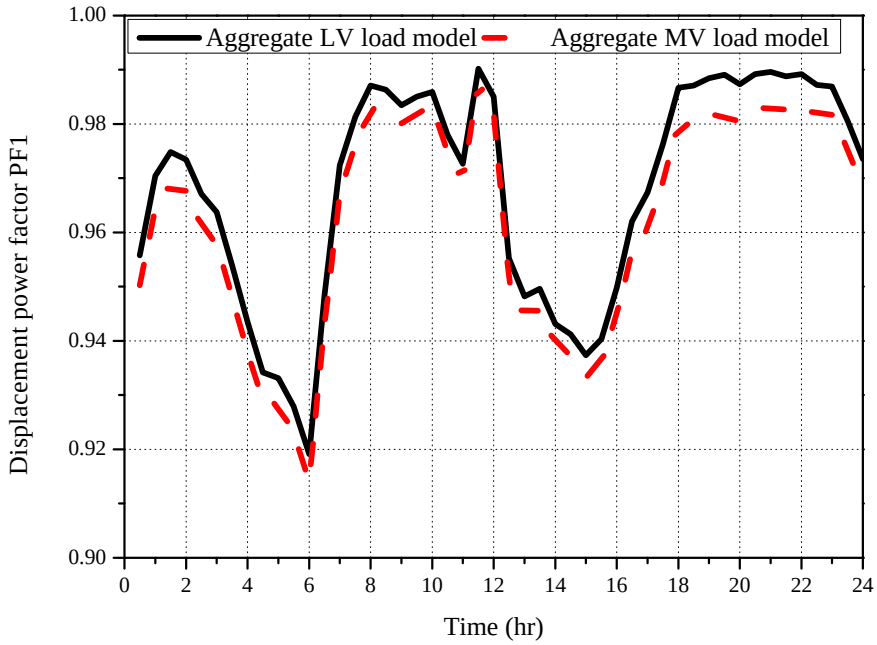

Figure 6.21: Comparison of displacement power factor values for MV and LV aggregate load models for UK residential load sector example.

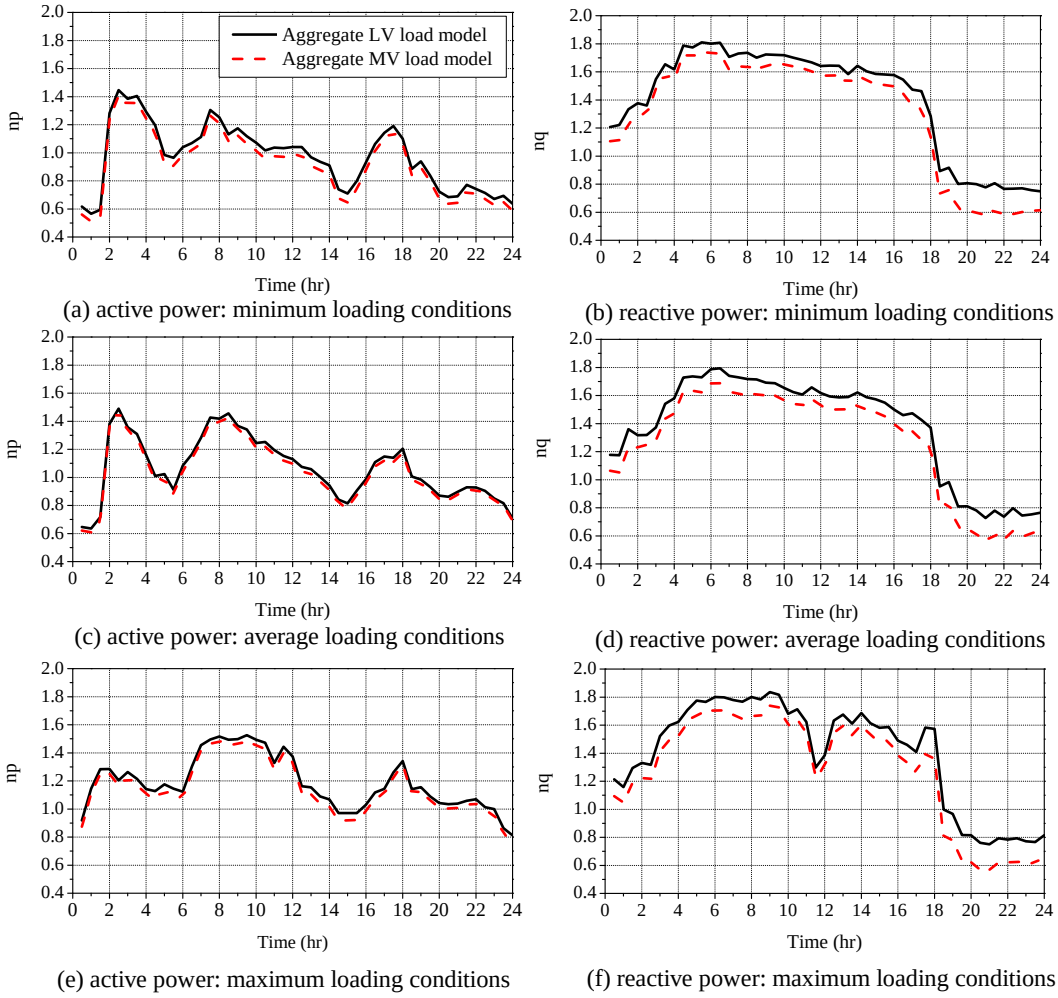

(a) active power: minimum loading conditions

(b) reactive power: minimum loading conditions

(c) active power: average loading conditions

(d) reactive power: average loading conditions

(e) active power: maximum loading conditions

(f) reactive power: maximum loading conditions

Figure 6.22: Comparison of MV and LV aggregate load models for UK residential load sector example, expressed in exponential form.

6.7 Conclusions

This chapter has presented a methodology for developing aggregate load models at the LV and MV levels of the power system. This aggregation methodology offers additional functionality which is not available in existing load modelling approaches, and also a better representation of the temporal variations in the electrical characteristics of the modelled load. Both of these features add considerable value to the developed load models, and represent one of the main contributions of this research. Within the description of the aggregation methodology, several important areas of the analysis were introduced, including the validation of the equivalent impedance network model, the influence of this impedance as the aggregate load model is converted from LV to MV and the ability to produce information on the harmonic emissions of the aggregate load. Further illustration of the aggregate harmonic emissions are included in the subsequent chapter, along with the use of the developed aggregate MV residential load sector models in power flow analysis.

Chapter 7

Case studies: Aggregation methodology and network analysis

7.1 Introduction

This thesis has presented a detailed discussion of individual and aggregate models of modern non-linear loads, and proposed a set of generic load models which are able to retain the most important electrical characteristics of these. For this purpose, a new aggregation methodology was presented, which combined the circuit-based load models with publicly available statistics to develop an entirely new set of aggregate load models. The analysis in Chapter 6 was primarily aimed at the improved representation of the UK residential load sector. In this chapter, the aggregation methodology is revisited to provide further details for two important areas.

This begins by converting available UK commercial load sector statistics into the corresponding aggregate load models. As was the case with the residential load sector, the developed aggregate commercial load sector models are another novel output of the research, as there are no publicly available load models for the UK commercial load sector. The second subject which is considered is the addition of MG within the load modelling framework.

Although the focus of this research is in the development of load models for power systems studies, rather than the power system analysis itself, two examples are included in the final sections of this chapter to illustrate the use of the developed load models. Both case studies are placed in a DSM context, as this is one area of analysis which can be substantially improved with increased levels of load modelling detail. The first case study illustrates how the developed load models can be used to assess the impact of a simple DSM scenario on the overall network performance, including: power flows, voltage profiles and harmonic emission levels. The second example demonstrates the impact of the developed MV aggregate load models on the results obtained for identifying the optimal location of loads for implementing DSM actions in the distribution network.

The network and MG models used in the analysis have been provided by parallel research streams within the IES, [175] and [178], respectively, while their application to optimal power flow (OPF) techniques in the distribution network is also part of an internal collaboration [179].

7.2 Aggregation methodology: Commercial load sector

In the UK, the commercial load sector is responsible for around 30% of the annual electricity demand [58], and the characteristics of this load sector are significantly different to the UK residential load sector. With respect to the electronic devices, there is a much bigger contribution of lighting load (as discussed in Chapter 4), as well as a greater penetration of three-phase motors. The other notable difference in the commercial load sector is the period of demand, which, for the majority of commercial load subsectors, will occur within typical UK working hours (from approximately 08:00 - 18:00 hours).

It is the combination of the commercial and industrial load sectors which will, normally, have the biggest influence on the sustained period of high demand during the daytime hours. This period of loading coincides with the times of the highest probability of system faults [175], and efforts in modelling this load sector may help to provide better information to actions aimed at improving network reliability performance. The relatively high penetration of motor load also makes this load sector important for power system stability analysis [39].

The commercial load sector includes many different public services, illustrated in Figure 7.1. The analysis in this thesis will consider the overall commercial load sector, as the development of load models for specific subsectors requires access to data and measurements which are not publicly available. If such datasets were available, the aggregation methodology and load library could be applied to develop the corresponding load models. It should also be noted that a typical MV aggregate load is likely to consist of a mix of different commercial subsectors, and the development of specific commercial load models is required only for the analysis of specific sections of the network.

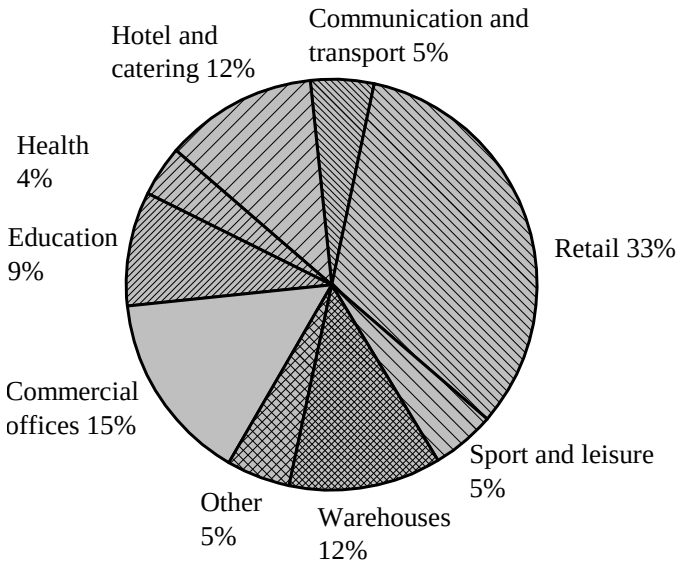

Figure 7.1: Contribution of commercial subsectors to the total commercial load sector demand [58].

The aggregation methodology described in Chapter 6 is employed again in this section. This begins by considering the typical demand curves of the commercial load sector for characteristic loading conditions (minimum, maximum and year average) and the contribution of individual load types to the total demand. In the next stage, the data is converted into the corresponding load categories and subcategories to allow for the representation of the total aggregate demand using the generic models developed in this thesis. The generic models are then combined to develop the aggregate load model.

7.2.1 Load demand curves

Power demand in the commercial sector is driven by the specific processes required to provide the necessary public service. As standard working hours are between 08:00 - 18:00, the maximum demand is expected during this period. This is confirmed by the aggregate load curves of the commercial load sector presented in Figure 7.2, in which the average curve values have been calculated from all data presented in [17]. The most important observation which can be taken from these curves is that the shape of the load profile is very similar for all three loading conditions.

As with the residential load sector, the (fundamental) reactive power demand is represented using the displacement power factor PF_1 and is an output of the modelling approach. The changes in PF_1 values are the result of changes in the load composition, and are less pronounced for the commercial load sector (cf. corresponding residential demand in Figure 6.2 on Page 151). In the residential sector, the diurnal variations in the displacement power factor follow the same general trend, which is also visible in the commercial load sector. Overall, the displacement power factor will improve during typical working hours, with a higher value for maximum loading conditions. This is a result of the loads within the aggregate load mix and requires a more detailed analysis of the load structure for a full explanation.

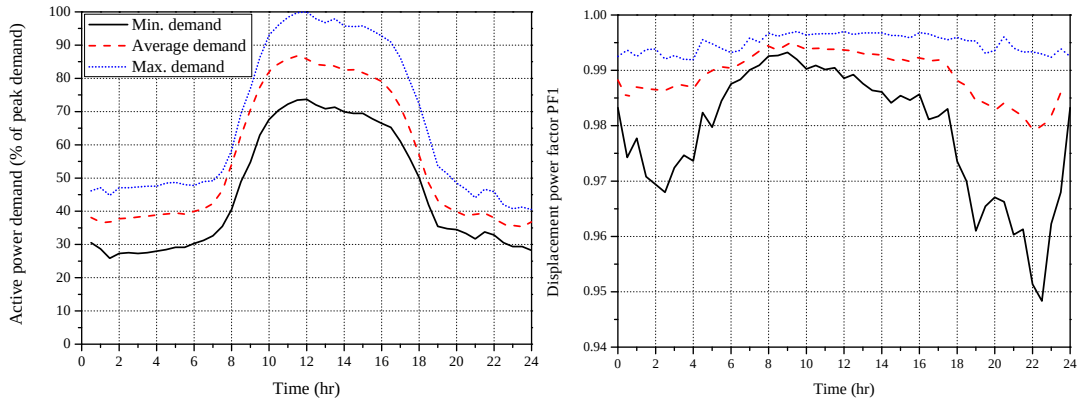

(a) active power [17]

(b) displacement power factor

Figure 7.2: Typical aggregate daily load demand curves for the UK commercial load sector for three characteristic loading conditions.

7.2.2 Load structure

Figure 7.4 (shown on page 180) illustrates how the load curves of the overall UK commercial load sector can be decomposed into the corresponding load mixes. The electrical devices and equipment are divided into the same types of loads as the residential load sector, i.e.CE and ICT equipment; cooking load; 'wet' load; 'cold' load; space heating (SH); water heating (WH) and lighting load. Direct and storage space and water heating units have been grouped together as, for aggregate load modelling, there is no difference in their operation.

The original dataset in [17] was found to overestimate the contribution of lighting load, in comparison with more established statistics in [58]. Therefore, the load profile has been adjusted to give a better representation of the overall commercial load sector. To achieve this, a two stage readjustment process was performed.

Stage 1

In this stage, the annual contribution of each load type is calculated and compared with statistics presented in [58] to identify the differences (i.e. load types with the biggest error). The 'other' load type, which is present in the vast majority of all available statistics (due to the inherent uncertainty in load decomposition) is then converted into the load types which displayed the biggest consumption error. This is an important stage in the process as all demand must be assigned to a specific electrical load for more accurate load model development. This stage is performed with respect to both the time of operation and the physical operation characteristics of the loads. For example, readjusting demand to increase the cooling load during the night-time hours for winter loading conditions is not physically sensible.

Stage 2

In the second stage, the modified contribution of each load type is calculated to identify any remaining errors in the annual consumption. An iterative process is then invoked to shift the error from the identified loads with the biggest positive error to the biggest negative error, i.e. to retain the overall energy balance, and then to the load type(s) with the second largest error and so forth.

The readjustment routine is terminated when all loads are within a predefined tolerance limit, taken as plus/minus 5% in this research. A reasonably large tolerance is applied as the identification of loads within the aggregate demand is inherently inaccurate. Even well established statistics, such as [58] used in this thesis, will have inaccuracies introduced by the data collection or applied analytical modelling methods, as well as the use of 'other' loads which are not well defined. Therefore, an ideal match to these statistics is not the ultimate goal and a more robust approach is to perform a sensitivity analysis to identify the influence of changes within the aggregate load mix on the desired features, in this case the electrical characteristics of the aggregate load model. This is discussed in more detail in Section 7.2.5.

The results of the load readjustment are presented in Figure 7.3, which compares the annual contribution of each load type to the total commercial load sector statistics in [58]. It can be seen that the modified load data provides a better match with the available load statistics than the original input dataset in [17].

The most notable variations between the input dataset and the load statistics is in the lighting load, which is overestimated in [17], and space heating and catering loads, which are underestimated. Therefore, this 'extra' lighting load is mostly redistributed to raise the contribution of space heating and catering loads. The 'other' load type has been allocated among the fully defined load types. The fact that the modified data is, generally, slightly overestimating the contribution of each load type is a consequence of reassigning the 'other' load type.

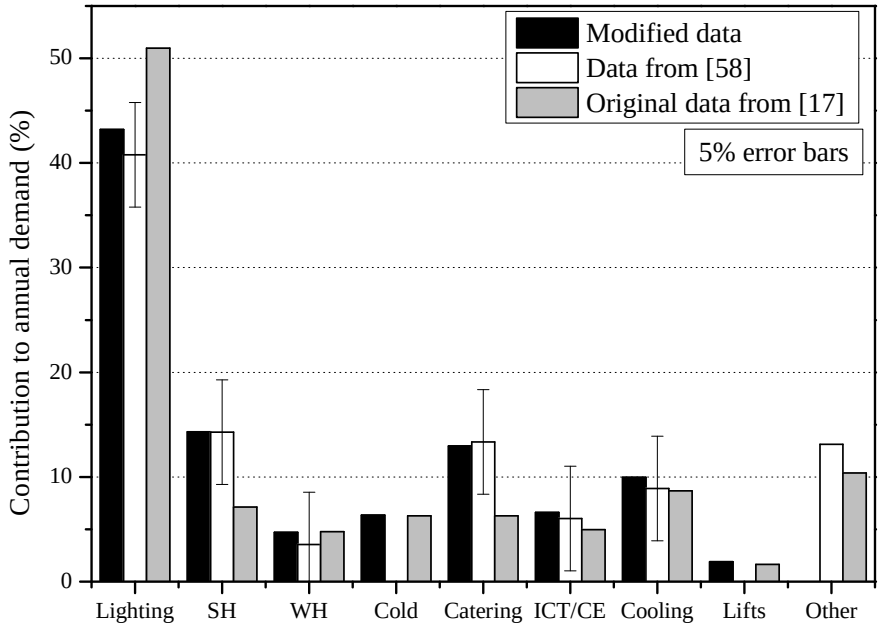

Figure 7.3: Contribution of load types to the overall commercial load sector annual consumption.

The daily and seasonal variations are shown in more detail in Figure 7.4. From these curves, the large contribution of lighting load to the overall demand is clearly visible. The majority of the lighting demand is concentrated in the typical working hours, but there is always a base load. As expected, the lighting demand will increase in winter months.

The other significant seasonal variations occur in the heating and cooling load types. The cooling load type is not present during the maximum, i.e. winter, loading conditions but will form a significant proportion of the total demand during the minimum, i.e. summer, loading conditions. The opposite trend is observed for the heating load type, with a large contribution to the demand of maximum loading conditions. As previously stated, these curves represent the overall UK commercial load sector, and the load composition is expected to vary between the different commercial load subsectors.

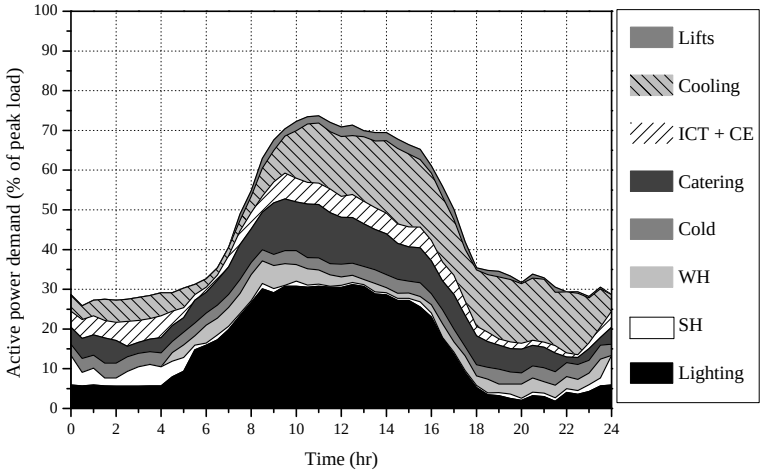

(a) minimum loading conditions

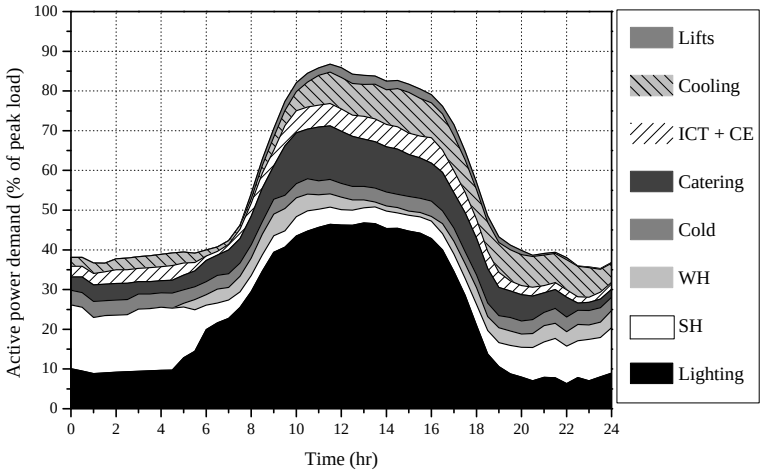

(b) year average

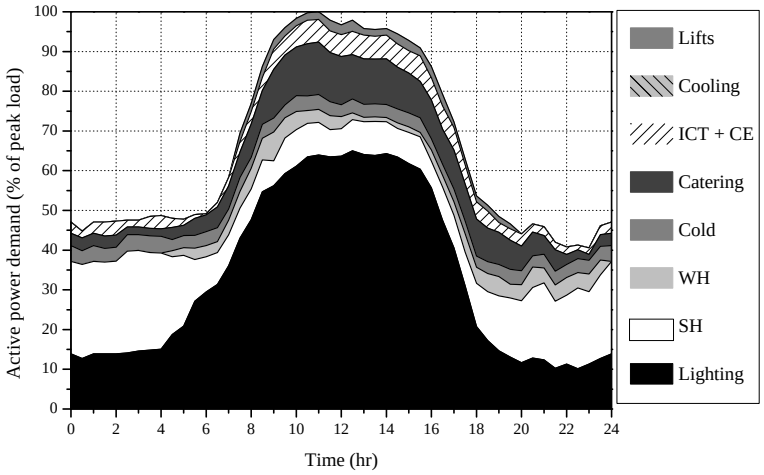

(c) maximum loading conditions

Figure 7.4: Decomposition of the UK commercial load sector into load types for three characteristic loading conditions, based on data in [17] and modified using statistics in [58].

7.2.3 Conversion of load type to load category

The next stage in the aggregation methodology is to convert the load structure curves into the corresponding load categories and subcategories. The load category definitions which have already been applied in the modelling of the residential load sector (given in Figure 6.4 on Page 154) are also generally applicable to the commercial load sector. However, some additional models are required and taken from literature, and are described in the appropriate sections.

Conversion of commercial lighting load type into corresponding load categories

As discussed in Chapter 4, the lighting technologies which are used in the commercial load sector have different requirements to those found in the residential load sector. Higher efficacy is required to light large spaces economically, and LFLs are the most dominant technology. The contribution of all light sources to the commercial lighting demand is given in Figure 7.5.

General lighting is defined as lighting used to produce lighting levels similar to domestic lighting, e.g. in restaurants or hotels. Therefore, this can be assumed to contain the same light source mixture as previously specified for the residential load sector. This consists of approximately 67% GILs and 33% CFLs and LFLs, with more details available in Section 6.4.3. Office lighting is exclusively LFLs, while 'industrial' lighting is defined as lighting required for warehouses and large leisure areas, and can be assumed to be HID lamps. Due to the substantial contribution of LFLs within the commercial load sector, they will have significant influence on the overall electrical characteristics of the aggregate demand. As models of these high power LFLs have not been developed within this thesis, the model from [39] is taken. It is also proposed that many of these ballasts will have been replaced by more sophisticated electronic control circuits, which exhibit electrical characteristics similar to PE a-PFC [18]. A 50/50 contribution is considered during model development but the contribution of lighting is subject to further sensitivity analysis in Section 7.2.6. These load categories are applied to convert the lighting load type into the corresponding load categories for use in the development of aggregate load models, as shown in Figure 7.5.

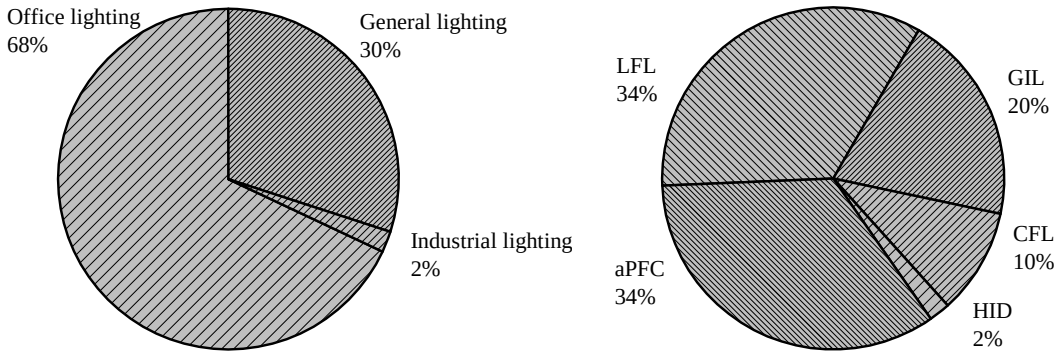

(a) by load type [180] **(b)** by load category

Figure 7.5: Conversion of commercial lighting load type into the corresponding load categories and subcategories.

As HID lamps have not been modelled in this thesis, a generic model from literature is taken to represent this load when developing the aggregate load model. The model from [39] is used to represent this load category (details of all identified lighting models have been presented in Section 4.2.1). These models for HID lamps and LFLs should be validated, and improved, if necessary, in future research to allow more confidence in the construction of load models for the commercial load sector.

Conversion of commercial space and water heating load type into corresponding load categories

The main operational principle of electrical space and water heating load does not change between load sectors. Therefore, this load is, again, assumed to be ideal constant resistive load. A more detailed discussion on the types of devices which are included in this group of loads is provided in Section 6.4.3.

Conversion of commercial 'cold' load type into corresponding load categories

The electrical processes performed by 'cold' loads in the commercial load sector are identical to those in the residential load sector. Therefore, the functional description is not repeated here (refer to Section 6.4.3 for further details). However, the size of some of the 'cold' loads used in the commercial load sector will necessitate a three-phase connection. In this thesis, it is assumed that 75% of motors are single-phase, while the remaining 25% are three-phase. This assumption is similar to a general rule from [62] stating that the motor contribution is around 70:30 (single-phase:three-phase) in the commercial load sector.

Conversion of commercial catering load type into corresponding load categories

As there are no statistics on the specific composition of the catering load in the commercial load sector, it is proposed to have the same load mix as the residential load sector. The contribution of the load categories to this load type are, therefore, 81% resistive and 19% PE p-PFC.

Conversion of commercial electronics load types into corresponding load categories

The consumer electronics load type is not well defined for the commercial load sector, so ICT and CE are grouped together as power electronic loads. There is very little available data on these load types for the UK commercial load sector; however, the most detailed available EU statistics indicate that the ratio of computer load to general office equipment, in terms of annual consumption, is approximately 60:40 [160]. This limited dataset requires additional assumptions, which are defined as:

- For computer load, the ratio of desktop to laptops is 75% desktop and 25% laptop. One monitor is assumed per desktop.
- For office equipment, printers are considered to account for 50% of consumption, based on two factors: the high rated power when in use and the relatively high stand-by power of larger appliances, which can be around 50 W for typical commercial applications. All other loads are assumed to be low-power electronic devices (i.e. PE no-PFC).

Applying these rules to the demand statistics produces the corresponding load category data given in Figure 7.6, with the penetration of technologies within each load type (e.g. the percentage of laptops with PE p-PFC) taken to be the same as the residential load sector.

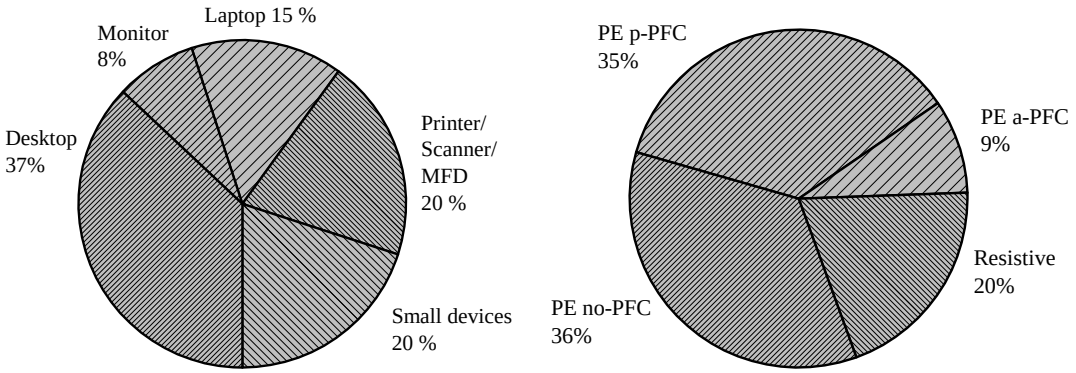

(a) by load type **(b)** by load category

Figure 7.6: Conversion of commercial power electronics load types into the corresponding load categories and subcategories.

Conversion of commercial 'cooling' load into corresponding load categories

Typical AC loads will include a start and run capacitor motor, i.e. CSR motor category, for the compressor (constant torque motor load) and a CSR motor for the fan (quadratic torque motor load) [181]. However, they can also be drive controlled three-phase induction motors. As there are no available statistics, a 75:25 contribution is again assumed between single-phase and three-phase units. The generic three-phase drive-controlled motor in [18] is used to represent this load category, with details presented in Table 7.1. The contribution of the fan load to the total cooling load is around 12% of the total power demand [181].

These statistics are used to obtain the contribution of the different load categories in Figure 7.7.

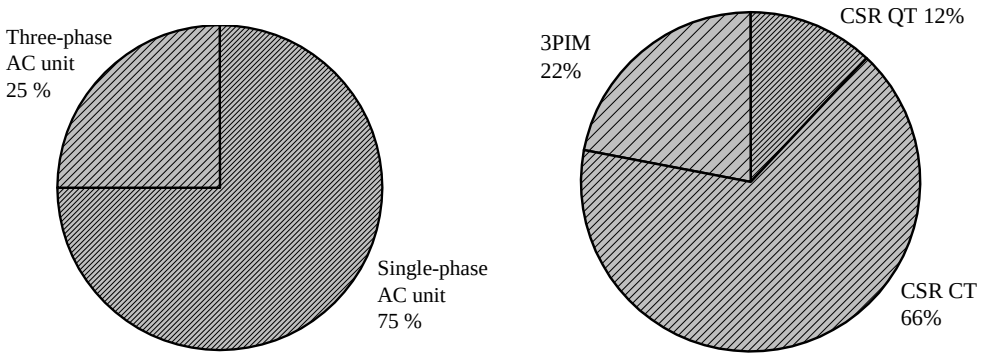

(a) by load type **(b)** by load category

Figure 7.7: Conversion of commercial 'cooling' load types into the corresponding load categories and subcategories.

Conversion of commercial lift load into corresponding load categories

There is no guidance in the available literature on the modelling of this load type, and is assumed to be a generic drive-controlled three-phase IM. This assumption is based on the fact that the majority of commercial properties with lifts will be larger buildings which are likely to include connection to a three-phase supply, which will require motors of typical maximum rated power around 15 kW [182, 183]. The model for this is taken from [18].

7.2.4 Aggregate load composition by load categories

The aggregate demand profiles as represented by load types (Figure 7.4) are converted into the corresponding load model categories and subcategories, with the results displayed in Figure 7.8. These results show that the largest contribution to the total demand are from the resistive and LFL loads, with an increasing penetration of motor load, from the AC units, during the summer months.

These load curves provide insight into the displacement power factors displayed in Figure 7.2. In the winter loading conditions, the displacement power factor during the night-time period is close to unity, as the main increase in load is due to resistive loads which will act to improve the value of overall aggregate load displacement power factor. During the typical working period, the value of PF_1 is generally increased due to the combined effect of the lighting, electronic and motor loads, which dominate the reactive power characteristics. In the summer months (i.e. minimum demand), the increased use of motor loads for AC units, and the resulting additional reactive power demand, will act to lower the displacement power factor.

The models of the load categories which have not been previously introduced are shown in Table 7.1. The motor load models are available from the previous research at the IES as part of the load library, while models of LFL and HID lamps are taken from [39]. From these models it is clear that the reactive power characteristics of the LFL will show significant variation as a result of changes in the supply voltage magnitude. This effect is a result of the saturation of the magnetic ballast, which, as previously indicated, are being replaced by more sophisticated electronic control circuits. As LFLs are one of the most dominant load categories in the commercial load sector, this behaviour will also be visible in the reactive power response of the aggregate commercial load model.

Table 7.1: Models for commercial load sector subcategories taken from literature.

Ref.	Load	PF_1	Exp.		Polynomial/ZIP model					
			n_p	n_q	Z_p	I_p	P_p	Z_q	I_q	P_q
[39]	HID	0.96	ns	ns	0.28	0.38	0.34	2.52	-6.51	4.99
[39]	LFL	0.96	ns	ns	-6.27	12.97	-5.69	8.16	-12.26	5.14
[18]	3PIM ASD	0.984	0	-0.5	0	0	1	1.22	0.45	-0.67
[18]	3PIM $RSIR_{CT}$	0.83	-0.1	1.44	0.27	-0.63	1.36	1.55	-1.7	1.15
where: 3PIM ASD represents generic drive controlled 3PIM.										

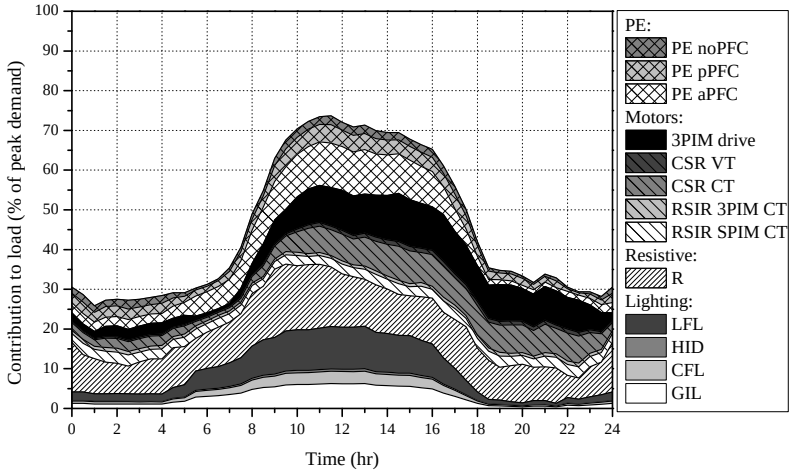

(a) minimum loading conditions

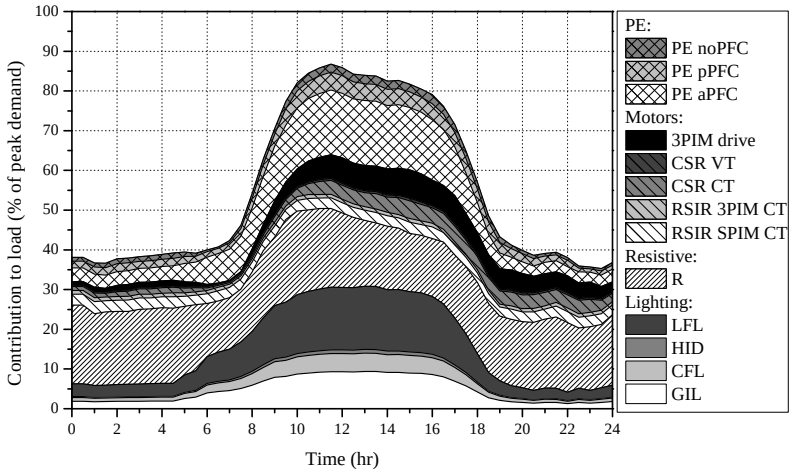

(b) average loading conditions

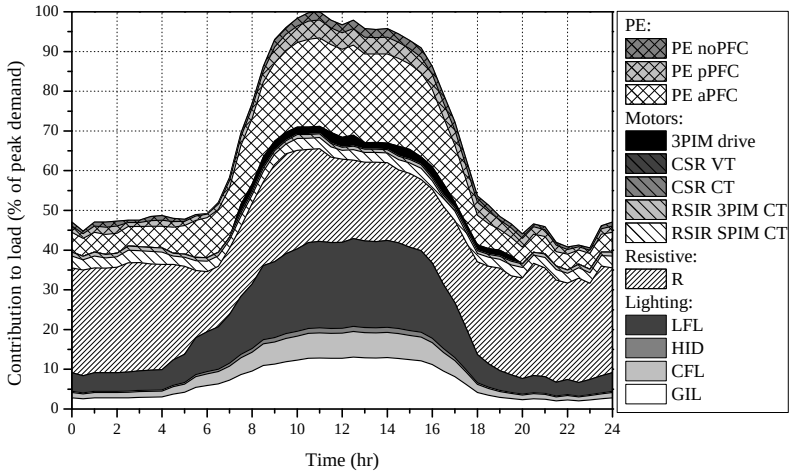

(c) maximum loading conditions

Figure 7.8: Decomposition of commercial load sector demand curves into load categories for three characteristic loading conditions.

7.2.5 Low-voltage aggregate load characteristics

Using the same technique of summing the input current waveforms of the individual load categories, the instantaneous current waveform of the LV aggregate commercial load is obtained. By performing a voltage sweep of the supply voltage magnitude, the exponential and polynomial/ZIP load model interpretations of the aggregate load characteristics are extracted. Again, the exponential load model coefficients are used for display purposes in Figure 7.9, with all exponential and polynomial/ZIP load model coefficients included in Appendix H.

For active power characteristics, the results for the different loading conditions are similar during the typical working hours. The seasonal variations observed between the minimum and maximum demand cases can be attributed to the electrical characteristics of the heating and cooling loads, respectively. The larger contribution of motor load during the minimum loading period will lower the value of n_p. Although the increased contribution of heating load in the winter months will act to raise the value of n_p, this is offset by the higher demand for lighting loads, which, for the LFL loads considered in this thesis, tend towards to constant current and constant power loads. However, the effect of the increased heating load for the maximum loading conditions is more pronounced during the night-time periods.

As expected, the exponential load model value which describes the reactive power characteristics is quite high, as a result of the LFL and motor load. The largest value is noted around 6am for all cases, as the contribution of lighting increases at a faster rate than the other reactive power loads during this period. Throughout the day, the use of these other loads will reduce the variations in the reactive power characteristics and the values of n_q are approximately constant for longer periods of time. However, the value will rise again during the evening, as the use of other loads reduces and lighting load again becomes more dominant within the load mix.

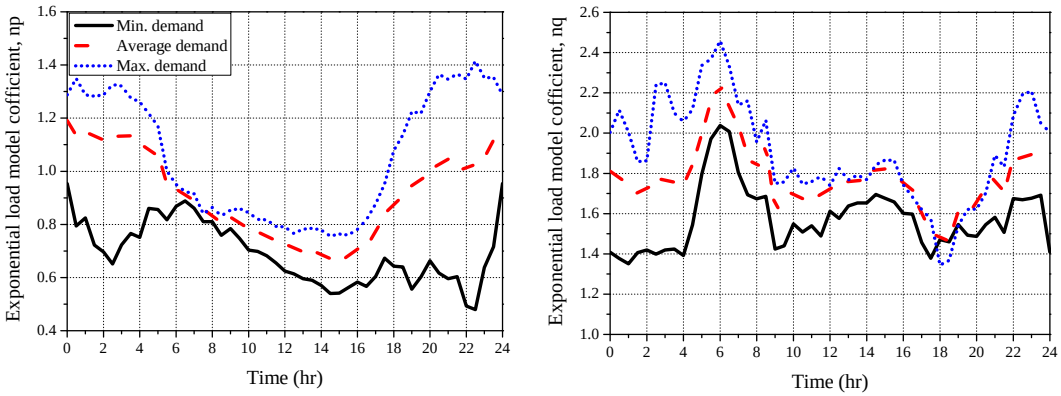

(a) active power (b) reactive power

Figure 7.9: Variation in aggregate LV commercial load model represented by the exponential load model form.

Although it is hard to validate the proposed models with existing commercial load sector models, the values can be compared to provide reassurance on the overall trends displayed by the model values in Figure 7.9. The existing commercial load sector model in [1] (given in Table 6.2 on page 145) present n_p values between 0.99 for summer and 1.3 for winter, with corresponding n_q values of 3.5 and 3.1. It is not specified for which time of day the models are applicable, although it may be assumed with some confidence that the values will be representative of the typical working hours demand. Although slightly lower, the active power characteristics displayed by the model developed in this thesis exhibit the same trend. However, it is difficult to compare the reactive power characteristics due to the multitude of technological changes, e.g. proliferation of drive controlled motors, and legislative measures, e.g. the introduction of harmonic legislation (which has been shown to have a substantial impact on the power electronics and lighting load categories), which have taken place since the development of the model in [1] (in 1994).

Comparing with most recent available commercial load sector model [62], from the US in 2004, requires converting the polynomial/ZIP load model coefficients into the equivalent exponential load model parameters. Using (2.6) and (2.7) to convert the data in Table 6.2 returns: n_p = 0.57 and n_q = 1.9, which are again close to those presented in Figure 7.9. As stated, these comparisons do not serve to validate the developed UK commercial load sector models, but do give some confidence in the electrical behaviour of the developed models.

7.2.6 Sensitivity analysis of aggregate commercial load sector model

As the lighting load accounts for almost 40% of the total demand in the commercial load sector, the representation of this load should play a central role in the modelling effort. The various lighting technologies found in the commercial load sector have been discussed in Section 7.2.3 which has shown LFL to be the dominant technology. LFLs can be supplied from conventional magnetic ballasts or from more sophisticated electronic control circuits, and a 50/50 ratio was assumed during the commercial load sector model development. In order to quantify the influence of this load on the aggregate commercial load characteristics, the aggregate model is built for two cases: assuming 100% penetration of conventional ballast (denoted LFL Type I in Figure 7.10) and 100% penetration of electronic control circuits (denoted as LFL Type II in Figure 7.10).

Increasing the contribution from the conventional ballast will raise the values of n_p and n_q, and lower the aggregate displacement power factor. Although the changes in n_p and PF_1 are relatively modest, there is a notable change in the reactive power characteristics. Due to the highly non-linear performance of the ballast, this will raise the aggregate exponent to between the second and third power. The steeper gradient of the $Q_1 - V$ curve, in comparison with the relatively linear $P - V$ characteristic, will influence the power factor values for changes in supply voltage magnitude.

The electronic control circuits allow for better regulation of the voltage and current at the tube terminals, therefore improving performance and lifetime. As previously stated, due to the rated power of these devices, it is expected that they will have electrical characteristics similar to PE a-PFC [18], in order to satisfy the requirements of harmonic legislation given in [20]. As this technology is introduced in large numbers, the gradient of both the $P-V$ and Q_1-V characteristic will reduce. Again, the effect on the reactive power demand is much more pronounced. This is because the a-PFC is modelled with ideal operation, i.e. with unity power factor, and the reactive power characteristics are determined by the remaining capacitive CFL loads and induction motor loads. The local interaction of these loads, and the significantly reduced reactive power demand due to removal of lighting load, will result in a very high value of displacement power factor.

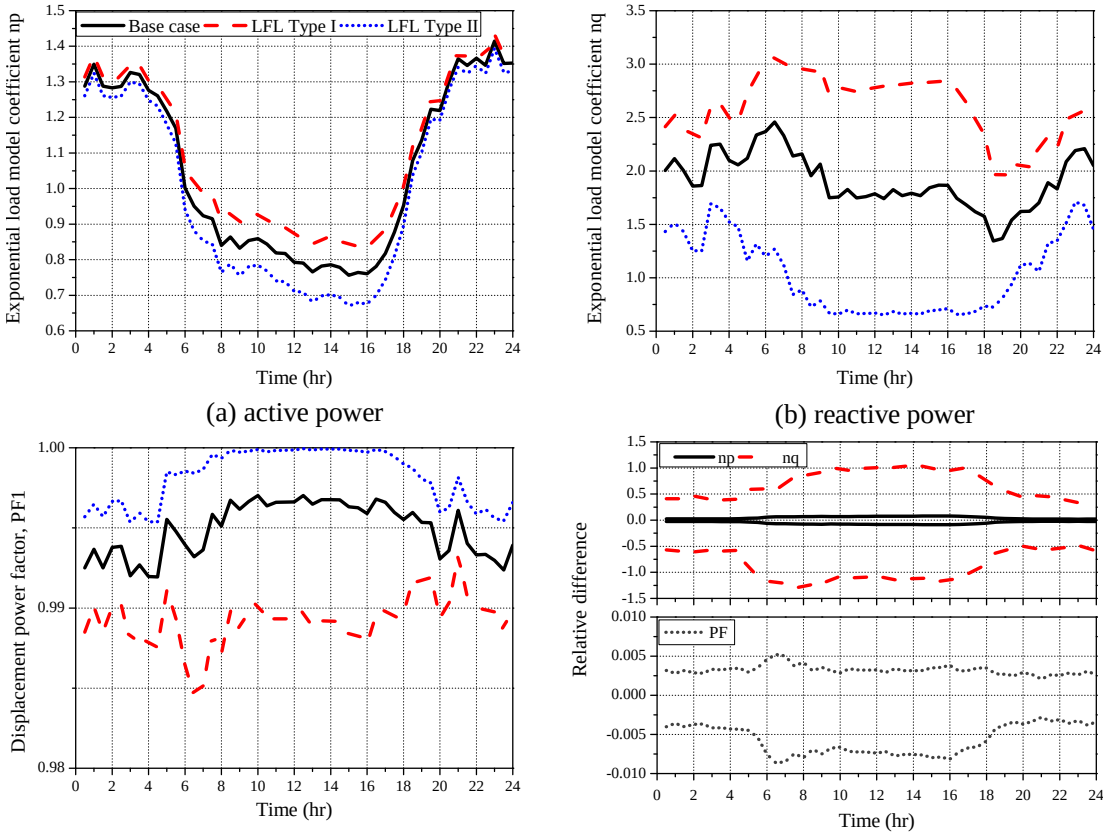

Figure 7.10: Impact of changing LFL load on aggregate commercial load sector electrical characteristics (maximum loading conditions).

Additional sensitivity analysis on the commercial load sector is performed by adjusting the contribution of each load by plus and minus 5%, with all other loads proportionally adjusted, i.e. scaled down or up. This proportional adjustment alters the load mix under the aggregate demand curve (i.e. the decomposition under the envelope) rather than the actual load demand (which is represented by the envelope). The upper and lower boundary results, displayed in

Figure 7.11, are obtained by simulating every new load mix and identifying the maximum and minimum parameter value from all simulated load compositions.

This was performed for the average loading conditions, and the variations in load model parameter values are comparable with the results in Figure 7.10. The exception is the reactive power characteristic, which is less sensitive to changes in the load composition than for changes in the technology of the lighting load category. The reactive power demand will also influence the displacement power factor, which shows a slightly wider range of values for changes in the load composition.

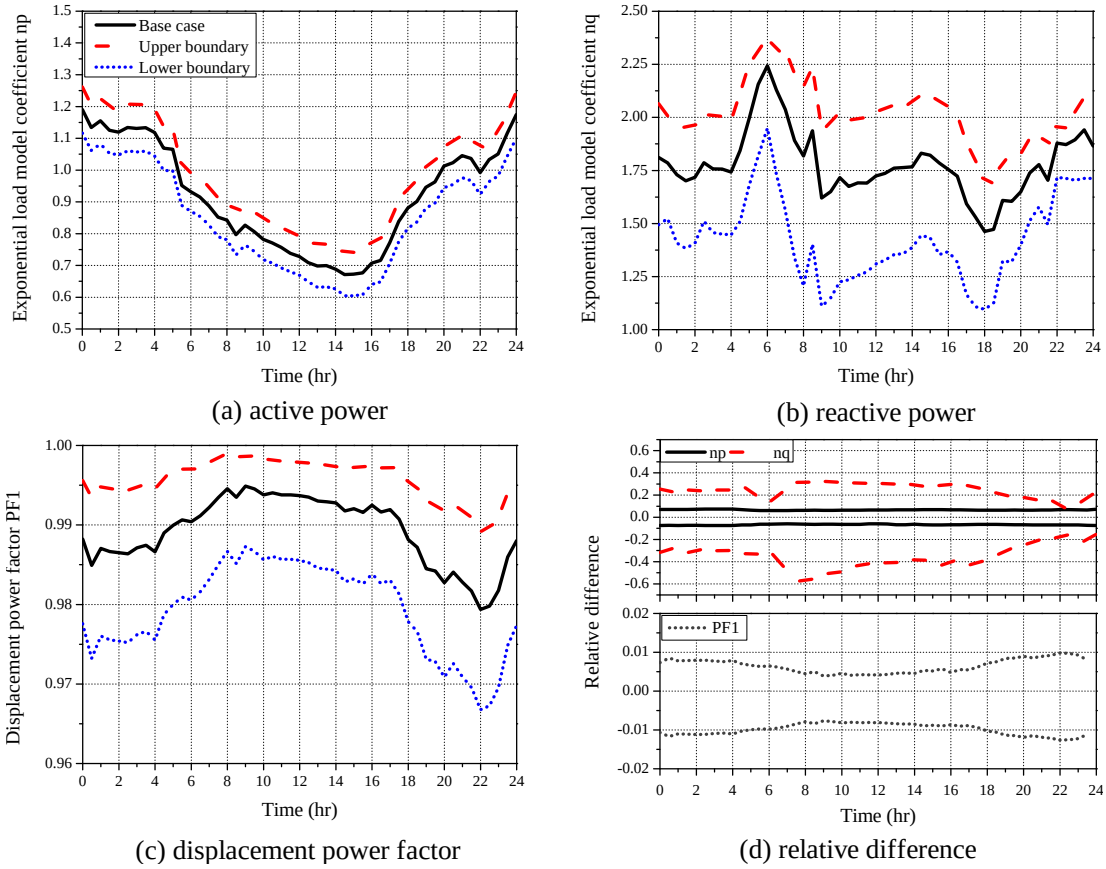

(a) active power

(b) reactive power

(c) displacement power factor

(d) relative difference

Figure 7.11: Impact of load composition changes on the aggregate commercial load sector electrical characteristics (average loading conditions).

7.2.7 Discussion of results

The application of the aggregation methodology to the commercial load sector further demonstrates the benefits of using both the methodology and the load model library. There is likely to be greater variability in the electrical characteristics of the commercial load sector, due to the large number of subsectors, which cannot be adequately covered within this research. However, the model for the overall commercial load sector provides some insight into the likely electrical characteristics of the commercial load sector which are not currently available for UK-based loads.

The analysis has shown that the most important load within the commercial load sector is LFL, which has the greatest influence on the electrical characteristics of the aggregate model. This suggests that further investigation and development of an updated load model for this load category should be included in the load library, to allow for the further improvement and development of a more accurate commercial load sector model, as well as the required subsector load models, in the future research.

The model development stopped at the LV aggregate model and did not extend to the model representation at the MV level. This stage is not necessary, as the results presented in Chapter 6 have thoroughly covered this stage of the aggregation methodology. Furthermore, the typical aggregate load at the MV level is likely to include a mix of load sectors, so the development of aggregate MV load models should be performed for the appropriate weighting of different load sectors, rather than to each load sector individually.

7.3 Aggregation methodology: Microgeneration

The deployment of various LV MG technologies, e.g. solar-photovoltaic (PV), small-scale wind turbines (WT) and combined heat and power (CHP) systems, is expected to increase in future electricity networks. It is estimated, for example, that the installed capacity of small-scale WTs in the UK could be as high as 1.3 GW by 2020 [184]. As these technologies will be installed and operated in parallel with the LV network load, they will have an impact on the performance of the LV network and will alter the aggregate electrical characteristics (as viewed from the MV load supply point). Therefore, MG technologies should be included in the development of MV aggregate load models.

Recent statistics, taken from [6], suggest that almost half (40%) of network operators do not currently consider these technologies within the LV aggregate load model. This may be due to the reasonably low penetration of MG, as the influence on the network operation may be negligible for low levels of installation. However, as the number of MG units within the LV network rises, their impact on many network performance aspects, e.g. reduction of losses due to reduced demand, possible increase in voltage distortion due to inverter interface connection etc. [185, 186], will increase. In extreme cases, the installed MG capacity may be so large as to result in reversed power flows, and export from the LV network back into the distribution system. This will require the use of active distribution network cells (ADNC) modelling techniques.

This thesis suggests that the effect of MG can be included within the aggregation methodology, as presented in the flowchart in Figure 6.1. As the research presented in this thesis is primarily interested in the development of aggregate load models for power system analysis, the most important step is to quantify the changes in the electrical characteristics of the MV aggregate load model as a result of installed MG. Accordingly, only brief details of the MG modelling effort are included here (full details are available in [178]). It is shown that even a modest

MG penetration of 10% may have a considerable impact on the electrical characteristics of the aggregate load/demand in which it is included.

7.3.1 Modelling of microgeneration technologies

As shown in the aggregation methodology flowchart (Figure 6.1, Page 150), three datasets are required to include MG in the aggregate model development process. These are analogous to the datasets used for the load model development which have been presented in this thesis:

- MG energy resources: which specifies the available primary energy resources (e.g. wind) for conversion to power generation (comparable to the load demand curves).
- MG structure and composition: which specifies the contributions of different MG technologies to the total installed MG capacity (analogous to the load categories).
- Generic models of MG: representation of the installed MG technologies in a form suitable for use in power system analysis (the equivalent of the generic load models).

These datasets are now briefly described for use in the aggregation methodology. Although the installed MG technology will be determined by the locally available resources, the effect of MG on the electrical characteristics of the aggregate load are investigated using only small-scale wind energy systems, defined as less than 2.5 kW [178], in this research. This MG technology was selected to allow for collaboration with parallel research in [178].

Small-scale wind turbine modelling

The vast majority of small-scale WTs will utilise a permanent magnet synchronous generator (PMSG) with an inverter interface for the grid connection. In this configuration, the variable magnitude and frequency of the PMSG power output is regulated by the rectifier and inverter, which will export power to the grid at the required frequency and magnitude. The basic components of a generic small-scale wind energy system are shown in Figure 7.12.

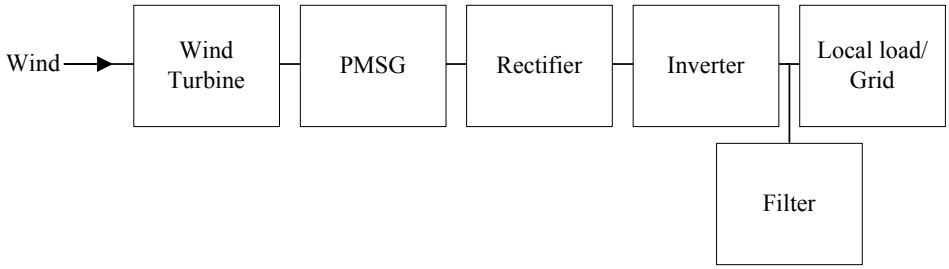

Figure 7.12: Main components of a PMSG based small WT system.

For use in the aggregation methodology to develop steady-state aggregate load models, the most important details are the active and (fundamental) reactive power demands. Research in [178] has developed a generic aggregate model of small-scale WTs, given in (7.1) overleaf, from a large database of manufacturers' power curves. This steady-state model includes the efficiency of both the electromechanical conversion (typically around 80%) and the inverter system (typically around 90%) [187].

$$P_{WT_{aggregate}} = -10.3v + 3.83v^2 - 0.11v^3 \tag{7.1}$$

where: v is the input wind speed (m/s) and $P_{WT_{aggregate}}$ is the power output of the aggregate wind-based MG model.

The performance of the inverter interface will determine the electrical characteristics of the small-scale wind energy system, and it is assumed to operate at unity power factor in accordance with legislation [188]. For the purpose of this research, it is also assumed that the output filter is ideal, supplying an ideal sinusoidal waveform, with no harmonic content, to the local grid. This effectively makes the MG act as a negative load within the LV network, which is adequate for the development of MV aggregate steady-state load models with low MG penetration levels. In reality, however, the inverter interface will introduce high frequency harmonics in the LV network. These will typically lie out with the frequency range analysed in this research, and is not considered further.

Resources modelling

Wind energy resources exhibit significant short, medium and long-term variations (i.e. hourly, daily, weekly and seasonal variations). It is, therefore, necessary to perform temporal assessment of wind energy resources by taking into account both daily (time of the day) and seasonal (day/month of the year) variations. Additionally, wind energy resources will also vary at different geographic locations (spatial variations), i.e. within different load subsectors.

In this research, the aim is to capture the full extent of the impact of the LV MG on the aggregate load characteristics at the MV level. To achieve this, processed wind speed measurements taken in the Edinburgh city area are analysed to identify the maximum and mean wind resource value for each time step (i.e. half-hour period) within a 30-day period. As both wind and load are highly variable, a 30-day period (i.e. plus/minus 15 days) is selected to cover the possible range of wind speeds that may occur around the time of year of each characteristic loading condition. The minimum value is omitted, as the minimum measured value for each time step was always zero for the measured dataset (i.e. there may be no wind at any hour of any during year). Although this analysis presents a simplified assessment of a complex natural resource, this information is all that is required to quantify the possible impact on the aggregate MV characteristics for load model development. A more thorough analysis, from which the data presented here is extracted, is available in [178].

The maximum and mean values for summer and winter, i.e. minimum and maximum loading conditions, are presented in Figure 7.13. The highest wind speeds measured during the maximum loading conditions are generally higher than the corresponding values for minimum loading conditions. The difference in the mean value is less pronounced, but there will still be an improved performance of the small-scale wind energy system for maximum loading

conditions, as the power output varies with the cube of wind speed (7.1). The final observation on Figure 7.13 is that, for this measured location, the wind turbine will almost never produce rated power output during the summer period.

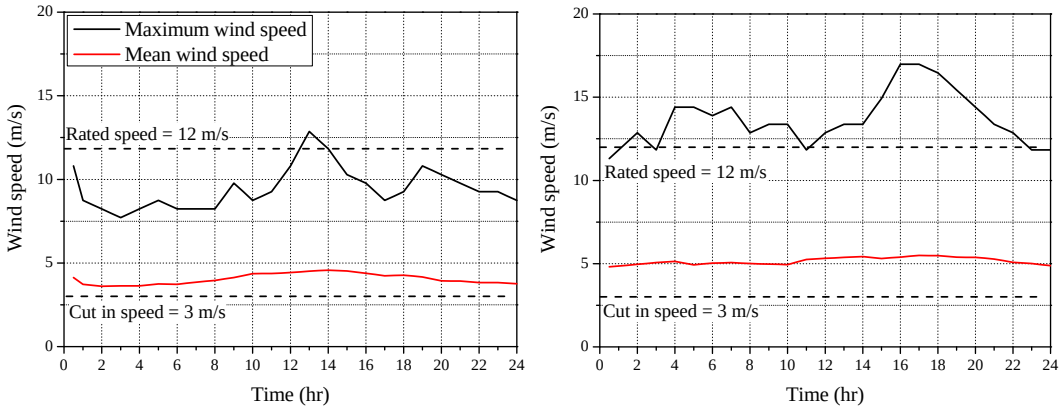

(a) minimum loading conditions **(b)** maximum loading conditions

Figure 7.13: Measured wind speed assessment for time of year corresponding to minimum and maximum loading conditions.

7.3.2 Aggregate low-voltage microgeneration model

Initial analysis of the impact of MG on residential load is simply assessed by combining the processed wind speed measurements with the generic WT model to calculate the typical maximum and mean power outputs of the MG . This power output is then subtracted from the demand curves to examine the effect on the active and reactive power demand of the residential load sector. This does not include the effect of interactions between the MG, the connected load and the supply network, e.g. reduction in network losses, which is considered further in the following section.

In this example, the assumed penetration of small-scale wind-based MG is taken as 10% of the peak load (i.e. maximum winter demand). Although the penetration is small, the maximum possible load which may be offset by small-scale wind-based MG can reach up to 30% of the instantaneous power demand. This is possible during both the maximum and minimum loading conditions, as shown in Figures 7.14 and 7.15.

For the analysed location, the probability of occurrence of characteristic wind speeds during the maximum loading conditions can be expressed using the Weibull distribution, which shows that the probability of wind speeds higher than 12 m/s (i.e. rated speed) and lower than 3 m/s (i.e. cut in speed) are approximately 2.5 %, and 16 %, respectively. The probability of the mean value is around 39 %. For the minimum summer loading condition, the probability of maximum and zero WT outputs for the same 12 m/s and 3 m/s input wind speeds are less than 1 % and around 21 %, respectively, while the probability of the mean value is approximately 53%.

As the MG devices are assumed to operate at unity power factor, there is no ability to provide reactive power support to the network. This will lower the value of displacement power factor of the aggregate load, as the local supply of active power within the aggregate load will reduce the power imported from the distribution network while the reactive power demand will remain unchanged.

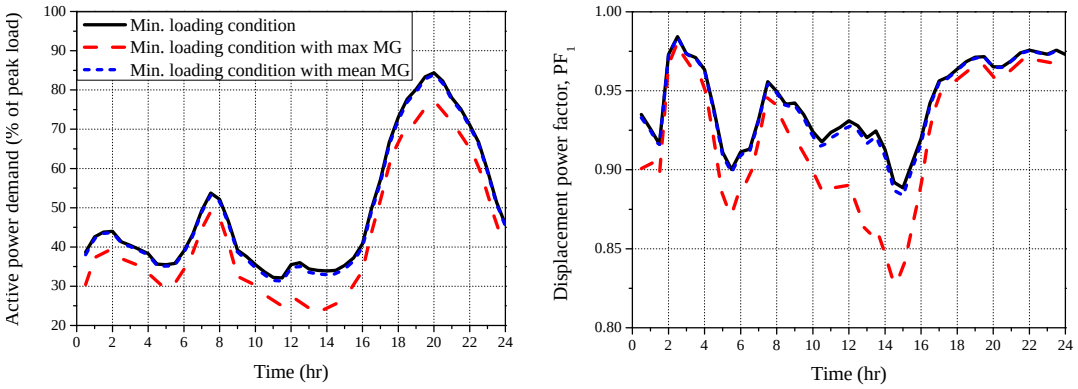

(a) active power (b) displacement power factor

Figure 7.14: Impact of aggregate LV MG model on demand for minimum loading conditions.

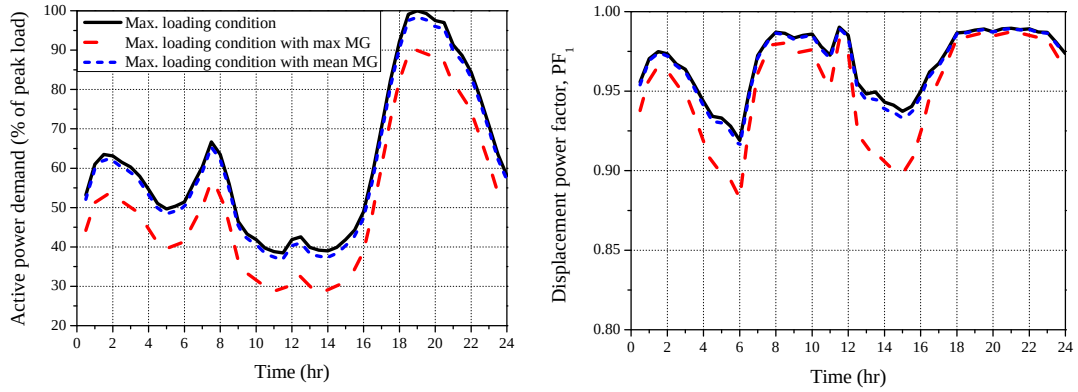

(a) active power (b) displacement power factor

Figure 7.15: Impact of aggregate LV MG model on demand for maximum loading conditions.

7.3.3 Aggregate load characteristics with microgeneration

The changes on the power curves is expected, but requires further simulation to investigate the overall effect of MG on the electrical characteristics of the aggregate load model. To quantify this, the effect of the network must be taken into consideration. In this example, the detailed LV urban network (introduced in Figure 6.17, Page 167) is again used to provide continuity in the presented results. MG is assigned at each load point of the network, as indicated by the black circles in Figure 7.16. A 10% MG penetration equates to one MG of rated power 2.25 kW per load group. All other network properties are unchanged.

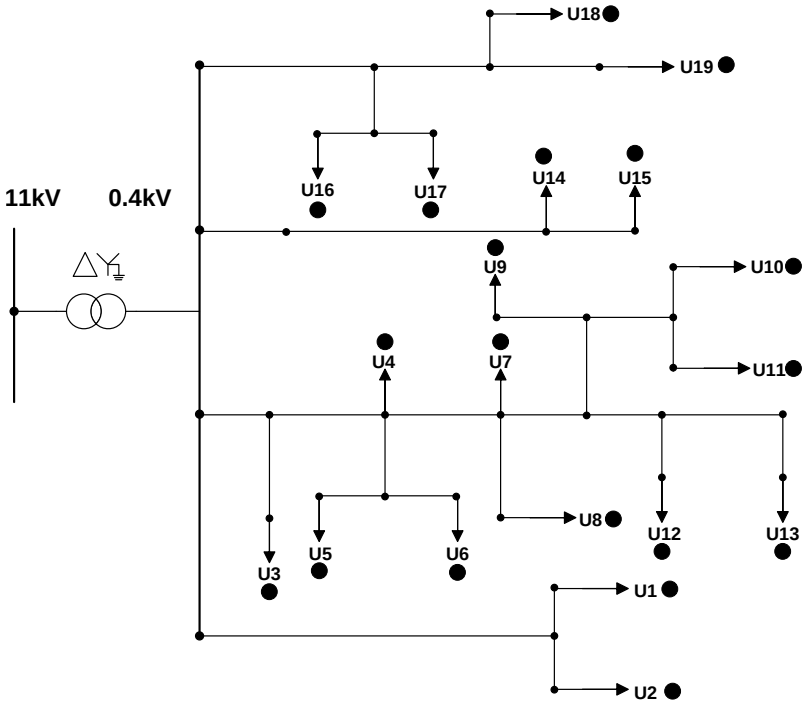

Figure 7.16: Urban network with connected microgeneration.

In Section 6.5.3, a network aggregation technique was introduced which allows for the representation of the entire LV network by a single equivalent impedance. As the network operation will change due to connection of MG units, this technique is again validated for the updated LV network configuration. The output from all MG units is connected in parallel with the aggregate LV load and supplied from the equivalent network impedance, as shown in Figure 7.17.

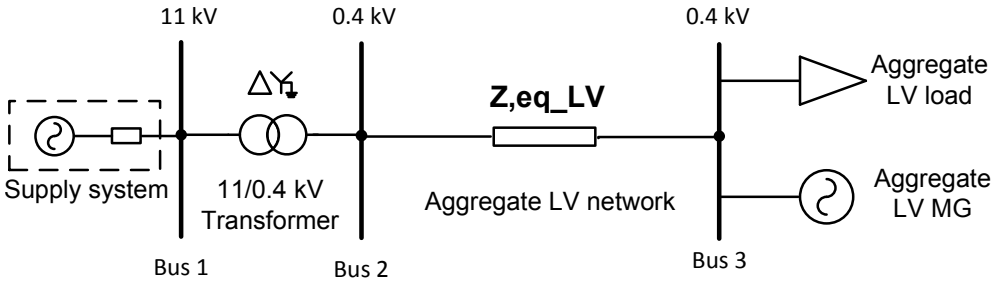

Figure 7.17: Equivalent network configuration with connected microgeneration.

Figures 7.18 and 7.19 compare the active and reactive power at the MV level for V = 0.8 pu and V = 1.2 pu, i.e. the maximum and minimum supply voltage magnitude considered in this research for load model development, for the detailed network and equivalent network configurations. There is negligible difference in the characteristics at the 11 kV busbar between the results obtained with the detailed network model and the corresponding results for equivalent network impedance model with MG. Therefore, the equivalent network can again be used for the development of aggregate MV load models which include the effect of MG.

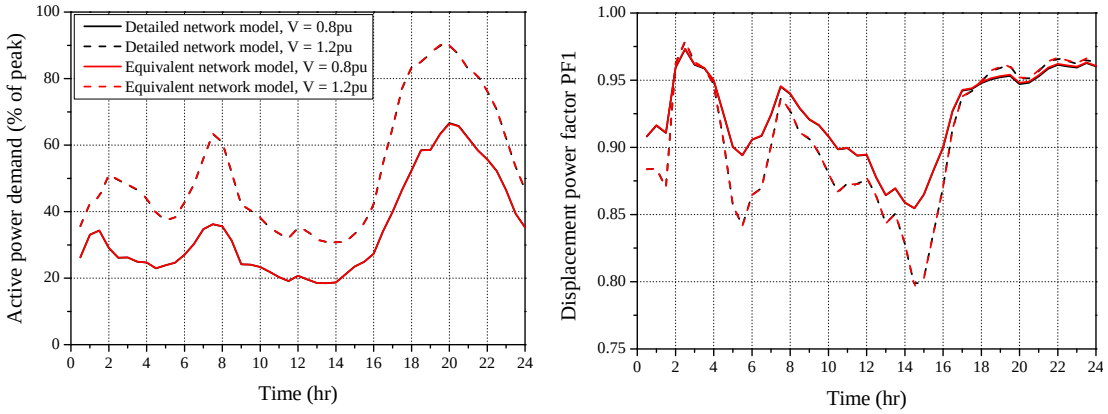

(a) active power demand (b) displacement power factor

Figure 7.18: Comparison of active and reactive power flows at 11 kV aggregate load supply point for detailed and equivalent network models for minimum loading conditions

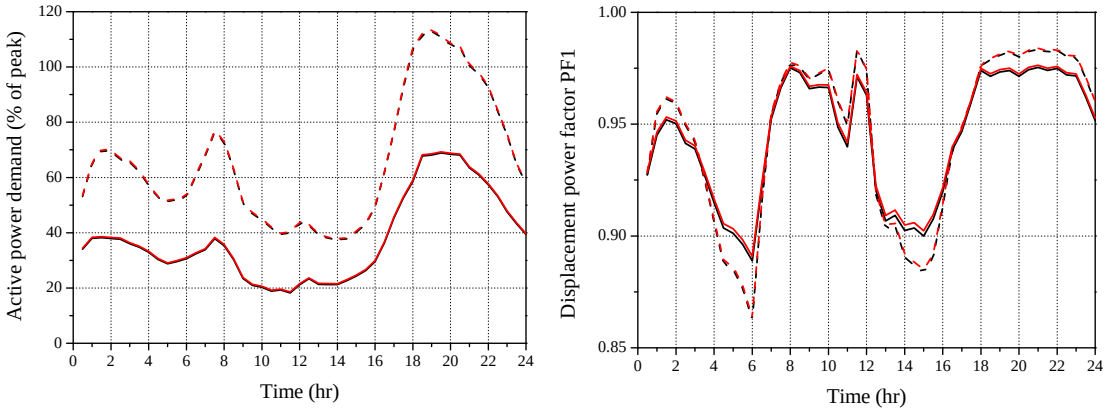

(a) active power demand (b) displacement power factor

Figure 7.19: Comparison of active and reactive power flows at aggregate point for detailed and equivalent network models for maximum loading conditions

It should be noted that it is unlikely that the MG units will remain connected for sustained under/over-voltage conditions of such severity. However, this hypothetical scenario provides a similar validation as the developed load models for the simulated network.

Due to the inverter interface, the MG units are modelled as a constant active power source, i.e. the device will output the power based on the available wind resources, regardless of the voltage in the LV network to which it is connected. Therefore, when operated in parallel with the LV load, it will act to reduce the demand of the constant power loads within the aggregate, even though the actual MG unit will supply all locally connected load. In the resulting mathematical derivations of the load model coefficients, this will resolve to raise the contribution of the constant impedance and constant current loads within the aggregate mix. This is confirmed by the simulation results in Figures 7.20 and 7.21, which show an increase in the MV aggregate load model coefficient with locally connected MG units.

The effect of MG on the aggregate MV load model is more pronounced for the maximum loading condition, i.e. the maximum load model coefficient value is higher. This is due to the larger percentage of resistive loads within the aggregate demand, from the increased use of heating loads (in comparison with the minimum loading conditions). As previously discussed, the constant impedance characteristic of these loads is reduced within the aggregate due to the large number of constant power electronic devices. However, when the MG is connected, the contribution of the constant power loads is reduced.

Although the installed MG is not participating in reactive power support within the LV network, it will still have a small effect on the reactive power characteristics at the MV level due to the participation of the supply network on the aggregate load characteristics. By supplying some local load, the power supplied from the MV network will reduce. The lower value of current flow through the network impedances will change the contribution of the network to the aggregate load, which, for this case, partly unloads the secondary distribution transformer and reduces the influence of this network component on the aggregate MV load characteristics.

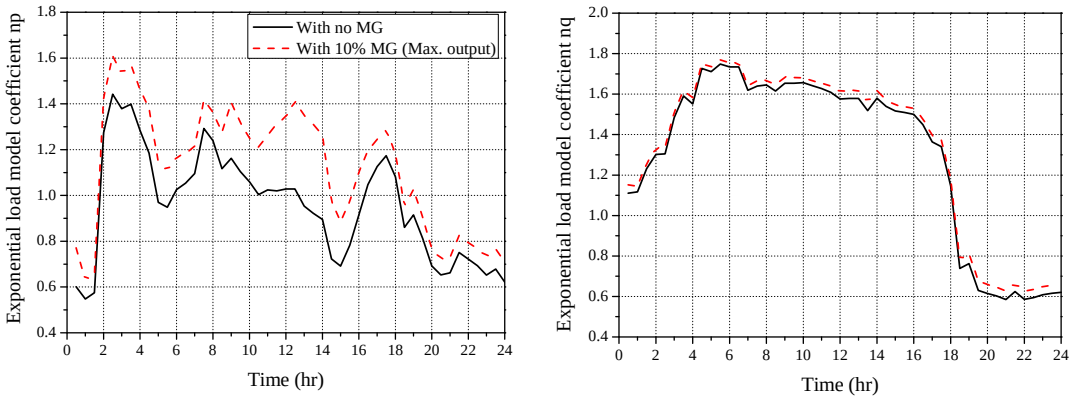

(a) active power (b) fundamental reactive power

Figure 7.20: Exponential load model model interpretation of MV aggregate load for minimum loading conditions with installed microgeneration.

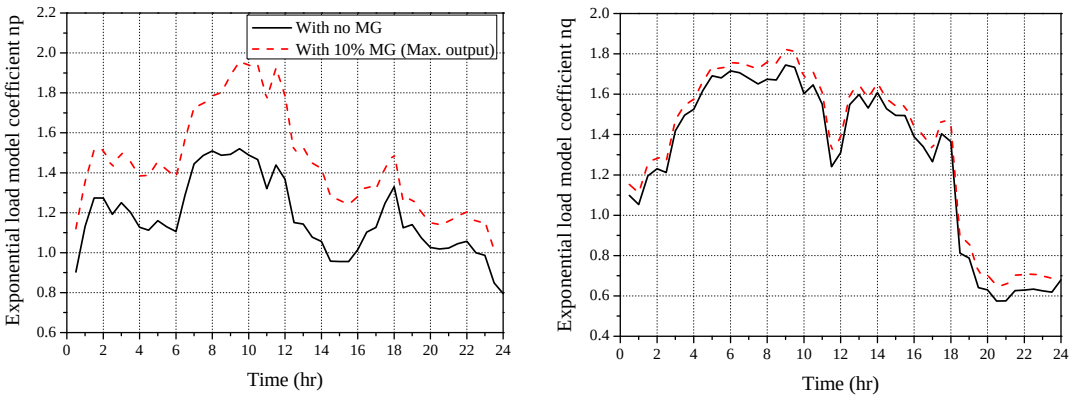

(a) active power (b) fundamental reactive power

Figure 7.21: Exponential load model model interpretation of MV aggregate load for maximum loading conditions with installed microgeneration.

7.3.4 Discussion of results

The results obtained in this case study show an extension of the aggregation methodology to include the effect of MG within the MV aggregate load model. Although the assumed penetration of MG is modest, it is shown that it may still have a significant impact on the steady-state load model coefficients of the aggregate load representation. This indicates that, if the penetration of LV MG increases in the future, it will be even more important to consider their impact and effects on all aspects of power system analysis.

Treating the MG as a negative load is adequate for this analysis. Although the MG will 'offset' a portion of the load, this will change the losses within the network and alter the influence of the network on the aggregate load model. Although the results in Figures 7.20 and 7.21 suggest that this will reduce the constant power characteristic, the result is more complicated due to the interaction with the supply network impedance, and the effect cannot be calculated by simply reducing the contribution of this component and scaling the remaining load.

To illustrate this, the MV aggregate load model coefficients are recalculated by simply reducing the active power load model coefficient by the output of the MG, i.e. (7.2). This load is then proportionally redistributed to the constant current and constant impedance load model coefficients in (7.3) - (7.5).

$$P_{p,new} = P_{p,old} - P_{MG_{\%}} \tag{7.2}$$

$$Z_{p,new} = \frac{P_{p,old} - P_{p,new}}{Z_{p,old} + I_{p,old}} Z_{p,old} \tag{7.3}$$

$$I_{p,new} = \frac{P_{p,old} - P_{p,new}}{Z_{p,old} + I_{p,old}} I_{p,old} \tag{7.4}$$

$$n_{p,new} \approx \frac{Z_{p,new} \times 2 + I_{p,new} \times 1 + P_{p,new} \times 0}{Z_{p,new} + I_{p,new} + P_{p,new}} \tag{7.5}$$

where: $Z_{p,old}$, $I_{p,old}$ and $P_{p,old}$ are the aggregate MV load model coefficients before connection of MG, $P_{MG_{\%}}$ is the generation of the MG as a percentage of the total demand, $Z_{p,new}$, $I_{p,new}$ and $P_{p,new}$ are the MV load model coefficients calculated by assuming MG as a negative constant power load and $n_{p,new}$ is the equivalent value of exponential load model with MG connected.

An example of this calculation, for maximum loading conditions, is presented in Figure 7.22, which clearly illustrates the error introduced by simply reducing the constant active power demand without correct representation of the interaction with the network impedance. With an expected increase in the penetration of MG, it is believed that the development of a quick analytical method for this purpose would offer some value to the power system community and is presented as an area of further work in Chapter 8.

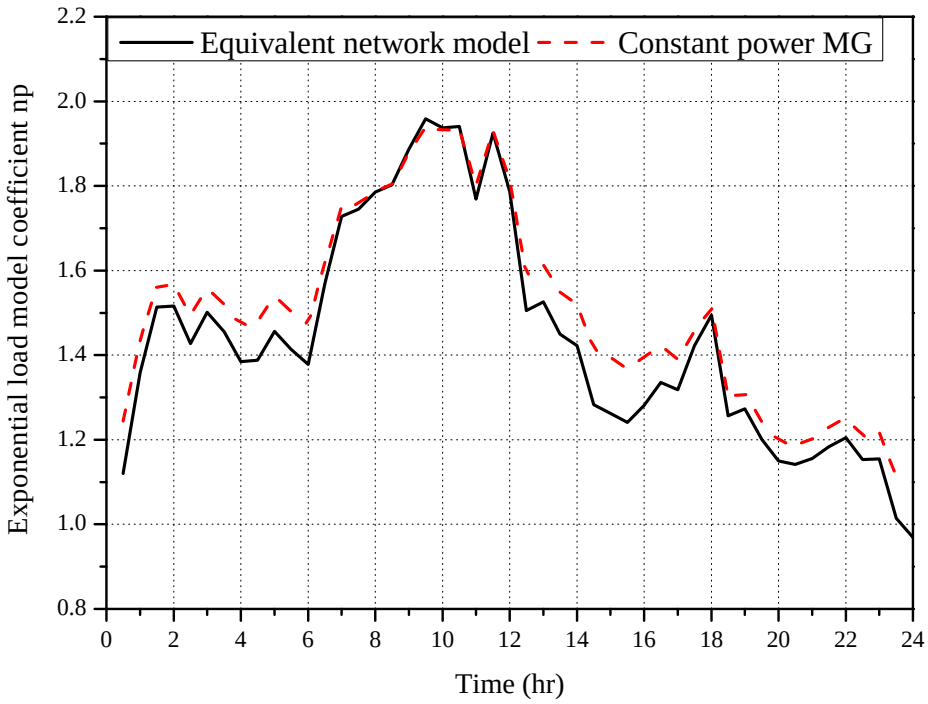

Figure 7.22: Illustration of error introduced in MV aggregate load model by representing MG as negative constant power load with consideration of the network impedance.

7.4 Network analysis

The main contributions of this thesis are in the development of aggregate load models, and, consequently, there was only limited time available to implement these models in power system studies. However, some applications of the developed load models are introduced in this section to highlight their flexibility and use in power system analysis. Two case studies are presented, both of which are set in the DSM research area, as this possible functionality of future ”smart grids” is particularly pertinent to load modelling.

Although DSM actions have been applied in power systems for several decades, e.g. in large industrial customers or through the use of electrical storage heating units in the residential load sector, it may be necessary to extend these actions to help manage network contingencies as the network becomes operated closer and closer to its operational limits. There is a certain potential to exploit advances in ICT technologies to increase the participation of residential and commercial load sectors within the DSM framework to provide network support. However, the majority of residential and commercial customers are deeply embedded within the LV networks, and this will require coordinating large groups of customers to achieve the volume of demand required to make a significant contribution to network support. For this purpose, the load modelling approach presented in this thesis can be of value, as it allows for improved representation of these LV loads, without significantly increasing the simulation time or complexity of simulations.

The first case study considers the effect of simple DSM actions within the LV network, and the propagation of changes from the LV load up to the grid supply point (GSP) on the primary winding side of the 33/11 kV distribution transformer. The purpose of this example is to highlight the ability of the developed models to represent a number of electrical characteristics and supply/load interactions. The second case study will show how the developed MV aggregate load models can be directly applied within an OPF analysis and their influence on the results.

Clearly, an accurate assessment of DSM functionalities and scenarios requires a large number of network simulations. This is beyond the scope of the research presented in this thesis, but is discussed as an area of further work in Chapter 8.

7.4.1 Case study: Low-voltage/medium-voltage network analysis

Using DSM to reduce the peak residential demand will help to defer investment in electricity networks, relieve possible overloading of network components and generally improve network performance. Although the control of active power is the main focus of most DSM schemes, the results presented in this section show how the developed models can be used to quantify the changes in reactive power demand and harmonic content of the aggregate load, which inevitably occur as a result of modifications of the active power demand.

The availability of residential loads for DSM is determined by the characteristics of individual loads and consumer routines. Many loads are unsuitable for even short-term load shifting due to their role in modern life, e.g. lighting, PCs, TVs and cooking appliances. The remaining load is generally suitable for DSM, but some load types offer more potential to DSM schemes than others. Due to the cyclical nature of operation, 'cold' loads are suitable for only a short-term deferral, while storage heating loads are mostly already used with off-peak tariffs. Therefore, this example assumes that 'wet' loads are the most readily available for residential DSM schemes.

The selection of the best/optimal DSM scheme will depend on the amount of load required for a particular corrective or preventive/protective action. This will vary from network to network, but can be assessed by OPF techniques (which is considered in the next example). This case study considers a simple DSM scheme in which an arbitrary amount, taken as 40% of all 'wet' loads present during the peak loading period (18:00 - 22:00 hour, Figure 7.23), is controlled. The load is reconnected in the same manner it was removed, i.e. the DSM portion of the load is simply delayed until a specified time. Therefore, this four-hour DSM load block can be reconnected at either: 22:00 (DSM 1), 02:00 (DSM 2), 06:00 (DSM 3), 10:00 (DSM 4) or 14:00 (DSM 5) in the daily load profile, as shown in Figure 7.23. More sophisticated reconnection schemes may aim to improve system performance by evenly redistributing the DSM load; however, reconnecting the load in blocks can be considered as a 'worst-case' scenario and may simply create new peak loading conditions. This will also demonstrate the possible range of operating conditions across the entire 24 hour period.

As well as the current load mix, the wholesale substitution of GILs with CFLs, an expected near future change in the residential load sector, is also considered. The two scenarios are defined as:

- Present scenario: the residential load mix is based on currently available load statistics.
- Near future scenario: all GILs are replaced with CFLs.

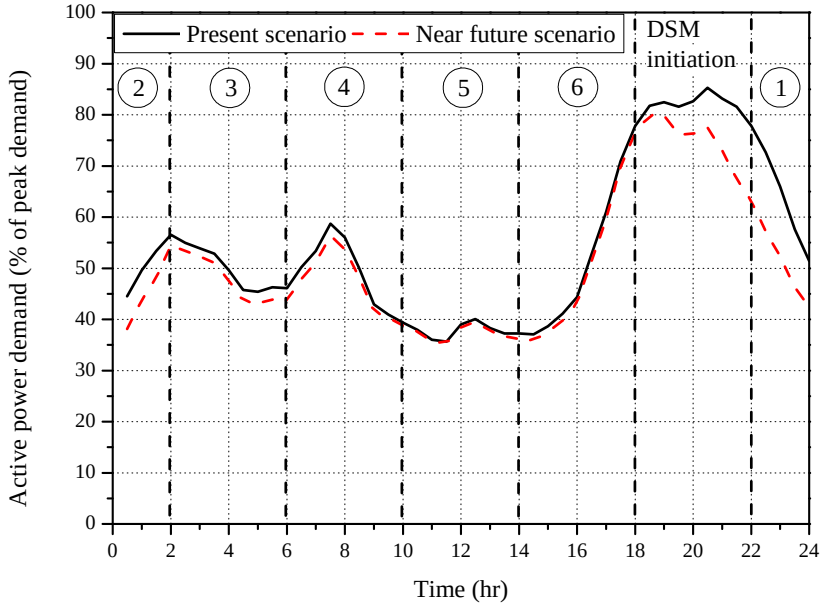

Figure 7.23: Specification of DSM windows and 'present' and 'near future' scenario load curves.

In the near future scenario, the lighting demand is proportionally reduced to reflect the expected savings (based on current trends/guidelines) of GIL to CFL replacement, while the contribution of all other loads is kept constant. This is taken as a four-fold reduction of the current GIL lighting demand (as shown in Figure 6.13 on Page 163).

For this study, the LV urban network is extended to include the 11 kV distribution network up to the GSP on the primary winding side of the 33/11 kV transformer. The network diagram is displayed in Figure 7.24, with additional parameter values of the MV section of the network included in Appendix I. The 33/11 kV transformer is the only component operating with active voltage control and uses an OLTC to regulate the voltage at the secondary side of the transformer within the prescribed range of $\pm$ 6 %. The 11/0.4 kV transformer is manually adjusted for expected seasonal variations in loading conditions, which is taken as a 1:1 ratio for the average loading conditions in this example.

The network model was built in MATLAB/Simulink software and populated with the previously developed generic load models. This software was chosen to allow for correct connection of the circuit-based load models, and also for the connection of inverter interfaced MG in future research. This model allows for analysis of changes in active/reactive power demand flows, system losses, voltage profiles and propagation of harmonics as a result of the previously defined DSM actions on both the 'present' and 'near future' scenario.

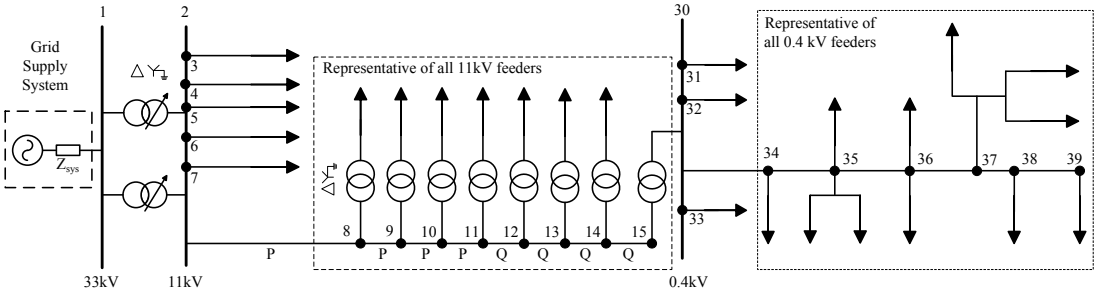

Figure 7.24: Typical UK network configuration supplying urban residential load.

Power flows

A comparison between the aggregate active and reactive power demands at the 33 kV bus (Bus 1 in Figure 7.24) for the 'present' and the 'near future' scenario is shown in Figure 7.25. Therefore, the presented results do not just show the load demand, they also include the network losses. The shaded area in the results plots corresponds to the difference between the base case of each scenario to the resulting value after removal/reconnection of DSM load. The physical interpretation of this shaded area is that connecting, or disconnecting, less than the full 40% of 'wet' load will produce a result within the boundaries of this area.

A 3.3 % reduction of peak active demand is recorded when the devised DSM scheme is implemented in the 'present' scenario. During the period of implemented DSM scheme (18:00-22:00 hours), total active power demand is reduced by 4.4%. When DSM is applied to the 'near future' scenario, the peak active demand experiences a reduction of 6.3%. In this 'near future' DSM case, total active power demand is reduced by 5% during the DSM reduction period.

The change from GILs to CFLs will not only reduce the peak active power, but, as CFLs are a capacitive load, they will also act as local reactive power support. This will slightly improve the displacement power factor in the evening, when lighting forms a significant percentage of the UK residential load. However, as shown in Figure 7.25, the effect of this local compensation does not propagate to the MV level, which can be attributed to the mainly inductive nature of the supply network components.

When the DSM load is reconnected, there is a corresponding increase in both active and reactive power demands, which is visible in both scenarios. In the 'present' scenario, reconnecting the DSM load in Region 1 will essentially just shift the peak until 22:00 hours. When the DSM load is reconnected in the system, the displacement power factor will reduce due to the motor load component of the 'wet' load. The changes in active and reactive power demands will also instigate changes in current flows and associated losses in the system. However, in the devised DSM scenarios the total daily demand does not change (all disconnected load is reconnected later), and there is only a negligible, i.e. less than 1%, difference in total system losses.

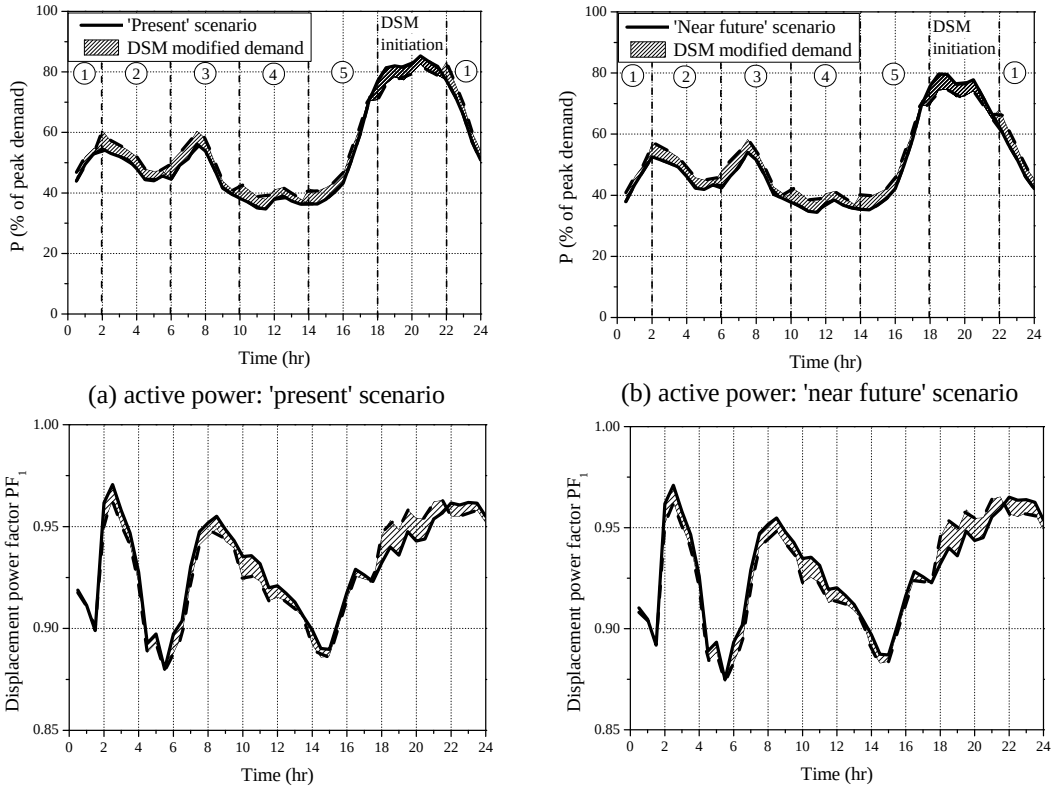

(a) active power: 'present' scenario

(b) active power: 'near future' scenario

(c) displacement power factor: 'present' scenario

(d) displacement power factor: 'near future' scenario

Figure 7.25: Comparison between aggregate active power demand and displacement power factors for 'present' and 'near future' scenarios.

Voltage profiles

The operation of the 33/11 kV OLTC transformer regulates the voltage at the secondary winding (i.e. Bus 2, Figure 7.24), in order to maintain the voltage of all LV customers within the prescribed limit of +10/-6% of the nominal voltage. The OLTC transformers will control voltage taking into account the expected voltage drop, ensuring that the voltage at the furthest away customer is still within the regulated limits. This assumes that the OLTC transformer will react every time the voltage of the last supplied LV customer is about to breach the constraints, and will remain in the set position as long as voltage is within the stipulated limits. In the future, smart metering of residential customers may allow DNOs to analyse real-time information on network voltages, which, if required, can be used to apply appropriate voltage control.

The changes in daily LV network voltage profiles are shown in Figure 7.26 for the first and last (Bus 30 and Bus 39, Figure 7.24) supplied LV customers, from which several observations can be made. Reducing the active power demand by DSM action in the 'present' scenario will actually increase the number of tap-change operations. There is very little effect of reconnection, as the voltage profile is generally within the limits without the need for OLTC action. However, reconnection of the DSM load in the night time hours (DSM 2), actually improves

the voltage profile, despite the increased load, as a result of the additional operations of the OLTC transformer.

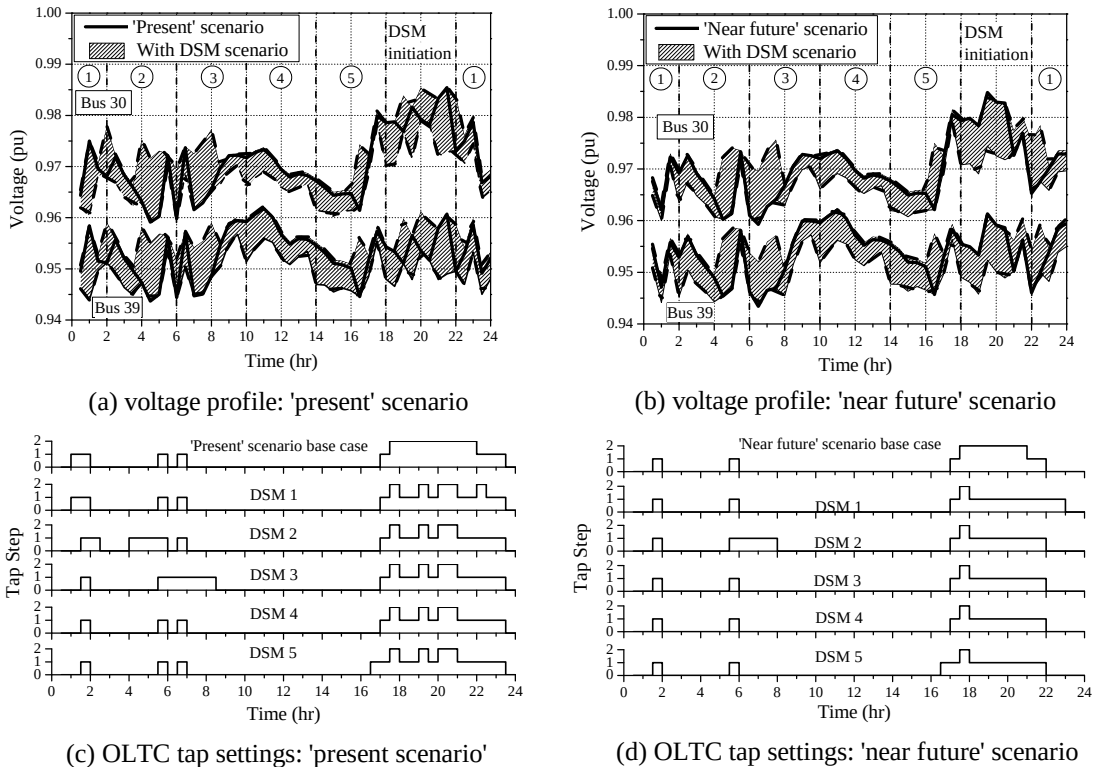

(a) voltage profile: 'present' scenario

(b) voltage profile: 'near future' scenario

(c) OLTC tap settings: 'present scenario'

(d) OLTC tap settings: 'near future' scenario

Figure 7.26: Comparison between LV voltage profiles for 'present' and 'near future' scenarios.

Overall, there are fewer OLTC operations for the 'near future' scenario, where the reduced active power demand during peak loading conditions, and local reactive power support, will result in the OLTC transformer performing less tap-changes. This trend is obviously highly dependent upon the configuration and exact loading conditions of the network. However, the results seem reasonable, as the substitution of GILs with CFLs will reduce both active and reactive power flows within the network, so a two-fold improvement in the voltage profile can be expected. This effect is displayed by the thick black plot in Figure 7.26, where it is shown that the voltage profile is higher during the evening periods for the 'near future' scenario.

Harmonic emissions

As shown in this thesis, the complex interactions between the network (i.e. source impedance) and loads will require detailed network and load models to accurately analyse the effect of changes in load structure on harmonics power flows. For the individual cases of power electronics and CFL loads, examples have shown that they will have a significant effect on the total THD of the connected load, as the resulting harmonic currents will interact with the system/source impedance, usually resulting in the distortion of the supply voltage waveform. This, in turn, will modify the harmonic emission of the load. Harmonic attenuation should also

be considered when analysing aggregate systems, as neglecting this may severely overestimate the harmonic propagation in the power system. This is illustrated in Figure 7.27, which displays the current THD as simulated for the last LV customer (Bus 39, Figure 7.24) with and without the proper representation of harmonic attenuation.

In Figure 7.27, the 'no attenuation' case corresponds to the results when the load model is supplied by a 'stiff grid' (exhibiting ideally sinusoidal voltage waveform). In this case, current THD values are much higher than when the model is adjusted to include harmonic attenuation (denoted as 'with attenuation'), resulting in distortion of the supply voltage waveform. These results confirm that harmonic emissions cannot be accurately assessed using fixed current harmonic sources and that harmonic power flow analysis should include the ability to correctly represent the interactions between supply system and load.

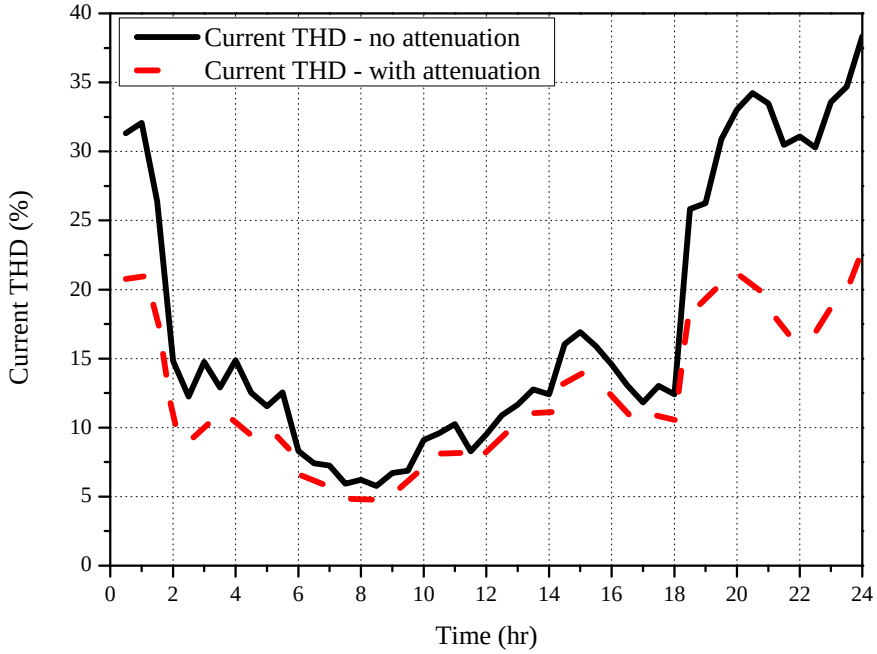

Figure 7.27: Comparison between daily variations in current THD values for 'present' scenario with and without the effect of harmonic attenuation.

The total harmonic emissions of the aggregate load is determined by the structure/mix of the individual loads and their interactions with each other and the network. Therefore, any DSM scheme which actively controls (i.e. changes) the load profile will alter the load mix and, therefore, the harmonic emissions. The results in Figure 7.28 give an illustration of how these results will change over the 24hr period and compare the simulated values at the LV aggregate feeder and the MV GSP.

For both scenarios, the highest levels of current and voltage THD occur during the evening, when the use of non-linear loads is at its highest. The replacement of GILs with CFLs in the 'near future' scenario results in a considerable increase in both current and voltage THD

values in the evening, as CFLs are a non-linear load with very high THD levels. The aggregate current THD levels will increase by around 5% but there is a significant peak in the voltage THD value, which increases from 2.1% to 4.1% at the LV level. Due to the cancellation with the other LV feeders within the 11 kV distribution network, the voltage THD at the GSP is still relatively low. The system transformers will also contribute to this phenomenon. The zero phase sequence harmonics which will flow through the neutral conductor, i.e. the triplen harmonics, will not transfer from the primary to the secondary of the delta-wye 11/0.4 kV transformer. However, they will circulate within the delta winding, which may result in increased heating in the transformer winding. The propagation of harmonics from LV (Bus 30, Figure 7.24) to MV (Bus 1, Figure 7.24) is shown in Figure 7.28 and 7.29. All voltage THD values are within the stipulated operating limits. The recommendations for voltage THD values are specified in guidelines in [189], in which the voltage THD levels are limited to 5% for V $\leq$ 1 kV, 4% for 6.6 kV $\leq$ V $\leq$ 20 kV and 3% for 22 kV $\leq$ V $\leq$ 400 kV.

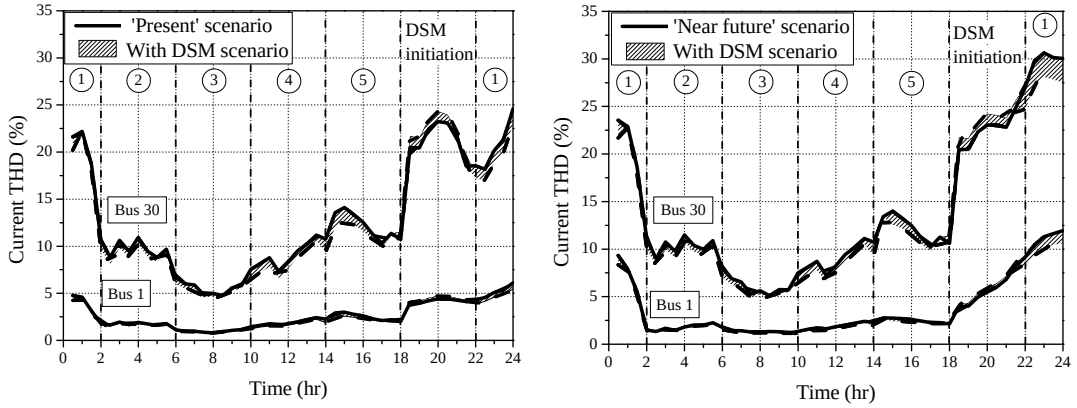

(a) 'present' scenario (b) 'near future' scenario

Figure 7.28: Comparison between current THD levels for 'present' and 'near future' scenarios.

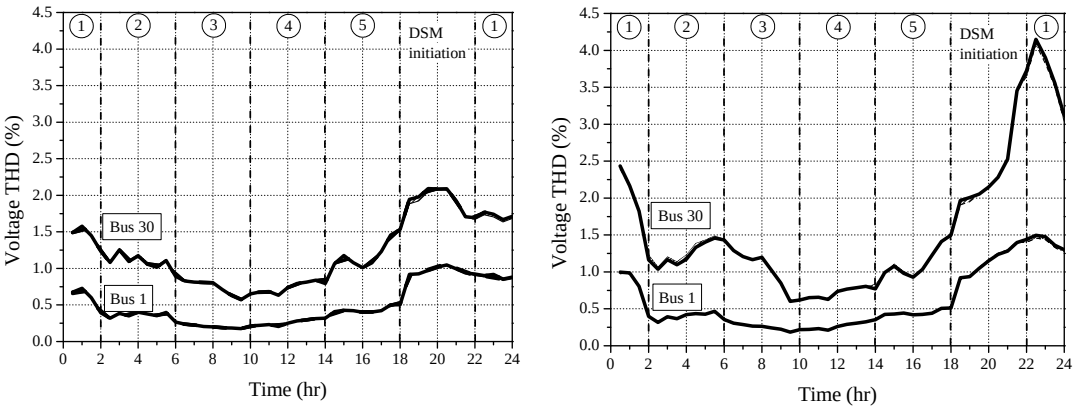

(a) 'present' scenario (b) 'near future' scenario

Figure 7.29: Comparison between voltage THD levels for 'present' and 'near future' scenarios.

As 'wet' load is modelled as drawing a continuous current waveform, consisting of resistive and reactive components, reconnecting the DSM block will act to reduce the aggregate current THD values. Conversely, removing this from the peak loading condition will increase the value of current THD. The results show that the influence of load changes will reduce towards the higher voltage levels, i.e. as the number of loads within the aggregate increases. The effect of the DSM action on the voltage THD levels is practically negligible. Again, this is a result of representation of a large number of LV networks in the distribution network model which will allow for harmonic cancellation and attenuation effects.

Discussion of results

Although the models developed in this research are able to provide information on the harmonic content of the aggregate load, the majority of results of the aggregation methodology have been presented using standard exponential and polynomial load model forms. The example in this section has served to illustrate how the developed load models can be used to allow for a more comprehensive analysis of network performance by including full representation of the harmonic emissions of non-linear loads. This was emphasised by the introduction of a 'near future' scenario, with increased contribution from CFL lighting loads, to show potential impacts of this LV network change on the performance of both the LV and MV networks.

It is difficult to accurately predict the effect of increased levels of non-linear loads within the LV network, as this will depend on many factors (including the strength of the system, the loading conditions and other changes in network operation). Therefore, it is hard to directly compare with results from similar studies, due to the difference in load composition and network characteristics. However, the studies show an expected increase in THD_V due to the increase in non-linear light sources [92], and increased use of non-linear loads generally [190]. A recent study in [93] suggests that the current THD levels in typical residential households will significantly increase with the replacement of GILs with CFLs. Although performed in laboratory conditions, with 'stiff grid' voltage waveform, it is possible to hypothesis that the interaction of this increased current THD with the supply system impedance will result in higher levels of voltage THD, as shown in this section.

In reality, the phase-out of GILs is likely to be protracted, and the use of halogen lamps will maintain a continuous current waveform within the lighting mix. For the possible time-scales involved, other changes in the load mix should also be considered. These may include the increasing proliferation of other non-linear loads, e.g. drive-controlled motors or EV battery chargers, as well as legislative changes, e.g. the reduction of the minimum rated power of devices required to meet harmonic limits from 75 W to 50 W (which is stated may be considered in [20]), or the large scale introduction of LV MG, which will all have an impact on this complex problem. These factors suggest that probabilistic modelling techniques should be employed to remove (or better represent) some of the uncertainties in the results. As shown in

previous chapters, the equivalent circuit models can be combined with Monte Carlo techniques to simulate large datasets for the non-linear loads within the system. Combining this with some variation in the contribution of specific loads to the aggregate demands, as shown in the sensitivity analysis of the commercial load sectors, will allow for a more comprehensive analysis of these system effects. It should be reiterated, this functionality is included within the presented load aggregation methodology and by the specific approaches taken in developing the load models of the individual load categories.

7.4.2 Case study: Optimal power flow

The need for DSM actions is, generally, a response to the need to maintain the energy balance within the power system. In the future, this may exploit improved ICT/power system infrastructures to provide (near) real time response to faults within a power system, in which a reduction of loads in certain locations may negate the need to disconnect an entire section of the network. This is expected to be more prevalent within the distribution system, as the growing penetration of distributed generation may necessitate more flexibility within the network in the future. The aggregate MV load models developed in this thesis can be applied to this area of research, in order to offer improved and more accurate representation of the aggregate LV loads. Initial results of a collaboration with [179] are included here to illustrate how the application of the presented load models may influence the outcome of the DSM analysis.

Problem formulation

During a fault caused network contingency/constraint, disconnecting a portion of the load will allow the system to operate safely until the fault is cleared. The characteristics of the fault, e.g. the location and severity, will determine the amount and location of load which must be disconnected, which are referred to as 'load adjustments' in this thesis, to maintain the system within its operational limits. This problem is addressed by an OPF formulation to minimise the amount of load adjustments which are required to bring the related network constraints under control. The OPF formulation is given in (7.6), with the network constraints defined by the set of rules in (7.7) - (7.10) overleaf.

$$minF\left(\Psi\right) = \sum_{i=1}^{N_{loads}} C_i MW_{0i}\left(1-\Psi_i\right) \tag{7.6}$$

where: Ψ_i is the load adjustment factor for the load connected at bus i, N_{loads} is the number of network load buses where DSM can be applied, C_i represents the cost of load adjustment at each bus and $MW_{0,i}$ is the initial active power of bus load i in MW.

The cost function C_i is set to an arbitrary value of '1' for the results presented in this section. However, it is perceived that this can be adjusted to provide a monetary value of DSM actions, allowing for cost-benefit analysis. A further discussion of this is presented in [179].

$$\Psi_{min,i} \leq \Psi_i \leq \Psi_{max,i} \tag{7.7}$$

$$MVA_i = \Psi_i \times MAV_0 \tag{7.8}$$

$$V_{min,j} \leq V_j \leq V_{max,j} \tag{7.9}$$

$$S_k \leq S_{max,k} \tag{7.10}$$

where: $\Psi_{min,i}$ and $\Psi_{max,i}$ are the minimum and maximum load adjustment factors for each load at bus i, MVA_0 and MVA_i are the initial and total load adjusted at load bus i, $V_{min,j}$ and $V_{max,j}$ are the minimum and maximum allowed voltages at each network bus j and S_k and S_{max} are the MVA power flow through network branch k and the maximum rating, respectively.

OPF implementation

This analysis is performed using a section of the Scottish Power distribution network, shown in Figure 7.30, with details taken from the Scottish Power Long Term Development Statement [191]. The time (i.e. hour of day) of peak demand during the maximum (i.e. day of the year) loading conditions are considered, as this represents the worst case fault condition. The network is populated with the MV aggregate load models developed in this thesis, with the equivalent impedance used to transform the LV models to the MV level (as described in Chapter 6). At each bus, the load sector mix (shown in Table 7.2) has been derived from measured data provided by the distribution network operator. Bus 1 supplies only commercial load sector, with a dedicated 33/6.6 kV supply transformer, while Bus 4 is 100% residential load. The other two buses are a mixture of residential, commercial and light industrial load sectors.

Table 7.2: Load sectors identified at the 11 kV nodes in the radial network.

Bus	Residential (%)	Commercial (%)	Industrial (%)	Peak demand (MW)
1	0	100	0	7.01
2	76	14	10	12.18
3	28	36	36	9.32
4	100	0	0	16.96

The light industrial load model from [62] is used to represent the industrial customers. This is justified by the fact that any larger industrial customers would be likely to have a dedicated power supply transformer. The composition of this load sector and the corresponding load models are shown in Table 7.3. As the OPF analysis is run in Siemens PSS®E software, only the polynomial/ZIP aggregate load model formulations could be implemented, and the industrial load model in Table 7.3 can be used directly in the aggregate load model development.

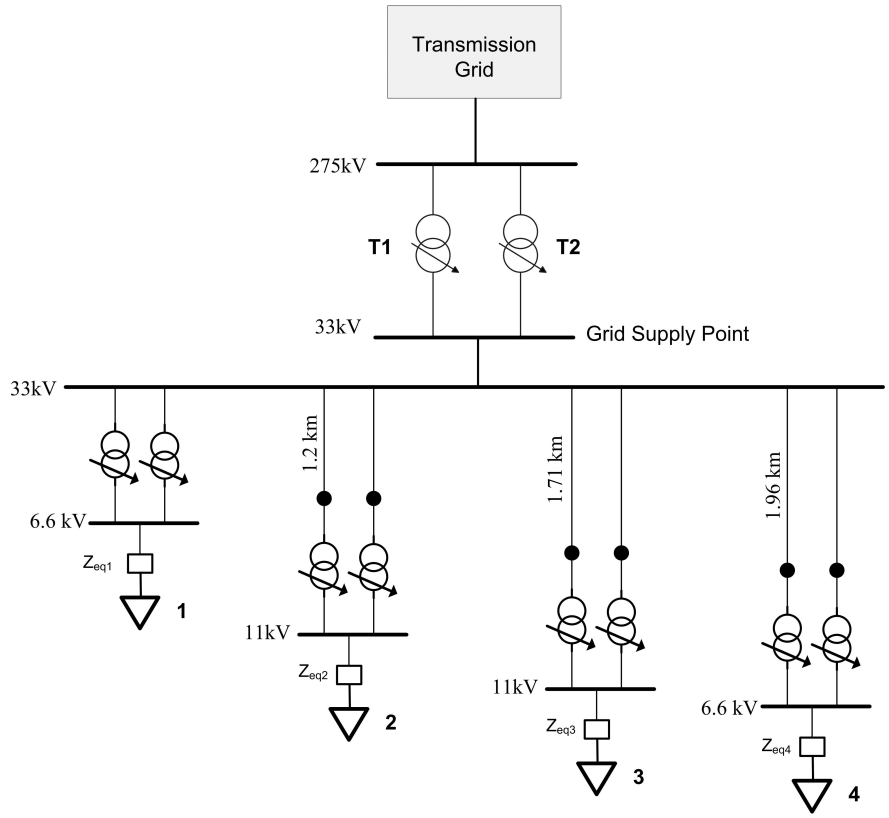

Figure 7.30: Scottish Power radial distribution network schematic [191].

Table 7.3: Composition of industrial load model [62].

Load	%	PF_1	Polynomial/ZIP model					
			Z_p	I_p	P_p	Z_q	I_q	P_q
Small motor	42.1	0.83	1.35	-0.98	0.63	2.31	-3.72	2.4
Large motor	9.3	0.835	0.46	0.73	-0.19	2.17	-3.03	1.87
GILs	8.7	1	1	0	0	-	-	-
HID	14.1	0.96	0.28	0.38	.34	2.52	-6.51	4.99
Electronics	25.8	1	0	0	1	-	-	-

Results

An upstream network contingency is simulated by faulting one of the 132/33 kV transformers. As each transformer is rated at around 70% of peak load, a fault in one transformer will result in an overload in the remaining transformer (during times of peak demand). Using the OPF formulation, the amount of load at Buses 1, 2, 3 and 4 required to clear the upstream contingency is calculated. As with the previous example, it is assumed that residential 'wet' load is available for DSM actions. The impact of removing all 'wet' load on the aggregate load model coefficients is displayed in Figure 7.31. It can be seen that there is only a small change in the electrical characteristics of the aggregate load (as represented by the exponential load

model coefficient values), due to the relatively low contribution of this load type to peak loading conditions. The values of active power coefficients will reduce as a consequence of the large contribution of resistive load (i.e. for water heating and clothes drying) being removed from the load mix. As the reactive power characteristics of all the motor loads within the residential aggregate are quite similar, removing the 'wet' load motors has an almost negligible effect on the steady-state reactive power characteristics.

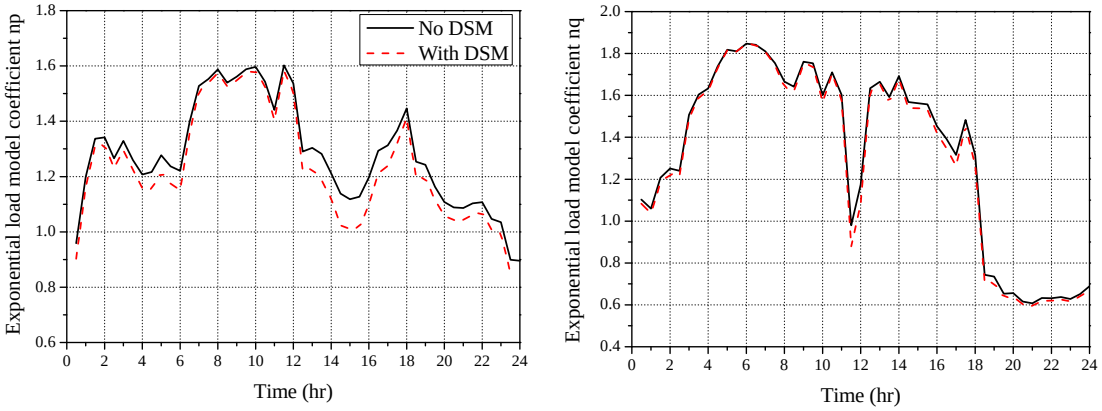

(a) active power (b) fundamental reactive power

Figure 7.31: Changes in the electrical characteristics of LV aggregate residential load due to disconnection of 'wet' load.

It can be seen that the optimal location for load reduction is at Bus 4, as this location requires the lowest value of load to be disconnected to alleviate the upstream fault. This can be attributed to increased system impedance between Bus 4 and the GSP. Therefore, reducing the load at Bus 4 will also have the greatest reduction in network losses, which also serves to unload the remaining distribution transformer. However, the main interest for this case study is the difference in the amount of load required to alleviate the network contingency between the different load models.

Table 7.4: Load sectors identified at the 11 kV nodes in the radial network.

Load adjustment (MW)				
Bus	Constant Power	Constant Current	Constant Impedance	Developed Model
1	-1.66	-1.68	-1.99	-1.67
2	-1.61	-1.64	-1.98	-1.64
3	-1.54	-1.57	-1.93	-1.59
4	-1.26	-1.35	-1.78	-1.41

The results indicate that modelling all bus demands as constant power loads will produce results which are overly optimistic. This can be explained by comparing theoretical cases of voltage dependent and voltage independent loads. If the load is voltage independent, the power demand is constant and equal to the rated/nominal power, regardless of the supply voltage. For the case

of voltage dependent load, the inherent voltage drop in the distribution system, will cause the power demand of the load to reduce from this rated/nominal value. As the OPF formulation is trying to find the amount of load which is required to alleviate the network contingency, this will iteratively remove load and recalculate the new loading conditions. As the load is removed, the voltage gradient in the system will improve, and the demand of the connected load will increase. Therefore, relatively speaking, more load has to be removed by the system operator when using voltage dependent load models. This effect is more pronounced for the constant impedance load model, as the demand varies to the square of the supply voltage magnitude.

At the maximum loading times, the active power characteristics of the residential load model will lie between constant current and constant impedance loads, which explains the obtained result. The difference between assuming constant power load is approximately 12%, while the difference with constant current load is around 4.5%. This is quite a substantial difference in the simulation results and highlights the value of increased levels of load modelling detail in the network analysis of DSM scenarios.

Discussion of results

Although brief, this analysis has considered the implication of incorporating the aggregate load models developed in this thesis in power system analysis. In this example, a difference of 4.5% and 12% was estimated between the developed models and the typical assumptions of constant power or constant current load models, respectively. In absolute values, this corresponds to approximately 60 kW or 150 kW, which is a considerable difference when compared to the typical residential load sector demand conditions. Assuming a peak demand of around 2 kW for maximum loading conditions, this equates to a difference of around 30 to 75 households. Accurately predicting these effects will, therefore, help to maintain service to the network while minimising the 'human cost', in terms of the number of affected or disconnected customers.

This analysis has considered only one characteristic loading condition, which, albeit the 'worst case' scenario, does not include wider system effects, such as locally connected generation, or the effect of load reconnection. Accordingly, the analysis should be extended to consider multiple periods of time to allow for the reconnection of the deferred load, and the resulting changes in system performance. As shown in the previous example, this can be easily included within the aggregation methodology provided in this thesis.

7.5 Conclusions

The purpose of this chapter was to demonstrate the flexibility of the developed load models and the aggregation methodology. Aggregate LV load models of the UK commercial load sector have been presented, based on a thorough review of commercial load use statistics. No existing models of the UK commercial load sector have been identified in the available literature, and the models produced in this thesis should go some way to filling this knowledge gap. However, as discussed in the analysis, there is expected to be variations in the electrical characteristics of different commercial load subsectors. It is likely that these variations will be relatively insignificant at the MV level and perhaps the generic commercial load sector model presented in this chapter can be applied, but more detailed models may be required to analyse specific areas of the lower voltage networks.

The development of commercial load sector models followed the same steps of the aggregation methodology as the residential load sector in the previous chapter. However, a further use of the aggregation methodology has been covered in this chapter by including the effects of LV MG within the aggregate load model. It was shown that the equivalent network impedance introduced in Chapter 6 can again be used to represent the combined electrical characteristics of LV load and MG at the MV level. This analysis also demonstrated that simply considering the LV MG as a negative load at the MV level will not accurately represent the overall electrical characteristics of the LV network with connected MG. Therefore, the interactions between load, generation and network should be considered when developing MV aggregate load models when MG is installed within the LV network.

The final section of this chapter has included some example results from network studies to illustrate how the developed load models can be used for a range of power system analysis. As emphasised throughout the thesis, flexibility in the load model aggregation methodology will allow for the representation of the load characteristics in a number of forms and maximise the use of the models. Although one of the most important features of the proposed aggregation methodology is in the ability to retain information on the harmonic emissions of the loads, by reproducing the instantaneous input current waveforms, the majority of discussions of the electrical characteristics of the developed aggregate models have used the exponential load model interpretation. In this chapter, the simulation of harmonics by the developed load models has been demonstrated in more detail. The final example from this chapter has emphasised the need for a more accurate load modelling process to accurately assess the implementation of DSM scenarios within the distribution network. It was shown that the aggregation methodology presented in this research can be used for this purpose, as it allows for the development of load models which are more representative of the downstream load than those modelled using typically applied load modelling assumptions.

Chapter 8

Conclusions and further work

This final chapter offers a review of the research presented in this thesis, and its contribution to the load modelling research area. The practical implications and limitations are also addressed. From these discussions, areas of further work and improvements to methodologies are identified.

8.1 Thesis summary

This thesis has presented a load modelling aggregation methodology which covers several levels of aggregation and voltage levels, starting with consideration of the individual devices and moving up to the medium-voltage (MV) level. This multi-scale approach includes improved representation of the electrical characteristics of the individual loads within the aggregate demand and allows for the development of load models in a number of widely used forms. The main contributions of this can be divided into two main areas: modelling of modern non-linear loads, which are covered in Chapters 3 - 5, and the development of the aggregation methodology, which is described in Chapters 6 and 7. General conclusions and discussions of the individual chapters are now presented.

Chapter 2 contained a concise overview of the load modelling research area and can standalone as an introduction to the power system load modelling research area. The results of a recent load modelling survey were used to introduce existing load modelling approaches, against which the work in this thesis should be evaluated.

The modelling of the **power electronics load category** was introduced in **Chapter 3**. This load category includes both the consumer electronics and information and communication technology (ICT) load types and, therefore, represents a significant portion of the total demand. The analysis of several measurements of the typical devices covered by this load category revealed differences between the electrical characteristics, which were grouped into three general subcategories. These variations are a result of the introduction of harmonic legislation in 2001 in the EU and has been shown to have a significant impact on the way these loads draw power from the electricity network. As the most important existing research of this load was performed prior to this date, this suggests that updated load models are required for this load category.

The load model development process began with the derivation of analytical expressions, which were based on the operation of the equivalent circuit model commonly used to model power electronics load. The analytical model was validated against measurements of actual devices and shown to accurately reproduce the considered electrical properties of the load. This tool can be implemented in a wider range of software than the equivalent circuit, which requires the use of electrical components, and offers reduced simulation times. This is an important feature for aggregate load model development as the simulation of a large number of devices is essential for providing confidence in the model.

The next stage in the model development process defined typical (or generic) values of each component within the equivalent circuit model, and identified expected tolerances for each. The influence of the individual components was scrutinised and led to the definition of operational boundaries, produced by finding the minimum and maximum value of each electrical characteristic from every combination of component values. The boundaries were compared against measured data for a number of devices and shown to incorporate the vast majority of measured values. This stage represents one of the main outcomes of this research, and the defined range of values can be applied to probabilistic modelling techniques to simulate a large number of individual devices, e.g. to characterise the harmonic emissions for use in harmonic power flows.

Such an approach was implemented in the next stage of the model development process, with a Monte Carlo routine applied to simulate a large number of individual devices to quantify the levels of harmonic cancellation present in the aggregate power electronics load mix. It has been shown that this effect will result in differences between the characteristics exhibited by the individual devices and the aggregate load, and should be acknowledged within the aggregate model development. Although it was not possible to validate the aggregate load model, the ability to represent the variations of the individual devices provides some level of confidence in the aggregate load model representation.

The final analysis performed in Chapter 3 was dedicated to comparing the electrical characteristics of the generic model, i.e. one equivalent circuit model configured with the generic value of each component, with the simulated aggregate results. It was shown that the effect of harmonic cancellation within each subcategory will manifest as an error in the total harmonic distortion (THD) of the current waveform, and the distortion and true power factor. This error is less than 10% across the entire voltage range for individual power electronics subcategories, and the error is subsequently reduced to less than 5% for current THD and less than 2% for all other electrical properties for a more representative aggregate load consisting of different subcategories. This is an important outcome of the research as it significantly reduces the computational intensity required in the development of larger aggregate loads, i.e. load sector model which were considered later in this thesis.

Chapter 3 introduced several important aspects of the modelling approach which are applied in the remainder of thesis. This is continued in **Chapter 4** which addressed the representation of the **energy efficient lighting load category** within the aggregate load modelling framework. This analysis primarily focussed on **compact fluorescent lamps** (CFLs) as they are expected to become the dominant lighting technology in the residential load sector in the near future. It was shown that the electrical characteristics of all measured CFLs of rated power less than or equal to 25 W were similar as a result of the introduction of the harmonic legislation. An equivalent circuit representation was presented by defining an equivalent dc link resistance, which was shown to retain the electrical behaviour of the measured CFLs.

The aggregate load model development followed the steps outlined in Chapter 3 and it was shown that there are relatively low levels of harmonic cancellation within the aggregate CFL load. These results were validated by measurement of different compositions of CFL load, which provides verification of the aggregate model development process. Improved matching with the measured data was achieved by modelling every individual CFL within the aggregate, although when representing the entire aggregate load by the generic CFL model, i.e. one equivalent circuit model configured with the generic values, the largest recorded error was 5%. This set of results clearly highlights the functionality of the multi-scale aggregation process applied in this research and the ability to develop models of different aggregate levels for use in power system analysis.

This detailed investigation into CFL loads was supplemented by initial results into the modelling of **light-emitting diode** (LED) **light sources** (LED LSs). The results indicate that there is still great variability in the electrical characteristics, i.e. in the electronic control circuits, of these loads, and the development of a generic model is not possible at this time. However, as LED LSs are likely to become prevalent in the residential load sector in the future, some simple load models, in standard exponential and polynomial/ZIP forms, are proposed for use in power system studies (which have not been identified during the literature review). More detailed modelling of these loads should be considered in future research.

Another important (expected) future load is the subject of analysis in **Chapter 5**, which assesses a range of measurements of **electric vehicle** (EV) **battery chargers**. Due to the commercial sensitivity of the measured data, there was limited access to the charging circuits and it was not possible to fully characterise the charging circuit using the approach refined in Chapters 3 and 4. However, it was shown that the equivalent circuit model is also able to reproduce the instantaneous input current waveforms of a number of EV battery chargers, proving its value as a flexible load modelling tool.

Several differences were observed between the measured data and the 'typical' EV battery charger characteristics presented in literature. Conclusions cannot be drawn on this limited dataset but it does indicate that there may be potential differences between the expected operation (i.e. ideal device connected to ideal supply conditions) and the actual operation (i.e. when

supplied from actual low-voltage (LV) networks). This may impact on the number of EV battery chargers which can be connected to LV networks without breaching network performance criteria and should be carefully considered within power system analysis.

Chapter 5 also included details on the representation of the EV battery, which will determine the power drawn from the supply network. Therefore, it is deserving of increased levels of modelling effort. It was shown that a simple equivalent battery resistance will allow for the development of an equivalent dc link resistance; while a more detailed electrochemical impedance spectroscopy (EIS) approach can be used to develop an electrical equivalent circuit model (EECM) which can analyse changes that may occur in the battery impedance due to use, i.e. wear and tear, and variations in ambient conditions. Time constraints and measurement availability limited the depth of analysis possible for this load, but the main modelling requirements have been addressed to support future research in this area.

For use in the power system analysis, the developed aggregate load models of the individual load categories (and subcategories) must be combined to represent typical customer groups. The **load modelling aggregation methodology** proposed for this purpose was described in **Chapter 6**. The UK **residential load sector** was taken as an example to illustrate the various stages of the process: starting from the conversion of the aggregate demand composition to load categories, to the construction of the LV aggregate load model and the transformation of this to the MV level for direct implementation in distribution network analysis. By using the generic aggregate load category models, the load sector aggregate model is constructed from the instantaneous input current waveforms of the individual load categories. Therefore, it contains more information than existing aggregate load sector models, which generally contain information of only the active and reactive power characteristics. An additional feature of the developed aggregate load models which was demonstrated in this chapter is the representation of the temporal changes in the electrical characteristics, which were shown to exhibit short (i.e. diurnal) and long (i.e. seasonal) variations as a result of changing load composition. By comparison, existing load models will typically present one set of load model parameters for each characteristic loading condition.

The transformation of the aggregate load model from LV to MV level was achieved by connecting the LV aggregate model to a generic LV network, and observing the changes at the MV aggregation point. As the majority of LV networks are complex electrical systems, with a large number of feeders and load points, it was proposed to simplify this stage through the use of network reduction techniques identified in literature, but which had not previously been applied to the load modelling research area. It was shown that this technique can be applied for load modelling purposes, thereby, significantly reducing the computational requirements without compromising the accuracy of the developed MV load model. This stage is important within the aggregation process as it was shown that the network can alter the electrical characteristics, as the point of aggregate representation moves from LV to MV.

The UK residential load models developed are another novel output of the research, as there is no comparable dataset for UK-based loads. However, as the output is obtained by the processing of publicly available statistics, this can be applied wherever similar datasets exist (some of which have been identified and can be found within the references of this thesis).

Further uses of the load modelling aggregation methodology were considered in **Chapter 7**. In this chapter, models for the UK **commercial load sector** were developed, highlighting the flexibility of the load model library. The load composition of the commercial load sector has several notable differences in comparison with the residential load sector, e.g. significantly higher contribution of lighting load, and the resulting differences in the electrical load model justify the effort in model development. Similar to the residential load sector models, the commercial load sector models have not been previously available for UK-based loads, so the combined set represents an entirely new dataset of UK-based load which can be applied for a more comprehensive network analysis.

As the ultimate aim of the aggregation methodology is to represent the load characteristics for use in distribution network analysis, it should include all LV network components. This was considered in Chapter 6, but the connection of **microgeneration** (MG) in future electricity networks must also be considered. Initial results suggest that, even with a modest 10% penetration, there may be substantial changes in the electrical characteristics, as represented at the MV level. Although the MG operation was assumed to be constant power output (for the available wind resources at the considered time), it was shown that assuming this without correct representation of the LV network will introduce an error in the load modelling process.

The final sections of Chapter 7 presented some initial results from ongoing research to illustrate the flexibility of the developed load models within a **demand-side management** (DSM) context. One case study demonstrated further details on the harmonic emissions which are produced by the aggregate load model. This brief analysis was included as the aggregate characteristics have mostly been represented by the exponential and polynomial/ZIP load models in the previous chapters of the thesis. The polynomial/ZIP interpretations were applied in the second case study within a framework to assess the optimal location, and required magnitude, of load deferral to help alleviate an upstream network contingency. The differences in results obtained using the models developed in this research and the standard load model types (i.e. constant power, constant current and constant impedance) suggest that a more accurate consideration of the supplied load can go some way to help minimise the 'human cost', i.e. the number of households, which may be required to participate in DSM actions.

8.2 Implications of the research

The ultimate goal of this thesis was to develop aggregate load models for use in power system analysis. This adopted a multi-scale approach, starting from the individual devices and aggregating to various levels, which can be considered a novel approach. Due to the level of detail and effort placed in the development process, the presented aggregate load models are able to provide increased levels of detail on the load characteristics than comparable aggregate load models identified in literature.

From a power systems simulation perspective, the implications of the aggregation methodology are contained within the flexibility of the approach, as it allows for the aggregate load characteristics to be presented in a number of load model forms. Therefore, models for different areas of power system analysis can be developed during one aggregation procedure. This functionality is suited to the analysis of modern power systems, as increasing levels of model detail are applied in the analysis.

As the thesis has focussed on the model development, the practical implications of the research are harder to define. However, the second case study in Chapter 7 clearly illustrates the added value of the extra information available in the developed load models, when compared with standard load modelling assumptions. More accurate representation of the load will help to improve the results of network analysis (and their implementation in actual power systems) but will also ensure that the impact on the power systems users is minimised. This information will be of most use to distribution network operators, as the aggregation process has focussed on load representation at the MV level. Furthermore, the ability to predict background harmonic levels will also provide value to power system planning decisions relating to harmonic filters, including connection of wind farms to the distribution network and building design for commercial properties with significant amount of non-linear loads.

8.3 Limitations of the research

Validation of load models

One of the most challenging aspects of this work is the validation of the developed aggregate load models. This would require a large number of measurements performed on a specific area of the power system where the network and load configurations are relatively well known. As these measurements are not currently available, this final level of validation was not possible within the time-frame of this research. However, it was possible to validate other stages of the process, which provides confidence in the final result. For the non-linear load categories modelled in this thesis, a large number of measurements was used to highlight the accuracy of the modelling approach. This is taken one step further for the CFL load, where the developed models were shown to be able to provide a good matching with the corresponding measured aggregate. The ability to reproduce the individual devices and the aggregate of these helps to remove some of the uncertainty in the overall aggregate load model.

Uncertainty modelling

The analysis presented in this thesis has attempted to group the entire residential and, to a lesser extent, commercial load sectors into five load categories. A thorough investigation of the electrical characteristics of modern loads, mostly through measurements and literature review, has been performed to provide subcategories to allow for the correct classification of these loads. This attempted to find the balance between functionality and ease of use.

Any attempts to classify the entire demand is bound to uncertainty. It is how this uncertainty is dealt with that defines how robust the approach is, which is demonstrated by the number of assumptions which must be made (and also in the judgements applied). In this thesis, access to measurements was used to remove as much of the uncertainty as possible. When this was not possible, a large number of data sources, ranging from technical literature to manufacturers' datasheets, were used to address knowledge gaps. When not even this level could be achieved, assumptions made were based on previous experience or rational logic.

However, the variability in demand is a major source of uncertainty itself, and probabilistic simulation techniques are normally applied at the LV level to remove as much of this uncertainty as possible. As the demand statistics used in this research are aggregate representations, some of this variability is removed, due to the larger sample size. Nevertheless, some sensitivity analysis should still be applied, as variations in the LV network will still exist (e.g. the aggregate demand measured at the MV level will exhibit slight day-to-day variations within the longer term seasonal swing). Some brief sensitivity analysis was performed to provide a basic insight into how the weighting of loads within the aggregate structure, i.e. the load composition, will influence the output of the aggregate load modelling efforts. More thorough analysis is suggested as an area of further work.

Integration of load models

The development of new modelling tools can only be considered successful if they are compatible with widely used softwares and the modelling approach presented in this thesis still has some work to do in overcoming these integration issues. However, the flexibility contained within the load modelling approach goes a long way to resolving these issues.

The proposal of the aggregation methodology began by considering the practical implementation of the aggregate load models. The use of the equivalent circuit model allows for more information of the aggregate load to be retained in the model development process, and can also be directly connected in some power system simulation softwares. However, this is not a widely recognised load model and the majority of results were represented by the exponential and polynomial/ZIP load models, which are still the most widely used load model forms. This was also the form which best served collaboration with colleagues in the Institute for Energy Systems.

As illustrated throughout the thesis, the models can also be integrated with harmonic power flow software. If required, the aggregation methodology can be extended to develop models in a specific form. However, as the results are already in the most commonly used forms, it is unlikely that this will be necessary (unless developing dynamic models, which are discussed in the following section).

8.4 Further work

8.4.1 Development of dynamic load models

As shown in literature, the equivalent circuit model is able to reproduce the inrush current conditions which may arise in modern power electronics loads due to sudden, i.e. step changes, in the supply voltage magnitude. One of the next logical steps in the load development process is to investigate whether any modifications in the analytical model are required to reproduce this, as a slightly more complex form may be required to represent the dc-dc electronic converters during these operating conditions. This should also include correct representation of the time-varying characteristics of the NTC thermistor, which will have a significant influence on the magnitude of current drawn from the network. As the configuration of CFLs (and also higher power LED LSs) is generally similar, these loads may also exhibit dynamic behaviour and a detailed study should be performed to quantify any potential impacts on the operation of the power system.

8.4.2 Development of LED LS load model

The analysis in Chapter 4 presented measurements which had been performed on currently available LED LSs. It was shown that this new lighting technology will present another non-linear load within the power system. However, the electrical characteristics of all measured LED LSs had noticeable differences and it was not possible to identify a typical, i.e. generic, set of values. A more thorough analysis of this technology should be performed to quantify the number of likely circuit topologies. Once these have been identified, load models should be developed. This should start from a detailed full circuit model, and then analyse the dc link voltage and current waveforms in order to define an equivalent resistance. As shown in Chapter 4, the modelling of the actual LEDs is relatively straightforward and the other component blocks within the drive circuit can perhaps be modified from existing full circuit models.

8.4.3 Development of LFL load model

Chapter 7 demonstrated that the electrical characteristics of the commercial load sector will be severely influenced by the use of LFLs. As this model is not currently included within the load library, this should be developed. This will allow for the development of more accurate commercial load sector models.

8.4.4 EV battery chargers

In the future, electric vehicle battery chargers are likely to become a more common load within the LV network. Due to the large rated power of these devices, even a modest penetration level will see them become a significant part of the aggregate demand. Therefore, accurate models of this load should be available for use in power system analysis. The work presented in this thesis has outlined several of the main steps which are required to develop the required models for both the EV battery and the EV battery charger. This analysis should be extended to identify and model a detailed full circuit model of the battery charger to verify the equivalent dc link resistance proposed in this research.

The simple analysis in this thesis has shown possible variations in the EV battery impedance, due to changes in the ambient temperature. It is also reported in literature that the impedance will change with age. The effect of this should be assessed by EIS, as the impedance of the battery will dictate the power demand of the EV battery charger, and may have an impact on network operation. The development of more detailed models,which can also include the effect of performance degradation on the EV battery (if the battery is represented by the EECM), will allow for more accurate studies of EV charging algorithms. However, this will require access to measurements of actual EV batteries and EV battery chargers.

8.4.5 Load aggregation

As this thesis is focussed on the development of aggregate load models for power system analysis, there are several possible areas to extend this work which may be generally defined as 'load aggregation'. It was proposed in Chapter 6, and, to a lesser extent, in Chapter 7, that there are possible subsectors within each major load sector, i.e. highly-urban, urban etc. The range of variations introduced by these different network configurations should be assessed to determine if this level of user division is necessary in the aggregate model development process. The initial sensitivity analysis performed on the commercial load sector load types should also be extended to include the possible variations within the load categories, and a similar analysis should be performed for the residential load sector. Furthermore, the developed residential load sector model contained a proportion of space and water heating which is representative of the overall UK residential load sector demand characteristics. As the use of these loads will not be present within every LV network, a residential load model should be developed with varying penetration levels of of space/water heating load. It can be hypothesised that the average value of the active power load model coefficient will reduce, making the actual demand in the LV network less sensitive to variations in the supply voltage magnitude.

Finally, the variation in load models for individual appliances (which are available using the defined range of parameter values) should be used in conjunction with model development procedures for individual households. Examples of this are available in [177] and will allow for the development of more detailed models for the analysis of LV networks.

8.4.6 Future load scenarios

The range of loads available within the developed load library can be used to analyse the impact of possible future load scenarios on the power system operation. Possible scenarios include: the proliferation of drive controlled motors within the residential load sector and the change of harmonic legislation from 75 to 50 W appliances. Further exploration of DSM scenarios should form a significant part of future load scenarios, and can be combined with other expected changes, such as coordinated charging of EVs and MG (discussed in the following section).

8.4.7 Combination with microgeneration

The results in Chapter 7 indicate that even small penetrations of MG can alter the electrical characteristics (as viewed from the MV supply point). More analysis is required in this area to fully consider all possible load/generation combinations, and also different MG technologies (e.g PV). As significant penetrations of MG are more likely in the near future, this analysis should incorporate any expected changes in load, e.g. the increased use of LED LSs, or network operation, e.g. DSM, which may exist. Furthermore, the approach applied to the development of MG models in [178] is comparable to the approach applied in this thesis, therefore, the MG models are also able to provide information on the harmonic current injections. The combination of the two sets of models will allow for a detailed power quality assessment of future networks.

8.4.8 Analytical LV/MV transformation

The equivalent network impedance has been shown to allow for the quick, but accurate, transformation of aggregate LV load characteristics to the MV level. However, this requires the representation of the equivalent network components, i.e. the equivalent feeder and secondary distribution transformer, in power system simulation software and must also include a voltage sweep to allow for fitting of the exponential or polynomial/ZIP load model coefficients. A mathematical derivation of the equivalent network impedance load flow will allow for the quick transformation of LV load model parameters to the MV, without the need for any software, or simulation of multiple voltage conditions. The value of this would be significantly increased if large penetrations of MG were present, as this method could be combined with probabilistic techniques which are typically used when simulating this particular scenario.

Bibliography

[1] P. Kundur, *Power system stability and control*, EPRI series, New York: McGraw-Hill, 1994.

[2] D. J. Hill, "Nonlinear dynamic load models with recovery for voltage stability studies," *IEEE Trans. Power Delivery*, vol. 8, no. 1, pp. 166-176, Feb. 1993.

[3] IEEE Task Force on Load Representation for Dynamic Performance, "Standard load models for power flow and dynamic performance simulation," *IEEE Trans. Power Delivery*, vol. 10, no. 3, pp. 1302-1313, Aug. 1995.

[4] IEEE Task Force on Load Representation for Dynamic Performance, "Load representation for dynamic performance analysis," *IEEE Trans. Power Delivery*, vol. 8, no. 2, pp. 472-482, May 1993.

[5] IEEE Task Force on Load Representation for Dynamic Performance, "Bibliography on load models for power flow and dynamic performance simulation," *IEEE Trans. Power Syst.*, vol. 10, no. 1, pp. 523-538, Feb. 1995.

[6] K. Yamashita, S. Martinaz Villanueva and J. V. Milanovic, "Initial results of international survey on industrial practice on power system load modelling conducted by CIGRE WG C4.605," presented at CIGRE Int. Symp., Bologna, Italy, Sept. 13-15, 2011.

[7] D. Singh, R. K. Misra and D. Singh, "Effect of load models in distributed generation planning," *IEEE Trans. Power Syst.*, vol. 22, no. 4, pp. 2204-2212, Nov. 2007.

[8] K. Qian, C. Zhou, M. Allan and Y. Yuan, "Load modelling in distributed generation planning," in *Proc. Int. Conf. Sustainable Power Generation and Supply*, Nanjing, China, Apr. 2009.

[9] D. Kirschen and G. Strbac, "Why investments do not prevent blackouts," *The Electricity J.*, vol. 17, no. 2, pp. 29-36, Mar. 2004.

[10] L. M. Hajagos and B. Danai, "Laboratory measurements and models of modern loads and their effect on voltage stability studies," *IEEE Trans. Power Syst.*, vol. 13, no. 2, pp. 584 - 592, May 1998.

[11] K.-W. Louie, "A new approach to compose load devices in electric power systems," *Int. J. of Applied Science and Engineering*, vol. 2, no.2, pp. 197 - 210, 2004.

[12] N. Lu, Y. Xie, Z. Huang, F. Puyleart, S. Yang, "Load component database of household appliances and small office equipment," in *Proc. IEEE PES General Meeting*, Pittsburgh, PA, Jul. 2008.

[13] I. Richardson, M. Thomson, D. Infield and C. Clifford, "Domestic electricity use: A high-resolution energy demand model," *Energy and Buildings*, vol. 42, no. 10, pp. 1878 - 1887, Oct. 2010.

[14] I. Richardson, M. Thomson and D. Infield, "A high-resolution domestic building occupancy model for energy demand simulations," *Energy and Buildings*, vol. 40, no. 8, pp. 1560-1566, 2008.

[15] I. Richardson, M. Thomson, D. Infield and A. Delahunty, "Domestic lighting: A high-resolution energy demand model," *Energy and Buildings*, vol. 41, no. 7, pp. 781-789, Jul. 2009.

[16] R. Yao and K. Steemers, "A method of formulating energy load profile for domestic buildings in the UK," *Energy and Buildings*, vol. 37, no. 6, pp. 663-671, Jun. 2005.

[17] Building Research Establishment, "The impact of changing energy use patterns in buildings on peak electricity demand in the UK," Tech, Rep. 243 752, Oct. 2008.

[18] C. E. Cresswell, "Steady-state load models for power system studies," Ph. D. thesis, Inst. For Energy Syst., Univ. Edinburgh, Edinburgh, UK, 2009.

[19] Design entry CIS. Cadence.

[20] *Electromagnetic compatibility (EMC), Part 3-2: Limits for Harmonic Current Emissions (Equipment Input Current Less Than or Equal to 16 A Per Phase)*, IEC 61000-3-2, 2006+A2:2009.

[21] *Electromagnetic compatibility (EMC), Part 3-12: Limits for Harmonic Currents Produced by Equipment Connected to Public Low-Voltage Systems With Input Current Greater Than 16 A and Less than 75 A per-phase*, IEC 61000-3-12, 2004.

[22] A. J. Collin and S. Z. Djokic, "Voltage disturbances and inrush current of dc power supplies," *Renewable Energy & Power Quality J.*, No. 8, April 2010, ISSN 2172-038X.

[23] A. J. Collin, C. E. Cresswell and S. Z. Djokic, "Harmonic cancellation of modern switch-mode power supply load," in *Proc. 14th IEEE Int. Conf. on Harmonics and Quality of Power*, Bergamo, Italy, Sept. 2010.

[24] S. Z. Djokic, A. J. Collin and C. E. Cresswell, "The future of residential lighting: Shift from incandescent to CFL to LED light sources," in *Proc. Illuminating Engineering Society of North America Annual Conf.*, Seattle ,WA, Nov. 2009.

[25] S. Z. Djokic, A. J. Collin and C. E. Cresswell, "Comparison of low-power and high-power CFL and LED light sources," in *Proc. Illuminating Engineering Society of North America Annual Conf.*, Seattle ,WA, Nov. 2009.

[26] A. J. Collin, S. Z. Djokic, H. F. Thomas and J. Meyer, "Modelling of electric vehicle chargers for power system analysis," in *Proc. IEEE Electrical Power Quality and Utilisation Conf.*, Lisbon, Portugal, Oct. 2011.

[27] A. J. Collin, J. L. Acosta, B. P. Hayes and S. Z. Djokic, "Component-based aggregate load models for combined power flow and harmonic analysis," in *Proc. 7th IET Mediterranean Conf. on Power Generation, Transmission Distribution and Energy Conversion*, Agia Napa, Cyprus, Nov. 2010.

[28] A. J. Collin, I. Hernando-Gil, J. L. Acosta and S. Z. Djokic, "An 11kV steady-state residential aggregate load model. Part 1: Aggregation methodology," in *Proc. IEEE PES PowerTech*, Trondheim, Norway, Jun. 2011.

[29] A. J. Collin, J. L. Acosta, I. Hernando-Gil and S. Z. Djokic, "An 11kV steady-state residential aggregate load model. Part 2: Microgeneration and demand-side management," in *Proc. IEEE PES PowerTech*, Trondheim, Norway, Jun. 2011.

[30] J. L . Acosta, A. J. Collin, B. P. Hayes and S. Z. Djokic, "Micro and small-scale wind generation in urban distribution networks," in *Proc. 7th IET Mediterranean Conf. on Power Generation, Transmission Distribution and Energy Conversion*, Agia Napa, Cyprus, Nov. 2010.

[31] A. J. Collin, I. Hernando-Gil, J. L. Acosta, I-S.Ille and S. Z. Djokic, "Realising the potential of smart grids in LV networks. Part 1: Demand-side management," in *Proc. IEEE PES Innovative Smart Grid Technologies Europe*, Manchester, UK, Dec. 2011.

[32] A. J. Collin, I. Hernando-Gil, J. L. Acosta, I-S.Ille and S. Z. Djokic, "Realising the potential of smart grids in LV networks. Part 2: Microgeneration," in *Proc. IEEE PES Innovative Smart Grid Technologies Europe*, Manchester, UK, Dec. 2011.

[33] B. P. Hayes, A. J. Collin, I. Hernando-Gil, J. L. Acosta, S. Hawkins, G. P. Harrison, and S. Z. Djokic, "All-scale modelling of wind generation and responsive demand in power system studies," in *Proc. IEEE PES General Meeting*, San Diego, CA, Jul. 2012.

[34] I-S.Ille, I. Hernando-Gil, A. J. Collin, J. L. Acosta, and S. Z. Djokic, "Reliability performance assessment in smart grids with demand-side management," in *Proc. IEEE PES Innovative Smart Grid Technologies Europe*, Manchester, UK, Dec. 2011.

[35] I. Hernando-Gil, I-S.Ille, A. J. Collin, J. L. Acosta, and S. Z. Djokic, "Impact of DG and energy storage on distribution network reliability: a comparative analysis," in *Proc. 2nd IEEE Energycon*, Florence, Italy, Sept. 2012.

[36] I. Hernando-Gil, I-S. Ilie, A. J. Collin, J. L. Acosta, B. P. Hayes and S. Z. Djokic, "Coordinated control of micro-generation and demand-side management in smart grids," in *IEEE PES MixGenera Conf.*, Madrid, Spain, Nov. 2011.

[37] B. P. Hayes, A. J. Collin, J. L. Acosta and S. Z. Djokic, "Assessment of the influence of distributed generation and demand side management on transmission system performance," in *Proc. 7th IET Mediterranean Conf. on Power Generation, Transmission Distribution and Energy Conversion*, Agia Napa, Cyprus, Nov. 2010.

[38] CIGRE WG C4.605, "Modelling and aggregation of loads in flexible power networks," in press, 2013.

[39] Electrical Power Research Institute (EPRI), "Advanced load modeling," Tech. Rep. 1007318, Sept. 2002.

[40] M. T. Au and J. V. Milanovic, "Development of stochastic aggregate harmonic load model based on field measurements," *IEEE Trans. Power Delivery*, vol. 22, no. 1, pp. 323-330, Jan. 2007.

[41] P.C. Krause, O. Wasynczuk and S. D. Sudhoff, *Analysis of electric machinery and drive systems*, 2nd ed. New York: McGraw-Hill, 2002.

[42] Electrical Power Research Institute (EPRI), "Measurement-based load modeling," Rep. 1014492, Sep. 2006.

[43] T. Y. J. Lem and R. T. H. Alden, "Comparison of experimental and aggregate induction motor responses," *IEEE Trans. Power Syst.*, vol. 9, no. 4, pp.189- 1900, Nov. 1994.

[44] T. Y. J. Lem abd R. T. H. Alden, "Comparison of experimental and aggregate induction motor responses," *IEEE Trans. Power Delivery*, vol. 9, no. 4, pp. 1895-1900, Nov. 1994.

[45] S. A. Y. Sabir and D. C. Lee, "Dynamic load models derived from date acquired during system transients," *IEEE Trans. Power Apparatus and Syst.*, vol. PAS-101, no. 9, pp. 3365-3372, Sept. 1982.

[46] H. Renmu, M. Jin and D. J. Hill, "Composite load modeling via measurement approach," *IEEE Trans. Power Syst.*, vol. 21, no. 2, pp. 663- 672, May 2006.

[47] M. T. Au and J. V. Milanovic, "Establishing harmonic distortion level of distribution network based on stochastic aggregate harmonic load models," *IEEE Trans. Power Delivery*, vol. 22, no. 2, pp. 1086-1092, Apr. 2007.

[48] A. Mansoor, W. Grady, A. Chowdhury and M. Samotyi, "An investigation of harmonics attenuation and diversity among distributed single-phase power electronic loads," *IEEE Trans. Power Delivery*, vol. 10, pp. 467-474, Jan. 1995.

[49] A. Bendre, D. Divan, W. Kranz and W. E. Brumsickle, "Are voltage sags destroying equipment?," *IEEE Industry Applications Magazine*, vol. 12, no. 4, pp. 12- 21, July-Aug. 2006.

[50] N. K. Medora, A. Kusko and M. Thompson, "Impact of line voltage sag on switch mode power supply operation," in *Proc. IEEE Conf. on Industrial Electronics and Applications*, Singapore, Jun. 2008.

[51] M. Rylander, W. M. Grady, A. Arapostathis, and E. J. Powers, "Power electronic transient load model for use in stability studies of electric power grids," *IEEE Trans. Power Systems*, vol. 25, no. 2, pp. 914 - 921, May 2010.

[52] A. Mansoor, W. M. Grady, R. S. Thallam, M. T. Doyle, S. D. Krein and M. J. Samotyj, "Effect of supply voltage harmonics on the input current of single-phase diode bridge rectifier loads," *IEEE Trans. Power Delivery*, vol. 10, no. 3, pp. 1416-1422, Jul. 1995.

[53] E.F. El-Saadany and M.M.A. Salama, "Reduction of the net harmonic current produced by single-phase non-linear loads due to attenuation and diversity effects," *Int. J. of Electrical Power & Energy Syst.*," vol. 20, no. 4, pp. 259-268, May 1998.

[54] N. Sayed, A. Stankovic and L. Nerone, "A new mathematical tool to meet IEC 61000-3-2," J. of Illuminating. Eng. Soc., vol. 33, pp. 67-74, 2004.

[55] L. Korunovic, D. Stojanovic and J. V. Milanovic, "Identification of static load characteristics based on measurements in medium-voltage distribution Network," *IET Generation, Transmission & Distribution*, vol. 2, no. 2, pp. 227-234, Mar. 2008.

[56] W. Xu, E. Vaahedi, Y. Mansour and J. Tamby, "Voltage stability load parameter determination from field tests on BC Hydro's system," *IEEE Trans. Power Syst.*, vol. 12, no. 3, pp. 1290-1297, Aug. 1997.

[57] D. Kosterev, A. Meklin, J. Undrill, B. Lesieutre, W. Price, D. Chassin, R. Bravo and S. Yang, "Load modeling in power system studies: WECC progress update," in *Proc. IEEE PES General Meeting*, Pittsbugh, PA. Jul. 2008.

[58] Dept. of Energy and Climate Change (DECC), "Energy consumption in the UK 2011," UK government, London, UK, Jul. 2012. [Online]. Available: https://www.gov.uk/government/publications/energy-consumption-in-the-uk

[59] C. Concordia and S. Ihara, "Load representation in power system stability studies," *IEEE Trans. Power Apparatus and Systems*, vol. PAS-101, no. 4, pp. 996 - 977, Apr. 1982.

[60] L. Hajagos and B. Danai, "Laboratory measurements and models of modern loads and their effect on voltage stability studies," *IEEE Trans. Power Delivery*, vol. 13, no. 2, pp. 584 - 592, May 1998.

[61] K. W. Louie, "A new approach to compose load devices in electric power systems," *Int. J. of Applied Science and Engineering*, vol. 2, no. 2, pp. 197 - 210, Jul. 2004.

[62] Electrical Power Research Institute (EPRI), "Advanced load modeling - Entergy pilot study," Tech. Rep. 1011391, Dec. 2004.

[63] N. Lu, Y. Xie, Z. Huang, F. Puyleart and S. Yang, "Load component database of household appliances and small office equipment," in *Proc. IEEE PES General Meeting*, Pittsburgh, PA, Jul. 2008.

[64] ON Semiconductor. [Online]. Available: http://www.onsemi.com/

[65] additional a-PFC circuit *IEEE Standard for Safety Levels with Respect to Human Exposure to Radio Frequency Electromagnetic Fields, 3 kHz to 300 GHz*, IEEE Std C95.1, 1999.

[66] *Electromagnetic compatibility (EMC): Requirements for Household Appliances, Electric Tools and Similar Apparatus*, BSI EN 55014-1:2006 +A2:2011.

[67] N. Mohan, T. M . Undeland and W. P. Robbins, *Power electronics: converters, applications and design*, 3rd ed. NewYork: Wiley, 2002.

[68] Ametherm, *Inrush current*, 2010. [Online]. Available: http://www.ametherm.com/inrush-current/surge-current-causes-and-prevention.html.

[69] A. Bennacer and A. Coltart, private communication, Dec. 2008.

[70] Power Factor Correction Handbook, 4th ed., ON Semiconductor, Phoenix, AZ, 2011. [Online]. Available: http://www.onsemi.com/pub_link/Collateral/HBD853-D.PDF

[71] XP Power, Power supply technical guide: Issue 2, 2007. [Online]. Available: http://www.xppower.com/pdfs/techguide.pdf

[72] Simulink 2009b. The MathWorks Inc.

[73] Pacific Power Source Inc. "AMX 360 linear AC power supply."

[74] *Voltage Characteristics of Electricity Supplied by Public Electricity Networks*, BS EN 50160, 2010.

[75] *Electromagnetic Compatibility (EMC): Testing and Measurement Techniques. Voltage Dips, Short Interruptions and Voltage Variations Immunity Tests*, IEC 61000-4-11, 2004.

[76] Rubycon, "Large can type aluminium electrolytic capacitors: USC series," 2010. [Online]. Available: http://www.rubycon.co.jp/en/catalog/e_pdfs/aluminum/e_usc.pdf

[77] A. Mansoor, W. Grady, P. Staats, R. Thallam, M. Doyle and M. Samotyj, "Predicting the net harmonic currents produced by large numbers of distributed single-phase computer loads," *IEEE Trans. Power Delivery*, vol. 10, no. 4, Oct. 1995.

[78] Coilcraft, "PFC Boost Inductor: document 737," 2009. [Online]. Available: http://www.coilcraft.com/pdf_viewer/showpdf.cfm?f=pdf_store:ja4224.pdf

[79] Coilcraft, "PFC Boost Inductor: document 607," 2009. [Online]. Available: http://www.coilcraft.com/pdf_viewer/showpdf.cfm?f=pdf_store:fa2890.pdf

[80] *Consideration of Reference Impedances and Public Supply of Network Impedance for Use in Determining Disturbance Characteristics of Electrical Equipment Having a Rated Current Less Than 75A Per Phase*, IEC 60725, 2005.

[81] W. M. Grady, A. Mansoor, E. F. Fuchs, P. Verde and M. Doyle, "Estimating the net harmonic currents produced by selected distributed single-phase loads: computers, televisions, and incandescent light dimmers," in *Proc. IEEE PES Winter Meeting*, New York, NY, Jan. 2002.

[82] MATLAB SimPowerSystem toolbox. The MathWorks Inc.

[83] MATLAB curve fitting toolbox, 2.1. The MathWorks Inc.

[84] P. Waide and S. Tanishima, "Light's labours lost: Policies for energy efficient lighting," Int. Energy Agency, Paris, France, 2006.

[85] EU Directive 2010/30/EU. Indication by labelling and standard produce information of the consumption of energy and other resources by energy-related products. [Online]. Available: http://eur-lex.europa.eu/LexUriServ/LexUriServ.do?uri=CELEX:32010L0030:EN:NOT

[86] EUROPA European Union, "Member states approve the phasing out of incandescent bulbs by 2012," IP/08/1909, 2009. [Online]. Available: http://europa.eu/rapid/press-release_IP-08-1909_en.htm

[87] Public Law 110-140 (2007, Dec. 19). H.R. 6 Energy independence and security act of 2007. [Online]. Available: http://www.gpo.gov/fdsys/pkg/PLAW-110publ140/pdf/PLAW-110publ140.pdf.

[88] *Light and Lighting - Lighting of Work Places, Part 1: Indoor Work Places*, BS EN 12464-1:2002.

[89] D. J. Pileggi, E. M. Gulachenski, C. E. Root, T. J. Gentile and A. E. Emanuel, "The effect of modern compact fluorescent lights on voltage distortion," *IEEE Trans. Power Delivery*, vol. 8, no. 3, pp.1451 - 1459, Jul. 1993.

[90] R. K. Rayudu, R. Rigo-Mariani and M. S. Witherden, "Effect of multiple compact fluorescent lamp usage on residential power quality," in *IEEE Int. Conf. Power System Technology*, Auckland, New Zealand, Oct. 2012.

[91] J. Meyer, P. Scegner and K. Heidenreich, "Harmonic summation effects of modern lamp technologies and small electronic household equipment," presented at CIRED, Frankfurt, Germany, Jun. 2011.

[92] A. M. Blanco and E. E. Parra, "Effects of high penetration of CFLs and LEDs on the distribution networks," in *Proc. 14th IEEE Int. Conf. on Harmonics and Quality of Power*, Bergamo, Italy, Sep. 2010.

[93] S. K. Ronnberg, M. H. J. Bollen and M. Wahlberg "Harmonic emission before and after changing to LED and CFL - Part I: Laboratory measurements for a domestic customer," in *Proc. 14th IEEE Int. Conf. on Harmonics and Quality of Power*, Bergamo, Italy, Sep. 2010.

[94] S. K. Ronnberg, M. Wahlberg and M. H. J. Bollen, "Harmonic emission before and after changing to LED and CFL - Part II: Field measurements for a hotel," in *Proc. 14th IEEE Int. Conf. on Harmonics and Quality of Power*, Bergamo, Italy, Sep. 2010.

[95] J. Yong, L. Chen, A. B. Nassif and W. Xu, "A frequency-domain harmonic model for compact fluorescent lamps," *IEEE Trans. Power Delivery*, vol. 25, no. 2, pp. 1182-1189, Apr. 2010.

[96] J. R. Ribeiro and F. J. Lange, "A new aggregation method for determining composite load characteristics," *IEEE Trans. Power Apparatus and Syst.*, vol. PAS-101, no.8, pp. 2869-2875, Aug. 1982.

[97] Dept. for Environment, Food and Rural Affairs (DEFRA), "BNDL01: Domestic lighting government standards evidence base 2009: Key inputs," UK Government, London, UK, Jun. 2010.

[98] Yong-Sik Youn, Gyun Chae and Gyu-Hyeong Cho, "A unity power factor electronic ballast for fluorescent lamp having improved valley fill and valley boost converter," in *28th Annual IEEE Power Electronics Specialists Conf.*, St Louis, MO, Jun. 1997.

[99] A. Campos, M. A. D. Costa, R. A. Pinto and R. N. Prado, "Fixed frequency self-oscillating electronic ballast to supply multiple lamps," in *35th Annual IEEE Power Electronics Specialists Conf.*, Aachen, Germany, Jun. 2004.

[100] M. A. Shafi and R. A. McMahon, "Influence of voltage and frequency dimming on power losses in HF electronic ballasts for compact fluorescent lamps," *IEEE Trans. Ind. Applications*, vol. 48, no. 2, pp. 839-845, Mar.-Apr. 2012.

[101] Philips Semiconductor, "Self oscillating circuit for CFL 10W and CFL 18W lamps," Tech. Rep. AN99065, Nov. 1999.

[102] M. Bairanzade, "Electronic lamp ballast design," ON Semiconductor, 2009. Tech. Rep. AN1543/D, 2009. [Online]. Available: http://www.onsemi.com/pub_link/Collateral/AN1543-D.pdf.

[103] U. Mader and P. Horn, "A dynamic model for the electrical characteristics of fluorescent lamps," in *Proc. IEEE Ind. App. Soc. Annu. Meeting*, Houston, TX, Oct. 1992.

[104] Y. Sun, "PSpice modeling of electronically ballasted compact fluorescent lamp systems," in *Proc. IEEE Ind. App. Soc. Annu. Meeting*, Toronto, Canada, Oct. 1993.

[105] T.-F. Wu, J.-C. Hung and T.-H. Yu, "A PSpice model for fluorescent lamps operated at high frequencies," in *Proc. 21st IEEE Int. Conf. Ind. Electron., Control and Instrumentation*, Orlando, FL, Nov. 1995.

[106] M. Sun and B. L. Hesterman, "PSpice high-frequency dynamic fluorescent lamp model," *IEEE. Trans. on Power Electron.*, vol. 13, no. 2, pp. 261-272, Mar. 1998.

[107] N. Omishi, T. Shiomi, A. Okude, and T.Yamauchi, "A fluorescent lamp model for high frequency wide range dimming electronic ballast simulation," in *Proc. 14th IEEE Annual Appl. Power Electronics Conf. and Expo.*, Dallas, TX, Mar. 1999.

[108] E. L. Corominas, J. M. Alonso, M. Rico-Secades, A. J. Calleja, J. Riba, and J. Cardesin, "Estimation of electrical characteristics of low power fluorescent lamps for optimized ballast design minimizing the number of lamp tests," in *Proc. IEEE Ind. App. Conf.*, Rome, Italy, Oct. 2000.

[109] M. Chen and Z. Qian, "A fluorescent lamp model based on its physical characteristics," in *Proc. 5th Int. Conf. Power Electron. and Drive Syst.*, Singapore, Nov. 2003.

[110] M. Perdigao and E. S. Saraiva, "Electronic ballast with wide dimming range: Matlab-simulink implementation of a double exponential fluorescent lamp model," presented at the 9th Spanish-Portuguese Conf. on Electrical Engineering, Marbella, Spain, Jun. - Jul. 2005.

[111] M. A. Shafi, R. A. McMahon, and S. Weier, "Investigation of losses in commercially available self-resonant ballasts for compact fluorescent lamps," in *Proc. IEEE Power Electron. Specialists Conf.*, Orlando, FL, Jun. 2007.

[112] J. Meyer, private communication, Mar. 2012.

[113] US Dept. Energy, Lighting Prize. [Online]. Available: http://www.lightingprize.org/

[114] US Dept. Energy, "Solid-state lighting research and development: Multi-year program plan," Apr. 2013. [Online]. Available: http://apps1.eere.energy.gov/buildings/publications/pdfs/ssl/ssl_mypp2013_web.pdf

[115] D. R. Nuttall, R. Shuttleworth, and G. Routledge, "Design of a LED street lighting system," in *Proc. 4th IET Conf. Power Electronics, Machines and Drives*, York, UK, Apr. 2008.

[116] L. Xingming and Z. Jing, "An intelligent driver for Light Emitting Diode Street Lighting," in *Proc. World Automation Congress*, Hawaii, HI, Sept. - Oct. 2008.

[117] B. Heffernan, L. Frater, and N. Watson, "LED replacement for fluorescent tube lighting," in *Proc. Australasian Universities Power Engineering Conf*, Perth, Australia, Dec. 2007.

[118] D. Ibrahim and M. Beasley, "The benefits of LED traffic lights in London and the pilot test sites," presented at 9th International Conf. on Road Transport Information and Control, 1998, Paper 454.

[119] UK Energy Research Centre, "Traffic signals," Quick hits, no. 3, Dec. 2006.

[120] Ray-Lee Lin, Yi-Chun Chang and Chia-Chun Lee, "Optimal design of LED array for single-loop CCM buck-boost LED driver," *IEEE Trans. Industry Applications*, vol. 49, no. 2, pp. 761-768, Mar.-Apr. 2013.

[121] Junming Zhang, Hulong Zeng and Ting Jiang, "A primary-side control scheme for high-power-factor LED driver with TRIAC dimming capability," *IEEE Trans. Power Electronics*, vol. 27, no. 11, pp. 4619-4629, Nov. 2012.

[122] Maxim Integrated, "Why drive white LEDs with constant current?," Application note 3256, 2004. [Online]. Available: http://www.maximintegrated.com/app-notes/index.mvp/id/3256

[123] P. Baureis, "Compact modeling of electrical, thermal and optical LED behavior," in *Proc. 25th Europena Solid-State Device Research Conf.*, Grenoble, France, Sep. 2005.

[124] G. Farkas, S. Haque, F. Wall, P. S. Martin, A. Poppe, Q. van Voorst Vader, and G. Bognar, "Electric and thermal transient effects in high power optical devices," in *Proc. 20th Annual IEEE Semiconductor Thermal Measurement and Management Symposium*, San Jose, CA, Mar. 2004.

[125] L. Marques, S. J. E. Mineiro, F. Antunes, and A. Perin, "Step down current controlled dc-dc converter to drive a high power LED matrix employed in an automotive headlight," presented at Brazilian Power Electronics Conference, 2005.

[126] M. Tyagi, *Introduction to semiconductor materials and devices*, 1st ed: John Wiley & Sons, 1991.

[127] Tech. Univ. Dresden, "Equipment harmonic database (PANDA)," 2013. [Online]. Available: http://www.panda.et.tu-dresden.de/cgi-bin/PANDA.cgi

[128] EEA, "Greenhouse gas emissions in Europe: A retrospective trend analysis for the period 1990-2008," report No. 6/2011, 2011. [Online]. Available: http://www.eea.europa.eu/publications/ghg-retrospective-trend-analysis-1990-2008

[129] International Energy Agency, "Technology roadmap for electric and plug-in hybrid electric vehicles," 2011. [Online]. Available: http://www.iea.org/publications/freepublications/publication/EV_PHEV_Roadmap.pdf

[130] UK Gov., "Plug-in Car Grant," 2010. [Online]. Available: https://www.gov.uk/government/publications/plug-in-car-grant

[131] P. T. Staats, W. M. Grady, A. Arapostathis and R. S. Thallam, "A statistical analysis of the effect of electric vehicle battery charging on distribution system harmonic voltages," *IEEE Trans. Power Delivery*, vol. 13, no. 2, pp. 640-646, Apr. 1998.

[132] J. C. Gomez and M. M. Morcos, "Impact of EV battery chargers on the power quality of distribution systems," *IEEE Trans. Power Delivery*, vol. 18, no. 3, pp. 975- 981, Jul. 2003.

[133] P. Richardson, D. Flynn and A. Keane, "Impact assessment of varying penetrations of electric vehicles on low voltage distribution systems," in *Proc. IEEE PES General Meeting*, Minneapolis, MN, Jul. 2010.

[134] S. Babaei, D. Steen, L. A. Tuan, O. Carlson and L. Bertling, "Effects of plug-in electric vehicles on distribution systems: A real case of Gothenburg," in *Proc. IEEE PES Innovative Smart Grid Technologies Europe*, Gothenburg, Sweden, Oct. 2010.

[135] K. Qian, C. Zhou, M. Allan and Y. Yuan, "Modeling of load demand due to EV battery charging in distribution systems," *IEEE Trans. Power Systems*, vol. 26, no. 2, pp. 802-810, May 2011.

[136] S. Acha, T. C. Green and N. Shah, "Optimal charging strategies of electric vehicles in the UK power market," in *Proc. IEEE PES Innovative Smart Grid Technologies*, Anaheim, CA, Jan. 2011.

[137] P. Richardson, D. Flynn and A. Keane, "Optimal charging of electric vehicles in low-voltage distribution systems," *IEEE Trans. Power Delivery*, vol. 27, no. 1, pp. 268-279, Feb. 2012.

[138] M. Yilmaz and P. T. Krein, "Review of battery charger topologies, charging power levels, and infrastructure for plug-in electric and hybrid Vehicles," *IEEE Trans. Power Elec.*, vol. 28, no. 5, pp. 2151-2169, May 2013.

[139] Electricycles. [Online]. Available: http://www.ecitywheels.com/electricycles/

[140] Verteci. [Online]. Available: http://www.verteci.com/

[141] J. Balcells and J. Garcia, "Impact of plug-in electric vehicles on the supply grid," in *Proc. IEEE Vehicle Power and Propulsion Conf.*, Lille, France, Sept. 2010.

[142] *Electric Vehicle Conductive Charging System - Part 21: Electric Vehicle Requirements for Conductive Connection to an A.C/D.C. Supply*, IEC 61851-21:2001.

[143] *Electric Vehicle Conductive Charging System - Part 22: AC Electric Vehicle Charging Station*, IEC 61851-22:2001.

[144] Axeon, "Our guide to batteries," [Online]. Available: http://www.axeon.com/Technology/Our-Guide-To-Batteries.aspx (subscription required).

[145] Gamry Inst., "Basics of electrochemical impedance spectroscopy", Application Note, Rev. 1.0, 2010. [Online]. Available: http://www.gamry.com/assets/Application-Notes/Basics-of-EIS.pdf

[146] R. Klein, N. A. Chaturvedi, J. Christensen, J. Ahmed, R. Findeisen, and A. Kojic, "Electrochemical model based observer design for a lithium-ion battery," *IEEE Trans. Control Syst. Technology*, vol. 21, no. 2, pp. 289-301, Mar. 2013.

[147] M. Charkhgard and M. Farrokhi, "State-of-charge estimation for lithium-ion batteries using neural networks and EKF," *IEEE Trans. Ind. Elect.*, vol. 57, no. 12, pp.4178-4187, Dec. 2010.

[148] I.-S. Kim, "Nonlinear state of charge estimator for hybrid electric vehicle battery," *IEEE Trans. Power Electronics*, vol. 23, no. 4, pp. 2027-2034, Jul. 2008.

[149] R. C. Kroeze and P. T. Krein, "Electrical battery model for use in dynamic electric vehicle simulations," in *Proc. IEEE Power Electronics Specialists Conf.*, Rhodes, Greece, Jun. 2008.

[150] M. Debert, G. Colin, M. Mensler, Y. Chamaillard and L. Guzzela, "Li-ion battery models for HEV simulator," Renault, Nov. 2008.

[151] B. Y. Liaw, G. Nagasubramanian, R. G. Jungst and D. H. Doughty, "Modeling of lithium ion cells: A simple equivalent-circuit model approach," in *Proc. 14th International Conf. on Solid State Ionics*, vol. 175, , pp. 835-839, Monterey, CA, Jun. 2003.

[152] J. -M. Lee, J. Lee, O. Nam, J. -H. Kim, B. H. Cho; H.-S. Yun, S.-S. Choi, K. Kim, J. H. Kim and S. Jun, "Modeling and real time estimation of lumped equivalent circuit model of a lithium ion battery," in *Proc. 12th International Power Electronics and Motion Control Conf.*, Portoroz, Slovenia, Aug. - Sept. 2006.

[153] S. Buller, M. Thele and R. W. A. A. De Doncker, "Impedance-based simulation models of supercapacitors and Li-ion batteries for power electronic applications," *IEEE Trans. Industrial Applications*, vol. 41, no. 3, pp. 742-747, May-Jun. 2005.

[154] Z. Zhang, "Charge/recharge efficiency and modelling of Li-ion batteries for electric vehicles," M.Sc dissertation, Inst. For Energy Syst., Univ. Edinburgh, Edinburgh, UK, 2010.

[155] ZSimpWin, EChem Software. [Online]. Availabe: http://www.echemsw.com/

[156] M. Kamachi, H. Miyamoto and Y. Sano, "Development of power management system for electric vehicle 'i-MiEV'," in *Proc. Int. Power Electronics Conf.,*, pp. 2949-2955, Sapporo, Japan, Jun. 2010.

[157] D. Huang and R. Billinton, "Effects of load sector demand side management applications in generating capacity adequacy assessment," *IEEE Trans. Power Syst.*, vol. 27, no. 1, pp. 335-343, Feb. 2012.

[158] G. J. Rogers, J. Di Manno R. T. H. Alden, "An aggregate induction motor model for industrial plants," *IEEE Trans. Power Apparatus and Syst.*, vol. PAS-103, no. 4, pp. 683-690, Apr. 1984.

[159] C. Noren and J. Pyrko, "Typical load shapes for Swedish schools and hotels," *Energy and Buildings*, vol. 28, no. 2, pp. 145-157, 1998.

[160] C. Noren, "Typical load shapes for six categories of Swedish commercial buildings," ISSN 0282-1990, 2007.

[161] J. P. Zimmermann, "End-use metering campaign in 400 households in Sweden: Assessment of the potential electricity savings," Enertech, Sept. 2009. [Online]. Available: http://www.enertech.fr/pdf/54/consommations%20usages%20electrodomestiques%20en%20Suede_2009.pdf

[162] H. Akbari, J. Eto, S. Konopacki, A. Afzal, K. Heinemeier, and L. Rainer, "Integrated estimation of commercial sector end-use load shapes and energy use intensifies in the PG&E Service Area," Energy and Environment Division, Univ. of California, Rep. LBL-34263, Dec. 1993. [Online]. Available: http://emp.lbl.gov/sites/all/files/lbnl-34263.pdf

[163] C. N. Jardine, "Synthesis of high resolution domestic electricity load profiles," presented at the First International Conference and Workshop on Micro-Cogeneration Technologies and Applications National Arts Centre, Ottawa, Ontario, 2008.

[164] UK Energy Research Centre (UKERC) Energy Data Centre. [Online]. Available: http://data.ukedc.rl.ac.uk/browse/edc/Electricity/LoadProfile/data

[165] Intertek, ”Household electricity survey: A study of domestic electrical product usage,” Tech. Rep. R66151, May. 2012.

[166] P. D. R. Stamminger, ”Synergy potential of smart appliances in smart domestic appliances in sustainable energy systems,” Smart-A, Oeko-Institut, Freiburg, Germany, Tech. Rep. D2.3, Nov. 2008.

[167] Commission for Energy Regulation, Smart Metering Project. [Online]. Available: http://www.ucd.ie/issda/data/commissionforenergyregulationcer/

[168] R. E. Brown and J. G. Koomey, ”Electricity use in California: Past trends and present usage patterns,” *Energy Policy*, vol. 31, no. 9, pp. 849-864, Jul. 2003.

[169] J. A. Fuentes, A. Gabaldon, A. Molina and E. Gomez, ”Development and assessment of a load decomposition method applied at the distribution level,” *IEE Proc. Generation, Transmission and Distribution*, vol. 150, no. 2, pp. 245-251, Mar. 2003.

[170] Schneider Electric, ”Adjustable Frequency Controllers”, Tech. Rep. SC100 R5-95. [Online]. Available: http://static.schneider-electric.us/docs/Motor%20Control/AC%20Drives/SC100.pdf

[171] R. Cao and E. R. Collins, ”The effects of load types on the behavior of AC motor drives during voltage sags,” in *Proc. 10th IEEE Int. Conf. on Harmonics and Quality of Power*, Rio de Janeiro, Brazil, Oct. 2002.

[172] Dept. for Environment, Food and Rural Affairs, ”BNDL01: Domestic lighting government standards evidence base 2009: Key inputs,” UK Government, London, UK, Jun. 2010

[173] M. Kay, Practical hydraulics, CRC Press, 1998.

[174] Department for Environment, Food and Rural Affairs (DEFRA), ”BNCE TV01: Televisions (TVs) government standards evidence base 2009: Key Inputs,” UK .Government, London, UK, Jun. 2010.

[175] I. Hernando-Gil, ”Integrated assessment of quality of supply in future electricity networks,” Internal Report, Inst. For Energy Syst., Univ. Edinburgh, Edinburgh, UK, 2011.

[176] P. Trichakis, P. C. Taylor, P. F. Lyons and R. Hair, ”Predicting the technical impacts of high levels of small-scale embedded generators on low-voltage networks,” *IET Renewable Power Generation*, vol. 2, no. 4, pp. 249 - 262, Dec. 2008.

[177] A. J. Collin, G. Tsagarakis, A. E. Kiprakis and S. McLaughlin, ”Multi-scale electrical load modelling for demand-side management,” in *Proc. IEEE PES Innovative Smart Grid Technologies Europe*, Berlin, Germany, Oct. 2012.

[178] J. L. Acosta, "Micro and small-scale generation in urban distribution networks," Ph. D. thesis, Inst. For Energy Syst., Univ. Edinburgh, Edinburgh, UK, 2012.

[179] B. P. Hayes, "Distributed generation and demand side management: Applications to transmission system operation," Ph. D. thesis, Inst. For Energy Syst., Univ. Edinburgh, Edinburgh, UK, 2013.

[180] Market Transformation Programme (MTP), "BNCL01: Commercial Lighting Government Standards Evidence Base 2009: Key Inputs", Jul. 2010.

[181] K. Tomiyama, J. P. Daniel and S. Ihara, "Modeling air conditioner load for power system studies," *IEEE. Trans. Power Syst.*, vol.13, no.2, pp.414-421, May 1998.

[182] Toshiba, "Spacel-uni: Toshiba machine-room-less elevators." [Online]. Available: http://www.toshiba-elevator.co.jp/elv/infoeng/products/pd03.jsp

[183] Loher, "Drive systems for lifts." [Online]. Available: http://www.swe.siemens.com/spain/web/es/industry/drive_tech/flender/Documents/Folleto%20para%20motores%20para%20ascensores%20Loher.pdf

[184] British Wind Energy Association, "Small wind systems," UK Market report, 2009.

[185] M. Thomson and D.G. Infield, "Impact of widespread photovoltaics generation on distribution systems," *IET Renewable Power Generation*, vol. 1, no. 1, pp. 33-40, Mar. 2007.

[186] P. Trichakis, P. C. Taylor, P. F. Lyons and R. Hair, "Predicting the technical impacts of high levels of small-scale embedded generators on low-voltage networks," *IET Renewable Power Generation*, vol. 2, no. 4, pp. 249 - 262, Dec. 2008.

[187] N. Stannard, "Generator for, and modelling of, small-scale wind turbines," Ph.D. thesis, School of Engineering, Durham Univ., Durham, UK, 2008.

[188] *Recommendations for the Connection of Small-scale Embedded Generators (Up to 16 A per Phase) in Parallel with Public Low-Voltage Distribution Networks*, Engineering Recommendation G83/1-1, 2003.

[189] *Planning Levels for Harmonic Voltage Distortion and the Connection of Non-linear Equipment to Transmission and Distribution Systems in the United Kingdom*, Engineering Recommendation G5/4-1, Feb. 2001.

[190] N. Browne, S. Perera and P. F. Ribeiro, "Harmonic levels and television events," in *IEEE PES General Meeting*, Tampa, FL. Jun. 2007.

[191] Scottish Power, "Long term development statement," [Online]. Available: http://www.sppowersystems.co.uk/LT_statements/default.asp?NavID=9

[192] *IEEE Standard Definitions for the Measurement of Electric Power Quantities Under Sinusoidal, Non-sinusoidal, Balanced, or Unbalanced Conditions*, IEEE Std 1459-2010.

[193] G. James, Modern engineering mathematics, 3rd edition, Prentice Hall, 2001.

[194] Mathematica. Wolfram Research.

Appendix A

Electrical definitions

Definitions of electrical power quantities are taken from IEEE Standard 1459 [192].

A.1 Active power

$$P = \frac{1}{kT}\int_{\tau}^{\tau+kT} pdt = P_1 + P_H$$

where: p is the instantaneous active power ($= iv$), τ and $\tau + kT$ define the measurement time interval, T is the cycle time and P_1 and P_H are the fundamental and harmonic components of the active power demand.

$$P_1 = \frac{1}{kT}\int_{\tau}^{\tau+kT} v_1 i_1 dt = V_1 I_1 cos\theta_1$$

where: v_1 and i_1 are fundamental frequency components of instantaneous voltage and current, V_1 and I_1 are the rms values of the fundamental frequency components of voltage and current and θ_1 is the phase angle between the fundamental components of the voltage and current phasors.

$$P_H = \sum_{h\neq 1} V_h I_h cos\theta_h = P - P_1$$

where: V_h and I_h are the rms values of the component of voltage and current at frequency hf_1 and θ_h is the phase angle between the components of the voltage and current phasors V_h and I_h.

A.2 Fundamental reactive power

$$Q_1 = \frac{\omega_1}{kT}\int_{\tau}^{\tau+kT} i_1 \left[\int v_1 dt\right] dt = V_1 I_1 sin\theta_1$$

where: v_1 and i_1 are fundamental frequency components of instantaneous voltage and current, V_1 and I_1 are the rms values of the fundamental frequency components of voltage and current and θ_1 is the phase angle between the fundamental components of the voltage and current phasors.

A.3 Displacement power factor

$$PF_1 = cos\theta_1 = \frac{P_1}{S_1}$$

and

$$S_1 = V_1 I_1$$

where: P_1 and S_1 are the fundamental components of the active and apparent power and θ_1 is the phase angle between the fundamental components of the voltage and current phasors.

A.4 True power factor

$$PF = \frac{P}{S}\frac{[1+(P_H/P_1)]PF_1}{\sqrt{1+THD_I^2+THD_V^2+(THD_I THD_V)^2}} \approx \frac{1}{\sqrt{1+THD_I^2}}PF_1 \approx PF_d PF_1$$

where:

$$PF_d = \frac{[1+(P_H/P_1)]}{\sqrt{1+THD_I^2+THD_V^2+(THD_I THD_V)^2}} \approx \frac{1}{\sqrt{1+THD_I^2}}$$

and

$$S = \sqrt{(VI)^2}$$

where: P and S are the total active and apparent power (including harmonic components), THD_I is the total harmonic distortion of the current, THD_V is the total harmonic distortion of the voltage, PF_1 is the displacement power factor and PF_d is termed the distortion power factor.

The approximation can only be used when $THD_v < 5\%$ and $THD_i > 40\%$.

A.5 Total harmonic distortion

$$THD_\% = \sqrt{\sum_{h\neq 1}\left(\frac{|I_h|}{|I_1|}\right)^2} \times 100$$

where: I_h is the rms value of current component at frequency hf_1 and I_1 is the rms value of fundamental component of the current. Note: equivalent expression exists for voltage.

A.6 Harmonic diversity factor

$$DF_h = \left|\frac{\sum_{n\neq 1} I_h^n}{\sum_n^N |I_h^n|}\right|$$

where: $I_h^n = |I_h^n| \angle\theta_h^n$ is the harmonic vector current of order h injected by the n^{th} load.

Appendix B

Analytical model derivation

The model derivation is based on theory presented in [67, 193]. The coding and simplification of the model is performed in [194]. The derivation begins from matrix form of the differential equations:

$$\begin{bmatrix} \frac{di_{in}}{dt} \\ \frac{dv_{dc}}{dt} \end{bmatrix} = \begin{bmatrix} \frac{R}{L} & \frac{1}{L} \\ \frac{1}{C_{dc}} & \frac{1}{C_{dc}r_{eq}} \end{bmatrix} \begin{bmatrix} i_{in} \\ v_{dc} \end{bmatrix} + \begin{bmatrix} \frac{1}{L} \\ 0 \end{bmatrix} v_{rect}$$

where: R is the total resistance value of resistance in the conduction path, L is the total value of inductance in the conduction path, C_{dc} is the value of dc link capacitor, v_{rect} is the rectified ac input voltage, i_{in} is the instantaneous input current, v_{dc} is the instantaneous value of dc link voltage and r_{eq} is the equivalent dc resistance

Let:

$$A = \begin{bmatrix} \frac{R}{L} & \frac{1}{L} \\ \frac{1}{C_{dc}} & \frac{1}{C_{dc}r_{eq}} \end{bmatrix} \quad B = \begin{bmatrix} \frac{1}{L} \\ 0 \end{bmatrix}$$

and:

$$v = |v_s| \quad x = \begin{bmatrix} i_{in} \\ v_{dc} \end{bmatrix}$$

Therefore:

$$\frac{d}{dt}[x] = Ax + Bv$$

This set of equations can be solved by applying trapezoidal integration:

$$x(t) = x(t-\Delta t) + \int_{t-\Delta t}^{t} [A(t)\,x(t) + B(t)\,g(t)]\,dt$$

Which returns:

$$x(t) = x(t-\Delta t) + \int_{t-\Delta t}^{t} [A(t)\,x(t)]\,dt + \int_{t-\Delta t}^{t} [B(t)\,V(t)]\,dt$$

For small simulation time steps, it can be assumed that A and B are constant, i.e.

$$A(t-\Delta t) = A(t)$$
$$B(t-\Delta t) = B(t)$$

Therefore:

$$x(t) = x(t-\Delta t) + A\int_{t-\Delta t}^{t} x(t)\,dt + B\int_{t-\Delta t}^{t} V(t)\,dt$$

This is solved by trapezium rule:

$$T(h) = h\left(\frac{1}{2}f_0 + f_1 + \ldots + f_{n-1} + \frac{1}{2}f_n\right)$$

where:

$$h = \left(\frac{b-a}{n}\right)$$

and a and b are lower and upper limit of integration, i.e. t and Δt.

This implies that:

$$h = \frac{t-(t-\Delta t)}{1} = \Delta t$$

Which can be applied to simply the solution:

$$A\int_{t-\Delta t}^{t} x(t)\,dt = A\Delta t\left[\frac{1}{2}x(t-\Delta t) + \frac{1}{2}x(t)\right] = A\frac{\Delta t}{2}\left[x(t-\Delta t) + x(t)\right]$$
$$B\int_{t-\Delta t}^{t} V(t)\,dt = B\Delta t\left[\frac{1}{2}V(t-\Delta t) + \frac{1}{2}V(t)\right] = B\frac{\Delta t}{2}\left[V(t-\Delta t) + V(t)\right]$$

Substituting back into original equation for x,

$$x(t) = x(t-\Delta t) + A\frac{\Delta t}{2}\left[x(t-\Delta t) + x(t)\right] + B\frac{\Delta t}{2}\left[V(t-\Delta t) + V(t)\right]$$

Expanding terms:

$$x(t) = x(t-\Delta t) + A\frac{\Delta t}{2}x(t-\Delta t) + A\frac{\Delta t}{2}x(t) + \frac{\Delta t}{2}B\left[V(t-\Delta t) + V(t)\right]$$

Begin the simplication process by grouping similar terms:

$$x(t)\left[I - A\frac{\Delta t}{2}\right] = x(t-\Delta t)\left[I + A\frac{\Delta t}{2}\right] + \frac{\Delta t}{2}B\left[V(t-\Delta t) + V(t)\right]$$

where: Identity matrix $I = \begin{bmatrix} 1 & 0 \\ 0 & 1 \end{bmatrix}$

Rearranging:

$$x(t) = x(t-\Delta t)\left[I + A\frac{\Delta t}{2}\right]\left[I - A\frac{\Delta t}{2}\right]^{-1} + \frac{\Delta t}{2}B\left[V(t-\Delta t) + V(t)\right]\left[I - \frac{\Delta t}{2}A\right]^{-1}$$

Inverse matrix:

$$\left[I - A\frac{\Delta t}{2}\right]^{-1} = \begin{bmatrix} 1+\frac{\Delta t R}{2L} & \frac{\Delta t}{2L} \\ -\frac{\Delta t}{2C} & 1+\frac{\Delta t}{2CR_L} \end{bmatrix}^{-1} = \begin{bmatrix} \frac{2L(\Delta t+2CR_L)}{\alpha} & \frac{2C\Delta t R_L}{\alpha} \\ \frac{2\Delta t L R_L}{\alpha} & \frac{2CR_L(2L+\Delta t R)}{\alpha} \end{bmatrix}$$

where: common factor $\alpha = 4CLR_L + \Delta t^2(R+R_L) + 2\Delta t(L+CRR_L)$

Split x into two parts to simplify. Part one:

$$\left[I + A\frac{\Delta t}{2}\right]\left[I - A\frac{\Delta t}{2}\right]^{-1} = \begin{bmatrix} \frac{4CLR_L - \Delta t^2(R+R_L) + 2\Delta t(L+CRR_L)}{\alpha} & \frac{4C\Delta t R_L}{\alpha} \\ \frac{4\Delta t L R_L}{\alpha} & \frac{4CLR_L - \Delta t^2(R+R_L) - 2\Delta t(L+CRR_L)}{\alpha} \end{bmatrix}$$

where: α is as previously defined.

Part two:

$$\frac{\Delta t}{2}B\left[I - A\frac{\Delta t}{2}\right]^{-1} = \frac{\Delta t}{2}\begin{bmatrix} \frac{1}{L} \\ 0 \end{bmatrix}\begin{bmatrix} \frac{2L(\Delta t+2CR_L)}{\alpha} & \frac{2C\Delta t R_L}{\alpha} \\ \frac{2\Delta t L R_L}{\alpha} & \frac{2CR_L(2L+\Delta t R)}{\alpha} \end{bmatrix} = \begin{bmatrix} \frac{\Delta t(\Delta t+2CR_L)}{\alpha} & \frac{\Delta t^2 R_L}{\alpha} \end{bmatrix}$$

Therefore:

$$\begin{bmatrix} i_{in}(t) \\ v_{dc}(t) \end{bmatrix} = Mx(t-\Delta t) + N\left(v_s(t-\Delta t) + v(t)\right)$$

where: M and N are previously solved Part one and Part two.

Further simplification in Mathematica software yields the final set of recurrence relations.

Input current:

$$\begin{aligned} i_{in}(n+1) = \frac{1}{\alpha}\big(&4C_{dc}i_{in}(n)LR_{eq} + \Delta t^2\left(-i_{in}(n)(R+R_{eq}) + v_s(n)\right) + \ldots \\ &2\Delta\left(i_{in}(n)(L - C_{dc}RR_{eq}) + C_{dc}R_{eq}\left(-2v_{dc}(n) + v_s(n+1) + v_s(n)\right)\right)\big) \end{aligned}$$

DC link voltage:

$$\begin{aligned} v_{dc}(n+1) = \frac{1}{\alpha}\big(&4C_{dc}LR_{eq}v_{dc}(n) + 2\Delta t\left(2i_{in}(n)LR_{eq} - Lv_{dc}(n) + C_{dc}RR_{eq}v_{dc}(n)\right)\ldots \\ &+\Delta t^2\left(-Rv_{dc}(n) + R_{eq}\left(-v_{dc}(n) + v_s(n+1) + v_s(n)\right)\right)\big) \end{aligned}$$

where:

$$\alpha = 4C_{dc}LR_{eq} + \Delta t^2(R+R_{eq}) + 2\Delta t(L + C_{dc}RR_{eq})$$

Appendix C

MATLAB load models

Example MATLAB code is included for the:

- Single-phase equivalent circuit model
- Three-phase equivalent circuit model

Both equivalent circuit models are configured with constant power dc characteristics. To model CFL and EV battery charger loads, the expression of *RLOAD* (which represents the equivalent resistance r_{eq}) should be replaced with the appropriate expression from the main body text.

C.1 Single-phase equivalent circuit model

```
function [i] = SinglePhaseEquivalentCircuitModel(C, L, R, Prated,E,f,w,deltat,runtime)
% initialise counters
n=1; a=1; N=runtime/deltat;
% initialise variables
time=zeros(1,N+1); RLOAD=zeros(N,1); Vdc=zeros(N,1); Vs=zeros(N,1); i=zeros(N,1);
% define inital conditions
i(1)=0; Vdc(1)=317; t=0;time(1)=1e-6; Vs(1)=0; Vwave(1)=0; RLOAD(1)=Vdc(1)/Prated;
while time(n) <= runtime
    while Vdc(n) >= abs(Vs(n,1))
        n=n+1;
        time(n)=time(n-1) + deltat;
        i1=0;
        if time(n) >= runtime
            break
        else
            Vdc1=Vdc(n-1);
            RLOAD(n,1)=(Vdc(n-1)^2)/Prated;
            Vdc(n,1)= Vdc1*exp(-deltat/(C*RLOAD(n,1)));
            Vs(n,1)=abs(E*sin((w*time(n))));
            i(n,1)=0;
        end
    end
    if time(n) >= runtime
        break
    else
        while i(n,1) >= 0
            if time(n) >= runtime
                break
            end
            RLOAD(n+1)=(Vdc(n-1)^2)/Prated;
            beta=(4*C*L*RLOAD(n)+deltat^2*(R+RLOAD(n))+2*deltat*(L+C*R*RLOAD(n)));
            time(n+1)=time(n)+deltat;
            Vs(n+1,1)=abs(E*sin((w*time(n+1))));
            i(n+1,1)=(4*C*i(n)*L*RLOAD(n,1)+deltat^2*(-i(n)*(R+RLOAD(n,1))+Vs(n+1)...
            +Vs(n))+2*deltat*(i(n)*(L-C*R*RLOAD(n,1))+C*RLOAD(n,1)*(-2*Vdc(n)...
            +Vs(n+1)+Vs(n))))/beta;
            Vdc(n+1,1)=(4*C*L*RLOAD(n,1)*Vdc(n)+2*deltat*(2*i(n)*L*RLOAD(n,1)...
            -L*Vdc(n)+C*R*RLOAD(n,1)*Vdc(n))+deltat^2*(-R*Vdc(n)+RLOAD(n,1)...
            *(-Vdc(n)+Vs(n+1)+Vs(n))))/beta;
            n=n+1;
        end
    end
    time1=time(n);
    if time(n) >= runtime
        break
    end
end
```

C.2 Three-phase equivalent circuit model

```
function [i] = ThreePhaseEquivalentCircuitModel(C, L, R, Prated,E,f,w,deltat,runtime)

% initialise counters
n=1;a=1;

% initialise variables
N = runtime/deltat; % number of simulation data points
RLOAD = zeros(N,1);
Vdc = zeros(N,1);
vrect = zeros(N,1);
i = zeros(N,3);
time = zeros(N,1);
Vmax = zeros(N,1);
Vmin = zeros(N,1);

% define inital conditions
i(1)=0;Vdc(1)=570;t=0;time(1)=1e-6;RLOAD(1)=Vdc(1)/Prated;

% define three phase suply
Vs(1,1)=E*sin(w*time(1)); % V phase a
Vs(1,2)=E*sin(w*time(1)+2.0944); % V phase b
Vs(1,3)=E*sin(w*time(1)-2.0944); % V phase c

% calculate phase voltages
Vab = Vs(:,1)-Vs(:,2); % Vab = Va - Vb
Vac = Vs(:,1)-Vs(:,3); % Vac = Va - Vc
Vbc = Vs(:,2)-Vs(:,3); % Vbc = Vb - Vc

% find initial condition of vrect
V_abs(1) = abs(Vab);
V_abs(2) = abs(Vac);
V_abs(3) = abs(Vbc);
vrect(1) = max(V_abs);

while time(n) <= runtime

    % Capacitor discharge stage
    while Vdc(n) >= (vrect(n,1));
        n=n+1;
        time(n)=time(n-1) + deltat;
        i1=0;
        if time(n) >= runtime
            break
        else
            % Update dc link voltage
            Vdc1=Vdc(n-1);
```

```
        RLOAD(n,1)=(Vdc(n-1)^2)/Prated;
        Vdc(n,1)= Vdc1*exp(-deltat/(C*RLOAD(n,1)));

        % Update supply voltage
        Vs(n,1)=E*sin((w*time(n)));
        Vs(n,2)=E*sin((w*time(n)+2.0944));
        Vs(n,3)=E*sin((w*time(n)-2.0944));

        Vab = Vs(n,1)-Vs(n,2);
        Vac = Vs(n,1)-Vs(n,3);
        Vbc = Vs(n,2)-Vs(n,3);
        V(1) = abs(Vab);
        V(2) = abs(Vac);
        V(3) = abs(Vbc);

        vrect(n,1) = max(V);

        i(n,1)=0; i(n,2)=0; i(n,3)=0; % Input current is zero

        Vmax(n,1) = max(Vs(n,:)')';
        Vmin(n,1) = min(Vs(n,:)')';
    end
end

if time(n) >= runtime
    break
else

    % capacitor charging stage
    % define diode pairs from max and min of supply voltage
    Vmax(n,1) = max(Vs(n,:)')';

    if Vs(n,1) >= Vmax(n) % Diode 1
        if Vs(n,2) <= Vmin(n) % Diode 1 and Diode 6

            while i(n,1) >= 0
                if time(n) >= runtime
                    break
                end
                RLOAD(n+1)=(Vdc(n-1)^2)/Prated;
                beta=(4*C*L*RLOAD(n)+deltat^2*(R+RLOAD(n))+...
                 2*deltat*(L+C*R*RLOAD(n)));
                time(n+1)=time(n)+deltat;
                Vs(n+1,1)=E*sin((w*time(n+1)));
                Vs(n+1,2)=E*sin((w*time(n+1)+2.0944));
                Vs(n+1,3)=E*sin((w*time(n+1)-2.0944));

                Vab = Vs(n+1,1)-Vs(n+1,2);
```

```
            Vac = Vs(n+1,1)-Vs(n+1,3);
            Vbc = Vs(n+1,2)-Vs(n+1,3);

            V(1) = abs(Vab);
            V(2) = abs(Vac);
            V(3) = abs(Vbc);

            vrect(n+1,1) = max(V);

            i(n+1,1)=(4*C*i(n)*L*RLOAD(n,1)+deltat^2*(-i(n)*...
                (R+RLOAD(n,1))+Vs(n+1)+Vs(n))+2*deltat*(i(n)*...
                (L-C*R*RLOAD(n,1))+C*RLOAD(n,1)*(-2*Vdc(n)+...
                vrect(n+1)+vrect(n))))/beta;
            i(n+1,2)=(4*C*i(n)*L*RLOAD(n,1)+deltat^2*(-i(n)*...
                (R+RLOAD(n,1))+Vs(n+1)+Vs(n))+2*deltat*(i(n)*...
                (L-C*R*RLOAD(n,1))+C*RLOAD(n,1)*(-2*Vdc(n)+...
                vrect(n+1)+vrect(n))))/beta;
            Vdc(n+1,1)=(4*C*L*RLOAD(n,1)*Vdc(n)+2*deltat*...
                (2*i(n)*L*RLOAD(n,1)-L*Vdc(n)+C*R*RLOAD(n,1)*Vdc(n))...
                +deltat^2*(-R*Vdc(n)+RLOAD(n,1)*(-Vdc(n)+vrect(n+1)...
                +vrect(n))))/beta;
            n=n+1;
        end
    else % Diode 1 and Diode 2
        while i(n,1) >= 0
            if time(n) >= runtime
                break
            end
            RLOAD(n+1)=(Vdc(n-1)^2)/Prated;
            beta=(4*C*L*RLOAD(n)+deltat^2*(R+RLOAD(n))...
             +2*deltat*(L+C*R*RLOAD(n)));
            time(n+1)=time(n)+deltat;
            Vs(n+1,1)=E*sin((w*time(n+1)));
            Vs(n+1,2)=E*sin((w*time(n+1)+2.0944));
            Vs(n+1,3)=E*sin((w*time(n+1)-2.0944));

            Vab = Vs(n+1,1)-Vs(n+1,2);
            Vac = Vs(n+1,1)-Vs(n+1,3);
            Vbc = Vs(n+1,2)-Vs(n+1,3);

            V(1) = abs(Vab);
            V(2) = abs(Vac);
            V(3) = abs(Vbc);

            vrect(n+1,1) = max(V);

            i(n+1,1)=(4*C*i(n)*L*RLOAD(n,1)+deltat^2*(-i(n)...
             *(R+RLOAD(n,1))+Vs(n+1)+Vs(n))+2*deltat*(i(n)*...
```

```
                (L-C*R*RLOAD(n,1))+C*RLOAD(n,1)*(-2*Vdc(n)+...
                vrect(n+1)+vrect(n))))/beta;
               i(n+1,3)=(4*C*i(n)*L*RLOAD(n,1)+deltat^2*(-i(n)...
                *(R+RLOAD(n,1))+Vs(n+1)+Vs(n))+2*deltat*(i(n)*...
                (L-C*R*RLOAD(n,1))+C*RLOAD(n,1)*(-2*Vdc(n)+vrect(n+1)...
                +vrect(n))))/beta;
               Vdc(n+1,1)=(4*C*L*RLOAD(n,1)*Vdc(n)+2*deltat*...
                (2*i(n)*L*RLOAD(n,1)-L*Vdc(n)+C*R*RLOAD(n,1)*Vdc(n))...
                +deltat^2*(-R*Vdc(n)+RLOAD(n,1)*(-Vdc(n)+vrect(n+1)+...
                vrect(n))))/beta;

               n=n+1;
           end
       end
   elseif Vs(n,2) >= Vmax(n) % Diode 3
       if Vs(n,1) <= Vmin(n) % Diode 3 and Diode 1
           while i(n,2) >= 0
               if time(n) >= runtime
                   break
               end
               RLOAD(n+1)=(Vdc(n-1)^2)/Prated;
               beta=(4*C*L*RLOAD(n)+deltat^2*(R+RLOAD(n))...
                +2*deltat*(L+C*R*RLOAD(n)));
               time(n+1)=time(n)+deltat;
               Vs(n+1,1)=E*sin((w*time(n+1)));
               Vs(n+1,2)=E*sin((w*time(n+1)+2.0944));
               Vs(n+1,3)=E*sin((w*time(n+1)-2.0944));

               Vab = Vs(n+1,1)-Vs(n+1,2);
               Vac = Vs(n+1,1)-Vs(n+1,3);
               Vbc = Vs(n+1,2)-Vs(n+1,3);

               V(1) = abs(Vab);
               V(2) = abs(Vac);
               V(3) = abs(Vbc);

               vrect(n+1,1) = max(V);

               i(n+1,2)=(4*C*i(n,2)*L*RLOAD(n,1)+deltat^2*(-i(n,2)...
                *(R+RLOAD(n,1))+Vs(n+1,2)+Vs(n,2))+2*deltat*(i(n,2)...
                *(L-C*R*RLOAD(n,1))+C*RLOAD(n,1)*(-2*Vdc(n)+...
                vrect(n+1)+vrect(n))))/beta;
               i(n+1,1)=(4*C*i(n,2)*L*RLOAD(n,1)+deltat^2*(-i(n,2)*...
                (R+RLOAD(n,1))+Vs(n+1,2)+Vs(n,2))+2*deltat*(i(n,2)*...
                (L-C*R*RLOAD(n,1))+C*RLOAD(n,1)*(-2*Vdc(n)+...
                vrect(n+1)+vrect(n))))/beta;

               Vdc(n+1,1)=(4*C*L*RLOAD(n,1)*Vdc(n)+2*deltat*...
```

```
                (2*i(n,2)*L*RLOAD(n,1)-L*Vdc(n)+C*R*RLOAD(n,1)*Vdc(n))...
                +deltat^2*(-R*Vdc(n)+RLOAD(n,1)*(-Vdc(n)+...
                vrect(n+1)+vrect(n))))/beta;
               n=n+1;
           end
       else % Diode 3 and Diode 2
           while i(n,2) >= 0
               if time(n) >= runtime
                   break
               end
               RLOAD(n+1)=(Vdc(n-1)^2)/Prated;
               beta=(4*C*L*RLOAD(n)+deltat^2*(R+RLOAD(n))...
                +2*deltat*(L+C*R*RLOAD(n)));
               time(n+1)=time(n)+deltat;
               Vs(n+1,1)=E*sin((w*time(n+1)));
               Vs(n+1,2)=E*sin((w*time(n+1)+2.0944));
               Vs(n+1,3)=E*sin((w*time(n+1)-2.0944));

               Vab = Vs(n+1,1)-Vs(n+1,2);
               Vac = Vs(n+1,1)-Vs(n+1,3);
               Vbc = Vs(n+1,2)-Vs(n+1,3);

               V(1) = abs(Vab);
               V(2) = abs(Vac);
               V(3) = abs(Vbc);

               vrect(n+1,1) = max(V);

               i(n+1,2)=(4*C*i(n,2)*L*RLOAD(n,1)+deltat^2*(-i(n,2)*...
                (R+RLOAD(n,1))+Vs(n+1,2)+Vs(n,2))+2*deltat*(i(n,2)...
                *(L-C*R*RLOAD(n,1))+C*RLOAD(n,1)*(-2*Vdc(n)+...
                vrect(n+1)+vrect(n))))/beta;
               i(n+1,3)=(4*C*i(n,2)*L*RLOAD(n,1)+deltat^2*(-i(n,2)*...
                (R+RLOAD(n,1))+Vs(n+1,2)+Vs(n,2))+2*deltat*(i(n,2)*...
                (L-C*R*RLOAD(n,1))+C*RLOAD(n,1)*(-2*Vdc(n)+...
                vrect(n+1)+vrect(n))))/beta;

               Vdc(n+1,1)=(4*C*L*RLOAD(n,1)*Vdc(n)+2*deltat*...
                (2*i(n,2)*L*RLOAD(n,1)-L*Vdc(n)+C*R*RLOAD(n,1)*Vdc(n))...
                +deltat^2*(-R*Vdc(n)+RLOAD(n,1)*(-Vdc(n)+...
                vrect(n+1)+vrect(n))))/beta;
               n=n+1;
           end
       end
   else % Diode 5
       if Vs(n,1) <= Vmin(n) % Diode 5 and Diode 1
           while i(n,3) >= 0
               if time(n) >= runtime
```

```
            break
        end
        RLOAD(n+1)=(Vdc(n-1)^2)/Prated;
        beta=(4*C*L*RLOAD(n)+deltat^2*(R+RLOAD(n))...
         +2*deltat*(L+C*R*RLOAD(n)));
        time(n+1)=time(n)+deltat;
        Vs(n+1,1)=E*sin((w*time(n+1)));
        Vs(n+1,2)=E*sin((w*time(n+1)+2.0944));
        Vs(n+1,3)=E*sin((w*time(n+1)-2.0944));

        Vab = Vs(n+1,1)-Vs(n+1,2);
        Vac = Vs(n+1,1)-Vs(n+1,3);
        Vbc = Vs(n+1,2)-Vs(n+1,3);

        V(1) = abs(Vab);
        V(2) = abs(Vac);
        V(3) = abs(Vbc);

        vrect(n+1,1) = max(V);

        i(n+1,3)=(4*C*i(n,3)*L*RLOAD(n,1)+deltat^2*(-i(n,3)*...
         (R+RLOAD(n,1))+Vs(n+1,3)+Vs(n,3))+2*deltat*(i(n,3)*...
         (L-C*R*RLOAD(n,1))+C*RLOAD(n,1)*(-2*Vdc(n)+...
         vrect(n+1)+vrect(n))))/beta;
        i(n+1,1)=(4*C*i(n,3)*L*RLOAD(n,1)+deltat^2*(-i(n,3)*...
         (R+RLOAD(n,1))+Vs(n+1,3)+Vs(n,3))+2*deltat*(i(n,3)*...
         (L-C*R*RLOAD(n,1))+C*RLOAD(n,1)*(-2*Vdc(n)+...
         vrect(n+1)+vrect(n))))/beta;

        Vdc(n+1,1)=(4*C*L*RLOAD(n,1)*Vdc(n)+2*deltat*...
         (2*i(n,3)*L*RLOAD(n,1)-L*Vdc(n)+C*R*RLOAD(n,1)*Vdc(n))...
         +deltat^2*(-R*Vdc(n)+RLOAD(n,1)*(-Vdc(n)...
         +vrect(n+1)+vrect(n))))/beta;
        n=n+1;
    end
else % Diode 5 and Diode 6
    while i(n,3) >= 0
        if time(n) >= runtime
            break
        end
        RLOAD(n+1)=(Vdc(n-1)^2)/Prated;
        beta=(4*C*L*RLOAD(n)+deltat^2*(R+RLOAD(n))+...
         2*deltat*(L+C*R*RLOAD(n)));
        time(n+1)=time(n)+deltat;
        Vs(n+1,1)=E*sin((w*time(n+1)));
        Vs(n+1,2)=E*sin((w*time(n+1)+2.0944));
        Vs(n+1,3)=E*sin((w*time(n+1)-2.0944));
```

```
                    Vab = Vs(n+1,1)-Vs(n+1,2);
                    Vac = Vs(n+1,1)-Vs(n+1,3);
                    Vbc = Vs(n+1,2)-Vs(n+1,3);

                    V(1) = abs(Vab);
                    V(2) = abs(Vac);
                    V(3) = abs(Vbc);

                    vrect(n+1,1) = max(V);

                    i(n+1,3)=(4*C*i(n,3)*L*RLOAD(n,1)+deltat^2*(-i(n,3)*...
                     (R+RLOAD(n,1))+Vs(n+1,3)+Vs(n,3))+2*deltat*(i(n,3)*...
                     (L-C*R*RLOAD(n,1))+C*RLOAD(n,1)*(-2*Vdc(n)+...
                     vrect(n+1)+vrect(n))))/beta;
                    i(n+1,2)=(4*C*i(n,3)*L*RLOAD(n,1)+deltat^2*(-i(n,3)*...
                     (R+RLOAD(n,1))+Vs(n+1,3)+Vs(n,3))+2*deltat*(i(n,3)*...
                     (L-C*R*RLOAD(n,1))+C*RLOAD(n,1)*(-2*Vdc(n)+...
                     vrect(n+1)+vrect(n))))/beta;

                    Vdc(n+1,1)=(4*C*L*RLOAD(n,1)*Vdc(n)+2*deltat*...
                     (2*i(n,3)*L*RLOAD(n,1)-L*Vdc(n)+C*R*RLOAD(n,1)*Vdc(n))...
                     +deltat^2*(-R*Vdc(n)+RLOAD(n,1)*(-Vdc(n)+...
                     vrect(n+1)+vrect(n))))/beta;
                    n=n+1;
                end
            end
        end
    end
    time1=time(n);
    if time(n) >= runtime
        break
    end
end
```

Appendix D

Power electronics load models

D.1 Diversity factors

Table D.1: Calculated diversity factor values of power electronics loads for all harmonic orders.

Harmonic Number (N)	Diversity factor DF_h		
	PE no-PFC	PE p-PFC	Mixed aggregate
3	0.99763	0.99727	0.45478
5	0.99342	0.98846	0.33403
7	0.98713	0.9264	0.05012
9	0.97877	0.78415	0.38396
11	0.96836	0.85021	0.4625
13	0.95594	0.65227	0.35789
15	0.94153	0.63835	0.31702
17	0.92521	0.59982	0.40269
19	0.90703	0.42033	0.39862
21	0.88712	0.47003	0.3308
23	0.86576	0.3273	0.33715
25	0.84355	0.30389	0.36797
27	0.82217	0.2732	0.33401
29	0.80684	0.17998	0.27793
31	0.81459	0.2022	0.27221
33	0.8591	0.12781	0.27269
35	0.89793	0.1323	0.25788
37	0.9061	0.10918	0.25572
39	0.87001	0.0882	0.26756

D.2 Harmonic injections

D.2.1 PE no-PFC subcategory

Table D.2: Calculated aggregate input current harmonics of PE no-PFC subcategory for different system impedance values.

Harmonic Number (N)	System impedance value							
	Stiff grid		Min		Nom		Max	
	Mag. ($\%_1$)	Phase ($^\circ$)	Mag. ($\%_1$)	Phase ($^\circ$)	Mag. ($\%_1$)	Phase ($^\circ$)	Mag. ($\%_1$)	Phase ($^\circ$)
1	100	6.86	100	0.00	100	2.64	100	4.83
3	97.99	-159.03	96.17	-179.37	94.63	173.57	92.64	62.85
5	94.11	35.11	88.88	1.41	84.62	-10.54	79.23	241.26
7	88.501	-130.68	78.79	-178.16	71.23	164.70	62.07	54.51
9	81.44	63.64	66.82	1.68	56.1	-21.17	43.9	-135.83
11	73.231	-101.89	53.96	-179.35	40.93	151.08	27.51	28.76
13	64.24	92.81	41.25	-1.76	27.31	-40.10	15.12	-177.12
15	54.84	-72.18	29.6	173.54	16.53	121.80	8.69	-43.49
17	45.41	123.30	19.81	-15.19	9.76	-90.15	7.59	85.50
19	36.31	-40.54	12.52	148.55	7.47	45.86	7.26	-129.21
21	27.87	156.71	8.3	-59.44	7.33	-168.56	5.97	21.15
23	20.39	-4.29	6.99	87.31	6.88	-12.55	4.36	165.87
25	14.17	-162.29	6.87	-117.61	5.73	145.43	3.37	-59.27
27	9.54	44.88	6.57	45.10	4.34	-61.09	3.13	76.58
29	6.92	-100.41	5.79	-149.76	3.36	83.97	2.94	-139.74
31	6.33	119.25	4.7	13.89	3.051	-133.39	2.51	5.58
33	6.72	-25.21	3.74	173.02	3.001	16.00	2.04	145.89
35	7.05	-177.33	3.081	-33.15	2.781	170.40	1.79	-77.85
37	6.95	25.09	2.82	119.66	2.361	-35.95	1.71	61.94
39	6.39	-135.64	2.75	-83.51	1.951	112.49	1.57	-154.54

Note: all phase angles have been normalised to $\angle V_1 = 0$

D.2.2 PE p-PFC subcategory

Table D.3: Calculated aggregate input current harmonics of PE p-PFC subcategory for different system impedance values.

Harmonic Number (N)	System impedance value							
	Stiff grid		Min		Nom		Max	
	Mag. ($\%_1$)	Angle ($^\circ$)	Mag. ($\%_1$)	Angle ($^\circ$)	Mag. ($\%_1$)	Angle ($^\circ$)	Mag. ($\%_1$)	Angle ($^\circ$)
1	100	-17.85	100	-17.86	100	-18.02	100	-18.42
3	76.84	125.87	75.86	127.00	74.75	126.33	72.54	124.63
5	43.15	-94.43	41.28	-92.72	39.21	-94.36	35.24	-98.54
7	15.59	29.13	14.06	27.82	12.44	21.54	9.9	4.96
9	6.9	97.41	7.08	91.88	7.09	82.12	7.24	65.12
11	6.01	-163.76	5.8	-164.14	5.33	-172.38	4.47	168.85
13	2.89	-65.10	2.73	-74.04	2.52	-92.47	2.52	-127.41
15	2.26	6.01	2.4	2.10	2.36	-11.17	2.2	-35.85
17	1.66	108.14	1.58	103.56	1.38	84.22	1.19	40.19
19	0.92	-173.12	1.04	174.25	1.08	152.07	1.14	117.22
21	0.87	-88.13	0.92	-91.41	0.84	-111.37	0.69	-156.91
23	0.51	7.41	0.54	-7.53	0.54	-39.32	0.61	-89.62
25	0.39	77.87	0.51	70.72	0.51	48.03	0.44	0.54
27	0.32	175.28	0.35	166.37	0.31	132.90	0.34	65.64
29	0.18	-106.03	0.27	-122.85	0.29	-151.91	0.29	154.84
31	0.18	-21.78	0.23	-27.12	0.21	-57.61	0.19	-135.89
33	0.11	73.86	0.15	52.52	0.16	12.16	0.19	-52.11
35	0.08	146.19	0.11	137.15	0.13	106.51	0.12	24.74
37	0.07	-114.02	0.09	-128.19	0.08	-178.89	0.11	99.89
39	0.04	-32.37	0.08	-56.24	0.07	-95.53	0.07	-175.92
Note: all phase angles have been normalised to $\angle V_1 = 0$								

D.2.3 Mixed aggregate

Table D.4: Calculated aggregate input current harmonics of a mixed power electronics aggregate load for different system impedance values.

Harmonic Number (N)	System impedance value							
	Stiff grid		Min		Nom		Max	
	Mag. ($\%_1$)	Phase ($^\circ$)	Mag. ($\%_1$)	Phase ($^\circ$)	Mag. ($\%_1$)	Phase ($^\circ$)	Mag. ($\%_1$)	Phase ($^\circ$)
1	100	-13.95	100	-14.60	100	-15.13	100	-15.77
3	70.83	138.36	73.86	138.10	74.49	136.34	74.39	134.09
5	28.74	-70.86	34.45	-67.84	35.57	-71.03	35.06	-75.64
7	5.9	-61.38	2.07	144.87	3.55	112.85	3.544	93.06
9	19.35	73.31	15.45	49.61	13.05	38.25	10.994	30.59
11	15.43	-120.19	15.43	-150.97	13.28	-167.86	10.54	176.27
13	8.57	84.67	8.32	22.24	6.77	-9.67	4.8	-44.79
15	10.16	-62.11	5.28	-124.50	2.44	-164.97	0.65	93.83
17	9.19	119.52	5.91	57.98	3.08	25.81	1.05	-2.86
19	5.59	-48.66	4.42	-141.95	2.79	166.37	1.75	111.97
21	4.59	163.19	2.16	23.79	1.83	-62.58	1.75	-125.94
23	3.99	-5.26	1.22	-140.12	0.91	80.32	1.17	3.31
25	2.19	-173.09	1.33	26.83	0.63	-83.82	0.48	159.80
27	1.52	48.40	1.28	167.48	1.02	84.73	0.48	10.60
29	1.369	-105.64	1.06	-45.54	1.09	-126.52	0.66	156.31
31	0.89	106.23	0.79	127.90	0.78	25.10	0.61	-76.53
33	1.18	-23.66	0.83	-45.15	0.44	-166.98	0.47	54.85
35	1.27	176.15	0.87	124.17	0.39	8.42	0.3	214.51
37	1.11	18.34	0.69	-73.68	0.46	159.17	0.29	38.67
39	1.10	-136.86	0.47	92.14	0.48	-53.55	0.32	-166.53
Note: all phase angles have been normalised to $\angle V_1 = 0$								

Appendix E

Additional lighting material

E.1 Electrical characteristics of valley fill CFLs

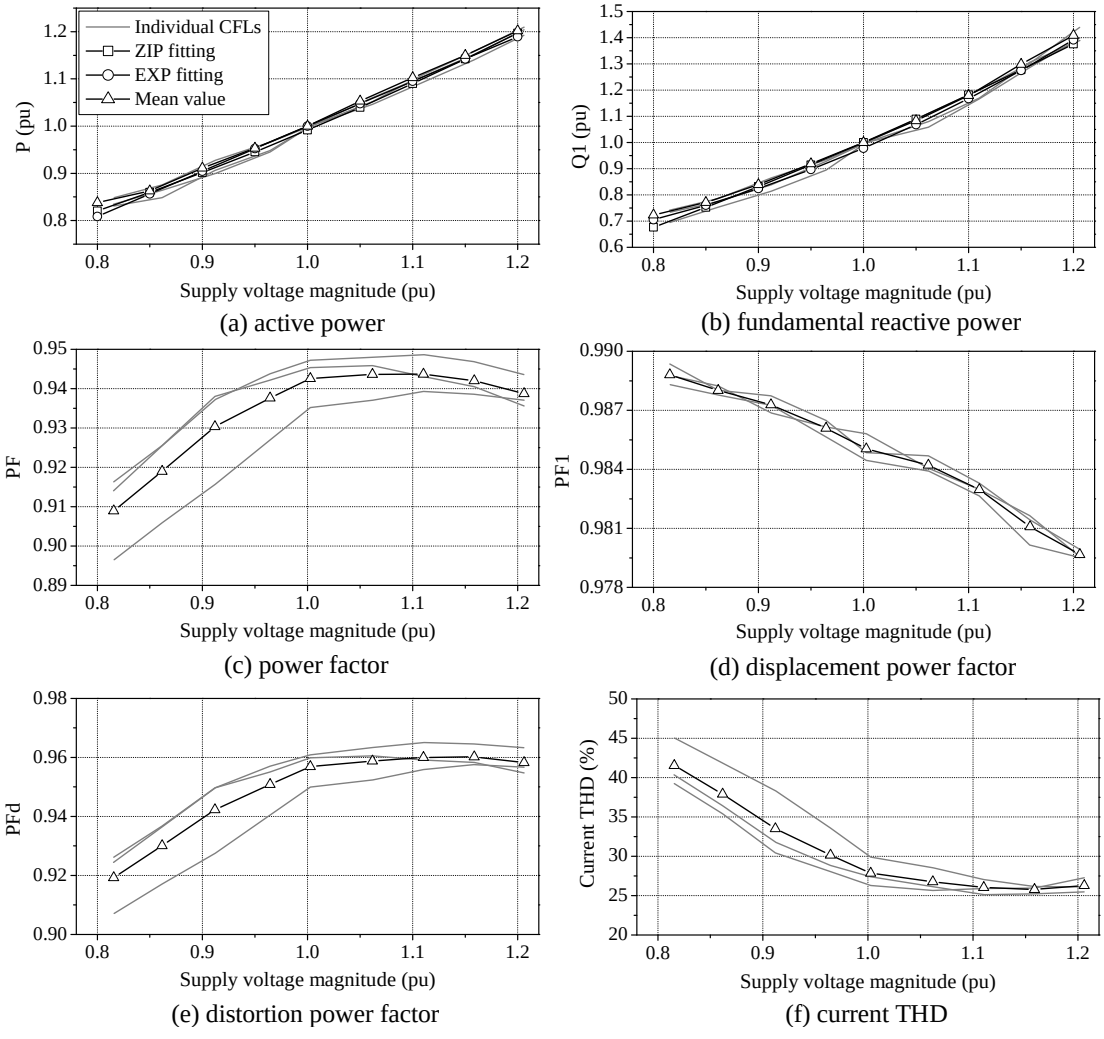

Figure E.1: Electrical characteristics of valley fill CFLs.

E.2 CFL diversity factors and harmonic emissions

Table E.1: Calculated diversity factor values and harmonic injections of aggregate CFL loads.

Harmonic Number (N)	Diversity Factor	Harmonic injections			
		Stiff grid		Distorted supply	
		Mag. ($\%_1$)	Phase (°)	Mag. ($\%_1$)	Phase (°)
1	-	100.00	27.35	100.00	29.51
3	0.996	79.99	-96.38	78.31	-90.47
5	0.979	49.86	146.49	51.75	162.19
7	0.904	25.33	49.91	36.37	67.01
9	0.874	18.84	-24.22	26.82	-29.57
11	0.860	17.41	-118.39	17.43	-119.247
13	0.739	12.34	144.96	13.79	162.69
15	0.659	8.99	64.12	12.00	74.27
17	0.652	8.39	-24.04	9.37	-11.03
19	0.532	6.59	-121.69	8.26	-94.81
21	0.419	4.57	151.56	6.77	176.51
23	0.405	4.03	66.67	5.54	95.61
25	0.326	3.35	-32.79	5.02	9.18
27	0.222	2.19	-129.09	3.87	-77.21
29	0.199	1.65	146.07	3.34	-154.35
31	0.191	1.48	44.03	2.97	118.05
33	0.159	1.07	-70.46	2.21	38.12
35	0.146	0.70	-174.72	2.09	-36.92
37	0.177	0.72	88.61	1.80	-121.82
39	0.196	0.84	-23.73	1.53	-193.32
Note: all phase angles have been normalised to $\angle V_1 = 0$					

E.3 Measured LED LS harmonic emissions

Shown overleaf.

Table E.2: Measured input current harmonics of HP LED LS.

Harmonic Number (N)	HP LED LS							
	1		2		3		4	
	Mag. ($\%_1$)	Phase (°)	Mag. ($\%_1$)	Phase (°)	Mag. ($\%_1$)	Phase (°)	Mag. ($\%_1$)	Phase (°)
1	100	50.45	100	30.01	100	30.77	100	21.59
3	58.98	-16.67	78.11	-81.80	66.04	-95.44	32.06	-91.13
5	20.52	-41.86	46.48	175.73	35.40	147.69	21.61	131.59
7	19.20	-42.91	24.63	100.45	19.67	73.34	19.71	-84.43
9	12.71	-66.72	21.93	35.69	19.14	6.27	22.77	-173.84
11	11.46	-69.83	19.38	-47.62	11.54	-75.15	19.00	60.68
13	9.39	-91.57	14.41	-122.74	5.86	-149.08	10.03	-7.67
15	8.31	-97.32	13.33	168.80	6.48	104.31	5.65	152.06
17	7.56	-116.83	12.57	89.72	7.24	19.34	5.97	37.43
19	6.65	-125.13	10.51	14.46	7.20	-34.54	14.02	-80.22
21	6.41	-142.53	9.92	-56.23	5.99	-97.03	9.40	-171.39
23	5.68	-152.82	9.57	-133.70	2.93	-156.39	7.241	53.23
25	5.68	-168.47	8.48	150.95	1.45	101.73	2.781	-132.48
27	5.12	178.78	8.14	78.93	2.66	-21.12	8.391	123.89
29	5.15	164.52	7.99	1.99	3.34	-80.61	6.09	8.14
31	4.75	150.32	7.33	-74.19	3.68	-132.91	6.37	-80.31
33	4.79	137.01	6.97	-147.52	2.67	170.72	0.86	74.16
35	4.54	121.79	6.81	136.87	1.56	116.66	2.72	-28.00
37	4.60	108.72	6.49	61.68	0.69	2.59	4.57	-165.29
39	4.50	92.16	6.39	-13.32	1.04	-116.67	4.24	135.87
Note: all phase angles have been normalised to $\angle V_1 = 0$								

Appendix F

Lithium-ion battery datasheet

The datasheet for the Li-ion battery used in Chapter 5 is included overleaf. The Li-ion battery was charged using the manufacturer recommended charger.

VARTA

LIC 18650-22 FC

Rechargeable Lithium-Ion Cylindrical

Data Sheet

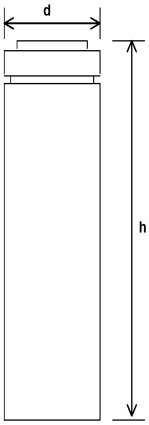

Type Designation	LIC 18650-22 FC
Type Number	56621
System	Li-Ion
UL Recognition	UL1642
Nominal Voltage	3.6V
Nominal Capacity, C	2200mAh
Minimum Capacity	2150mAh (at 0.2C and 20℃)
Dimensions	
Diameter (d)	18.4mm (max.)
Height (h)	65.0mm (max.)
Weight, approx.	44.5g
Charging Method	Constant Current + Constant Voltage
Charge Voltage	4.20V (+/- 50 mV)
Initial Charge Current	Standard Charge: 1100mA Rapid Charge: 2200mA
Charging Cut-Off (a) or b))	
a) by time	Standard Charge: 3h Rapid Charge: 2.5h
b) by min. current	0.05C
Discharge Cut-Off voltage	2.75V
Max. Continuous Discharge Current	4400mA
Operating Temperature	Charge: 0℃ to 45℃ Discharge: -20℃ to 60℃
Storage Temperature Capacity Recovery Rate [2)]	1 Year at -20 to 25℃ >80% 3 Month at -20 to 45℃ >80% 1 Month at -20 to 60℃ >80%
Impedance Initial	<100mΩ @ 1kHz
Life Expectancy [3)]	300 Cycles for ≥1505mAh

1) Prior to use read Handling Precaution and Prohibitions for VARTA Li-ion Batteries.
2) After storage at initial cell voltage of 3.6 to 3.9 V/cell; capacity 0.2C measured at 20℃.
3) Cell is to be charged at 0.8C to 4.2V with cutoff at 0.05C and discharged at 1.0C with cutoff at 2.75V, at 20℃

VARTA Microbattery GmbH
Daimlerstraße 1, 73479 Ellwangen, Germany
Tel.: +49 79 61 921-0
Telefax: +49 79 61 921-553

Appendix G

EV measurements

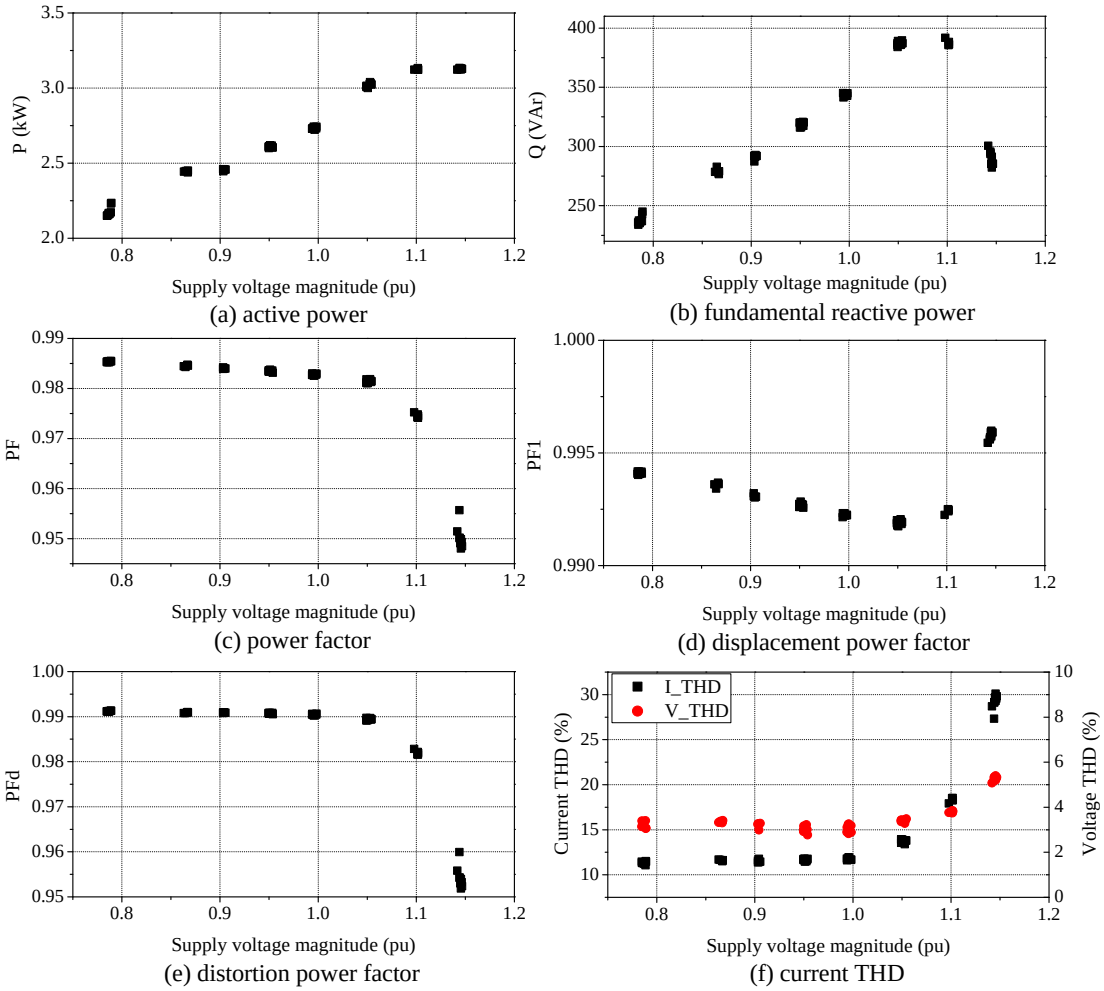

Figure G.1: Measured input electrical characteristics of EV Type III-A.

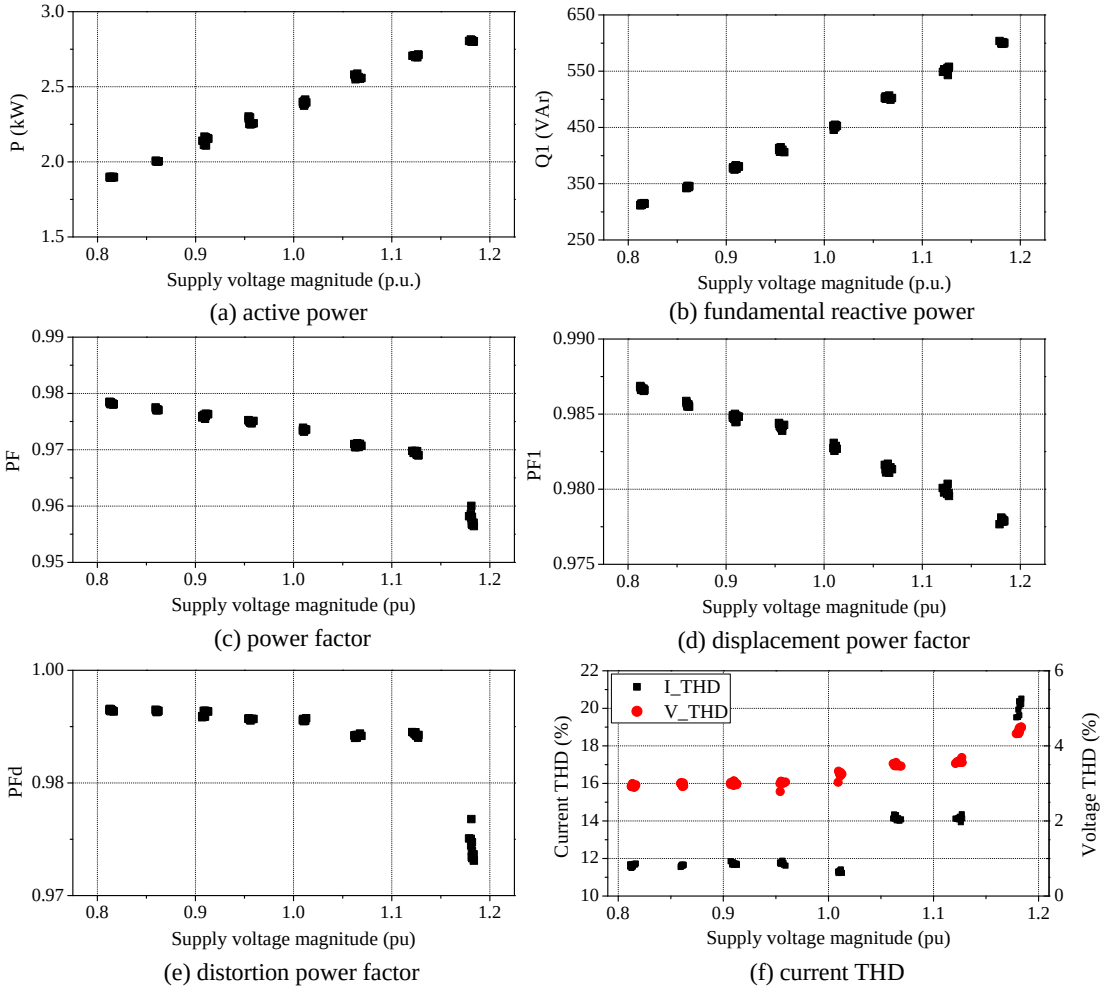

Figure G.2: Measured input electrical characteristics of EV Type III-B.

Appendix H

Load sector aggregate models

This appendix includes all load model coefficients for the following scenarios:

- Residential LV aggregate for minimum loading conditions
- Residential MV aggregate for minimum loading conditions
- Residential LV aggregate for average loading conditions
- Residential MV aggregate for average loading conditions
- Residential LV aggregate for maximum loading conditions
- Residential MV aggregate for maximum loading conditions
- Commercial LV aggregate for minimum loading conditions
- Commercial LV aggregate for average loading conditions
- Commercial LV aggregate for maximum loading conditions

All MV load models are obtained by connection to the generic UK urban LV distribution network.

Table H.1: Residential LV aggregate minimum loading condition.

Time (hr)	PF_1	Exp. Model		Polynomial/ZIP Model					
		n_p	n_q	Z_p	I_p	P_p	Z_q	I_q	P_q
0.5	0.93	0.62	1.21	0.25	0.13	0.63	0.84	-0.49	0.65
1.0	0.93	0.57	1.22	0.23	0.11	0.66	0.85	-0.50	0.65
1.5	0.92	0.59	1.33	0.26	0.07	0.67	0.97	-0.62	0.65
2.0	0.97	1.28	1.38	0.62	0.04	0.35	1.00	-0.65	0.65
2.5	0.98	1.45	1.36	0.71	0.02	0.27	0.99	-0.64	0.65
3.0	0.97	1.38	1.55	0.67	0.03	0.30	1.15	-0.78	0.63
3.5	0.97	1.41	1.65	0.68	0.04	0.28	1.24	-0.86	0.62
4.0	0.96	1.29	1.62	0.63	0.02	0.35	1.22	-0.85	0.63
4.5	0.94	1.20	1.79	0.58	0.02	0.40	1.36	-0.96	0.60
5.0	0.91	0.98	1.77	0.48	0.02	0.50	1.35	-0.96	0.60
5.5	0.90	0.96	1.81	0.47	0.02	0.51	1.38	-0.98	0.60
6.0	0.91	1.04	1.80	0.50	0.03	0.47	1.37	-0.97	0.60
6.5	0.91	1.07	1.81	0.52	0.02	0.46	1.38	-0.97	0.59
7.0	0.93	1.11	1.71	0.55	0.00	0.45	1.30	-0.91	0.62
7.5	0.96	1.30	1.73	0.64	0.01	0.35	1.32	-0.94	0.62
8.0	0.95	1.25	1.74	0.62	0.00	0.38	1.34	-0.97	0.63
8.5	0.94	1.13	1.70	0.56	0.01	0.44	1.31	-0.95	0.64
9.0	0.94	1.17	1.72	0.57	0.02	0.41	1.34	-0.98	0.64
9.5	0.93	1.12	1.72	0.55	0.00	0.44	1.35	-1.00	0.66
10.0	0.92	1.07	1.72	0.53	0.01	0.46	1.34	-0.98	0.65
10.5	0.92	1.02	1.70	0.50	0.02	0.49	1.32	-0.96	0.64
11.0	0.92	1.04	1.69	0.51	0.01	0.48	1.32	-0.97	0.66
11.5	0.93	1.03	1.67	0.51	0.01	0.48	1.31	-0.98	0.67
12.0	0.93	1.04	1.64	0.51	0.01	0.48	1.29	-0.96	0.67
12.5	0.93	1.04	1.64	0.51	0.01	0.48	1.30	-0.98	0.68
13.0	0.92	0.97	1.64	0.48	0.00	0.52	1.28	-0.94	0.66
13.5	0.92	0.94	1.58	0.46	0.00	0.54	1.21	-0.86	0.65
14.0	0.91	0.91	1.64	0.45	0.00	0.55	1.26	-0.90	0.64
14.5	0.89	0.74	1.60	0.37	0.00	0.63	1.20	-0.82	0.62
15.0	0.89	0.71	1.58	0.35	0.00	0.65	1.18	-0.79	0.62
15.5	0.90	0.80	1.58	0.40	0.00	0.60	1.19	-0.81	0.63
16.0	0.92	0.93	1.58	0.46	0.00	0.54	1.20	-0.85	0.65
16.5	0.94	1.06	1.55	0.52	0.01	0.47	1.20	-0.88	0.68
17.0	0.96	1.14	1.47	0.57	0.00	0.44	1.16	-0.87	0.71
17.5	0.96	1.19	1.46	0.59	0.00	0.41	1.17	-0.91	0.74
18.0	0.96	1.10	1.28	0.55	0.00	0.45	0.90	-0.54	0.64
18.5	0.97	0.88	0.89	0.44	0.00	0.56	0.35	0.18	0.47
19.0	0.97	0.94	0.92	0.46	0.00	0.53	0.39	0.12	0.48
19.5	0.97	0.84	0.80	0.42	0.00	0.58	0.23	0.34	0.43
20.0	0.97	0.72	0.81	0.36	0.00	0.64	0.25	0.30	0.45
20.5	0.97	0.68	0.80	0.34	0.01	0.65	0.27	0.26	0.47
21.0	0.97	0.69	0.78	0.31	0.07	0.62	0.27	0.24	0.49
21.5	0.97	0.77	0.81	0.32	0.13	0.55	0.33	0.15	0.52
22.0	0.98	0.74	0.77	0.29	0.16	0.55	0.28	0.20	0.52
22.5	0.97	0.71	0.77	0.28	0.15	0.57	0.29	0.18	0.53
23.0	0.97	0.67	0.77	0.24	0.19	0.57	0.31	0.14	0.54
23.5	0.98	0.69	0.76	0.25	0.19	0.56	0.30	0.16	0.54
24.0	0.97	0.64	0.75	0.23	0.18	0.59	0.28	0.18	0.53

Table H.2: Residential MV aggregate minimum loading condition.

Time (hr)	PF_1	Exp. Model		Polynomial/ZIP Model					
		n_p	n_q	Z_p	I_p	P_p	Z_q	I_q	P_q
0.5	0.93	0.56	1.11	0.28	0	0.72	0.91	-0.73	0.82
1.0	0.92	0.51	1.11	0.26	0	0.75	0.93	-0.76	0.83
1.5	0.91	0.54	1.23	0.27	0	0.73	1.03	-0.87	0.83
2.0	0.97	1.24	1.3	0.61	0	0.39	1.02	-0.76	0.74
2.5	0.98	1.4	1.3	0.69	0	0.31	0.99	-0.71	0.72
3.0	0.97	1.34	1.48	0.66	0	0.34	1.15	-0.85	0.7
3.5	0.97	1.36	1.59	0.67	0	0.33	1.24	-0.92	0.68
4.0	0.96	1.24	1.55	0.61	0	0.39	1.23	-0.94	0.71
4.5	0.94	1.14	1.72	0.56	0	0.44	1.37	-1.04	0.68
5.0	0.91	0.93	1.71	0.46	0	0.54	1.37	-1.07	0.7
5.5	0.90	0.9	1.75	0.45	0	0.55	1.4	-1.09	0.69
6.0	0.91	0.99	1.73	0.49	0	0.51	1.39	-1.08	0.69
6.5	0.91	1.02	1.73	0.5	0.01	0.49	1.39	-1.08	0.69
7.0	0.93	1.06	1.62	0.53	0	0.47	1.31	-1.04	0.73
7.5	0.95	1.26	1.64	0.62	0	0.38	1.32	-1.03	0.71
8.0	0.94	1.21	1.64	0.6	0	0.4	1.34	-1.07	0.73
8.5	0.94	1.08	1.61	0.54	0	0.47	1.32	-1.07	0.75
9.0	0.94	1.12	1.65	0.55	0	0.45	1.35	-1.07	0.73
9.5	0.93	1.06	1.65	0.53	0	0.48	1.36	-1.11	0.75
10.0	0.92	1.02	1.65	0.5	0	0.5	1.35	-1.09	0.73
10.5	0.91	0.96	1.64	0.47	0	0.53	1.34	-1.07	0.73
11.0	0.92	0.98	1.62	0.48	0	0.52	1.33	-1.08	0.74
11.5	0.92	0.97	1.61	0.48	0	0.52	1.33	-1.09	0.76
12.0	0.93	0.98	1.57	0.49	0	0.51	1.31	-1.07	0.77
12.5	0.92	0.98	1.57	0.49	0	0.51	1.32	-1.09	0.77
13.0	0.92	0.91	1.58	0.45	0	0.55	1.3	-1.06	0.76
13.5	0.92	0.88	1.51	0.43	0	0.57	1.24	-0.99	0.75
14.0	0.91	0.85	1.58	0.42	0	0.58	1.29	-1.03	0.74
14.5	0.89	0.68	1.54	0.34	0	0.67	1.24	-0.97	0.73
15.0	0.89	0.65	1.51	0.32	0	0.68	1.22	-0.95	0.73
15.5	0.90	0.74	1.51	0.37	0	0.63	1.22	-0.97	0.75
16.0	0.92	0.88	1.5	0.44	0	0.57	1.23	-1	0.77
16.5	0.94	1.02	1.45	0.5	0.01	0.49	1.22	-1.03	0.81
17.0	0.95	1.1	1.36	0.54	0	0.46	1.18	-1.02	0.85
17.5	0.95	1.15	1.34	0.57	0	0.43	1.19	-1.07	0.88
18.0	0.96	1.06	1.14	0.52	0.01	0.47	0.95	-0.78	0.83
18.5	0.96	0.84	0.73	0.42	0	0.58	0.5	-0.27	0.77
19.0	0.96	0.9	0.76	0.45	0	0.56	0.53	-0.31	0.78
19.5	0.96	0.79	0.62	0.4	0	0.61	0.42	-0.21	0.79
20.0	0.96	0.68	0.61	0.34	0	0.66	0.45	-0.3	0.84
20.5	0.96	0.64	0.6	0.32	0	0.68	0.47	-0.35	0.87
21.0	0.96	0.64	0.58	0.32	0	0.68	0.46	-0.34	0.88
21.5	0.97	0.73	0.62	0.36	0	0.64	0.49	-0.36	0.87
22.0	0.97	0.7	0.58	0.34	0.01	0.65	0.45	-0.31	0.87
22.5	0.97	0.67	0.59	0.33	0.01	0.66	0.45	-0.32	0.86
23.0	0.97	0.63	0.6	0.31	0.01	0.68	0.46	-0.32	0.86
23.5	0.97	0.65	0.61	0.31	0.02	0.67	0.43	-0.25	0.82
24.0	0.97	0.59	0.61	0.29	0	0.71	0.41	-0.2	0.8

Table H.3: Residential LV aggregate average loading condition.

Time (hr)	PF_1	Exp. Model		Polynomial/ZIP Model					
		n_p	n_q	Z_p	I_p	P_p	Z_q	I_q	P_q
0.5	0.94	0.65	1.18	0.26	0.12	0.62	0.81	-0.46	0.65
1.0	0.93	0.64	1.17	0.28	0.08	0.64	0.80	-0.44	0.64
1.5	0.92	0.72	1.36	0.33	0.06	0.61	0.99	-0.63	0.65
2.0	0.98	1.38	1.32	0.67	0.02	0.30	0.93	-0.57	0.63
2.5	0.99	1.49	1.32	0.73	0.02	0.25	0.93	-0.57	0.63
3.0	0.98	1.36	1.37	0.67	0.01	0.32	0.99	-0.62	0.64
3.5	0.97	1.31	1.54	0.64	0.02	0.34	1.15	-0.78	0.63
4.0	0.95	1.16	1.58	0.56	0.02	0.41	1.18	-0.80	0.62
4.5	0.91	1.01	1.73	0.48	0.03	0.48	1.30	-0.89	0.60
5.0	0.92	1.02	1.74	0.50	0.03	0.48	1.31	-0.92	0.60
5.5	0.90	0.91	1.73	0.45	0.01	0.54	1.31	-0.91	0.61
6.0	0.92	1.08	1.79	0.53	0.02	0.45	1.36	-0.95	0.59
6.5	0.93	1.17	1.79	0.57	0.02	0.41	1.36	-0.95	0.59
7.0	0.95	1.28	1.74	0.63	0.01	0.36	1.33	-0.95	0.62
7.5	0.97	1.43	1.73	0.70	0.01	0.29	1.33	-0.96	0.63
8.0	0.97	1.42	1.72	0.70	0.01	0.29	1.33	-0.97	0.64
8.5	0.97	1.46	1.71	0.71	0.01	0.27	1.32	-0.95	0.63
9.0	0.96	1.37	1.69	0.68	0.00	0.32	1.30	-0.94	0.64
9.5	0.96	1.34	1.69	0.66	0.00	0.34	1.30	-0.93	0.64
10.0	0.95	1.24	1.65	0.62	0.00	0.38	1.26	-0.89	0.63
10.5	0.95	1.25	1.62	0.62	0.00	0.38	1.23	-0.86	0.63
11.0	0.95	1.19	1.61	0.59	0.00	0.41	1.22	-0.86	0.64
11.5	0.94	1.15	1.66	0.57	0.00	0.43	1.29	-0.95	0.66
12.0	0.94	1.13	1.62	0.56	0.00	0.44	1.26	-0.93	0.67
12.5	0.94	1.07	1.59	0.53	0.00	0.47	1.23	-0.89	0.66
13.0	0.93	1.06	1.59	0.52	0.00	0.47	1.21	-0.87	0.65
13.5	0.92	1.00	1.59	0.49	0.01	0.50	1.20	-0.84	0.64
14.0	0.92	0.94	1.62	0.47	0.00	0.53	1.24	-0.88	0.64
14.5	0.91	0.84	1.59	0.42	0.00	0.58	1.18	-0.81	0.62
15.0	0.91	0.82	1.57	0.41	0.00	0.60	1.17	-0.80	0.62
15.5	0.92	0.91	1.55	0.45	0.00	0.55	1.16	-0.79	0.63
16.0	0.94	0.99	1.50	0.49	0.00	0.51	1.13	-0.78	0.65
16.5	0.95	1.11	1.46	0.55	0.00	0.45	1.11	-0.78	0.67
17.0	0.95	1.15	1.47	0.57	0.00	0.43	1.14	-0.83	0.69
17.5	0.95	1.14	1.43	0.56	0.00	0.44	1.08	-0.76	0.68
18.0	0.96	1.20	1.37	0.60	0.00	0.40	1.05	-0.74	0.70
18.5	0.97	1.01	0.95	0.50	0.01	0.50	0.43	0.09	0.48
19.0	0.97	0.98	0.98	0.48	0.01	0.51	0.48	0.02	0.50
19.5	0.98	0.93	0.81	0.46	0.02	0.53	0.26	0.29	0.45
20.0	0.97	0.87	0.81	0.42	0.02	0.56	0.28	0.26	0.47
20.5	0.98	0.86	0.78	0.41	0.05	0.55	0.25	0.28	0.47
21.0	0.98	0.90	0.73	0.40	0.08	0.51	0.20	0.33	0.47
21.5	0.98	0.93	0.78	0.38	0.17	0.45	0.31	0.17	0.53
22.0	0.99	0.93	0.74	0.37	0.18	0.45	0.26	0.22	0.52
22.5	0.98	0.90	0.80	0.34	0.22	0.44	0.36	0.07	0.57
23.0	0.98	0.85	0.74	0.32	0.21	0.47	0.28	0.18	0.54
23.5	0.98	0.82	0.75	0.31	0.20	0.50	0.29	0.18	0.54
24.0	0.97	0.71	0.76	0.27	0.16	0.57	0.30	0.17	0.53

Table H.4: Residential MV aggregate average loading condition.

Time (hr)	PF_1	Exp. Model		Polynomial/ZIP Model					
		n_p	n_q	Z_p	I_p	P_p	Z_q	I_q	P_q
0.5	0.93	0.62	1.06	0.26	0	0.74	0.79	-0.71	0.92
1.0	0.92	0.61	1.05	0.25	0	0.75	0.79	-0.72	0.93
1.5	0.91	0.69	1.23	0.29	0	0.71	0.96	-0.9	0.95
2.0	0.97	1.36	1.23	0.63	0	0.38	0.86	-0.69	0.82
2.5	0.98	1.47	1.25	0.68	0	0.32	0.86	-0.66	0.8
3.0	0.97	1.33	1.28	0.61	0	0.4	0.91	-0.74	0.83
3.5	0.97	1.28	1.44	0.58	0	0.42	1.07	-0.91	0.84
4.0	0.96	1.13	1.47	0.5	0	0.5	1.11	-0.96	0.84
4.5	0.94	0.98	1.63	0.43	0	0.58	1.25	-1.08	0.83
5.0	0.91	0.99	1.63	0.43	0	0.57	1.27	-1.1	0.84
5.5	0.90	0.88	1.62	0.38	0	0.62	1.27	-1.13	0.85
6.0	0.91	1.05	1.69	0.46	0	0.54	1.31	-1.13	0.82
6.5	0.91	1.13	1.69	0.5	0	0.5	1.31	-1.12	0.81
7.0	0.93	1.25	1.63	0.57	0	0.44	1.26	-1.1	0.84
7.5	0.95	1.4	1.61	0.64	0	0.36	1.24	-1.07	0.83
8.0	0.94	1.39	1.6	0.64	0	0.36	1.24	-1.08	0.84
8.5	0.94	1.43	1.61	0.66	0	0.34	1.23	-1.05	0.82
9.0	0.94	1.34	1.6	0.61	0	0.4	1.23	-1.06	0.83
9.5	0.93	1.31	1.6	0.59	0	0.41	1.23	-1.06	0.83
10.0	0.92	1.21	1.57	0.54	0	0.46	1.19	-1.02	0.83
10.5	0.91	1.22	1.54	0.55	0	0.46	1.16	-0.99	0.82
11.0	0.92	1.16	1.53	0.52	0	0.49	1.16	-0.99	0.83
11.5	0.92	1.12	1.58	0.49	0	0.51	1.23	-1.1	0.87
12.0	0.93	1.1	1.53	0.48	0.01	0.52	1.2	-1.08	0.88
12.5	0.92	1.04	1.5	0.46	0	0.55	1.17	-1.05	0.88
13.0	0.92	1.03	1.5	0.45	0	0.56	1.16	-1.02	0.87
13.5	0.92	0.97	1.5	0.42	0	0.58	1.15	-1	0.85
14.0	0.91	0.91	1.53	0.39	0	0.61	1.19	-1.05	0.87
14.5	0.89	0.81	1.5	0.35	0	0.66	1.14	-0.99	0.85
15.0	0.89	0.78	1.48	0.33	0	0.67	1.13	-0.99	0.86
15.5	0.90	0.88	1.45	0.38	0	0.63	1.11	-0.98	0.87
16.0	0.92	0.96	1.4	0.42	0	0.59	1.08	-0.96	0.89
16.5	0.94	1.08	1.35	0.48	0	0.53	1.05	-0.96	0.91
17.0	0.95	1.12	1.35	0.5	0	0.5	1.07	-1.02	0.95
17.5	0.95	1.11	1.29	0.49	0	0.51	1.02	-0.97	0.95
18.0	0.96	1.17	1.22	0.53	0	0.47	0.97	-0.94	0.97
18.5	0.96	0.98	0.81	0.43	0	0.57	0.48	-0.3	0.82
19.0	0.96	0.96	0.84	0.42	0	0.58	0.52	-0.36	0.84
19.5	0.96	0.91	0.66	0.4	0	0.61	0.37	-0.2	0.83
20.0	0.96	0.85	0.65	0.37	0	0.64	0.39	-0.26	0.87
20.5	0.96	0.84	0.61	0.36	0	0.64	0.38	-0.26	0.89
21.0	0.96	0.88	0.56	0.38	0	0.62	0.33	-0.22	0.89
21.5	0.97	0.91	0.61	0.39	0.01	0.6	0.4	-0.31	0.91
22.0	0.97	0.91	0.58	0.39	0.02	0.59	0.36	-0.27	0.91
22.5	0.97	0.89	0.64	0.37	0.04	0.59	0.43	-0.36	0.93
23.0	0.97	0.83	0.59	0.35	0.03	0.63	0.37	-0.26	0.9
23.5	0.97	0.8	0.62	0.34	0	0.66	0.36	-0.23	0.87
24.0	0.97	0.69	0.64	0.29	0	0.71	0.37	-0.22	0.85

Table H.5: Residential LV aggregate maximum loading condition.

Time (hr)	PF_1	Exp. Model		Polynomial/ZIP Model					
		n_p	n_q	Z_p	I_p	P_p	Z_q	I_q	P_q
0.5	0.96	0.92	1.21	0.41	0.09	0.50	0.84	-0.48	0.64
1.0	0.97	1.14	1.16	0.55	0.03	0.42	0.76	-0.38	0.62
1.5	0.97	1.28	1.29	0.62	0.03	0.35	0.91	-0.54	0.63
2.0	0.97	1.28	1.33	0.62	0.02	0.35	0.95	-0.58	0.63
2.5	0.97	1.20	1.32	0.59	0.02	0.39	0.93	-0.56	0.63
3.0	0.96	1.26	1.52	0.62	0.02	0.37	1.12	-0.75	0.63
3.5	0.95	1.21	1.60	0.59	0.03	0.38	1.19	-0.81	0.62
4.0	0.94	1.14	1.62	0.56	0.02	0.42	1.21	-0.83	0.62
4.5	0.93	1.13	1.71	0.55	0.01	0.43	1.29	-0.89	0.60
5.0	0.93	1.18	1.77	0.58	0.01	0.41	1.34	-0.94	0.59
5.5	0.93	1.14	1.77	0.56	0.01	0.43	1.33	-0.92	0.59
6.0	0.92	1.12	1.80	0.55	0.01	0.44	1.36	-0.95	0.59
6.5	0.95	1.30	1.80	0.64	0.01	0.35	1.37	-0.97	0.60
7.0	0.97	1.45	1.78	0.71	0.03	0.27	1.38	-1.01	0.63
7.5	0.98	1.49	1.77	0.71	0.06	0.23	1.38	-1.02	0.64
8.0	0.99	1.52	1.80	0.71	0.09	0.20	1.44	-1.10	0.67
8.5	0.99	1.49	1.78	0.69	0.11	0.20	1.41	-1.07	0.66
9.0	0.98	1.50	1.84	0.70	0.09	0.21	1.46	-1.11	0.65
9.5	0.99	1.53	1.82	0.72	0.08	0.20	1.46	-1.13	0.67
10.0	0.99	1.49	1.68	0.72	0.04	0.24	1.36	-1.07	0.71
10.5	0.98	1.47	1.71	0.71	0.04	0.25	1.38	-1.08	0.70
11.0	0.97	1.33	1.62	0.65	0.03	0.33	1.28	-0.96	0.68
11.5	0.99	1.44	1.30	0.71	0.01	0.28	1.01	-0.75	0.73
12.0	0.99	1.37	1.38	0.68	0.01	0.31	1.10	-0.84	0.74
12.5	0.96	1.16	1.63	0.56	0.04	0.40	1.29	-0.98	0.69
13.0	0.95	1.15	1.67	0.56	0.03	0.41	1.35	-1.06	0.71
13.5	0.95	1.09	1.61	0.53	0.01	0.45	1.28	-0.97	0.69
14.0	0.94	1.07	1.69	0.51	0.05	0.45	1.33	-1.00	0.67
14.5	0.94	0.97	1.61	0.46	0.04	0.50	1.25	-0.92	0.66
15.0	0.94	0.97	1.58	0.47	0.03	0.50	1.20	-0.85	0.65
15.5	0.94	0.97	1.59	0.46	0.04	0.50	1.22	-0.88	0.66
16.0	0.95	1.03	1.49	0.50	0.02	0.48	1.13	-0.79	0.66
16.5	0.96	1.12	1.46	0.55	0.01	0.44	1.12	-0.81	0.69
17.0	0.97	1.14	1.41	0.56	0.01	0.43	1.07	-0.76	0.69
17.5	0.98	1.26	1.58	0.57	0.11	0.32	1.31	-1.07	0.76
18.0	0.99	1.34	1.57	0.60	0.14	0.27	1.32	-1.09	0.77
18.5	0.99	1.14	1.00	0.51	0.11	0.38	0.57	-0.16	0.58
19.0	0.99	1.16	0.97	0.51	0.13	0.36	0.53	-0.10	0.57
19.5	0.99	1.09	0.82	0.47	0.15	0.38	0.32	0.17	0.51
20.0	0.99	1.04	0.81	0.44	0.16	0.40	0.34	0.13	0.53
20.5	0.99	1.03	0.76	0.42	0.18	0.40	0.28	0.20	0.52
21.0	0.99	1.04	0.75	0.42	0.19	0.39	0.28	0.19	0.53
21.5	0.99	1.06	0.79	0.43	0.18	0.38	0.34	0.10	0.55
22.0	0.99	1.07	0.78	0.44	0.19	0.38	0.33	0.12	0.55
22.5	0.99	1.01	0.79	0.40	0.20	0.40	0.36	0.08	0.57
23.0	0.99	1.00	0.77	0.40	0.19	0.41	0.33	0.12	0.56
23.5	0.98	0.86	0.77	0.35	0.17	0.49	0.31	0.15	0.54
24.0	0.97	0.81	0.82	0.36	0.10	0.55	0.36	0.10	0.55

Table H.6: Residential MV aggregate maximum loading condition.

Time (hr)	PF_1	Exp. Model		Polynomial/ZIP Model					
		n_p	n_q	Z_p	I_p	P_p	Z_q	I_q	P_q
0.5	0.95	0.87	1.09	0.43	0	0.57	0.9	-0.71	0.82
1.0	0.96	1.11	1.05	0.55	0	0.45	0.81	-0.58	0.78
1.5	0.97	1.25	1.19	0.62	0	0.38	0.93	-0.69	0.76
2.0	0.97	1.25	1.23	0.62	0	0.38	0.96	-0.72	0.76
2.5	0.96	1.17	1.21	0.58	0	0.42	0.96	-0.73	0.77
3.0	0.96	1.23	1.41	0.61	0	0.4	1.13	-0.87	0.74
3.5	0.95	1.18	1.49	0.58	0	0.42	1.2	-0.94	0.74
4.0	0.94	1.1	1.52	0.54	0	0.46	1.23	-0.97	0.74
4.5	0.93	1.08	1.61	0.54	0	0.47	1.3	-1.01	0.72
5.0	0.93	1.13	1.69	0.56	0	0.44	1.35	-1.05	0.7
5.5	0.92	1.1	1.68	0.54	0	0.46	1.34	-1.04	0.7
6.0	0.91	1.08	1.71	0.53	0	0.47	1.37	-1.07	0.69
6.5	0.94	1.26	1.7	0.62	0	0.38	1.36	-1.06	0.69
7.0	0.97	1.42	1.67	0.7	0	0.3	1.35	-1.05	0.7
7.5	0.98	1.46	1.64	0.72	0	0.28	1.32	-1.03	0.71
8.0	0.98	1.49	1.67	0.74	0	0.27	1.36	-1.08	0.72
8.5	0.98	1.46	1.66	0.72	0	0.28	1.34	-1.06	0.71
9.0	0.98	1.46	1.74	0.72	0	0.28	1.41	-1.11	0.7
9.5	0.98	1.49	1.73	0.73	0	0.27	1.41	-1.12	0.72
10.0	0.98	1.45	1.6	0.72	0	0.28	1.33	-1.09	0.76
10.5	0.97	1.43	1.64	0.71	0	0.3	1.36	-1.11	0.75
11.0	0.97	1.28	1.55	0.63	0	0.37	1.27	-1.03	0.76
11.5	0.99	1.4	1.23	0.69	0	0.31	1.02	-0.82	0.81
12.0	0.98	1.33	1.3	0.66	0	0.34	1.1	-0.93	0.83
12.5	0.95	1.11	1.54	0.55	0	0.45	1.3	-1.09	0.79
13.0	0.94	1.1	1.59	0.55	0	0.46	1.36	-1.16	0.8
13.5	0.95	1.04	1.53	0.51	0.01	0.49	1.29	-1.09	0.8
14.0	0.94	1.02	1.6	0.5	0.01	0.49	1.34	-1.11	0.77
14.5	0.94	0.92	1.52	0.46	0	0.55	1.28	-1.06	0.78
15.0	0.93	0.92	1.49	0.46	0	0.55	1.23	-1	0.77
15.5	0.94	0.92	1.49	0.46	0	0.55	1.25	-1.04	0.79
16.0	0.94	0.98	1.38	0.48	0.01	0.51	1.15	-0.95	0.8
16.5	0.96	1.08	1.34	0.53	0	0.47	1.15	-0.99	0.84
17.0	0.96	1.11	1.26	0.55	0	0.45	1.1	-0.96	0.86
17.5	0.97	1.23	1.4	0.6	0.01	0.39	1.27	-1.18	0.91
18.0	0.98	1.31	1.36	0.62	0.06	0.32	1.23	-1.13	0.9
18.5	0.98	1.11	0.81	0.54	0.02	0.44	0.67	-0.54	0.87
19.0	0.98	1.13	0.78	0.54	0.04	0.42	0.63	-0.48	0.86
19.5	0.98	1.06	0.63	0.49	0.07	0.44	0.48	-0.33	0.85
20.0	0.98	1.01	0.62	0.47	0.05	0.47	0.5	-0.37	0.87
20.5	0.98	1	0.57	0.45	0.1	0.45	0.45	-0.34	0.88
21.0	0.98	1.01	0.57	0.45	0.1	0.45	0.44	-0.32	0.87
21.5	0.98	1.03	0.62	0.46	0.1	0.44	0.48	-0.35	0.86
22.0	0.98	1.04	0.62	0.47	0.1	0.44	0.47	-0.31	0.84
22.5	0.98	0.98	0.63	0.44	0.1	0.46	0.48	-0.34	0.86
23.0	0.98	0.97	0.62	0.44	0.08	0.48	0.45	-0.29	0.84
23.5	0.98	0.82	0.61	0.4	0.02	0.58	0.44	-0.27	0.83
24.0	0.97	0.77	0.67	0.38	0	0.62	0.48	-0.29	0.81

Table H.7: Commercial LV aggregate minimum loading condition.

Time (hr)	PF_1	Exp. Model		Polynomial/ZIP Model					
		n_p	n_q	Z_p	I_p	P_p	Z_q	I_q	P_q
0.5	0.98	0.95	1.41	0.15	0.65	0.20	1.43	-1.49	1.06
1.0	0.97	0.79	1.38	0.06	0.67	0.27	1.30	-1.24	0.95
1.5	0.98	0.82	1.35	0.08	0.67	0.25	1.29	-1.25	0.96
2.0	0.97	0.72	1.41	0.09	0.54	0.37	1.35	-1.32	0.97
2.5	0.97	0.70	1.42	0.09	0.53	0.39	1.37	-1.35	0.98
3.0	0.97	0.65	1.40	0.07	0.52	0.42	1.33	-1.28	0.96
3.5	0.97	0.72	1.42	0.10	0.52	0.38	1.39	-1.40	1.01
4.0	0.97	0.77	1.42	0.12	0.52	0.36	1.41	-1.44	1.02
4.5	0.97	0.75	1.39	0.13	0.49	0.38	1.34	-1.32	0.98
5.0	0.98	0.86	1.54	0.00	0.85	0.14	1.76	-2.03	1.26
5.5	0.98	0.86	1.80	0.00	0.86	0.14	2.16	-2.58	1.42
6.0	0.98	0.82	1.97	0.00	0.82	0.17	2.70	-3.50	1.80
6.5	0.99	0.87	2.04	0.00	0.87	0.12	2.91	-3.86	1.95
7.0	0.99	0.89	2.01	0.00	0.89	0.10	2.88	-3.84	1.96
7.5	0.99	0.86	1.80	0.00	0.87	0.12	2.63	-3.54	1.90
8.0	0.99	0.81	1.69	0.00	0.82	0.17	2.52	-3.41	1.89
8.5	0.99	0.81	1.67	0.00	0.82	0.17	2.59	-3.58	1.99
9.0	0.99	0.76	1.69	0.00	0.76	0.23	2.69	-3.77	2.08
9.5	0.99	0.78	1.42	0.00	0.79	0.20	2.13	-2.89	1.76
10.0	0.99	0.75	1.44	0.00	0.75	0.24	2.10	-2.81	1.71
10.5	0.99	0.70	1.55	0.00	0.71	0.29	2.29	-3.08	1.80
11.0	0.99	0.70	1.51	0.00	0.70	0.29	2.26	-3.06	1.81
11.5	0.99	0.68	1.54	0.00	0.69	0.31	2.29	-3.11	1.81
12.0	0.99	0.66	1.49	0.00	0.66	0.33	2.22	-3.01	1.79
12.5	0.99	0.62	1.61	0.00	0.63	0.37	2.42	-3.29	1.87
13.0	0.99	0.61	1.58	0.00	0.62	0.38	2.39	-3.26	1.87
13.5	0.99	0.60	1.64	0.00	0.60	0.39	2.45	-3.33	1.88
14.0	0.99	0.59	1.65	0.00	0.59	0.40	2.44	-3.29	1.85
14.5	0.99	0.57	1.65	0.00	0.57	0.42	2.45	-3.32	1.87
15.0	0.98	0.54	1.70	0.00	0.54	0.45	2.49	-3.36	1.87
15.5	0.99	0.54	1.68	0.00	0.54	0.45	2.52	-3.42	1.91
16.0	0.98	0.56	1.66	0.00	0.56	0.43	2.41	-3.23	1.82
16.5	0.99	0.58	1.60	0.00	0.58	0.41	2.33	-3.12	1.79
17.0	0.98	0.57	1.60	0.00	0.57	0.43	2.18	-2.81	1.64
17.5	0.98	0.60	1.46	0.01	0.59	0.40	1.85	-2.30	1.44
18.0	0.98	0.67	1.38	0.12	0.42	0.45	1.69	-2.04	1.35
18.5	0.97	0.64	1.47	0.29	0.06	0.65	1.65	-1.88	1.22
19.0	0.97	0.64	1.46	0.32	0.00	0.68	1.58	-1.74	1.16
19.5	0.96	0.56	1.55	0.28	0.00	0.72	1.67	-1.83	1.16
20.0	0.97	0.60	1.49	0.30	0.00	0.70	1.61	-1.77	1.16
20.5	0.97	0.66	1.49	0.33	0.00	0.67	1.57	-1.70	1.12
21.0	0.97	0.62	1.55	0.31	0.00	0.69	1.73	-1.95	1.23
21.5	0.96	0.60	1.58	0.30	0.00	0.70	1.70	-1.86	1.16
22.0	0.96	0.60	1.51	0.30	0.00	0.70	1.57	-1.67	1.10
22.5	0.95	0.49	1.67	0.25	0.00	0.75	1.88	-2.12	1.25
23.0	0.95	0.48	1.67	0.24	0.00	0.76	1.84	-2.06	1.22
23.5	0.96	0.64	1.68	0.30	0.03	0.66	1.85	-2.08	1.22
24.0	0.97	0.72	1.69	0.21	0.30	0.49	1.89	-2.14	1.25

Table H.8: Commercial LV aggregate average loading condition.

Time (hr)	PF_1	Exp. Model		Polynomial/ZIP Model					
		n_p	n_q	Z_p	I_p	P_p	Z_q	I_q	P_q
0.5	0.99	1.19	1.81	0.19	0.80	0.00	2.11	-2.46	1.35
1.0	0.98	1.13	1.79	0.15	0.84	0.01	2.00	-2.26	1.26
1.5	0.99	1.16	1.73	0.16	0.83	0.01	1.96	-2.24	1.28
2.0	0.99	1.13	1.70	0.13	0.86	0.01	1.93	-2.20	1.28
2.5	0.99	1.12	1.72	0.13	0.86	0.01	1.96	-2.25	1.29
3.0	0.99	1.13	1.79	0.14	0.85	0.01	2.05	-2.37	1.32
3.5	0.99	1.13	1.76	0.14	0.86	0.01	2.04	-2.37	1.33
4.0	0.99	1.13	1.76	0.14	0.85	0.01	2.05	-2.39	1.34
4.5	0.99	1.12	1.74	0.13	0.86	0.01	2.00	-2.32	1.31
5.0	0.99	1.07	1.84	0.07	0.92	0.00	2.37	-2.96	1.59
5.5	0.99	1.07	2.00	0.07	0.92	0.00	2.71	-3.49	1.79
6.0	0.99	0.95	2.16	0.00	0.96	0.03	3.21	-4.35	2.14
6.5	0.99	0.93	2.24	0.00	0.94	0.05	3.36	-4.57	2.21
7.0	0.99	0.91	2.13	0.00	0.92	0.06	3.25	-4.47	2.22
7.5	0.99	0.89	2.04	0.00	0.90	0.09	3.20	-4.46	2.26
8.0	0.99	0.85	1.89	0.00	0.86	0.13	3.07	-4.33	2.27
8.5	0.99	0.84	1.82	0.00	0.85	0.14	3.04	-4.35	2.31
9.0	0.99	0.80	1.94	0.00	0.80	0.18	3.22	-4.59	2.38
9.5	0.99	0.83	1.62	0.00	0.83	0.15	2.67	-3.79	2.12
10.0	0.99	0.81	1.65	0.00	0.81	0.17	2.71	-3.85	2.14
10.5	0.99	0.78	1.72	0.00	0.79	0.20	2.81	-3.99	2.18
11.0	0.99	0.77	1.67	0.00	0.78	0.21	2.76	-3.92	2.16
11.5	0.99	0.76	1.69	0.00	0.76	0.22	2.79	-3.96	2.17
12.0	0.99	0.74	1.69	0.00	0.74	0.24	2.80	-4.00	2.19
12.5	0.99	0.73	1.72	0.00	0.73	0.25	2.88	-4.11	2.23
13.0	0.99	0.71	1.74	0.00	0.71	0.27	2.90	-4.14	2.25
13.5	0.99	0.70	1.76	0.00	0.70	0.28	2.92	-4.16	2.24
14.0	0.99	0.70	1.76	0.00	0.71	0.28	2.92	-4.15	2.24
14.5	0.99	0.69	1.77	0.00	0.69	0.29	2.93	-4.17	2.24
15.0	0.99	0.67	1.83	0.00	0.68	0.31	3.00	-4.25	2.25
15.5	0.99	0.67	1.82	0.00	0.68	0.31	3.00	-4.26	2.26
16.0	0.99	0.68	1.78	0.00	0.68	0.31	2.87	-4.05	2.17
16.5	0.99	0.71	1.76	0.00	0.71	0.28	2.86	-4.05	2.19
17.0	0.99	0.72	1.72	0.00	0.72	0.27	2.73	-3.81	2.08
17.5	0.99	0.77	1.59	0.00	0.78	0.22	2.42	-3.31	1.89
18.0	0.99	0.84	1.53	0.00	0.84	0.15	2.14	-2.80	1.66
18.5	0.99	0.88	1.46	0.00	0.87	0.12	1.82	-2.22	1.40
19.0	0.99	0.90	1.47	0.07	0.76	0.17	1.78	-2.13	1.35
19.5	0.98	0.95	1.61	0.18	0.58	0.24	1.90	-2.25	1.34
20.0	0.98	0.96	1.60	0.22	0.52	0.26	1.87	-2.18	1.31
20.5	0.98	1.01	1.65	0.27	0.46	0.26	1.84	-2.07	1.23
21.0	0.98	1.02	1.74	0.23	0.56	0.21	2.04	-2.39	1.35
21.5	0.98	1.05	1.78	0.25	0.55	0.21	2.03	-2.34	1.31
22.0	0.98	1.04	1.70	0.33	0.37	0.30	1.88	-2.11	1.22
22.5	0.98	0.99	1.88	0.19	0.62	0.20	2.19	-2.55	1.36
23.0	0.98	1.03	1.87	0.25	0.52	0.22	2.14	-2.46	1.32
23.5	0.98	1.05	1.89	0.17	0.71	0.12	2.19	-2.55	1.36
24.0	0.99	1.12	1.94	0.14	0.83	0.03	2.34	-2.80	1.46

Table H.9: Commercial LV aggregate maximum loading condition.

Time (hr)	PF_1	Exp. Model		Polynomial/ZIP Model					
		n_p	n_q	Z_p	I_p	P_p	Z_q	I_q	P_q
0.5	0.99	1.29	2.00	0.29	0.70	0.00	2.57	-3.20	1.63
1.0	0.99	1.35	2.12	0.35	0.64	0.00	2.75	-3.46	1.71
1.5	0.99	1.29	2.00	0.29	0.70	0.00	2.57	-3.20	1.63
2.0	0.99	1.28	1.86	0.29	0.71	0.00	2.43	-3.08	1.64
2.5	0.99	1.29	1.86	0.29	0.70	0.00	2.44	-3.08	1.64
3.0	0.99	1.33	2.24	0.33	0.66	0.00	2.83	-3.49	1.66
3.5	0.99	1.32	2.25	0.33	0.67	0.00	2.92	-3.66	1.74
4.0	0.99	1.28	2.10	0.28	0.71	0.00	2.69	-3.36	1.66
4.5	0.99	1.26	2.06	0.26	0.73	0.00	2.65	-3.30	1.66
5.0	1.00	1.22	2.12	0.23	0.77	0.00	3.24	-4.45	2.22
5.5	0.99	1.17	2.34	0.18	0.81	0.00	3.58	-4.93	2.35
6.0	0.99	1.00	2.37	0.02	0.97	0.00	3.80	-5.34	2.54
6.5	0.99	0.95	2.46	0.00	0.96	0.03	3.92	-5.50	2.58
7.0	0.99	0.92	2.33	0.00	0.93	0.05	3.81	-5.41	2.60
7.5	1.00	0.92	2.14	0.00	0.93	0.06	3.76	-5.50	2.74
8.0	1.00	0.84	2.16	0.00	0.85	0.13	3.76	-5.49	2.72
8.5	1.00	0.86	1.96	0.00	0.87	0.11	3.57	-5.30	2.73
9.0	1.00	0.83	2.06	0.00	0.84	0.14	3.73	-5.52	2.79
9.5	1.00	0.85	1.75	0.00	0.86	0.12	3.14	-4.62	2.48
10.0	1.00	0.86	1.76	0.00	0.87	0.12	3.21	-4.76	2.55
10.5	1.00	0.84	1.83	0.00	0.85	0.13	3.28	-4.82	2.55
11.0	1.00	0.82	1.75	0.00	0.83	0.15	3.15	-4.65	2.50
11.5	1.00	0.82	1.76	0.00	0.83	0.16	3.18	-4.70	2.52
12.0	1.00	0.79	1.79	0.00	0.80	0.18	3.26	-4.83	2.57
12.5	1.00	0.79	1.74	0.00	0.80	0.18	3.21	-4.78	2.57
13.0	1.00	0.77	1.82	0.00	0.77	0.21	3.34	-4.95	2.61
13.5	1.00	0.78	1.77	0.00	0.79	0.19	3.24	-4.81	2.57
14.0	1.00	0.79	1.79	0.00	0.80	0.19	3.29	-4.89	2.60
14.5	1.00	0.78	1.77	0.00	0.79	0.19	3.25	-4.82	2.57
15.0	1.00	0.76	1.84	0.00	0.77	0.22	3.36	-4.98	2.62
15.5	1.00	0.76	1.87	0.00	0.77	0.21	3.40	-5.03	2.64
16.0	1.00	0.76	1.86	0.00	0.77	0.21	3.35	-4.93	2.58
16.5	1.00	0.78	1.74	0.00	0.79	0.19	3.19	-4.73	2.54
17.0	1.00	0.82	1.68	0.00	0.83	0.16	3.00	-4.39	2.40
17.5	1.00	0.88	1.62	0.00	0.89	0.10	2.73	-3.91	2.18
18.0	1.00	0.95	1.57	0.00	0.96	0.03	2.51	-3.51	2.00
18.5	1.00	1.08	1.34	0.09	0.91	0.00	1.91	-2.52	1.61
19.0	1.00	1.14	1.37	0.14	0.86	0.00	1.83	-2.33	1.50
19.5	1.00	1.22	1.54	0.23	0.77	0.00	2.12	-2.75	1.63
20.0	0.99	1.22	1.62	0.22	0.78	0.00	2.05	-2.54	1.49
20.5	0.99	1.30	1.62	0.30	0.69	0.00	1.99	-2.41	1.42
21.0	1.00	1.36	1.70	0.37	0.63	0.00	2.33	-3.02	1.69
21.5	0.99	1.35	1.89	0.35	0.65	0.00	2.43	-3.04	1.61
22.0	0.99	1.37	1.83	0.37	0.63	0.00	2.24	-2.71	1.47
22.5	0.99	1.35	2.09	0.35	0.65	0.00	2.67	-3.33	1.66
23.0	0.99	1.41	2.19	0.42	0.58	0.00	2.67	-3.20	1.54
23.5	0.99	1.35	2.21	0.36	0.64	0.00	2.76	-3.39	1.62
24.0	0.99	1.35	2.05	0.36	0.64	0.00	2.66	-3.34	1.68

Appendix I

Distribution network data

Table I.1: Generic UK urban secondary distribution transformer values [175].

Operating Voltage (LV)	Vector Group	Rating (MVA)	Impedance		Tap range		Tap step (pu)
			R	X	Min	Max	
			(pu on 100MVA)		(pu)		
33/11	Dyn11	15	0.06	1	0.8	1.05	0.0143
11/0.4	Dny11	0.5	2.04	9.28	0.95	1.05	0.025

Table I.2: Generic UK urban MV/LV distribution network component values [175].

Id.	Type	CSA (mm^2)	Impedance					I_{max} (A)
			Positive seq.		Neutral	Negative seq.		
			R	X	R	R	X	
			Ω/km					
LV lines								
A	UG	300	0.100	0.073	0.1268	0.593	0.042	465
B	UG	185	0.163	0.074	0.168	0.656	0.05	355
C	UG	120	0.253	0.071	0.253	1.012	0.047	280
D	UG	95	0.320	0.0975	0.320	1.280	0.051	245
E	UG	70	0.443	0.076	0.443	1.772	0.052	205
L	UG	35	0.851	0.041	0.9	3.404	0.03	120
MV lines								
P	UG	185	0.12271	0.06575	-	0.85896	0.23011	415
Q	UG	95	0.14403	0.06662	-	1.00824	0.23318	355
Where: UG - underground cable and CSA is the cross sectional area.								